DESIGN, SYNTHESIS, CHARACTERIZATION AND SIMULATION OF POLYHEDRAL OLIGOMERIC SILSESQUIOXANE PORPHYRIN MOLECULES TO FABRICATE SELF-ASSEMBLED NANOPARTICLES AND THEIR USE FOR PHOTODYNAMIC THERAPY

by

Paula Loman-Cortes

A dissertation submitted to the faculty of
The University of North Carolina at Charlotte
in partial fulfillment of the requirements
for the degree of Doctor of Philosophy in
Nanoscale Science

Charlotte

2021

Approved by:

_____
Dr. Donald Jacobs

_____
Dr. Jordan Poler

_____
Dr. Thomas A. Schmedake

_____
Dr. Juan L. Vivero-Escoto

_____
Dr. Michael G. Walter

ABSTRACT

PAULA LOMAN-CORTES. Design, Synthesis, Characterization and Simulation of Polyhedral Oligomeric Silsesquioxane Porphyrin Molecules to Fabricate Self-Assembled Nanoparticles and Their Use for Photodynamic Therapy. (Under the direction of DR JUAN L VIVERO-ESCOTO)

Nanostructures can have a variety of functionalities, making them useful for many applications in energy, catalysis, medicine, biotechnology and other scientific fields. These functional nanostructures are built via the self-assembly of building blocks with particular physicochemical properties. Different molecular interactions participate in the self-assembly processes such as metallic, ionic, van der Waals forces, electrostatic, hydrophobic, H-bonding, and π- π stacking. Therefore, the building blocks are molecules that are pre-designed to supply these interactions in a given environment and can provide a desired functionality.

Polyhedral oligomeric silsesquioxane (POSS) is a promising scaffold to be used as building block for self-assembly and other applications. When covalently linked to a photosensitizer, POSS has an influence on the self-assembly behavior of the photosensitizer, modifying its properties, potentially enhancing its efficacy toward photodynamic therapy (PDT).

In this Thesis, I describe my work on the study of POSS-porphyrin derivatives as building blocks, their self-assembly and application in PDT. We envision that the chemical tunability of POSSs can be used as a promising option to improve the delivery and performance of photosensitizers.

DEDICATION

I would like to dedicate this work to Chloe, Oliver, Rodrigo and Frida for their encouragement and patience. You are my love light.

To Oliver's and Chloe's teachers throughout daycare and preschool, especially Ms. Summer, Ms. Latara, Ms. Free, Ms. Alexandra, Ms Melissa, Mrs Mathur, Mrs Chester, Mrs Waiman, Mrs Londono, Mrs Legeic and Mrs Rouse. It was invaluable to me that my children were cared for in such safe, happy, and enriching environments while I was working in this project. I am inspired by your dedication and hard work.

To Dr Vivero without whom I would have never completed this program. He is terrific mentor and a true friend who stood by me through rough times.

ACKNOWLEDGEMENTS

I am very grateful to Dr Vivero for his guidance, motivation, and patience throughout all my time in UNCC. I am also thankful for the support and guidance of my committee members, Dr Schmedake, Dr Poler, Dr Walter, and Dr Jacobs. Especially to Dr Jacobs who dedicated many hours of his time to patiently go through the simulation data with me. I greatly appreciate Dr Donovan-Merkert's encouragement and help every time I needed it.

I would like to thank all the fellow V-lab members for their companionship. And especially Paolo Siano and Alexis Johnston for all the work they did in relation to this project.

I am also grateful to Centro Nacional de Ciencia y Tecnología (CONACYT) for the scholarship 440854 that funded most of my time in the program and to the Graduate School who covered my first semester through the GASP program.

TABLE OF CONTENTS

LIST OF TABLES

LIST OF FIGURES

LIST OF ABBREVIATIONS

$^1O_2$	Singlet oxygen
ATPP	Aminophenyl trphenyl porphyrin
APTES	(3-aminopropyl) trihydroxysilane
BHT	Butylated hydroxytoluene
Ce6	Chlorin e6
CuAAC	Cu(I)-catalyzed [3+2] azide–alkyne cycloaddition
DCM	Dichloromethane
DI water	Deionized water
DIPEA	di-isopropyl ethyl amine
DLS	Dynamic light scattering
DMF	Dimethyl formamide
DMSO	Dimethysulfoxide
DPPC	1,2-dipalmitoylphosphatidylcholine
FRET	Förster type resonance energy transfer
GROMACS	GROningen MAchine for Chemical Simulations
IR	Infrared
LAMMPS	Large-scale Atomic/Molecular Massively Parallel Simulator
MW	Molecular Weight
OPLSA-AA	Optimized Potentials for Liquid Simulations All Atom
PBS	Phosphate buffer solution
PDT	

PEG	Photodynamic Therapy
PMF	Poly(ethylene) glycol
	Potential of mean force
POSS	Polyhedral oligomeric silsesquioxane
POSSP-IB	Hepta (isobutyl POSS) porphyrin
POSSP-Ph	Hepta (phenyl POSS) porphyrin
POSSP-TIB	Tetrakis[Hepta (isobutyl POSS)] porphyrin
RLS	Resonance light scattering
RNA	Ribonucleic Acid
ROS	Reactive Oxygen Species
RPMI	Roswell Park Memorial Institute
SEM	Scanning electron microscopy
SPCE	Simple point-charge (extended) water model
TATPP	Tetra(aminophenyl) porphyrin
TEM	Transmission electron microscope
THF	Tetrahydrofuran
TMAOH	Pentahydrate tetramethyl ammonium hydroxide
TNBC	Triple negative breast cancer
TPP	Tetraphenyl porphyrin
UV-vis	Ultra-violet visible spectroscopy

CHAPTER 1. INTRODUCTION.

Nanostructures can have a variety of functionalities, making them useful for many applications in energy, catalysis, medicine, biotechnology and other scientific fields.[2] These functional nanostructures are built via the self-assembly of building blocks with particular physicochemical properties. Different molecular interactions participate in the self-assembly processes such as metallic, ionic, van der Waals forces, electrostatic, hydrophobic, H-bonding, and π- π stacking. Therefore, the building blocks are molecules that are pre-designed to supply this interactions in a given environment and can provide a desired functionality.[3-4] Macromolecular self-assembly also produces materials with functional properties that depend on the spatial arrangement of constituent molecules. The morphology of such materials across a range of length scales is an important factor to consider for achieving particular function suitable for different applications[5-6]. In this Thesis, I describe my work on the study of polyhedral oligomeric silsesquioxanes (POSS) porphyrin derivatives as building blocks, their self-assembly and application in photodynamic therapy (PDT).

1.1 Polyhedral Oligomeric Silsesquioxane (POSS)

POSS molecules are nanostructures with the empirical formula $[RSiO_{1.5}]_n$ where n is usually 8, 10 or 12 and R is an organic functional group. The geometry can be random, ladder or cage. POSS cage molecules with n=8 is the most common, it can be regarded as a cube where the organic substituents are attached at the corners (Figure 1).[7] The size of these POSS cubes range between 1 and 3 nm.[8]

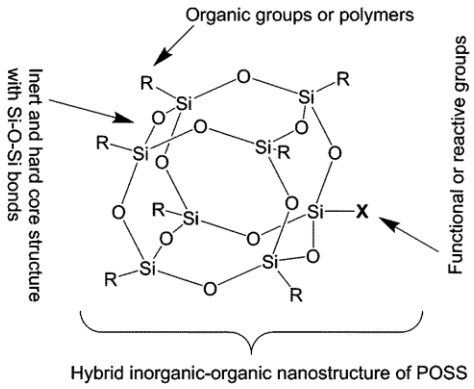

Figure 1. POSS general structure.[9]

By modifying the organic moieties, the chemical compatibility (solubility) and reactivity of the POSS molecules can be tuned. The organic substituents can be modified throughout the cage, providing different functionalities to render a wide variety of molecular interactions that can be used to build molecular clusters through self-assembly. The relatively large size and inert behavior of Si-O-Si core make them useful as molecular spacers. A spacer with interchangeable organic functionalities can greatly influence the self-assembly behavior of a system. These characteristics facilitate the self-assembly of POSS-containing materials of which there are plenty of examples in the literature

1.2 Strategies for synthesis and functionalization of POSS

1.2.1 Synthesis of POSS

POSS can be synthetized from the corresponding organotrichlorosilane or alkoxysilane by controlled hydrolysis and condensation[10-11]:

$$\boldsymbol{nXSiY_3 + 1.5nH_2O \rightarrow (XSiO_{1.5})\ \ n\ +\ 3nHY} \qquad (1)$$

Y is either Cl or an alkoxy group; and X is an organic group or H.

The condensation can be either complete, forming a functionalized cage, or incomplete, obtaining a ladder or a cage that is open in one corner that can be further functionalized with a silane precursor (Figure 2).[12] The cubic POSS (n=8) is commonly isolated by difference in solubility and

can take a long time to form, even months.[10-11, 13] The most common substituents, which are commercially available, that have been incorporated in the POSS cage are H, isobutyl, phenyl, methyl, benzyl, vynil, n-propyl, cyclohexane, aminopropyl, ammonium propyl, chloropropyl, and mercaptopropyl.[11] By using the open cage as starting material, POSS with multiple functionalities can be synthesized via the corner capping approach (Figure 2).[10-11]

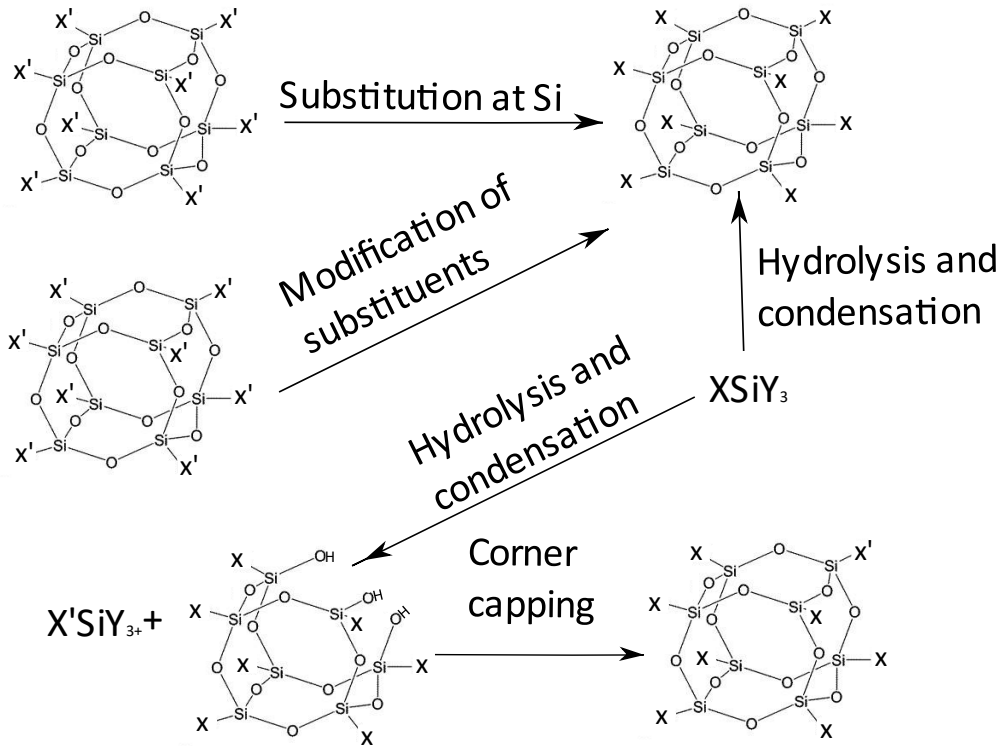

Figure 2. Routes to POSS synthesis.[11]

1.2.2 Functionalization of POSS

The most common methods for functionalization of a POSS cage after its condensation are the modification of the already existing functionalities or the introduction of a new ones through corner capping (Figure 2). Common functional groups for chemical modifications are:

aminopropyl, phenyl, and vinyl. A large variety of new functionalities have been introduced to POSS including azo, carboxylic acid, nitrile, sulfhydryl, epoxide, diverse polymers, and many others.[11, 14-19]

A very common method of modification is adding new molecules by nucleophilic addition to carbonyl groups; for example, reacting one or more aminopropyl groups from the POSS with an acyl chloride[20] or a carboxylic acid functionalized molecule afford amide bonds.[21-23]

Recently, "click" chemistry has been used by many groups to introduce diverse ligands to the POSS cage, particularly the Cu(I)-catalyzed [3+2] azide–alkyne cycloaddition (CuAAC)[24-26] and thiol-ene addition.[24, 27-28] Before the CuAAC reaction could be used successfully on POSS, several groups worked on the introduction of azido functionalities[JV1]. The azidation of octakis(3-chloropropyl) POSS is prone to suffer from cage rearrangement.[29] Heyl *et al.*[30] overcame this issue by converting the chloropropyl groups octakis(3-chloropropyl) to iodopropyl with NaI, tetrabutylammonium iodide and iodopropane in butanone and then performing the azidation with N,N,N′,N′-Tetramethyl guanidinium azide in $CHCl_3$. While Fabritz *et al.*[25] converted the chloropropyl groups to bromopropyl with LiBr in acetone and then performed the azidation using NaN_3 in DMF. Dr Chiara's group[26, 31] obtained the octa azide POSS from octa ammonium POSS by a diazo transfer approach using both the trifluoromethanesulfonyl azide and the more innocuous nonafluorobutanesulfonyl azide using $CuSO_4$ as a catalyst.

1.3 Use of POSS in biomedical applications[JV2][PL3]

POSS has been used extensively for biomedical applications. They have [JV4]been used in drug delivery, gene therapy, biomedical imaging and bone regeneration.[32] [JV5]They can be simultaneously

conjugated with multiple functional groups that provide drug carrying, targeting and/or enhanced solubility capabilities. Through its multiple arms, POSS can easily be incorporated in crosslinked polymers, fixing any functional groups into the polymer matrix. In addition, most of the POSS molecules studied are readily internalized in cells[33] and have shown low cytotoxicity.[34-35]

Some examples of biomedical applications that include the use of POSS are: the study of lecithin-carbohydrate interactions, the creation of supramolecular amphiphiles for cell adhesion and tissue engineering, and the hierarchical self-assembly of POSS-peptides and dendrimers in general that can later encapsulate therapeutic molecules for drug delivery.[14] [JV6][PL7]POSS have also been useful as building blocks to produce giant molecules. This strategy allows the design of different topologies such as tadpole, dumbbell, star-like or dendrimers. For example, Caihua *et al*.[36] created a star block copolymer by attaching 32 poly-caprolactonate chains to a POSS center. This molecule formed a micelle in water that could be loaded with the hydrophobic drug ibuprofen, which can be later released by controlling the temperature.

1.4 Use of POSS for PDT

1.4.1 Photodynamic therapy (PDT)

Photodynamic therapy is non-invasive therapeutic approach that involves the administration of a photosensitizer, which upon light irradiation reacts with molecular oxygen to generate reactive oxygen species (ROS) affording cell death as ultimate outcome.[37] Figure 3 summarizes the mechanisms by which the ROS are formed. After light irradiation, the photosensitizer is excited to the singlet state, S_1, where it can relax back to the ground state, S_0, via fluorescence or non-radiative decay or it can be converted to the triplet state, T_1, by intersystem crossing. While in the

triplet state, it can react with ambient molecules to produce the ROS following one of two paths (type I or type II PDT). In Type I the photosensitizer produces free radicals through an electron or hydrogen transfer process, these free radicals interact with water or oxygen molecules producing hydroxyl radicals or superoxide anions even in hypoxic conditions. In Type II the photosensitizer in the excited triplet state transfers its energy to an oxygen molecule also in its triplet state producing singlet state oxygen ($^1O_2$), which is highly cytotoxic.[38] Singlet oxygen is the most important component for PDT, but its diffusion length is typically very short (30 nm maximum); hence, the intracellular localization of the photosensitizer is very important for the effective PDT treatment.[39]

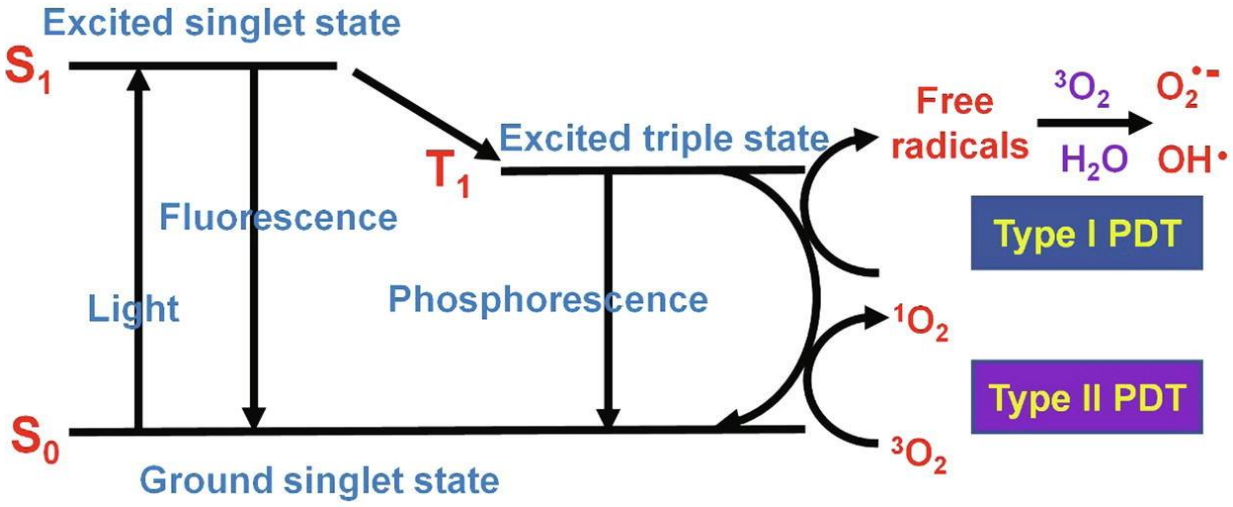

Figure 3. Jablonski diagram illustrating the formation of reactive oxygen species associated to PDT.[38]

Porphyrins are widely used photosensitizers for PDT applications because of their high singlet oxygen quantum yield,[40] with some of them showing a high affinity to tumor sites,[41] and an absorption wavelength longer than other types of photosensitizers (630–700 nm).[42] It has been

found that the affinity of porphyrin photosensitizers for tumor tissue increases as the molecule becomes more hydrophobic.[37, 43] One of the main challenges with porphyrins is their poor solubility in physiological conditions, which prevents their circulation in the bloodstream reducing their PDT efficacy.[37, 44]

1.4.2 Aggregation and quenching of porphyrin photosensitizers.

Porphyrins tend to aggregate in water-rich media, changing its photophysical properties. The aggregates usually have lower fluorescence and singlet oxygen quantum yields.[45] It is considered that the decrease of singlet oxygen production upon photosensitizer aggregation is a result of the quenching of its singlet excited state. Therefore, it is frequently accompanied by a decrease in the photosensitizer's fluorescence emission.[46]

There are two mechanisms to account for the self-quenching of porphyrins; the Förster type resonance energy transfer (homo-FRET) and exciton coupling. Homo-FRET depends on the overlap of the absorption and emission bands of the porphyrin molecules. It is inversely proportional to the sixth power of the distance between molecules, so it is very sensitive to this parameter. [47-49] In theory, this process should not involve a change in the fluorescence lifetime,[48-52] although an apparent increase in fluorescent lifetime was reported for homo FRET in tetraphenyl porphyrin (TPP).[47] [JV8][PL9]The second mechanism involves the interaction of the excited states of two or more molecules leading to a delocalization of the excitation over those molecules. This exciton coupling also depends on the distance and relative orientation of the molecules.[48, 53-54] Kasha's theory predicts total quenching for molecules that are stacked on top of each other and have no rotation relative to the other (H-aggregates, Figure 5).[53, 55] Also, Kasha aggregates, specifically J-

aggregates, can have a reduced fluorescence lifetime.[56] Although the formation of a Kasha aggregate can explain the quenching of fluorescence, the intercrossing to the triplet state is not equally weakened by the exciton coupling.[7,9,53] Both processes, homo-FRET and exciton coupling, can happen at the same time. Since both processes are dependent on the distance between the fluorophores, increasing the spacing between them should always reduce their effect.

Several strategies have been developed to prevent the aggregation of porphyrins. Direct chemical functionalization of photosensitizers has been widely explored to increase their solubility in water and reduce aggregation. For example, our group previously studied cationic porphyrins and the influence of the number of positive charges in their efficiency for PDT in Gram-negative bacteria.[57] Nevertheless, some of these approaches require long synthetic steps with tedious separation protocols affording usually low yields. Other alternatives have explored the encapsulation of porphyrins in liposomes, polymers, metal-organic frameworks, metallic or silica-based nanoparticles.[37] Our group has investigated the use of silica-based platforms for cancer treatment using PDT.[58-63]

1.4.3 Strategies to improve PDT using POSS

POSS molecules are an attractive platform for the delivery of porphyrins because they provide an absolute control on the chemical functionalization of the core structure. The modification of POSS-porphyrins render enhanced solubility, colloidal stability and targeting. Moreover, through its multiple functionalization sites, POSS can easily be incorporated in crosslinked polymers, fixing any functional groups into the polymer matrix. In addition, the large volume of POSS cage can

provide steric hinderance for preventing the aggregation of the poprphyrins, which is relevant to overcome the self-quenching effect.

Some reports have already been published on the investigation of POSS-porphyrins for PDT. It has been found that the POSS cage can be useful to conjugate a targeting agent to the photosensitizer system[64-65] and that it can prevent the aggregation induced quenching of the porphyrin, increasing its efficiency for PDT.[23-24, 66-70]

Lee and Kim[65] conjugated Protoporphyrin IX (PpIX) molecules and linolenic acid to a water soluble octammonium POSS. The molecule self-assembled into nanoparticles of ~120 nm in diameter due to strong hydrophobic interactions. Cellular uptake was enhanced, most likely due to the presence of linoleic acid. The nanoparticles also showed improvement in *in vitro* PDT efficacy; while dark toxicity was reduced, as compared with PpIX. Jin et al.[66] incorporated pendant isobutyl POSS monomers into an amphiphilic copolymer that alternates a tetraphenyl porphyrin with the POSS. With this arrangement the authors prevented the porphyrin aggregation and reduced the aggregation-induced quenching effect. The system then self-assembled into spherical nanoparticles with sizes dependent on the polymer length. Compared to the POSS-free polymeric nanoparticle, this system showed a higher fluorescence and singlet oxygen quantum yield as a clear indication that the POSS units contribute to the decrease of the aggregation between porphyrin units. *In vitro* data in A549 cells showed the time-dependent internalization of the nanoparticles and the enhanced PDT efficiency associated with the POSS units. Finally, the POSS containing polymeric nanoparticles have an excellent biocompatibility and anti-cancer capability for PDT of tumors *in vivo*. Bao, Wang et al.[68] modified tetrahydroxyphenyl porphyrin with POSS units containing long dodecyl alkyl chains. With this strategy the authors expected to overcome the lack of water solubility and aggregation of the photosensitizers. In addition, the authors also

wanted to amplify the singlet oxygen generation by energy transfer after the POSS-porphyrin unit has been wrapped by a semiconducting polymer forming nanoparticles.[71-73] Photophysical characterization of the nanoparticles showed an improved fluorescence quantum yield and singlet oxygen generation as an indication that the POSS scaffold and the long alkyl chains effectively reduces the aggregation of porphyrins and prevents the interaction with the semiconducting polymer. *In vitro* evaluation of the nanoparticles in HeLa cells demonstrated an improved fluorescence emission in biological media and PDT effect. Bao, Wang et al.[24] conjugated four POSS to a tetrahydroxyphenyl porphyrin (THPP) where the POSS arms were functionalized with PEG_{5000} to create water-soluble nanoparticles with an hydrodynamic diameter of 28 nm. The absorbance, fluorescence and $^1O_2$ generation were enhanced with respect to the control porphyrin due to the presence of POSS framework, which reduces the self-quenching effect between porphyrins. *In vitro* tests on HeLa cells showed lower dark toxicity, but enhanced toxicity under irradiation as compared with THPP.

1.5 Self-assembly of POSS molecules

1.5.1 POSS as a building block for self-assembly

POSS molecules have recently been used to develop hybrid systems with unique properties for self-assembly.[74-75] The intramolecular interactions in general can be used for encoding the molecular structure design. Examples of the interactions that have been used for the self-assembly of POSS molecules are electrostatic, hydrogen bonding, van der Waals, dipole-dipole, and aromatic π-π. Also, contributions from molecular packing constraints, interfacial curvature, matching of surface amphiphilicity and charge have been exploited.[76-77]

Being prone to self-assembly and crystallization, POSS is frequently used as a building block in amphiphilic systems, providing a specific interaction with the solvent (usually water) through its substituents.[32, 78-82] When POSS containing molecules undergo self-assembly, the POSS section tends to form a separate microdomain, often crystalline.[83-86] It is hypothesized that POSS molecules go through a nucleating effect for forming this nanocrystalline phase.[87-88] The substituents of the POSS are crucial in determining their self-assembly behavior by imparting specific chemical and physical properties that play a role in the self-assembly process.[89-90] For example, molecules that comprise of many POSS units with a variety of substituents that are not miscible tend to possess distinct microdomains as they form a hierarchical assembly.[91] Aromatic POSS substituents have shown to participate in the self-assembly through π-π interactions and stacking.[90] Although POSS molecules have a natural propensity to self-assemble and form hierarchical structures, when chemically coupled with other self-organizing molecules such as porphyrins, the scope of self-assembly control is increased.[74-75] The self-assembly tendency of POSS together with its biocompatibility has been exploited in many applications such as drug delivery and PDT. By forming POSS aggregates, it is possible to achieve lower levels of cytotoxicity and/or prevent aggregation quenching of POSS-fluorophore molecules,[92-95] including porphyrins.[23, 64-66, 70, 96]

The POSS cage has been used as a scaffold with photoluminescent molecules generating 3D structures that prevent both an excessive π-π stacking and a drop in their quantum yield. [1, 94, 97-98] For instance, a perylene diimide (PDI) dye was dotted with two POSS molecules on opposite sides, which promoted a dimer arrangement (Figure 4) that presented a significant red shift in the UV-Vis spectrum and an increased fluorescent emission, most likely due to J-aggregation.[1] POSS

molecules have been also used to prevent aggregation induced quenching in other luminescent materials such as quantum dots. [99-101] POSS molecules could provide the steric hinderance needed to prevent direct face to face stacking while the interaction between the organic moieties of the POSS could also have an influence on the resulting geometry. Other studies of self-assembly of POSS-based molecules (POSS-fullerene[7, 102] or forming super amphiphiles[78]) have shown a clear tendency of the POSS moieties to form microphases that contribute to the final shape of the self-assembled aggregate.

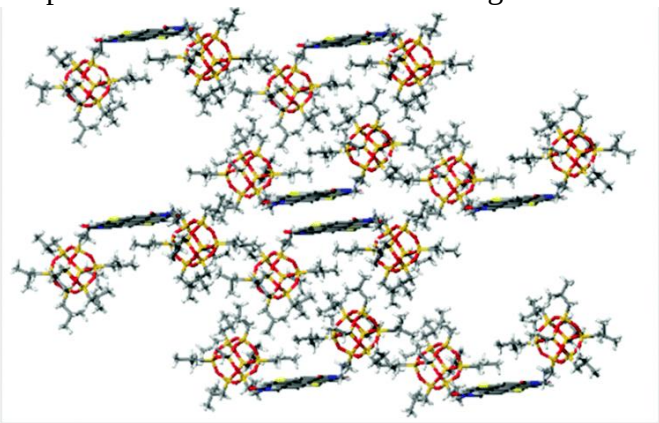

Figure 1 Self-assembly of POSS-PDI-POSS into J-aggregate dimers as an example of POSS directing the aggregation of a chromophore.[1]

1.5.2 Self-assembly of POSS-porphyrin molecules

Porphyrins are light absorbing molecules that are abundant in nature.[37] They are long known to self-aggregate;[103] however, porphyrins usually form irregular aggregates in solution that may not be suitable for specific applications.[99] However, if they stack forming specific geometries that afford coupling between their electronic transitions, this can give rise to optical and electronical properties that differ from the original individual molecules.[104] Features such as enhanced fluorescence, efficient charge transfer,[105-108] shifting of absorbance wavelength, and reduction of quenching at high concentrations are relevant for these aggregates.

The main unit of porphyrins (porphine) is composed of a planar aromatic heterocyclic compound (Figure 5a). This particular geometry allows for stacking between molecules. In addition, chemical

modifications on the meso-positions of the molecule can provide complementary mechanisms of molecular interaction.[37, 106] In general, the geometries of aggregates that present electronic coupling via π-π stacking are classified into two main groups: H- and J-aggregates (Figure 5b and c). In H-aggregates, the molecules are stacked face to face, while in J-aggregates they are staggered.[109] H-aggregation commonly results in the quenching of the emission processes, which it is usually not desired. Nevertheless, in some specific cases that can be an advantage. J-aggregates do not quench the chromophore emission and are linked to an increase in the charge separation distance in the exciton that leads to high efficiency as an electron donor.[105] Previous reports have shown that adding groups that provide steric repulsion such as ortho-substituted alkoxyphenyl groups at meso-positions[110-111] and a POSS molecule[101] can prevent porphyrin aggregation.

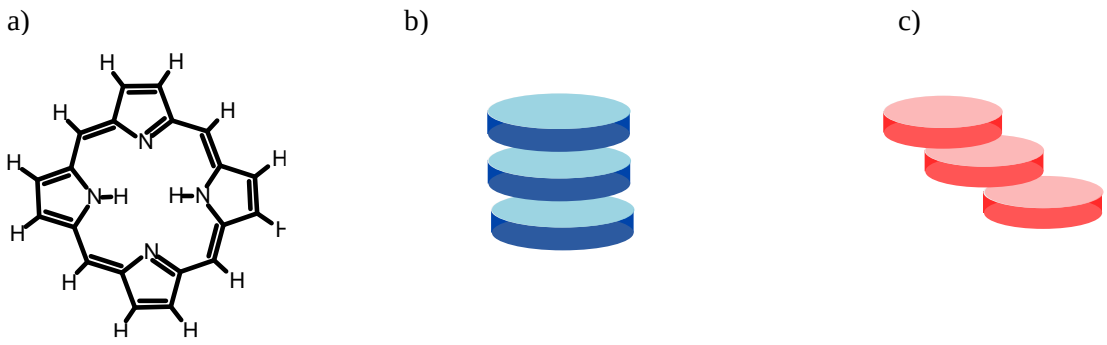

Figure 5. a) Illustration of porphine molecule, which is the main unit of porphyrins. Cartoon shows the stacking arrangement for b) H-aggregation and c) J-aggregation.

The controlled self-assembly of porphyrins can lead to small particles with diameters in the hundreds to thousands of nanometers. These particles are commonly prepared by the reprecipitation method, which relies on the differences in solubility of porphyrin molecules between two or more solvents. The approach follows the addition of a solvent with poor solubility

for porphyrin molecules to a porphyrin solution while mixing vigorously [99, 112-115], sometimes with the help of sonication.[116] This method is simple, reproducible and produces nanoparticles with narrow size distributions.[112, 117-118] The porphyrin particles obtained by this protocol have been studied for optics, theranostics, sensing, and catalysis.[119-123] The nanoscale arrangement makes the individual molecules less accessible from reactive species and therefore less prone to photobleaching.[124]

There have been studies of self-assembly of POSS-porphyrin molecules. For example, the self-assembly of isobutyl POSS linked to tetraphenyl porphyrin produced different geometries when varying the solvent ratio of $CHCl_3$ to hexane because hexane is much more compatible with the POSS than with the porphyrin. By varying the solvent polarity in this way, along with the concentration of POSS-porphyrin and the length of the linker between the POSS and the porphyrin, a wide range of morphologies and sizes were obtained including micelles and nanowires from 172 to 1205 nm in diameter.[74, 125] In another study, an ionic porphyrin-POSS adduct aggregates in acidic conditions because of the interactions of the protonated porphyrin. The growth of the aggregates is stabilized by the POSS steric hinderance, yielding spherical nanoparticles with sizes ranging from 20-80 nm.[126]

1.5.3 Optical properties of porphyrin aggregates.

In nanoscale systems, the electronic excitations differ from the ones in bulk materials. The excitons can be thought to be either a confined bulk-type exciton or a molecular exciton.[104] A difference of nanoscale excitons with bulk size excitons is that their size is not dictated by the electron-hole Coulomb interaction, but by the physical dimensions of the nanoparticle and/or the distribution of

the building blocks. Orbital mixing interactions between nanoparticle subunits can induce exciton delocalization over the subunits.[104]

The change in optical properties of agglomerates is usually explained using Kasha's theory of excitonic coupling[55] as a starting step.[127] Exciton effects are observed in a composite molecule were strong electronic transition exists between the sub-units. The exciton is split, provoking either shifts or splitting in the absorption bands. Kasha's theory regards a dye molecule as a point dipole and upon aggregation the energy of the excited states of the interacting dipoles is split as shown in Figure 6. The geometry in an H-aggregate causes the singlet excited state to have a higher energy than the monomer while in a J-aggregate the energy is lower. This is the origin of the characteristic blue and red shifts of H- and J-aggregates, respectively. In the H-aggregates, the excited state can go through vibronic relaxation causing a loss in emission intensity while in J-aggregates only the transition to the ground sate is allowed, causing a high quantum yield.[128]

The transition probabilities between the ground state and the split excitation states is given by the vector sum of the individual transition dipole moments. In the case of coplanar coupling (Figure 6a), one of the split exciton states is forbidden because the individual dipoles cancel each other, leaving only one observable transition.[129] Kasha's model limits the interaction to the nearest neighbors and the dipoles are assumed to be translationally equivalent.[130]

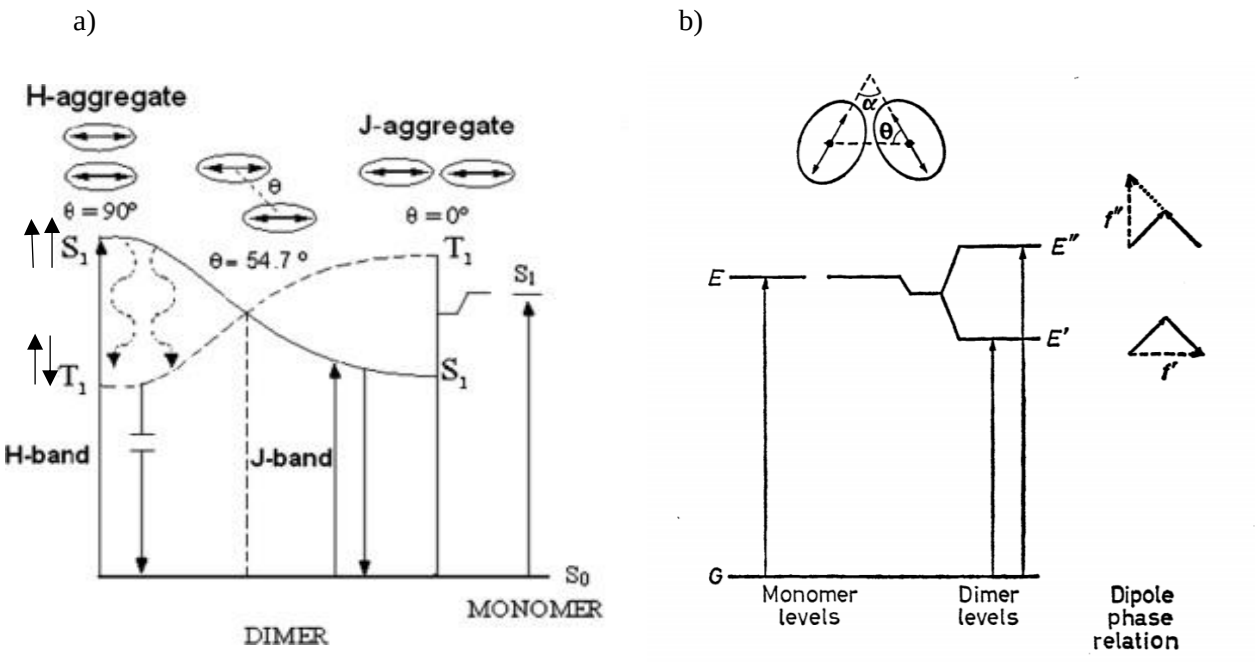

Figure 6. Point dipole approximation theory. a) Coplanar coupling. b) Oblique coupling.[128-129]

Experimentally accessible features of aggregates are spectral maxima, full width at half maximum (FWHM) of absorption and emission spectra and superradiance.[131] A decreased Stokes shift indicates a decrease in exciton phonon coupling.[131] The FWHM increases with temperature and with aggregate disorder. The extinction coefficient and fluorescence rate constant can decrease with aggregate disorder.[131] In J-aggregates, the emitting state has a transition dipole that is proportional to the square root of the number of chromophores in the aggregate and the radiative decay rate increases.[56] The ratio of the oscillator strengths of the first two vibronic peaks in the absorption spectrum increases with the exciton bandwidth in J-aggregates and decreases in H-aggregates. The ratio of the fluorescence vibronic peaks (0,0 / 0,1 peaks) increases with the number of chromophores over which the exciton is delocalized in J-aggregates, but decreases in H-aggregates.[56]

Besides absorbing light, aggregates also scatter it due to differences in polarizability with the solvent. This scattering is enhanced at wavelengths were absorption takes place and is called resonance light scattering (RLS). In monomeric solutions, this RLS is weak compared to the absorption but as the volume of the aggregate increases, the absorption increases linearly but the scattering depends on the square of it so it becomes more noticeable.[132]

1.6 Molecular dynamic simulations

1.6.1 Basic concepts of molecular dynamic simulations[JV10][PL11]

In each step of a molecular dynamic simulation, the forces exerted on each atom by all the system are calculated, and then the position and velocity of every atom is updated using Newton's laws of motion. The forces on the atoms are calculated using models known as force fields (OPLS-AA force field in this work). Typically, force fields include terms that incorporate electrostatic interactions, spring-like terms that set the preferred length of covalent bonds, and other terms to capture other interatomic interactions. Each step is usually only a few femtoseconds long and it is repeated the necessary number of times to get the desired simulation time, usually several hundred nanoseconds.[134] The algorithm is summarized in Figure 7.

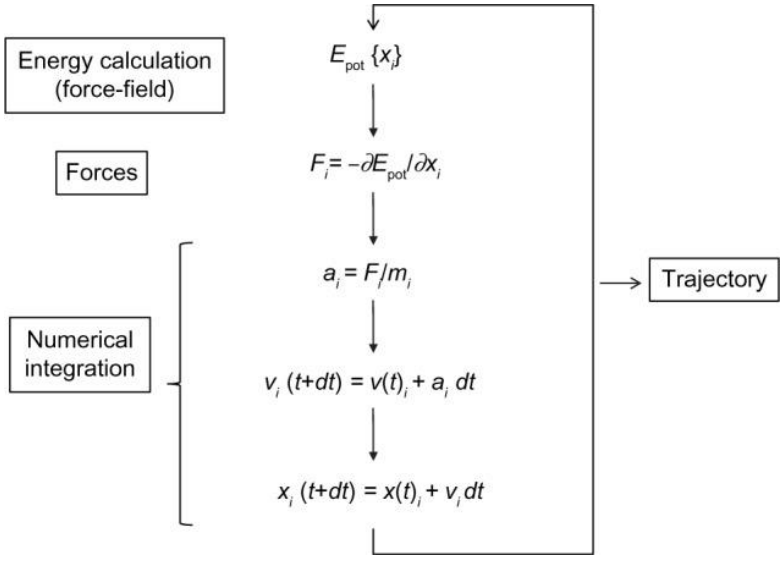

Figure 7. Molecular dynamics basic algorithm.[133]

1.6.2 Use of molecular dynamic simulations to study the self-assembly of POSS

Previous studies have employed MD simulations to glean insight about the self-assembly of POSS molecules. These works have focused on studying monofunctionalized systems or composites where POSS molecules are part of the whole platform.[79, 135-137] For example, in a study of self-assembly of monotethered POSS with tether lengths of 4-24 carbons and good or bad solvents for the tethers, it was found that the large volume and cubic geometry of the POSS cages together with their attractive interaction in a poor solvent induces a strong face to face local packing, corroborating the POSS strong tendency to self-assembly in a poor solvent.[135] In a recent work, a coarse-grained model was used to simulate the hierarchical self-assembly of a dendrimer with POSS at the core in water. POSS arms were amphiphilic PEG-based polymers of varying sizes. The obtained structures match the ones physically observed by TEM where a strong microphase separation was observed showing MD simulations can yield results close to real life experiments.[138] Furthermore, MD simulations of amphiphilic polymers containing POSS in water showed that the POSS units offered a second level of hierarchy in the resulting ordered structure and the MD simulation was useful for understanding the self-assembly process.[79] A study on self-assembly of POSS mono-tethered with either a phenyl, cyclopentyl or phenyl group using a coarse grained model found that short-range interactions (<5 Å), mainly van der Waals, promoted a face to face assembly of the POSS cages while the long-range coulombic interactions (>10 Å) were responsible for corner-edge, corner-corner and edge-edge arrangements. They also observed that in the phenyl substituted POSS, π-π interactions were a strong driving force for self-assembly and that they acted cooperatively with H bonds to determine the final assembly shape. They did not observe a strong drive to self-assembly for the isobutyl substituted POSS but although the solvent

used in the simulation is not mentioned, it does not seem to be water so they would not be observing any hydrophobic effect.[137]

1.6.3 Use of molecular dynamic simulations to study the interaction with a phospholipid bilayer

The passive diffusion of a molecule through the cell membrane can be studied by MD simulations and there are many examples of the study of the permeability of a molecule through a phospholipid bilayer as a tool for analyzing the cell uptake by this mechanism.[139-141] The field dedicated to model phospholipid bilayers is very large and the complexity of the simulations has grown rapidly with the advances in hardware capacity and software optimization. Traditionally the phospholipids have been modeled using the CHARMM and Berger force fields which have been optimized to reproduce their experimental characteristics.[142] When studying the permeation across a bilayer of molecules, the free energy profiles, diffusion coefficients and permeability coefficients have been calculated. The results tend to be qualitatively consistent with experiments, but the actual values obtained are difficult to compare to the experimental ones. Simulations are often done on simple, pure lipid bilayers while the real membranes are much more complex.[143]

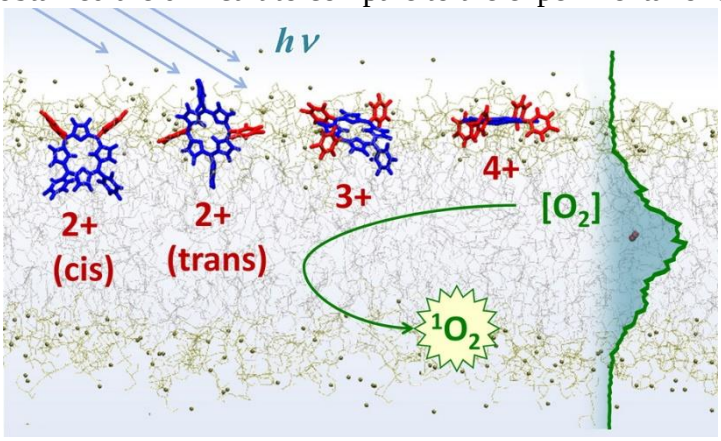

Figure 8. Interaction of porphyrins with varying number of positive charges with a phospholipid bilayer. Red indicates the presence of the charges.[144]

There is a previous work studying the insertion of porphyrins in a phospholipid bilayer that notes the influence and position of cationic charges on the orientation and depth in

which the porphyrins are inserted into the bilayer. Since oxygen is more soluble in the hydrophobic region of the bilayer and hence more abundant there, the porphyrins that can go deeper into this region are thought to be more efficient as photosensitizers for photodynamic therapy (Figure 8).[144]

1.7 Summary/outline of the dissertation

1.7.1 Goal/Hypothesis

The main goal of this Thesis project was to investigate the effect of different functional groups in POSS molecules on the self-assembly and PDT performance of POSS-porphyrin molecules. We hypothesized that by taking advantage of the structural and chemical properties of POSS, the self-assembly of porphyrins can be performed in a controlled fashion. In this Thesis, we focused our efforts on the synthesis and characterization of three POSS-porphyrin derivatives and studying their performance as photosensitizer agents for photodynamic therapy. By using molecular dynamic simulation, we explored the effect of functional moieties that can drive the self-assembly through the hydrophobic effect, π-π interaction or H-bonding.

1.7.2 Description of each chapter

Chapter 1 depicts basic principles on the synthesis, functionalization and application of POSS in biomedicine. It also gives an in-depth description of the main concepts related to the self-assembly of POSS and POSS-porphyrins, and PDT applications. Basic concepts of molecular dynamic simulation used in this Thesis are also described.

Chapter 2 describes the synthesis and characterization of three POSS-porphyrin derivatives using different substituents on the POSS cage. The structural and physicochemical properties of these POSS-porphyrin molecules are depicted in this Chapter. The in vitro PDT effect of these POSS-porphyrins is also discussed. Finally, MD simulations with lipid bilayers are used to describe the POSS-porphyrin interactions and account for the PDT results.

Chapter 3 outlines the Molecular Dynamics simulations on the self-assembly of the POSS-porphyrins. The MD results depicts the final arrangement of the assemblies and shed light on the mechanism of the assembly.

Chapter 4 reports our preliminary results on the fabrication of POSS-porphyrins nanomaterials in water. The influence of the steric hinderance combined with directing hydrophobic/aromatic agents on the self-assembly is studied. The resulting optical properties are analyzed.

Chapter 5 summarizes the main conclusions of this work and gives future directions that can be pursued in this field.

CHAPTER 2. SYNTHESIS AND CHARACTERIZATION OF POSS-PORPHYRIN MOLECULES CONTAINING DIFFERENT FUNCTIONAL GROUPS.

Some of the results reported in this Chapter have already been published: Molecules (2020), 25(21), 4965. I also acknowledge the contribution of Alexis Johnston (MS Chemistry '20) and Paolo Siano (MS Chemistry '20) in some of the results reported in this Chapter.

2.1 Introduction[JV12]

Both POSS and porphyrins are very prone to self-assembly. In porphyrins, the assemblies can altered optical and electronic properties, which is not always desirable. The chemical addition of POSS to the porphyrin molecule changes the relative orientation and spacing within the porphyrins. While the driving force for the self-assembly of porphyrins is usually π-π interactions, the molecular interactions of the POSS unit will depend on its substituents. In this work, we are testing POSS-porphyrins containing POSS units with different substituents such as isobutyl and phenyl.

In this chapter, three POSS-porphyrin (POSSP) derivatives were designed, synthesized, characterized, and applied for PDT *in vitro*. The synthesized molecules are: 5-(4-[3-(3-(3,5,7,9,11,13,15-heptaisobutyl pentacyclo[9.5.1.1(3,9).1(5,15).1(7,13)]octasiloxane) propyl) ureido] phenyl)-10,15,20-(triphenyl)porphyrin (POSSP-IB), 5-(4-[3-(3-(3,5,7,9,11,13,15-heptaphenyl pentacyclo[9.5.1.1(3,9).1(5,15).1(7,13)]octasiloxane) propyl) ureido] phenyl)-10,15,20-(triphenyl)porphyrin (POSSP-Ph) and (tetra-(4-[3-(3-(3,5,7,9,11,13,15-heptaisobutyl pentacyclo[9.5.1.1(3,9).1(5,15).1(7,13)]octasiloxane) propyl) ureido] phenyl)-10,15,20-(triphenyl)porphyrin (POSSP-TIB) (Figure 9).[JV13] Two different substituents for the POSS cage were

chosen, isobutyl and phenyl, to synthesize POSSP derivatives. The goal for this selection was to evaluate the influence of the substituents on the self-assembly of POSSP. The isobutyl POSS cage is expected to interact through van der Waals and hydrophobic interactions. While the phenyl POSS should present π-π forces that could afford interactions between themselves or with the porphyrin. Moreover, a third POSSP molecule containing four POSS was fabricated with the purpose of testing the effect of the increased steric hinderance.

To afford the molecules shown in Figure 9, we used the corner-capping approach to add an amino propyl group to the POSS molecules (Figure 9d).[145-146] Then, the amino group was be converted to an isocyanate group using triphosgene.[147] Finally, the resulting isocyanate POSS derivatives were reacted with either (*p*-aminophenyl)-10,15,20-triphenyl porphyrin (ATPP) or 5,10,15,20-tetra(*p*-aminophenyl) porphyrin (TAPP) to afford the final molecules.

The structural, photophysical and photochemical properties of these molecules were evaluated using different spectroscopic and spectrometric techniques as described below. The use of this POSSP derivatives for PDT was also carried out using cancer cells. Finally, MD simulations to account for the interactions of POSSP-IB and POSSP-Ph with the cell membrane were also perfomed.

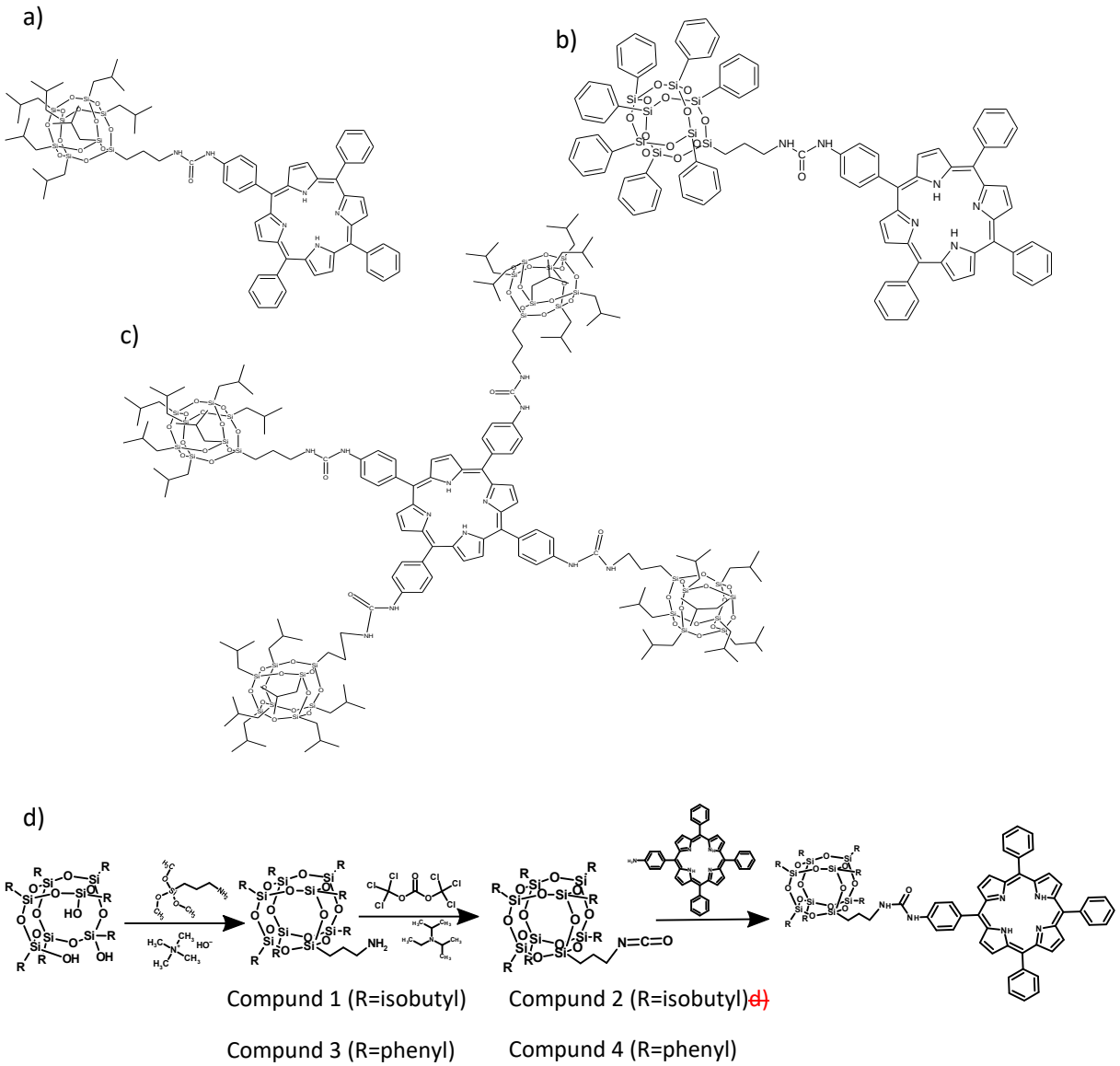

Figure 9. Target POSS-porphyrin molecules. a) POSSP-IB. b) POSSP-Ph. c) POSSP-TIB. d) Synthesis of POSS-porphyrin compounds. Corner capping the corresponding trisilanol produces an aminopropyl POSS which is in turn phosgenated to afford an isocyanate POSS. The reaction of the isocyanate POSS with an aminophenyl porphyrin yields the final POSS-porphyrin molecules.

2.2 Materials and methods

2.2.1 Materials

All commercial solvents were of reagent grade or higher and were used as received. Experiments with moisture/air-sensitivity were performed using anhydrous solvents and under nitrogen atmosphere in a Schlenk line. Silica G60 (70-230 mesh) was used for column chromatography. Trisilanol hepta(isobutyl) POSS and trisilanol hepta(phenyl) POSS were purchased from Hybrid Plastics. (3-aminopropyl) triethoxysilane (APTES) was acquired from Alfa Aesar. Pentahydrate tetramethyl ammonium hydroxide (TMAOH) in methanol and N,N'-diisopropylethylamine were supplied from Sigma-Aldrich. Roswell Park Memorial Institute (RPMI 1640), fetal bovine serum (FBS), penicillin-streptomycin (pen-strep), phosphate buffer saline (PBS, 1X), and trypsin were purchased from Corning. 5-(4-aminophenyl)-10,15,20-(triphenyl)porphyrin (ATPP), 5,10,15,20-tetra(4-aminophenyl) porphyrin (TAPP) and 5,10,15,20-(tetraphenyl)porphyrin (TPP) were purchased from Frontier Scientific (Logan, UT, USA).

2.2.2 Methods

NMR spectra were recorded at room temperature in $CDCl_3$ or DMSO-d_6 using either a 300 MHz or a 500 MHz JEOL NMR spectrometer. Mass spectra were collected by a MALDI-TOF Voyager Biospectrometry Laser MALDI or a Thermo Scientific MSQ Plus MASS Detector. UV-vis spectra were obtained on a Cary 300 UV-visible spectrophotometer. Photophysical properties of the POSSP were measured using a RF-5301 PC Shimadzu fluorimeter.

2.2.2.1 UV-Vis/Fluorescence spectroscopy

The UV–Vis spectra were recorded from 300 to 800 nm using solutions of POSSP-IB, POSSP-Ph and POSSP-TIB in THF (6.6 µM) [JV14][PL15] in quartz cuvettes (1 cm path length). Similar conditions were used for the parent porphyrins (TPP, ATPP, and TAPP). The fluorescence spectra for POSSPs and parent porphyrins were obtained in the same solutions described above using an excitation wavelength of 520 nm. The fluorescence spectra were recorded from 600 to 800 nm. The extinction coefficients were obtained using the Beer's Law equation from the linear regression of absorption values vs. concentration, several concentrations in THF ranging from 0.1 to 10 µM were used. Similar conditions were used for the parent porphyrins (TPP, ATPP, and TAPP).

2.2.2.2. Fluorescence Quantum Yield

The fluorescence quantum yields for air-saturated solutions (Φ_F) in THF [JV16][PL17] were determined using the comparative method. TPP was used as a reference with a fluorescence quantum yield of 0.12 in benzene.[148] The POSSPs concentrations ranged from 0.1 to 10 µM (THF). The excitation wavelength was 520 nm and the excitation and emission slit width were 2 nm. The fluorescence quantum yields were measured according to the comparative method described by Equation (1).

$$\Phi_{F,Sample} = \Phi_{F,Reference} (m_{Sample}/m_{Rerefence}) (\eta^{2}_{Sample}/\eta^{2}_{Rerefence}) \quad (1)$$

where $\Phi_{F,Reference}$ represents the fluorescence quantum yield of a fluorophore reference (TPP), m is the slope of the plotted data relative to the area of the emission peak against the absorption of the fluorophore and η is the refractive index.[149]

2.2.2.3. Singlet Oxygen Quantum Yield

The $^1O_2$ quantum yields (Φ_Δ) were determined through an indirect method using dimethylanthracence (DMA) as the singlet oxygen probe. Several solutions containing DMF were air saturated and prepared with DMA (50 µM) and the POSSPs or parent porphyrins (TPP, ATPP, and TAPP) (5 µM). These solutions were covered with aluminum foil to avoid any premature quenching. Quartz cuvettes (1 cm × 1 cm) were filled with 1 mL of the solution, placed in a spectrofluorophotometer (xenon lamp, Shimadzu RF-5301 PC) and irradiated at 515 nm for 600 s. The absorbance decay of DMA was monitored at 380 nm, which was corrected from light scattering by subtracting the spectra of POSSPs. The Φ_Δ was calculated using Equation (2).

$$\Phi_{\Delta,S} = \Phi_{\Delta,R} (m_{Sample}/m_{Rerefence}) (1-10^{-absReference}/1-10^{-absSample}) \quad (2)$$

where $\Phi_{\Delta,S}$ is the singlet oxygen quantum yield of the sample and m is the slope of the plotted data relative to the area of the emission peak against the absorption of the reference.[148]

Alexis Johnston carried out all the *in vitro* experiments.

2.2.2.4 Cell Culture

MDA-MB-231, a human invasive TNBC cell line, was purchased from American Type Culture Collection (ATCC). Breast cancer cells were cultured in RPMI 1640 medium supplemented with 10% FBS and 1% pen-strep at 37 ◦C with 5% CO_2 atmosphere. The culture media was changed every other day. All cell cultures were maintained in 25 or 75 cm^2 cell culture flasks and the cells were passaged at 70–80% confluency every 2–4 days.

2.2.2.5 In Vitro Cyto- and Phototoxicity

The phototoxicities of ATPP, TAPP and the POSS-porphyrins tested using the MTS assay. MDA-MB-231 cells were seeded in a 96-well plate at a density of 5×10^3 cells per well in 100 µL of complete media and incubated at 37 °C in 5% CO_2 atmosphere for 24 h. After removing the cell culture medium, different concentrations (0.01–0.5 µM) were prepared in cell media from a stock solution in DMSO with a final volume of the organic solvent smaller than 1%. After a 48-h incubation, the culture media was removed, and the cells were washed twice with phosphate buffer solution. MDA-MB-231 cells were illuminated with red light (630 nm) at a fluence rate of 24.5 mW/cm^2 for 20 min. Control experiments were maintained in the same conditions, but in the dark. After irradiation, the media was replaced with fresh media and the cells were allowed to grow for an additional 24 h. The cyto- and phototoxicities of the porphyrins and POSS-porphyrins were evaluated following the same protocol, but using concentrations ranging 0.01–100 µM. To quantify the phototoxic or dark toxicity effects of the experiments described above, the treated MDA-MB-231 cells were subjected to a cell viability assay using the CellTiter 96® Aqueous solution assay. To perform the assay, the cell media was removed, and the cells were washed once with phosphate buffer solution. Fresh media (100 µL) and 20 µL of CellTiter 96® were added into each well and incubated for 2–3 h at 37 °C in 5% CO_2 atmosphere. The cell viability (%) was calculated as: viability = $(As_{ample}/A_{control}) \times 100\%$, where A_{sample} and $A_{control}$ denote absorbance values of the sample and control wells measured at 490 nm, respectively. The results are reported as the average ± SD of three experiments. The IC_{50} values were determined using GraphPad Prism (v8.1.2 for macOS, La Jolla California, CA, USA) fitting the viability data to a sigmoidal curve.

2.2.2.6 Flow Cytometry

Six-well plates were prepared with 1×10^5 MDA-MB-231 cells per well in complete RPMI media (2 mL) and incubated at 37 °C in 5% CO_2 for 48 h. The media was removed from each well and media solutions of control porphyrin (ATPP) and the POSS-porphyrins (2 mL, 0.5 µM) were added to the wells. The cells were incubated at 37 °C in 5% CO_2 atmosphere for 24 h. The cell media was removed from the wells, and the cells were washed with phosphate buffer solution two times. The cells were incubated for 3–5 min in the presence of trypsin (500 µL). Cells were removed and transferred to a centrifuge tube. Media (500 µL) was added to each well to remove any remaining cells and mixed with the previous solution. The cell pellet was obtained after centrifugation (2.5k RPM, 10 min). The supernatant was discarded, and phosphate buffer solution (500 µL) was added to each tube. The cell pellet was mixed and transferred to flow cytometry tubes. The cell internalization of the studied compounds was measured as the percentage of positive cells using a flow cytometer (BD LSRFortessa).

2.2.2.7 Statistical Analysis

All data in the manuscript are presented as mean ± SD unless mentioned otherwise. To compare ΦΔ values, the statistical analysis was performed with one-way ANOVA using Tukey's multiple comparison test. To calculate the singlet oxygen quantum yields (n = 3) and IC_{50} values (n = 6) for the cell viability studies, GraphPad prism software was used. Cellular uptake using flow cytometry was evaluated with a minimum of 5000 gated cells. All the statistical analyses were performed using GraphPad Prism (v8.2.0 for Windows) with $\alpha = 0.05$ and reported as asterisks assigned to the p-values: **** $p \leq 0.0001$, *** $p \leq 0.001$, ** $p \leq 0.01$, * $p \leq 0.05$ and ns $p > 0.05$.

2.2.2.8 MD simulation of interaction with a phospholipid bilayer

We simulated the interaction of POSSP-IB, POSSP-Ph and ATPP as a control with lipid bilayer using molecular dynamics. The molecules are shown in Figure 10.

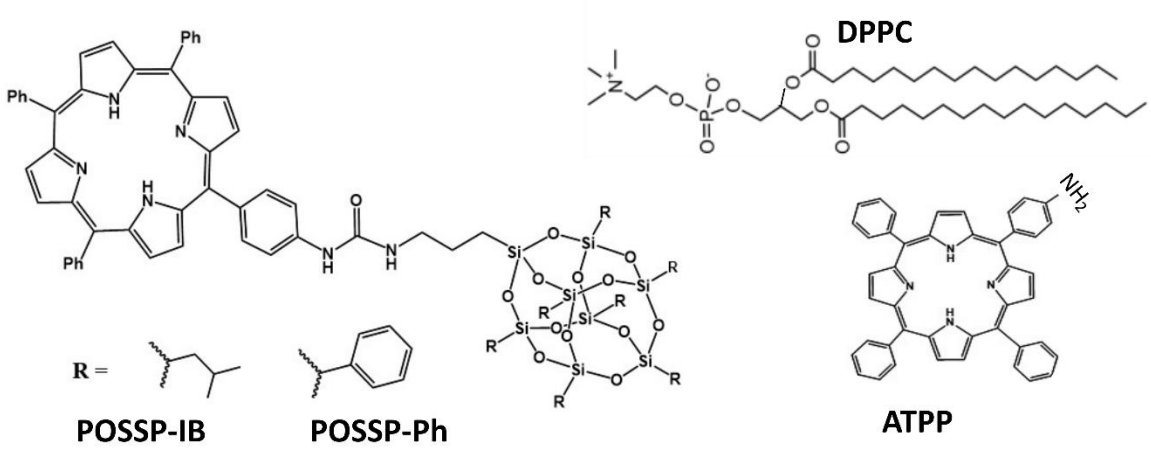

Figure 10. Structures of phospholipid DPPC, control porphyrin ATPP, POSSP-IB and POSSP-Ph.

We used the commonly employed phospholipid 1,2-dipalmitoylphosphatidylcholine (DPPC) to construct a model bilayer.[150] The hydrated DPPC was developed by Tieleman and Berendsen and consists of 128 DPPC molecules and 3655 water molecules.[151] The structure and force field parameters for DPPC were downloaded from http://wcm.ucalgary.ca/tieleman/downloads.

We ran all simulations on Grommacs 2019.2[152-153] For the POSS-porphyrin molecules, we used the OPLSA-AA force field parameters obtained in a previous work using the LigParGen software (Chapter 3).[154-157] Since they were initially in a format compatible with the LAMMPS software, we carefully converted them to the units and conventions used in Gromacs. For the phospholipids we used the Berger parameters[158] because they are widely used and validated and are compatible

with the OPLS-AA forcefield.[159-161] We scaled the 1,4 interactions of the Berger lipid headgroups independently using the method devised by Neal and collaborators.[160, 162-163][JV18] Water was simulated using the extended simple point charge (SPC/E)[164] model.

The POSS-porphyrin molecules were added in random positions on top of the hydrated DPPC structure using Packmol.[165] We placed either 1 or 4 POSS-porphyrin molecules in each simulation to have a total of six systems. The single molecule simulations were taken as a control and the four molecule simulations were done to study the effect of the self-assembly on the interaction of the molecules with the bilayer.[JV19] We added 2700 (one POSS-porphyrin) or 4100 (4 POSS-porphyrins) water molecules on top of the hydrated DPPC bilayer to solvate the POSS-porphyrins. All bonds to H atoms restrained using the LINCS algorithm.[166] Three-dimensional periodic boundary conditions were applied. The cutoffs for vdW and short-range Coulombic interactions were both 12 Å. Long range electrostatic interactions were calculated through the particle-mesh Ewald method.[167-168] The temperature was kept at 323 K (above DPPC phase transition which is 315 K)[169] using the Nose-Hover thermostat.[170] Pressure was set at 1 bar and controlled semi-isotropically by a Parrinello-Rahman barostat.[171] In both the thermostat and the barostat, water, DPPC and POSS-porphyrin molecules were coupled independently. The systems first went through a steepest descent minimization, then 100 ps of NVT and 1 ns on NPT for equilibration. The POSS-porphyrins were held in place by positional restraints during that process. Afterward, NPT production simulation was carried out.

The symmetric potential of mean force (PFM) calculations were done by using umbrella sampling.[150, 172] We obtained 31 configurations along the z-axis from a steered MD simulation. The distance between the molecules COM and the bilayer center in each configuration differed by about 0.1 nm. Each window was equilibrated by 5 ns followed by 5 ns of production run.

The PFM profile was obtained using the Weighted Histogram Analysis Method (WHAM)[173] as implemented in GROMCAS.[174] Overlap histograms are in Figure 11.

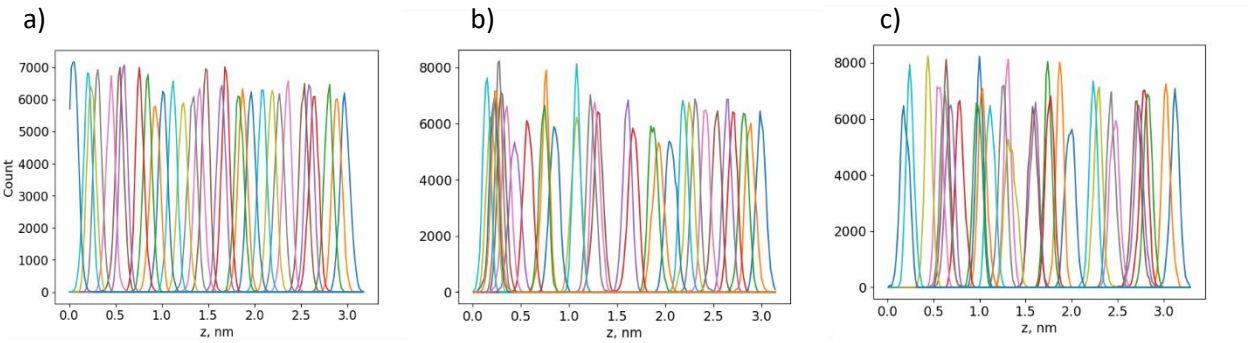

Figure 11. Histograms from the WHAM analysis, showing enough overlap. a) ATPP, b) POSSP-IB, c) POSSP-Ph.

Partial densities were calculated using the GROMACS gmx density tool. COM trajectories and molecules visualization were done using the VMD software.[175]

The deuterium order parameter (S_{CD}) was calculated using the GROMACS gmx order tool and averaged in the time period 180-200 ns. To investigate the structural changes of the bilayer in the vicinity of the porphyrin molecules, we also evaluated the S_{CD} only in DPPC molecules that were within 5 Å of a porphyrin molecule at 180 ns.

Hydrogen bonds were detected using the GROMACS tool gmx hbonds using the default cutoff values for Hydrogen - Donor – Acceptor angle (30°) and Donor-Acceptor distance (0.35 nm).

To characterize the relative orientation of the porphyrin molecules with respect to the bilayer normal, we defined a plane for each porphyrin molecule by employing a least-squares fitting procedure with respect to a planar surface to the displacements of heavy atoms comprising the

porphyrin core without including the phenyl groups. Then we obtained the tilt angle, α, of the porphyrins by calculating the angle of this plane to the z-axis.

2.2 Synthesis and structural characterization of the POSS-porphyrins[JV20]

2.2.1 Synthesis and structural characterization of hepta-isobutyl-POSS-triphenyl ureido porphyrin molecules (POSSP-IB).

2.2.1.1 Synthesis of Aminopropyl hepta(isobutyl) POSS (1-(3-amino)propyl-3,5,7,9,11,13,15-heptaisobutyl pentacyclo[9.5.1.1(3,9).1(5,15).1(7,13)]octasiloxane) (1)

The synthesis of compound [JV21]1[JV22]was carried out as previously reported with slight modifications.[145] Trisilanol hepta(isobutyl) POSS (2.00 g, 2.52 mmol) was dispersed in ethanol (12.5 mL) under stirring (550 rpm) followed by the addition of APTES (424 µL, 435 mg, 1.97 mmol) and TMAOH (40 µL, 0.06 mmol, 25% w/v). The mixture was stirred (700 rpm) for 43 h at 40 °C. A significant amount of aminopropyl hepta(isobutyl) POSS precipitated during the reaction time. The dispersion was centrifuged, and the supernatant discarded. The solid product was washed twice with acetonitrile. The product was dried under vacuum for 48 h (Yield = 84% wt). ^{1}H-NMR (Figure A1)[JV23][JV24] (300 MHz, $CDCl_3$, ppm) δ: 2.67 (t, 2H, -CH_2-N-), 1.85 (m, 7H, -CH-), 1.52 (m, 2H, -CH_2-), 0.94 (d, 42H, CH_3), 0.60 (m, 16H, -Si-CH_2-); ^{29}Si-NMR (Figure A2) (99 MHz, $CDCl_3$, ppm) δ: -66.8, -67.2, -67.4. FTIR (Figure A3) (cm^{-1}): 2953, 2906 and 2870 (C-H), 1600 (N-H), 1465 (C-N), 1228 (Si-C), 1081 (Si-O-Si), 955 (Si-O-Si), 740 (Si-C). MALDI-TOF (Figure A4) (m/z): $[M]^+$ = 873.01 observed; $[M]^+$ = 873.31 calcd.

2.2.1.2 Synthesis of isocyanato propyl hepta(isobutyl) POSS (1-isocyanatopropyl-3,5,7,9,11,13,15-heptaisobutyl pentacyclo[9.5.1.1(3,9).1(5,15).1(7,13)]octasiloxane) (2)

The synthesis of compound 2[JV25] was carried out as previously reported with slight modifications[147]. Compound 1 (150 mg, 0.172 mmol) was dissolved in dry dichloromethane (2 mL) at room temperature, and the solution was stirred slowly (300 rpm) under nitrogen atmosphere. DIPEA (60 µL, 44.5 mg, 0.34 mmol) and triphosgene (25.5 mg, 0.086 mmol) were added to this solution under slow stirring and N_2 atmosphere. After 3 h, the stirring speed and the nitrogen flow were increased to cause the evaporation of the solvent (evaporation time: 10 min). The product was washed twice with acetonitrile. Compound 2 was dried under vacuum for 48 h (Yield = 71% wt). ^{1}H-NMR (Figure A5)[JV26] (300 MHz, $CDCl_3$, ppm) δ: 3.28 (t, 2H, -CH_2-N=C=O), 1.85 (m, 7H, -CH-), 1.71 (m, 2H, -CH_2-), 0.94 (d, 42H, CH_3), 0.66 (t, 2H, -Si -CH_2-), 0.60 (m, 14H, -Si -CH_2-); ^{29}Si-NMR (Figure A6)[JV27] 99 MHz, $CDCl_3$ ppm) δ: -67.1, -67.4, -67.7. FTIR (Figure A7)[JV28] (cm^{-1}): 2954 and 2870 (C-H), 2273 (N=C=O), 1465 (C-N), 1229 (Si-C), 1084 (Si-O-Si), 955 (Si-O-Si), 739 (Si-C).

2.2.1.3 Synthesis of hepta(isobutyl)-POSS-Porphyrin (5-(4-[3-(3-(3,5,7,9,11,13,15-heptaisobutyl pentacyclo[9.5.1.1(3,9).1(5,15).1(7,13)]octasiloxane) propyl) ureido] phenyl)-10,15,20-(triphenyl)porphyrin) (POSSP-IB)

Compound 2 (20 mg, 0.022 mmol) was dissolved in dry dichloromethane (2 mL) at room temperature. To this solution, 5-(4-aminophenyl)-10,15,20-(triphenyl)porphyrin (ATPP) (28 mg, 0.045 mmol) and excess DIPEA were added. The final solution was stirred at room temperature for 48 h in a sealed flask. The product was separated using column chromatography on silica gel (DCM:MeOH; 99:1). After purification, POSSP-IB was dried and obtained as a dark powder

(Yield = 82 % wt). ^{1}H-NMR (Figure A9 and Figure A10)[JV29] (300 MHz, $CDCl_3$, ppm) δ: 8.87 (m, 8H, Py-H), 8.18 (m, 8H, Ph-H), 7.74 (m, 11H, Ph-H), 3.34 (t, 2H, -CH_2-N-), 1.88 (m, 7H, -CH-), 1.76 (m, 2H, -CH_2-), 0.96 (d, 42H, CH_3), 0.71 (t, 2H, -Si-CH_2-), 0.61 (m, 14H, -Si -CH_2-); ^{29}Si-NMR (Figure A12)[JV30] (99 MHz, $CDCl_3$, ppm) δ: -67.0, -67.1, -67.3. FTIR (Figure A13)[JV31] (cm^{-1}): 3318 (N-H), 2925 and 2870 (C-H), 1655 (C=O), 1465 (C-N), 1227 (Si-C), 1084 (Si-O-Si), 966 (Si-O-Si), 700 (Si-C). MALDI-TOF (Figure A14)[JV32] (m/z): $[M-1]^+$ = 1527.55 observed; $[M]^+$ = 1528.55 calcd.

2.2.2 Synthesis of Phenyl-POSS-Porphyrin (POSSP-Ph)

2.2.2.1 Synthesis of Aminopropyl hepta(phenyl) POSS (1-(3-amino)propyl-3,5,7,9,11,13,15-heptaphenyl pentacyclo[9.5.1.1(3,9).1(5,15).1(7,13)]octasiloxane) (3)

The synthesis of compound 3[JV33] was carried out as previously reported with slight modifications.[176] Trisilanol hepta(phenyl) POSS (2.48 gr, 2.7 mmol) was dispersed under stirring (500 rpm) in toluene (4.0 mL) and placed in a dry ice/acetone bath at -10 °C for 5 min. To this solution, APTES (616 µL, 600 mg, 2.7 mmol) was added. The final dispersion was allowed to warm up to room temperature under stirring (500 rpm) for 16.5 h. Then, acetonitrile (20 mL) was added to precipitate the product. Finally, the supernatant was removed after centrifugation and the final product was washed twice with acetonitrile. Compound 3 was dried under vacuum for 48 h (Yield = 61% wt). ^{1}H-NMR (Figure A15 and Figure A16)[JV34] (300 MHz, $CDCl_3$, ppm) δ: 7.74 (m, 14H, Ph-H), 7.44 (m, 7H, Ph-H), 7.37 (m, 14H, Ph-H), 2.66 (t, 2H, -CH_2-N-), 1.62 (m, 2H, -CH_2-), 0.83 (t, 2H, -Si-CH_2-); ^{29}Si-NMR (Figure A18)[JV35] (99 MHz, $CDCl_3$, ppm) δ: - 64.5, -77.8, -78.3. FTIR (Figure A19)[JV36] (cm^{-1}): 3073 (N-H), 3051 (C-H, sp2), 2921 (C-H, sp3), 1595 (N-H), 1431 (C-N), 1082 (Si-O-Si),

1027 (Si-O-Si), 780 (Si-C). MALDI-TOF (Figure A20)[JV37] (m/z): $[M]^+$ = 1013.13 observed; $[M]^+$ = 1013.29 calcd.

2.2.2.2 Synthesis of isocyanato propyl hepta(phenyl) POSS (1-isocyanatopropyl-3,5,7,9,11,13,15- heptaphenyl pentacyclo[9.5.1.1(3,9).1(5,15).1(7,13)]octasiloxane (4)

Compound 3 (174 mg, 0.172 mmol) was dissolved in dry dichloromethane (2 mL) at room temperature and the solution was stirred slowly (300 rpm) under nitrogen atmosphere. Triphosgene (25.5 mg, 0.086 mmol) and DIPEA (60 µL, 44.5 mg, .34 mmol) were added to this solution under slow stirring and N_2 atmosphere. After 3 h, the stirring speed and the nitrogen flow were increased to cause the evaporation of the solvent (evaporation time: 10 min). The product was washed twice with acetonitrile twice. Compound 4 was dried under vacuum for 48 h (Yield = 78% wt). ^{1}H-NMR (Figure A21)[JV38] (300 MHz, $CDCl_3$, ppm) δ: 7.71 (m, 14H, Ph-H), 7.41 (m, 7H, Ph-H), 7.38 (m, 14H, Ph-H), 3.18 (m, 2H, -CH_3-N=C=O), 1.56 (m, 2H, -CH_2-), 0.91 (t, 2H, -Si-CH_2-); ^{29}Si-NMR (Figure A22)[JV39] (99 MHz, $CDCl_3$, ppm) δ: -65.3, -77.6, -78.1. FTIR (Figure A23)[JV40] (cm^{-1}): 3073 (C-H, sp2), 2933 (C-H, sp3), 2271 (N=C=O), 1600 (C=O), 1431 (C-N), 1085 (Si-O-Si), 1027 (Si-O-Si), 743 (Si-C).

2.2.2.3 Synthesis of hepta(phenyl)-POSS-Porphyrin (5-(4-[3-(3-(3,5,7,9,11,13,15-heptaphenyl pentacyclo[9.5.1.1(3,9).1(5,15).1(7,13)]octasiloxane) propyl) ureido] phenyl)-10,15,20-(triphenyl)porphyrin) (POSSP-Ph)

Compound 4 (22 mg, 0.022 mmol) was dissolved in dry dichloromethane (2 mL) at room temperature. To this solution, 5-(4-aminophenyl)-10,15,20-(triphenyl)porphyrin (ATPP) (28 mg,

0.045 mmol) and excess DIPEA were added. The final solution was stirred at room temperature for 48 h in a sealed flask. The product was separated using column chromatography on silica gel (Toluene:MeOH; 80:1). After purification, POSSP-Ph was dried and obtained as a dark powder (Yield = 73% wt). ^{1}H-NMR (Figure A25)[JV41] (300 MHz, $CDCl_3$, ppm) δ: 8.83 (m, 8H, Py-H), 8.21 (m, 8H, Ph-H), 7.80-7.74 (m, 25H, Ph-H), 7.44 (m, 7H, Ph-H), 7.37 (m, 14H, Ph-H), 3.34 (t, 2H, -CH_2-N-), 1.41 (t, 2H, -CH_2-), 0.96 (t, 2H, -SiCH_2-); FTIR (Figure A26)[JV42] (cm^{-1}): 3645 (-NH-CO-NH), 3380 (-NH-), 3062 (C-H, sp2), 2960 (C-H, sp3), 1737 (C=O), 1469 (C-N), 1135 (Si-O-Si), 1109 (Si-O-Si), 742 (Si-C). MALDI-TOF (Figure A27)[JV43] (m/z): $[M-2]^+$ = 1665.72 observed; $[M]^+$ = 1668.33 calcd.

2.2.3 Synthesis of tetra-Isobutyl-POSS-Porphyrin (POSSP-TIB) (tetra-(4-[3-(3-(3,5,7,9,11,13,15-heptaisobutyl pentacyclo[9.5.1.1(3,9).1(5,15).1(7,13)]octasiloxane) propyl) ureido] phenyl)-10,15,20- (triphenyl)porphyrin)

Compound 2 (120 mg, 0.132 mmol) was dissolved in dry dichloromethane (2 mL) at room temperature. To this solution, 5,10,15,20-tetra(4-aminophenyl)porphyrin (TAPP) (30 mg, 0.045 mmol) and excess DIPEA were added. The final solution was stirred at room temperature for 48 h in a sealed flask. The product was separated using column chromatography on silica gel (DCM:MeOH; 5:1). After purification, POSSP-TIB [JV44]was dried and obtained as a dark red powder (Yield = 83 % wt). ^{1}H-NMR (Figure A29 and Figure A30)[JV45] (300 MHz, $CDCl_3$, ppm) δ: 8.87 (m, 8H, Py-H), 8.05 (m, 8H, PhH),7.80- 7.70 (m, 8H, Ph-H), 3.34 (t, 8H, -CH_2-N-), 1.88 (m, 28H, -CH-), 1.76 (m, 8H, -CH_2-), 0.94 (d, 168H, CH_3), 0.70- 0.60 (m, 64H, -Si -CH_2-); FTIR (Figure A31)[JV46] (cm^{-1}): 3345 (-NH-CO-NH-), 3056 (CH, sp2), 2922 (C-H, sp3), 1436 (C-N), 1088 (Si-O-Si),

1000 (Si-O-Si), 733 (Si-C). MALDI-TOF (Figure A32)[JV47] (m/z): $[M-4H]^+$ = 4267.39 observed; $[M]^+$ = 4271.46 calcd.

2.2.4 Results and discussion of the structural characterization of the molecules

POSS molecules contain a wide variety of chemical properties that allow multiple functionalization.[11, 15] In this work, POSS-porphyrin (POSSP) molecules were designed to contain different functional groups such as alkyl and aromatic (Figure 9). The synthesis of the POSS-porphyrin derivatives containing hydrophobic groups, isobutyl (POSSP-IB and POSSP-TIB) and phenyl (POSSP-Ph), was carried out through a multi-step approach (Figure 9d). First, commercially available heptaisobutyl- or heptaphenyl-trisilanol POSS was functionalized with aminopropyl trimethoxysilane via a corner capping reaction under basic conditions to insert an aminopropyl arm.[10] The amine group on these compounds was transformed to an isocyanate by using triphosgene. The successful formation of the cyanate group was shown by the FT-IR stretching vibration at 2273 cm^{-1}. Finally, aminophenyl triphenyl porphyrin was reacted with the isocyanate group forming an urea bond to obtain either POSSP-IB or POSSP-Ph. We also synthesized a tetra-substituted POSS-porphyrin (POSSP-TIB) by reacting an excess of propyl-isocyanate hepta(isobutyl) POSS with tetra-aminophenyl porphyrin following the same reaction as above. The spectroscopic characterization of the three POSS porphyrins demonstrated the successful synthesis of these compounds. Characteristic vibrations in the FT-IR spectra showed the presence of the urea bond at ~1650 cm^{-1} and the Si-O-Si framework at ~1084, 966 and 700 cm^{-1}, which are characteristic of the siloxane cage. Confirmation for the fabrication of these POSSP molecules was obtained by ^{29}Si NMR with diagnostic signals at −67.0, −67.1 and −67.3 ppm for POSSP-IB and at −65.3, −77.8 and −78.1 ppm for POSSP-Ph. In addition, MALDI-TOF

mass spectrometry was used to further corroborate the synthesis of the actual POSSP products, showing the expected molecular ions at $[M - H]^+ = 1527.55$, $[M - 3H]^+ = 1665.24$ and $[M - 4H]+ = 4267.39$, for POSSP-IB, POSSP-Ph and POSSP-TIB, respectively.

2.3 Spectroscopic characterization of the POSS-porphyrin molecules.[JV48][JV49]

The UV–Vis and fluorescence spectra of the POSSPs was measured and compared with the parent porphyrins. Normalized absorption spectra of the POSSP solutions in tetrahydrofuran (THF) showed the typical Soret and Q bands for porphyrins in the ranges of 410–420, 510–530, 545–565, 585–595 and 645–660 nm (Figure 12). The Soret band wavelengths and the corresponding extinction coefficient values are presented in Table 1. The steady-state fluorescence emission spectra with normalized intensities showed two characteristic emission peaks for free-base porphyrins in the ranges of 650–660 and 715–720 nm (Figure 13). The specific emission wavelengths for the POSSPs are provided in Table 1. The S- and Q-bands of POSSPs are slightly blue-shifted with respect to their parent porphyrin, ATPP or TAPP, most likely due to the change in the electron-donating effect of the nitrogen substituent in the para (4-phenyl) position when it is chemically transformed from an amine to an urea group, as has been reported in the literature.[177]

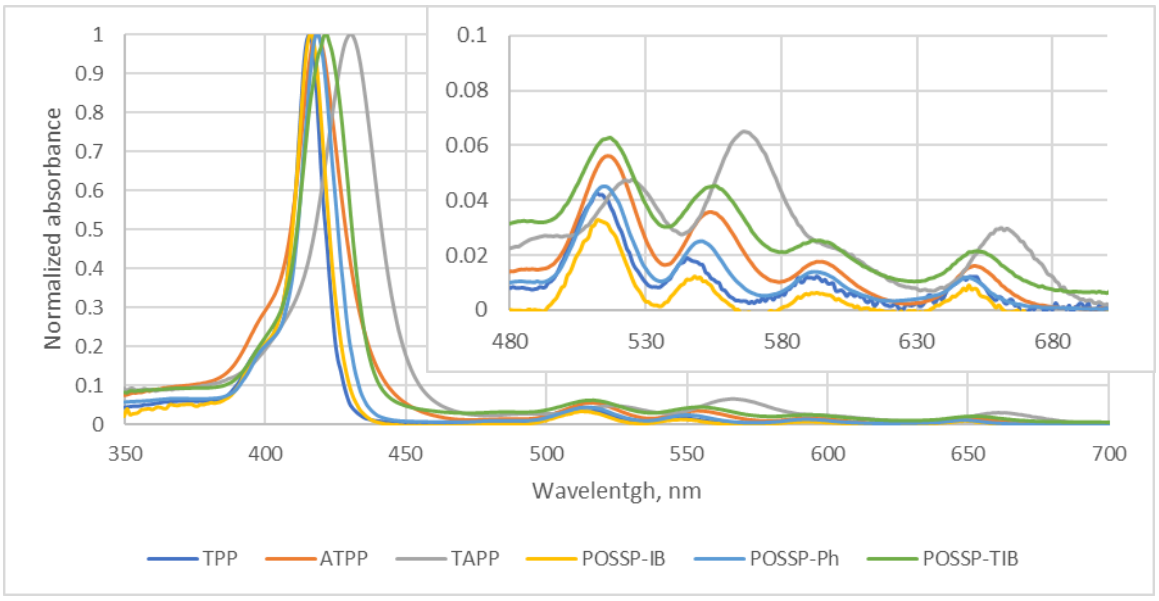

Figure 2. Normalized UV-Vis absorption of porphyrins and POSS-porphyrins in THF.

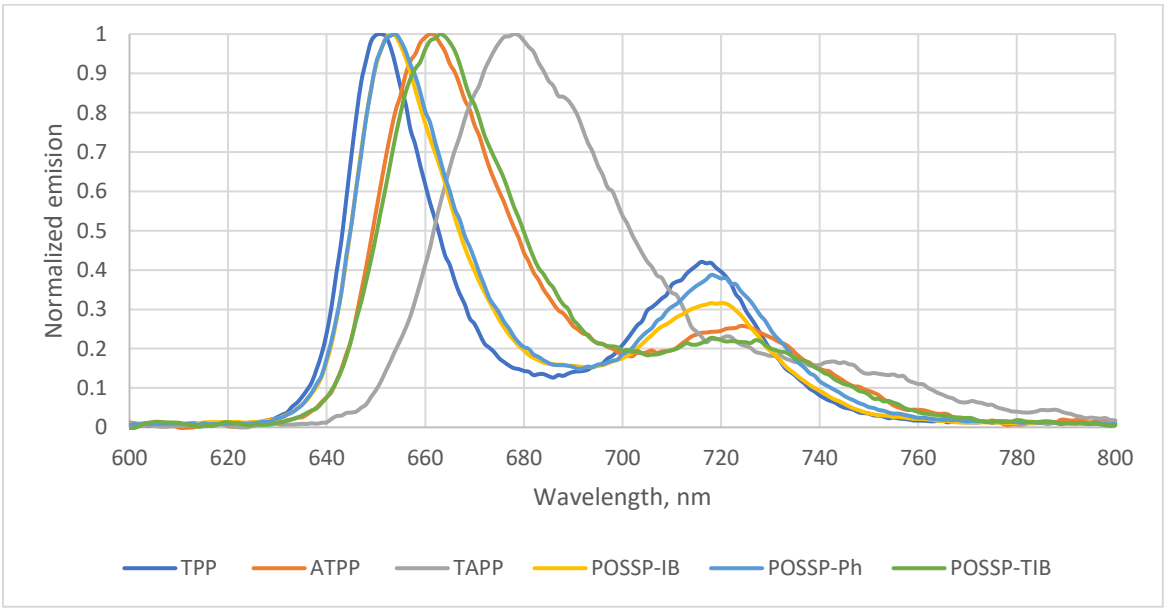

Figure 13. Normalized fluorescence emission in THF

Table 1. Photophysical and photochemical properties of POSSPs.

Molecule	**λ_{Soret} (nm) [$\varepsilon \times 10^3$ (M^{-1} cm^{-1})] (n = 3)**	**$\lambda_{Emission}$ (nm)**	**Φ_Δ (n = 3)**	**Φ_F (n = 3)**
TPP	416, 434 ± 30	651, 717	0.62	0.12
ATP	419, 275 ± 26	661, 745	0.45 ± 0.02	0.21 ± 0.02
TAPP	431, 154 ± 32	678, 787	0.59 ± 0.01	0.16 ± 0.01
POSSP-IB	416, 22.1 ± 8.3	653, 720	0.82 ± 0.01	0.14 ± 0.01
POSSP-Ph	419, 46.2 ± 9.0	653, 719	0.60 ± 0.02	0.13 ± 0.01
POSSP-TIB	422, 117.3 ± 34.4	663, 719	0.70 ± 0.01	0.13 ± 0.02

The fluorescence quantum yields (Φ_F) were determined to indirectly characterize the efficiency of the POSSP compounds to undergo intersystem crossing (ISC) from the excited state to the triplet state, which is an essential step in ROS generation.[57] Porphyrin derivatives typically exhibit a low Φ_F, because the majority of photons that they absorb undergo ISC to an excited triplet state. Φ_F in THF was calculated relative to tetraphenylporphyrin (TPP) in benzene. The data show that the POSSPs have lower Φ_F values compared to the parent porphyrins (Table 1), as a possible indication of a more efficient ISC. The $^1O_2$ quantum yield (Φ_Δ) of the POSSP compounds in dimethyl formamide (DMF) was indirectly determined using 9,10-dimethylanthracene (DMA) as $^1O_2$ probe. DMA reacts with $^1O_2$, undergoing a 1,4-cycloaddition that is detected as a decrease in the intensity of the DMA absorption band at 379 nm. The Φ_Δ was calculated relative to the reference TPP (Φ_Δ = 0.62)[178] using the slope of the time-dependent decomposition of DMA plots (Ln([DMA_0]/[DMA]) versus irradiation times (Figure 14) and Equation (2).[178]

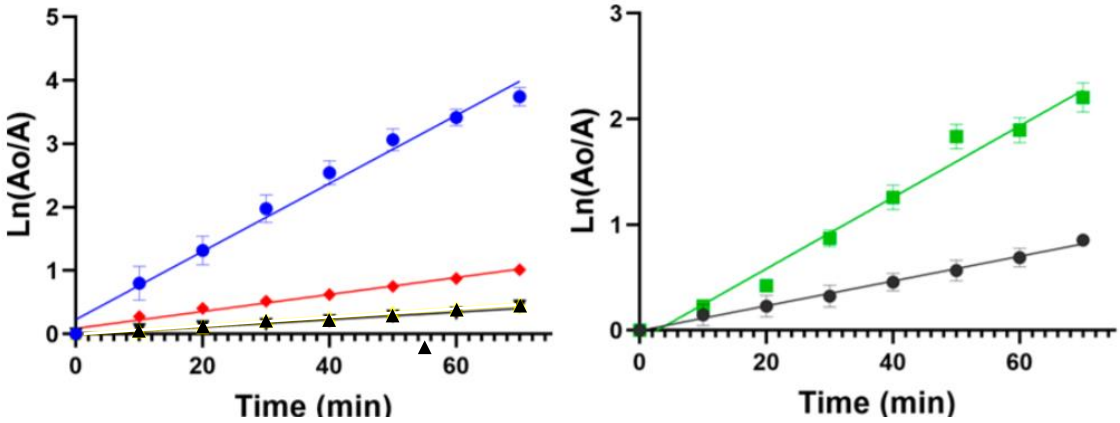

Figure 14. Time-dependent decomposition of DMA plots[JV50]. POSSP-IB (blue), POSSP-Ph (red), POSSP-TIB (green); ATPP (black) and TAPP (dark gray).

The experimental protocol was validated by comparing tetrahydroxy-phenyl-porphyrin and tetraamino-phenyl-porphyrin molecules with known Φ_Δ in DMF ($\Phi_\Delta = 0.57 \pm 0.03$ and $\Phi_\Delta = 0.58 \pm 004$).[42] The measured quantum yield values matched the literature values within ±3% error, with a Φ_Δ values of 0.59 ± 0.01 and 0.58 ± 0.01 for tetrahydroxy-phenyl-porphyrin and tetraamino-phenyl-porphyrin molecules, respectively. The Φ_Δ values obtained for POSSPs are shown in Table 1. Interestingly, all the Φ_Δ values for the POSSP are higher than those corresponding to the parent porphyrins ($p < 0.0001$, Table 1). The POSSP-IB, POSSP-Ph and POSSP-TIB showed an increase in the Φ_Δ values by 82%, 33% and 19%, respectively. The Φ_Δ values for the POSSPs follow this trend POSSP-IB > POSSP-TIB > POSSP-Ph. The Φ_Δ value could depend on the following factors: (i) triplet state properties, including quantum yield, lifetime, and energy; (ii) the ability of substituents to quench $^1O_2$; and (iii) the efficiency of energy transfer from the excited triplet state to ground state molecular oxygen.[179] In the case of porphyrins, the triplet state after irradiation could be inhibited by mutual energy transfer since these molecules favor π-stacking, also known

as self-quenching effect.[180] This effect results in a decline of the ability of porphyrins to generate $^1O_2$. However, due to the unique 3D structure of POSS, its steric hindrance suppresses self-quenching of the excited states of porphyrins resulting in the observed enhancement of Φ_Δ for POSSPs.[24, 66] It is also relevant to point out that the increase in the Φ_Δ values for the POSSPs may have a major impact on their PDT performance.

2.4. Photodynamic Therapy of Triple-Negative Breast Cancer Using POSS-Porphyrin Molecules

Triple-negative breast cancer (TNBC) subtype is characterized by the lack of targetable markers, which accounts for about 10–20% of the newly diagnosed breast cancer cases.[181] Approximately 50% of the patients diagnosed with early-stage TNBC experience recurrence, and 37% die within the first five years after surgery.[182] As TNBC lacks targetable receptors, patients with TNBC are treated with conventional chemotherapy and radiotherapy, which are associated with toxic side effects and development of resistance leading to aggressive relapse and distant metastasis.[183] PDT has been used to treat different types of cancer such as those originated in the skin, head and neck, breast and lung.[184-185] Recently, PDT has been explored as a promising alternative to treat TNBC.[61, 186-188] In this work, the cytotoxicity and phototoxicity of POSSPs in a tripe negative breast cancer cell line (MDA-MB-231) were evaluated using the MTS assay. As expected, no major cytotoxicity was observed in the range of concentration tested in the absence of light (Figure 15a). Photosensitizers are only toxic through the generation of reactive oxygen species after excitation with light and in the presence of molecular oxygen.[189] To compare the PDT performance of all the POSSPs developed in this work, due their hydrophobicity, a non-toxic amount of DMSO was used to carry out these experiments. As shown in Figure 15b and Table 2, at the highest concentration

evaluated (0.5 µM), POSSP-IB showed a reduction in cell proliferation of 43 ± 4% followed by POSSP-TIB with 19 ± 3%. POSSP-Ph did not show significant phototoxicity at the highest concentration. Interestingly, this trend in cell phototoxicity, POSSP-IB > POSSP-TIB > POSSP-Ph, follows a similar trend as the Φ_Δ values. This corroborates the importance of the singlet oxygen generation for the PDT effect.

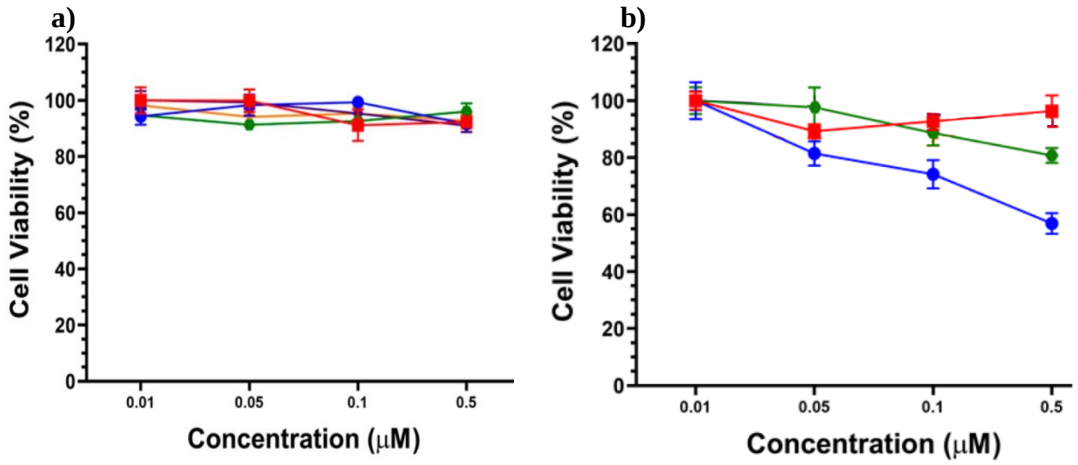

Figure 15. a) Cytotoxicity and b) dose–response plot for the phototoxicity of POSSP-IB (blue), POSSP-Ph (red), POSSP-TIB (green) in MDA MB231 cells

Table 2. Phototoxicity at 0.5µM

Molecule	**Cell viability at 0.5µM under light irradiation (%) (n=3)**
ATPP	124 ± 9
POSSP-IB	57 ± 4
POSSP-Ph	96 ± 6
POSSP-TIB	81 ± 3

The uptake of POSSPs by MDA-MB-231 cells was analyzed by flow cytometry. MDA-MB-231 cells were inoculated with the POSSPs at a concentration of 0.5 μM for 24 h. The flow cytometry data (Figure 16) show that POSSP-Ph and POSSP-TIB were internalized in a much higher percentage than POSSP-IB. It seems that, in this case, the photochemical properties of the POSSPs, in particular $^1O_2$ generation, play a major role in the PDT outcome. This hypothesis is supported by the results obtained with the porphyrin control (ATPP) where a low Φ_Δ value was obtained, but a high internalization in MDA-MB-231 cells was observed, and minimal PDT effect was obtained (Table 2), most likely related to its low Φ_Δ value (Table 1). Nevertheless, it is important not to rule out other factors such as the subcellular localization of these compounds.

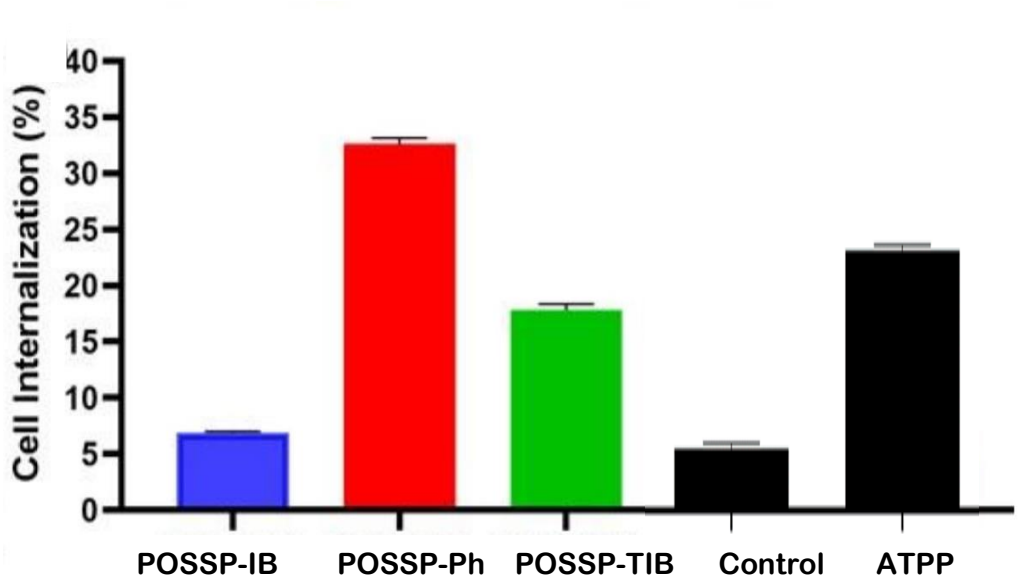

Figure 16. Internalization of POSS-porphyrins in MDA-MB-231 cells using flow cytometry.

2.5 POSS-porphyrins self-assembly and permeation into a phospholipid bilayer

POSS molecules are prone to self-assembly in aqueous environment. This feature has been used by several groups to create self-assembled structures that are stable in water and can be used to

carry hydrophobic agents into the cell. [64-66] So, when studying the diffusion of POSS molecules through a lipid bilayer, it is important to also analyze the influence of its self-assembled structures. Here, we analyzed the diffusion of POSS-porphyrins through a phospholipid bilayer by using MD simulations. We studied the effect of the POSS cage substituents on the self-assembly of the molecule. To the best of our knowledge, there are no MD simulations of the interaction of a POSS molecules with lipid bilayers.

2.5.1 Permeation of single POSSP molecule through the DPPC bilayer

First, we run MD simulations to analyze the interaction of a single molecule with the lipid bilayer. Our results show that for both POSSP molecules, POSSP-IB and POSSP-Ph, or control porphyrin, the porphyrin portion of the molecule was inserted into the bilayer. It has been reported in the literature that hydrophobic molecules in general diffuse more easily into a lipid bilayer due to the interaction with the hydrophobic acyl region.[190] In porphyrins, specifically, it has been reported that their hydrophobicity determines how deep does the molecule is inserted into a bilayer.[144]

Figure 17 shows the partial densities of the DPPC bilayer regions, showing the average densities of each component along the z axis. Comparing the values among the three different single-molecule simulations and the control bilayer, the positions relative to the bilayer center at which the curves cross are all within ±0.1 nm between systems. This shows that the prescence of the molecules did not alter the position in the z-axis at which the different components of the bilayer are located.[JV51] Figure 18a shows how ATPP penetrated the bilayer deeper than the porphyrin portion of POSSP-IB or POSSP-Ph, most likely because the POSS cage prevents its further

insertion Figure 18e and Figure 19a[JV52] show the change of position of both the porhyrin and POSS, respectively, along the simulation. [JV53] The porphyrin in the three molecules enter the bilayer and travel some distance with a direction toward the bilayer center. The POSS cages, on the other hand, never enter the bilayer and stay on top of the headgroups. MD simulation of only the POSS-IB and POSS-Ph cages show that these molecules did not pass through the lipid bilayer (Figure 17a).

The tilt angles in Figure 18b [JV54]show how the porphyrins are close to parallel to the bilayer normal (cos(α) is close to 1) when inserting into the bilayer and this is exemplified for POSSP-IB in Figure 18d. This orientation presents the least steric hinderance. POSSP-IB stays aligned to the bilayer normal during the rest of the simulations, while ATPP is freer to vary this angle, probably because the POSSP molecules are constrained by the POSS cage that is sitting on top of the bilayer.

The potential of mean force in Figure 18c force shows a preference of the molecules to be on the headgroups region of the DPPC bilayer, presenting an energetic barrier for their insertion all the way to the bilayer center.[JV55] This may be due to the steric effect of the POSS in the POSSP molecules and to the polar amino group in ATPP, having a repulsive interaction with the hydrophobic acyl chains of the bilayer. This is in agreement with the configuration of the molecules at the end of the simulations (Figure 19b-d).

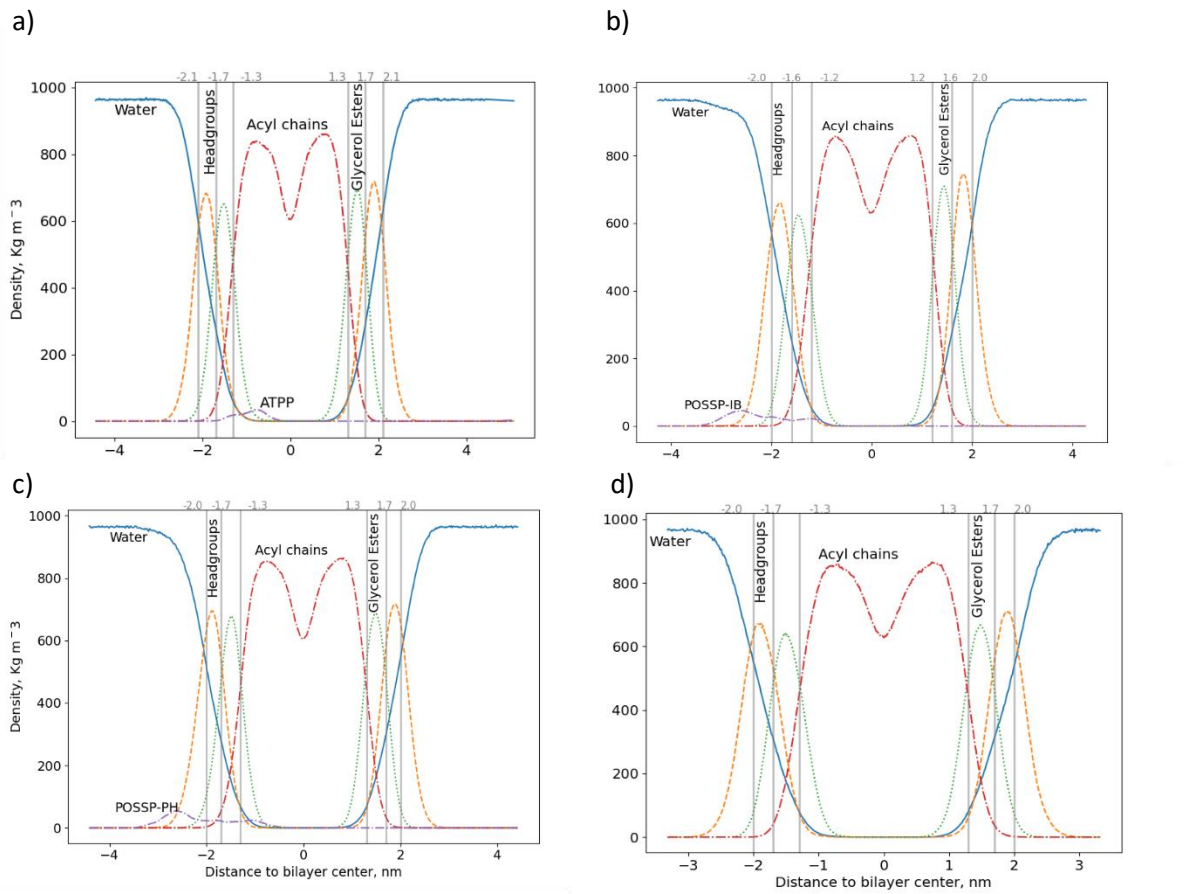

Figure 17. Partial density profiles of the systems with only one POSS-porphyrin or porphyrin molecule, averaged in 180-200 ns (0-20 ns for DPPC). The numbers and vertical lines in grey mark the points where the DPPC curves cross. a) ATPP. b) POSSP-IB. c) POSSP-Ph. d) DPPC with no porphyrins.

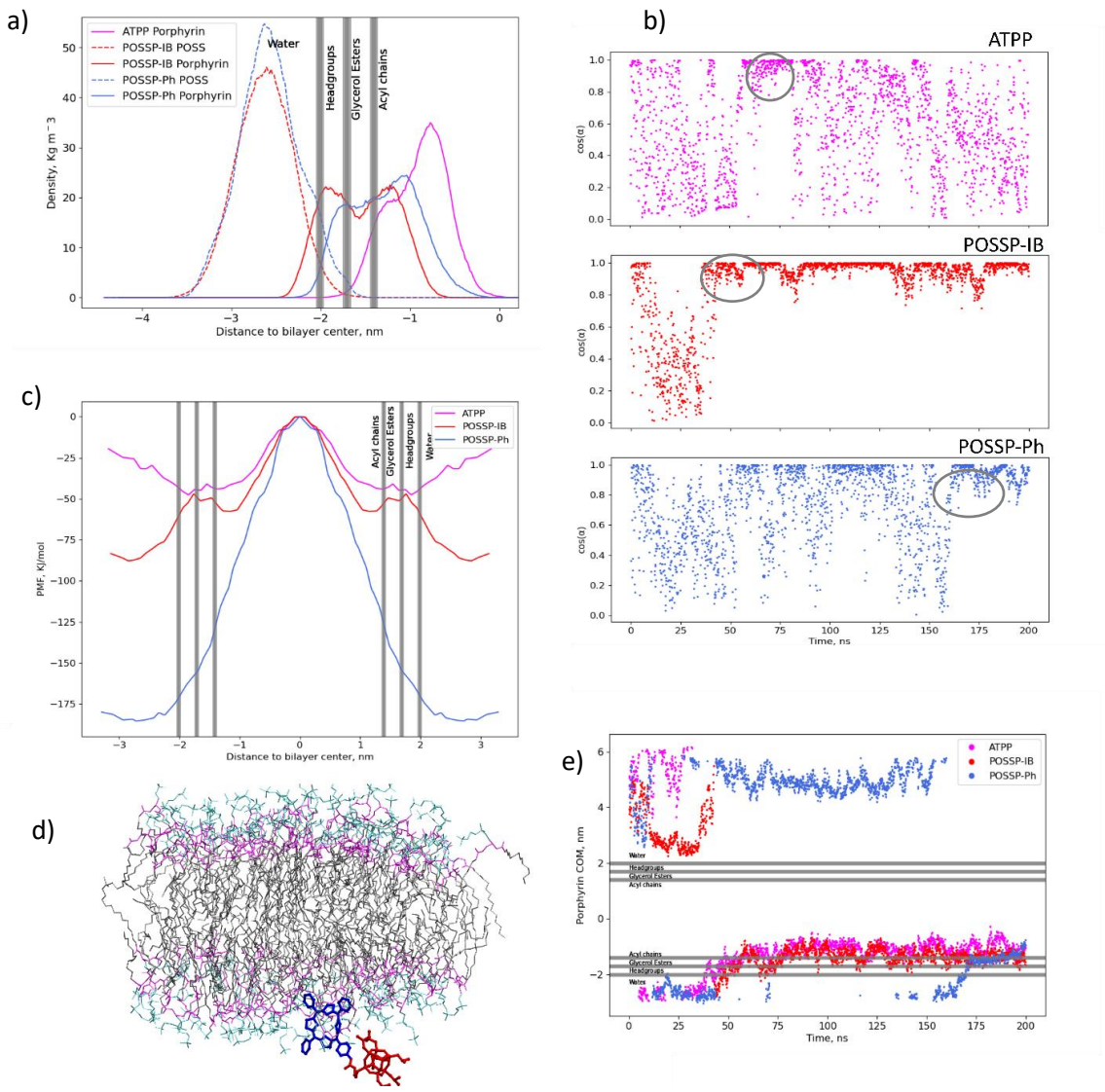

Figure 18. Individual molecules simulations. a) Partial density profile averaged in 180-200 ns showing penetration of the POSS and porphyrins. b) Tilt angle, α, of the porphyrin planes with respect to the bilayer normal direction. The circels indicate the point in time at which the molecules were inserted into the bilayer. c) Potential of mean force curves. e) COM of the porphyrin moiety along the simulation. d) POSSP-IB at 68 ns, the porphyrin plane is parallel to the bilayer normal. Headgroups in cyan, glycerol esters in magenta, acyl chains in gray, porphyrin in blue and POSS

cage in red, water omitted for clarity. The gray lines in a,c and e are a rough indication of the location of the regions of the DPPC bilayer.

As the porphyrins penetrate into the bilayer, some of the hydrogen bonds between the porphyrin core and water are substituted by hydrogen bonds with the phospholipids headgroups. Figure 20 quantifies the number of hydrogen bonds to the porphyrin core along the simulations. The porphyrin core forms hydrogen bonds to the DPPC headgroups while inserted in that region. It also has a strong tendency to form hydrogen bonds with water even in the hydrophobic region of the bilayer.[JV56] The formation of hydrogen bonds to the headgroups may stabilize the insertion of the porphryins to the bilayer, compensating the loss of hydrogen bonds to water.

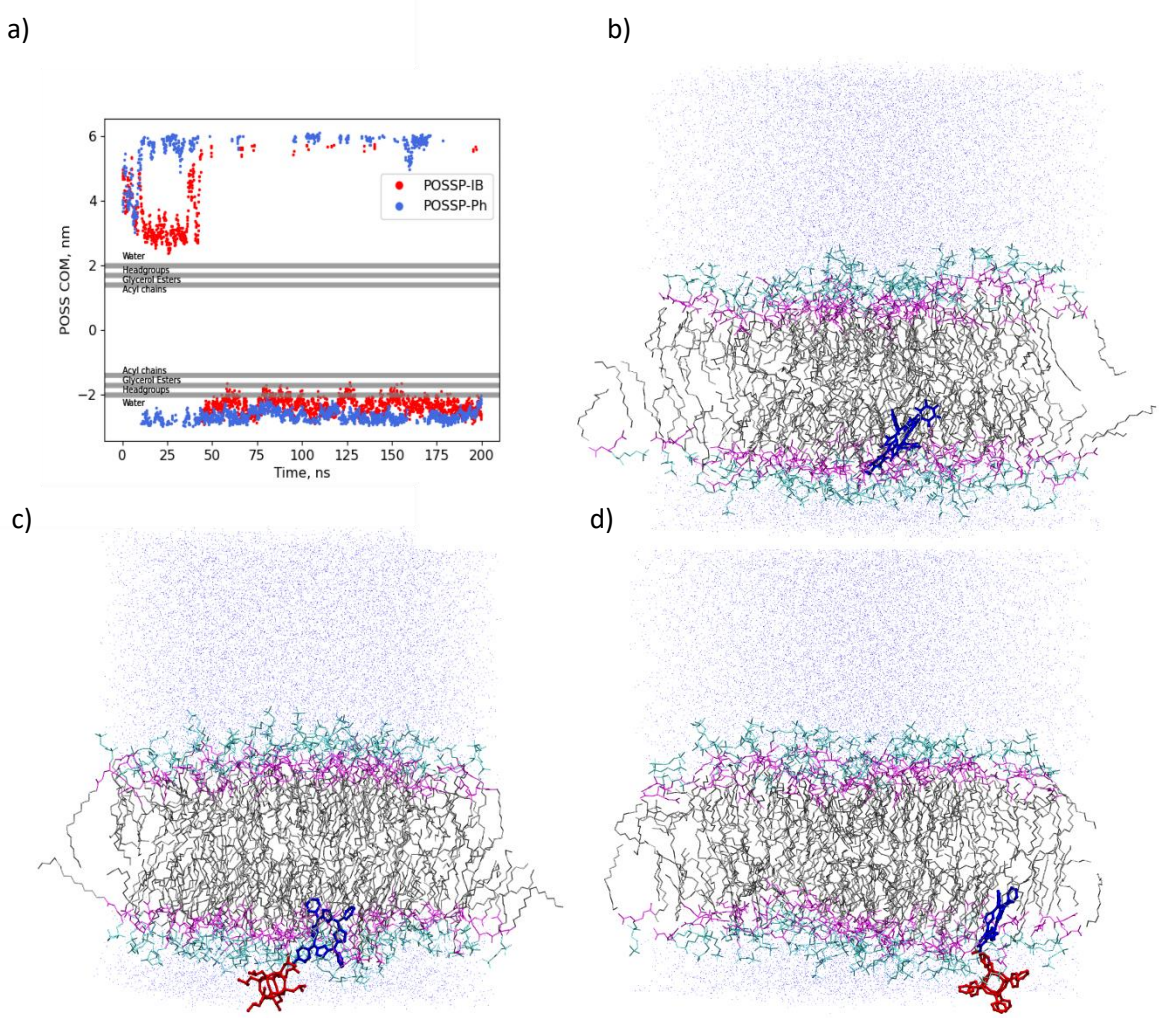

Figure 19 a) COM of the POSS cage along the simulation. In both POSSP-IB and POSSP-Ph the POSS cages tend to stay at the water phase although the isobutyl POSS sometimes goes into the headgroups region. b,c,d) End of the simulations at 200 ns. Water in light blue, headgroups in cyan, glycerol esters in magenta, acyl chains in gray, porphyrin in blue and POSS cage in red. b) ATPP. c) POSSP-IB. d) POSSP-Ph.

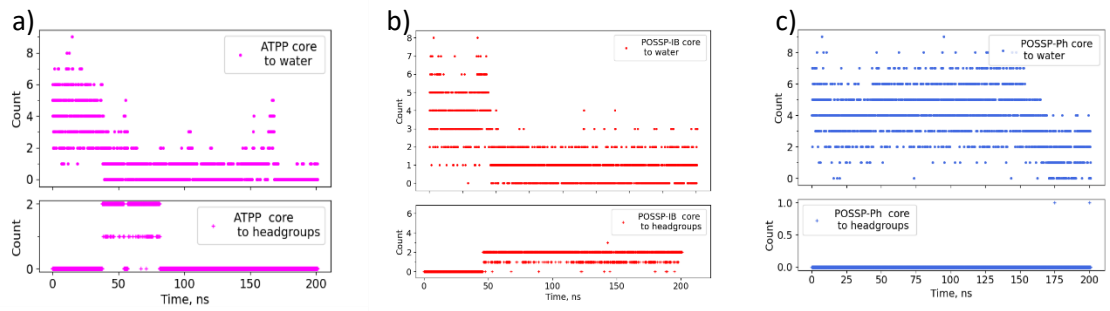

Figure 20. Number of hydrogen bonds detected from the porphyrin core to either water or DPPC headgroups in the single-molecule systems. a) ATPP. b) POSSP-IB. c) POSSP-Ph.

The bilayer thickness and area per lipid are an indication of the packing of the phospholipids in the membrane and the general integrity of the bilayer and can have an effect on the cell function.[191-193] To explore the effect of the porphyrins in the physical properties of the bilayer, Table 3 shows the calculated bilayer thickness and area per lipid for all the systems. The experimental area per lipid of DPPC is 63.0 ± 1.0 $Å^2$ at a temperature of 323K and its thickness, measured as the distance between phosphate groups in the upper and lower leaflets of the bilayer in the electron density profile, is approximately 38.0 Å at 323K.[194] The values calculated for the porphyrin molecules systems do not differ significatively to the lone DPPC bilayer so no . The deuterium order parameter (S_{CD}) gives information about the order of the phospholipids in the membrane, it is related to the relative orientation of the methylene groups and its value can go from 0 (complete disorder) to 0.5 (completely ordered state).[195] The order of the phospholipids affects the fluidity of the bilayer and also has an effect on the cell function.[193] Figure 21 shows the order parameters for the individual molecules systems compared to the lone DPPC bilayer where no effect of the porphyrins on the phospholipids order is observed. The simulations did not find any type of damage to the bilayer caused by the molecules studied.

Table 3. Bilayer properties averaged over 0-20 ns for DPPC and 180-200 ns for the others. The bilayer thickness was measured as the distance between the mean positions of the phosphate groups of each monolayer.

System	DPPC	ATPP (1)	POSSP-IB (1)	POSSP-Ph (1)	ATPP (4)	POSSP-IB (4)	POSSP-Ph (4)
Bilayer thickness, Å	37.5±0.4	38.0±0.5	37.3±0.5	38.2±0.5	37.8±0.4	36.9±0.5	37.6±0.4
Area per lipid, $Å^2$	61.9±1.0	60.8±0.9	62.1±1.0	60.8±0.8	61.1±0.9	63.4±1.0	61.7±0.8

In conclusion for the three systems with only one porphyrin or POSS-porphyrin molecule, the porphyrin section of the three molecules gets inserted into the DPCC bilayer in a similar fashion, with the porphyrin plane parallel to the bilayer normal, minimizing steric hindering. The POSS cage in the POSS-porphyrins does not prevent the porphyrin from being inserted into the bilayer.

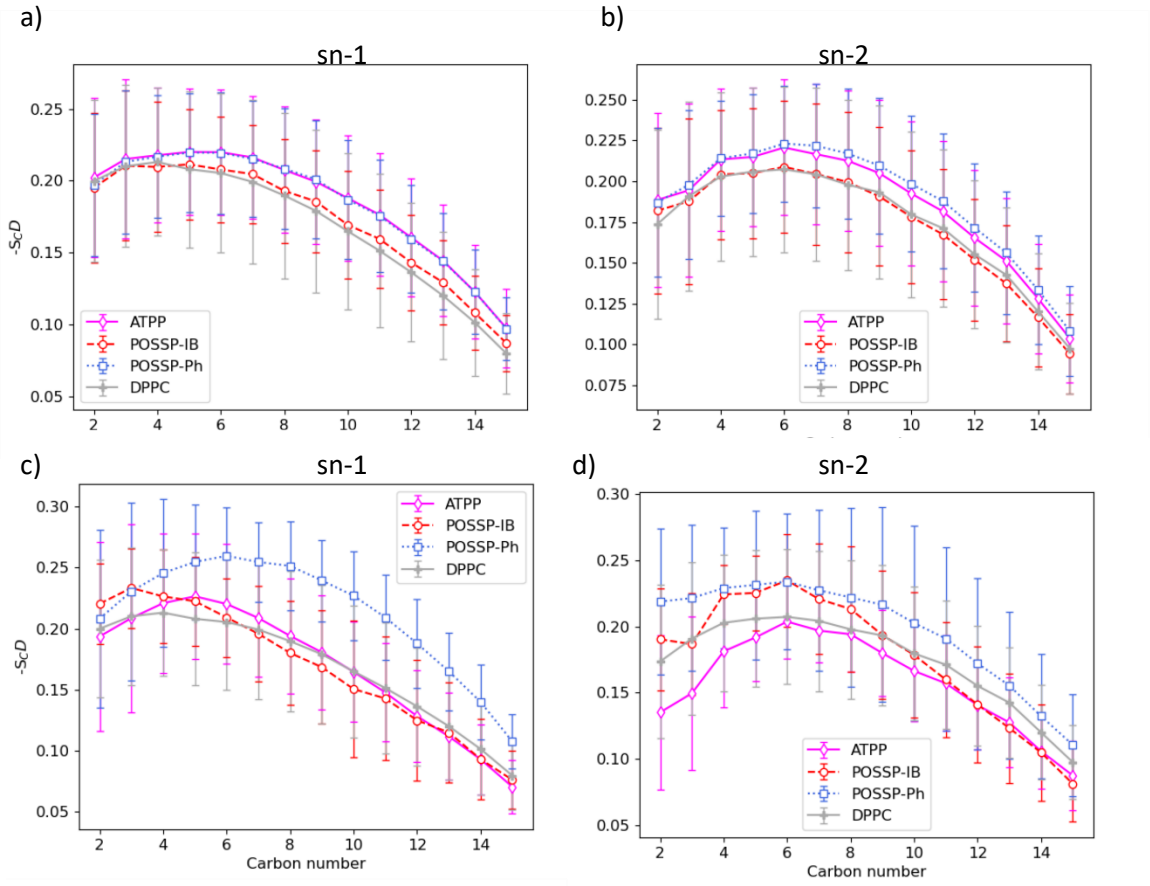

Figure 21. Single molecule systems, deuterium order parameters (S_{CD}) evaluated for the two DPPC lipid acyl chains (sn-1 and sn-2) averaged over 0-20 ns for DPPC and 180-200 ns for the other systems. a,c) all phospholipids in the bilayer b,d) only phospholipids within 5 Å of the porphyrin

2.5.2 Effect of self-assembly in permeation through the DPPC bilayer

We performed simulations using four molecules [JV57]of each compound tested in this study, POSSP-IB, POSSP-Ph and ATPP, to determine whether there is an effect of the aggregation of the POSSP molecules on their interaction with the lipid bilayer. Once formed, the POSSP aggregates should be small enough to avoid interactions with itself across the periodic boundary conditions of the simulation box (percolation). Having the experience from the simulation

described in Chapter 3, we approximated than a four molecules POSSP aggregate would be small enough to avoid this problem but still show their characteristic self-assembly features. Figure 22 shows the results from these simulations. Interestingly, contrary to the findings describe in the previous section, the MD data clearly depicted a different interaction of the aggregates as compared with the single molecules. Figure 22a and 22b show that ATPP form stacks by molecular interactions. We hypothesize that the particular arrangement of this stacks prevents the penetration of porphyrin through the lipid bilayer. POSS-Ph and POSSP-IB also produced aggregates through different molecular interactions. An in-depth MD study of the mechanisms for the self-assembly of these molecules is depicted in Chapter 3 of this Thesis. In the case of POSSP-IB aggregate due to its particular morphology after self-assembly, three of the porphyrins units are inserted in parallel to the lipid bilayer, similar as in the case of the single molecule (Figure 22a and 22c). This finding is especially significant for the use of these POSSP molecules as photosensitizers since there is a much larger damage to the cell membrane. In addition, it has been reported that the concentration of molecular oxygen increases along the lipid bilayer, being the highest in the hydrophobic region.[144] In the case of the POSSP-Ph aggregate, only one of the four porphyrins penetrated the lipid bilayer; while the other ones were sitting flat on top of the headgroups (Figure 22a and 22d). Most likely due to the formation of stacks that prevent them to penetrate the lipid bilayer. This trend of the interactions of ATPP, POSSP-IB and POSSP-Ph with the lipid bilayer follows the experimental data obtained for the PDT efficacy with cancer cells (section 2.4), with POSSP-IB being the most efficient to eliminate cells.

Figure 23 shows the density profiles of the DPPC regions for the four molecules system, showing, as in the individual molecules simulations, no major effects on the bilayer.

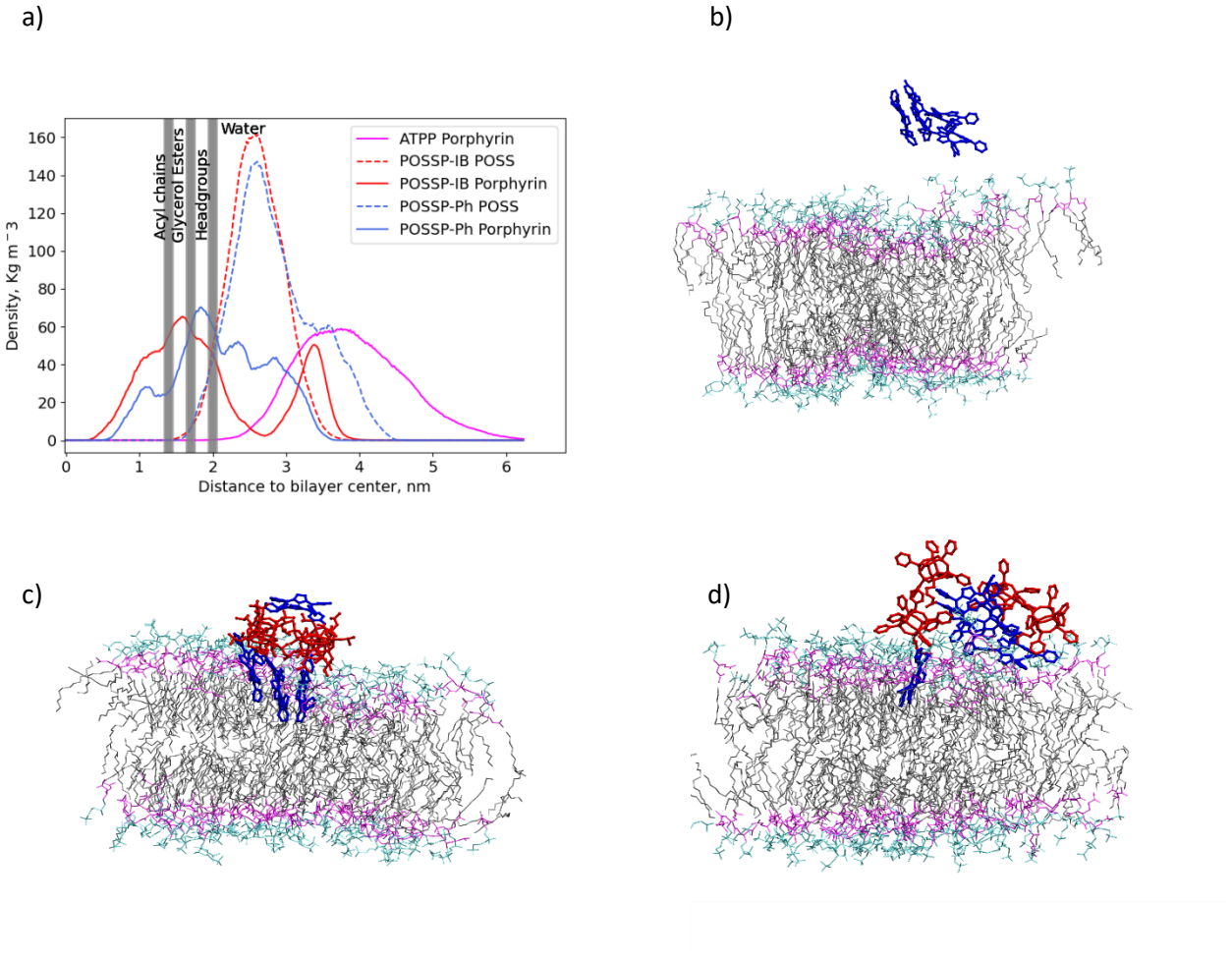

Figure 22. Position of the POSS-porphyrins relative to the DPPC bilayer center for simulations with four molecules. a) Partial density profile averaged in 180-200 ns showing penetration of the POSS and porphyrin moieties in each system in the coordinate perpendicular to the DPPC bilayer normal. The gray vertical lines are a rough indication of the location of the regions of the DPPC bilayer. a-d) Final configuration of the systems. Headgroups in cyan, glycerol esters in magenta, acyl chains in gray, porphyrin in blue and POSS cage in red, water omitted for clarity. b) ATPP. C) POSSP-IB. d) POSSP-Ph

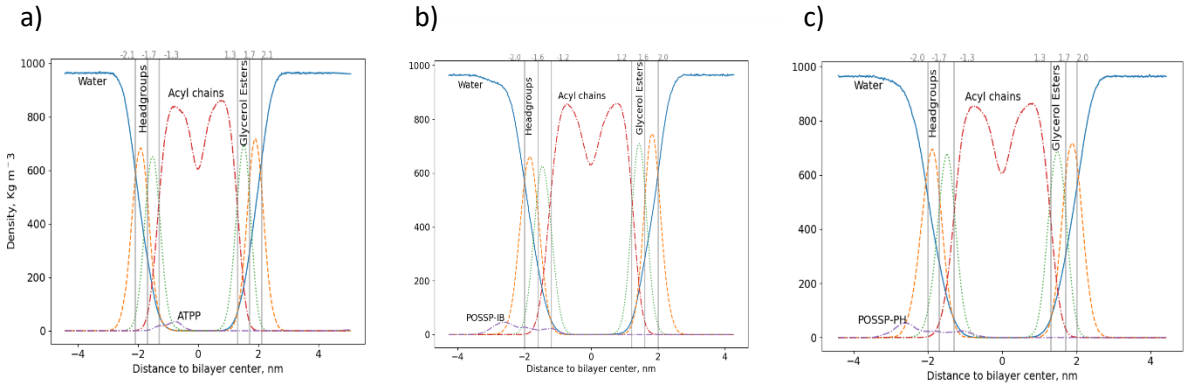

Figure 23. Partial density profiles of the systems with four POSS-porphyrin or porphyrin molecule, averaged in 180-200 ns. The numbers and vertical lines in grey mark the points where the DPPC curves cross. a) ATPP. b) POSSP-IB. C) POSSP-Ph.

Figure 24a-c depict the time evolution of the interaction between the individual porphyrin moieties associated with each aggregate (ATPP, POSSP-IB or POSSP-Ph) with respect to the lipid bilayer. Figure 24b clearly shows that after 100 ns the porphyrin units associated with POSSP-IB-1, 3 and 4 penetrate the lipid bilayer. Moreover, the angle of these porphyrins molecules once inside the bilayer (Figure 24e) is close to be parallel to the bilayer normal ($\cos(\alpha)$ is close to 1) similar to the single porphyrins as described in the previous section. POSSP-Ph aggregate only show one porphyrin (number 4) passing through the bilayer and reaching the hydrophobic region after 125 ns (Figure 24c). The tilt angle of this porphyrin show that it is close to be parallel to the bilayer normal (Figure 24f). The angle for POSSP-Ph 2 and 3 show that they are parallel, but these molecules did not pass through the lipid bilayer. Interestingly, POSSP-Ph molecule 1 is perpendicular to the normal and the end of the simulation and stays in the

headgroups region (Figure 24f). In the case of the ATPP aggregate, the four porphyrins did not penetrate the lipid bilayer. Like the individual molecules systems, the porphyrins enter the bilayer with their planes parallel to the bilayer normal.

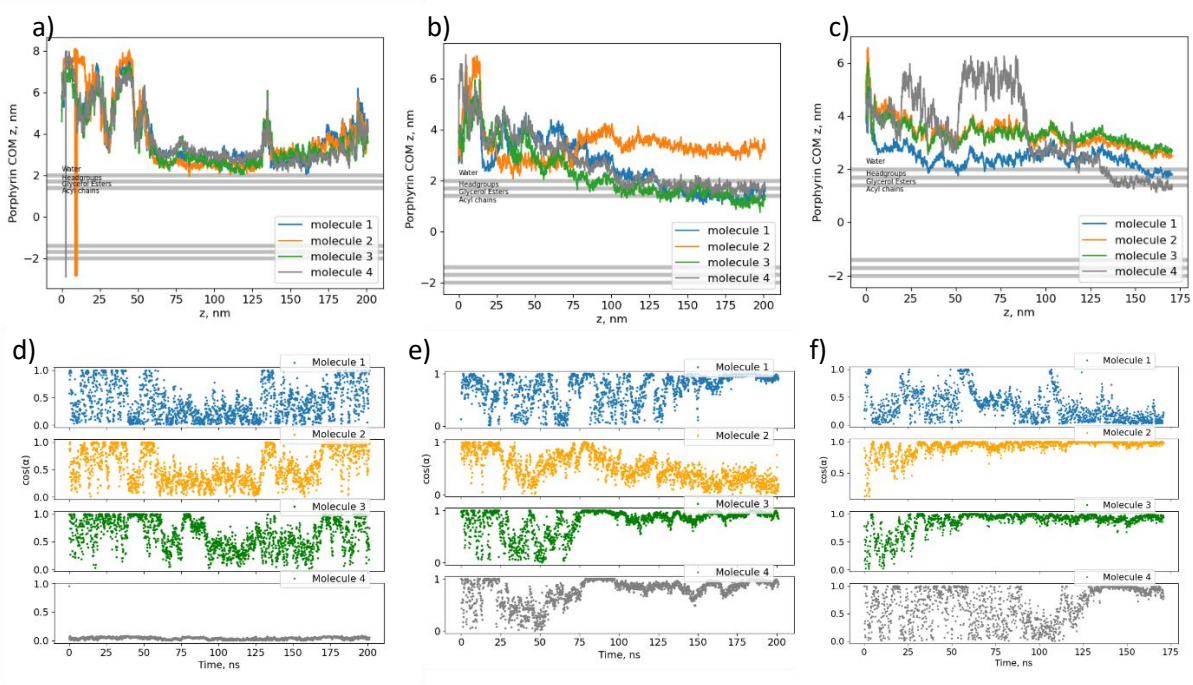

Figure 24. a-c) z component of the four porphyrin COM vs the bilayer center. d-f) tilt angle of the molecules. a,d) ATPP. b,e) POSSP-IB. c,f) POSSP-Ph.

It is important to point out that for the three systems; ATPP, POSSP-IB and POSSP-Ph, the self-assembly process to afford the aggregates occurs around 60 ns, which is before the molecules start to get close to the bilayer. As shown in Figure 25, ATPP molecules form stacks resulting in an aggregate that cannot be inserted in the lipid bilayer. When aggregate, POSSP-Ph molecules also form stacks through the porphyrin portion. However, POSPP-IB molecules self-assembled

mostly through the hydrophobic interaction between POSS cages, preventing the formation of stacks between the porphyrins. More details about the mechanism of self-assembly for these molecules will be provided in Chapter 3.

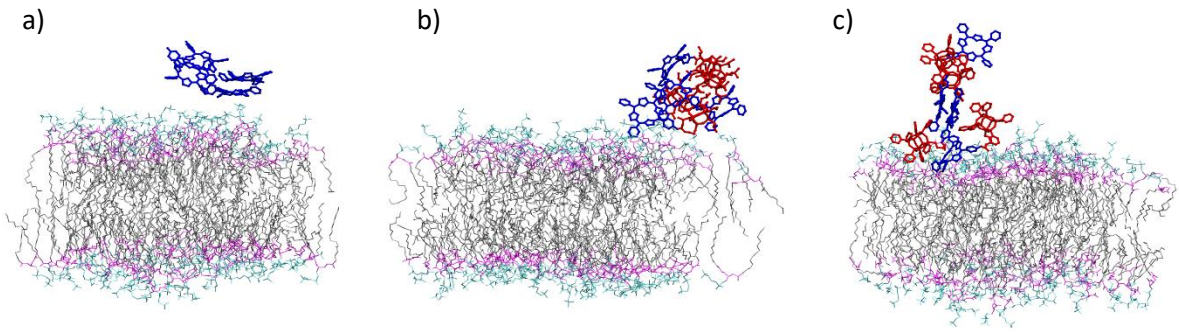

Figure 25. Aggregate formation for a) ATPP, b) POSSP-IB, and c) POSSP-Ph at 60 ns. ATPP forms stacks between the porphyrins; while POSSP-IB does not show any stack formation and POSSP-Ph shows few stacks. Headgroups in cyan, glycerol esters in magenta, acyl chains in gray, porphyrin in blue and POSS cage in red, water omitted for clarity.

Figure 25 shows the deuterium order parameters for the four molecules systems where is there no indication of the porphyrins altering significatively the order of the phospholipids.

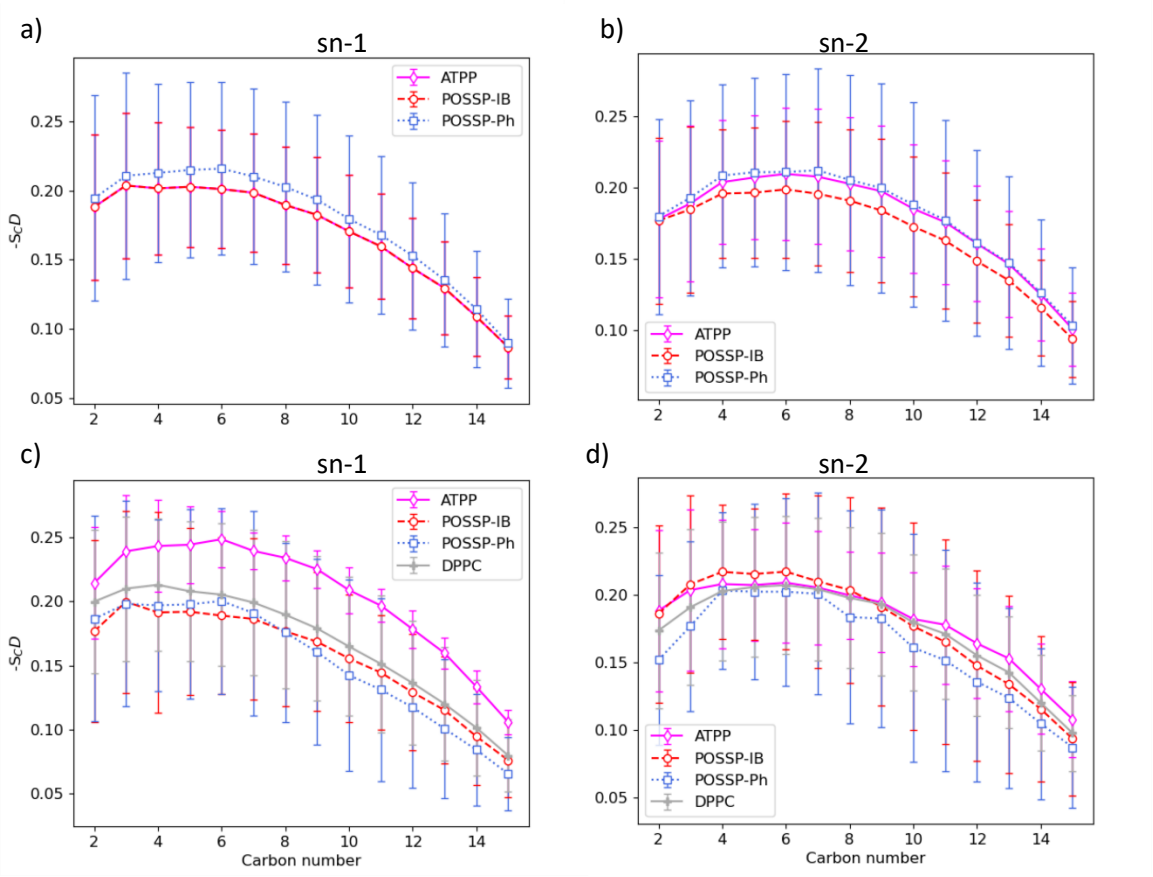

Figure 25. Four molecule systems, deuterium order parameters (S_{CD}) evaluated for DPPC lipid acyl chains (sn-1 and sn-2) averaged over 0-20 ns for DPPC and 180-200 ns for the other systems. a,c) all phospholipids in the bilayer b,d) only phospholipids within 5 Å of the porphyrin

2.6 Conclusions[JV58]

POSSP-IB, POSSP-Ph and POSSP-TIB were successfully synthesized. Relative to the parent porphyrins, the POSS-porphyrins presented lower fluorescence and higher singlet oxygen quantum yields. The increase in singlet oxygen quantum yield can be explained by a decrease in the aggregation induced quenching effect, directly associated with the the steric effect of the POSS cages, this hypothesis will be further analyzed in Chapter 3. The *in vitro* PDT experiments

showed that POSSP-IB has the highest PDT efficiency at the concentration tested in our experiment to eliminate MDA-MB-231 cells followed by POSSP-TIB and POSSP-Ph. MD simulations of the aggregates associated to these molecules shed light to account for this trend with POSSP-IB having a much better insertion of the porphyrin units than the POSSP-Ph.

MD simulations show the importance of considering the influence of self-assembly when the interaction of POSSP molecules with lipid bilayer is studied. Contrary to MD simulations of a single molecule; where all the porphyrin portions associated with ATPP, POSSP-IB or POSSP-Ph are inserted into the lipid bilayer, the aggregates produced by that molecules have a different performance. Single molecules follow the most favorable insertion mode for the porphyrins, which minimizes the steric impediment with the lipid bilayer by arranging its molecular plane parallel to the bilayer normal. Nevertheless, in the case of the self-assembled clusters, this particular geometrical arrangement can be prevented by the stacking between the porphyrins like in the case of ATPP aggregates. POSSP-IB molecules self-assembled mainly through hydrophobic effect (Chapter 3 will describe more in detail the mechanism) preventing the stacking between porphyrins. Therefore, favoring their insertion into the hydrophobic region.

CHAPTER 3. MD SIMULATIONS OF THE SELF ASSEMBLY OF POSS-PORPHYRINS[JV59]

The results reported in this Chapter have been submitted to Materials Today Communications (MTCOMM-D-21-02606), which are currently under revision. The work was done in collaboration with Dr. Donald Jacobs.

3.1 Introduction

Being prone to self-assembly and crystallization, POSS is frequently used as a building block of amphiphilic systems, providing a specific interaction to the solvent through its substituents.[32, 78-82] When POSS containing molecules progress through self-assembly, the POSS section tends to form a separate microdomain, often crystalline.[83-86] POSS has been shown to have a nucleating effect for forming this nanocrystalline phase.[87-88] The substituents of the POSS are crucial in determining their self-assembly behavior by imparting specific physicochemical properties that play a role in the self-assembly process.[89-90] For example, molecules that comprise of many POSS units with a variety of substituents that are not miscible tend to possess distinct microdomains as they form a hierarchical assembly.[91] Aromatic POSS substituents have shown to participate in the self-assembly mechanism through π-π interactions and stacking.[90] Although POSS molecules have a natural propensity to self-assemble and form hierarchical structures, when chemically coupled with other self-organizing molecules such as porphyrins, the scope of self-assembly control is increased.[74-75] The self-assembly tendency of POSS together with its biocompatibility has been exploited in many applications such as photodynamic therapy, where it is possible to achieve lower levels of cytotoxicity and/or prevent aggregation quenching of POSS-photosensitizer molecules,[92-95] including porphyrins.[23, 64-66, 70, 96][JV60]

Previous studies have employed MD simulations to glean insight about the self-assembly of POSS molecules. These works have focused on studying monofunctionalized systems or composites

where POSS molecules are part of the whole platform. In a study describing the self-assembly of monotethered POSS, it was found that the large volume and cubic geometry of the POSS cages together with their attractive interaction in a poor solvent induces a strong face to face local packing.[135] In another study comparing the behavior of POSS with phenyl, isobutyl and cyclopentane substituents, the self-assembly with sorbitol revealed that is necessary to have cooperative π-π interactions and H bonding so that the molecules would form an adduct.[136] In a recent work, a coarse-grained model was used to simulate the hierarchical self-assembly of POSS containing dendrimers. The obtained structures match the ones physically observed by TEM where a strong microphase separation was observed.[138] Furthermore, MD simulations of amphiphilic polymers containing POSS showed that the POSS units offered a second level of hierarchy in the final ordered structure.[79, 196] A study on self-assembly of POSS monotethered with a hydrocarbon using a coarse grained model found that short-range van der Waals interactions (<5 Å) promoted a face to face assembly of the POSS cages while the long-range coulombic interactions (>10 Å) were responsible for corner-edge, corner-corner and edge-edge arrangements.[137] In this work, we employ MD simulations at the all-atom level to study the self-assembly of POSS-porphyrins.

We have carried out MD simulation for the self-assembly of three different POSS-Porphyrin molecules (Figure 9). The main goal of this study was to determine the influence of the functional groups in the POSS molecules on the aggregation of the POSS-porphyrin building blocks. Our results suggest that in water, the difference in hydrophobicity between the isobutyl groups compared to the phenyl groups in the POSS cage cause a different arrangement of the POSS molecules within the aggregates. Specifically, the MD data shows that the POSS section associated with isobutyl moieties tend to cluster tightly and exclude water, while the porphyrin portion of the POSS-porphyrin interact with water molecules, causing the space between the porphyrin moieties

to increase, resulting in a reduction of the number of contacts between porphyrins. Whereas a similar effect is observed for the phenyl POSS cage, the aggregation between POSS moieties is not as predominant as in the isobutyl POSS case, presumably due to a lower hydrophobicity. In addition, the phenyl substituents have a π-π interaction to the porphyrin, keeping them closer to the phenyl POSS, so when the molecules aggregate, the porphyrins tend to make more contact with each other. In the case of POSSP-TIB, the four isobutyl cages keep the porphyrins distant from each other, making almost no contact. We also studied the solvation changes upon aggregation, and the geometry of the different systems to explain the differences in the arrangement of the final systems. Understanding the factors that control the self-assembly of the POSS-porphyrin system provides insight for how to mitigate aggregation induced quenching (AIQ) of the excited states due to the proximity and relative orientation of the porphyrin molecules as well as enhancing interesting optical and electronic properties.

3.2 Methods

3.2.1 Modeling and simulation procedure

Three POSS-porphyrin molecules (Figure 9) were simulated using LAMMPS software.[197-198] We employed the OPLS-AA (Optimized Potentials for Liquid Simulations – All Atom) force field. Water was simulated using the extended simple point charge (SPC/E) model.[164] The water molecule bond length and bond angle were constrained using the SHAKE algorithm,[199] which eliminates fast degrees of freedom and reduces the number of variables to track.[200] The complete force field parameters for the porphyrin and POSS-porphyrin molecules were obtained using the LigParGen software[154-156] as downloaded from the GitHub repository.[157] LigParGen is an

extension of the BOSS[201-202] software which was obtained from the Jorgensen group. The 1.14*CM1A-LBCC charge model[155] provided with the LigParGen software was used.

For POSSP-Ph and POSSP-TIB the parameterization methodology was modified due to their large size. Their parameters were obtained by combining overlapping fragments of the molecules following the steps described in previously published works for the parametrization of large molecules.[203-204] In the case of POSSP-Ph, a fragment containing the POSS cage and the urea bond joined to a phenyl group (Figure 26a) was parametrized using LigParGen. Following that first level of parametrization, the phenyl ring opposite to the POSS was removed. Then, the porphyrin force field parameters and topology obtained from the POSSP-IB molecule were combined to create a new porphyrin fragment. The fragments were joined using Moltemplate[205] creating a new bond between the porphyrin and the urea group as shown in Figure 26b. The corresponding coefficients were copied from the analogous ones in POSSP-IB. Moltemplate[205] calculates the dihedral and improper coefficients automatically. For POSSP-TIB, the IBPOSS fragment (Figure 26c) was extracted from the POSSP-IB parametrization. Then three copies of this IBPOSS fragment were joined to the POSSP-IB molecule (after deleting the corresponding H atoms in the porphyrin phenyls) as described in Figure 26d. As a final step, the new bonds and coefficients were obtained using the same procedure as described for POSSP-Ph.

For each simulation, 20 molecules were randomly placed in a 100 Å periodic cubic box and then 32,000 water molecules were added to the box using Packmol.[165] With these values, the density would be roughly around 1 g/cm^3 in random positions, leaving on average 2 Å between them. The largest molecule, POSSP-TIB was around 50 Å in its largest dimension so we made the simulation box to have double that size on each side. Twenty molecules were the largest number of POSSP-TIB molecules that could fit in the 100 Å box, which corresponds to a concentration of 33.2 M.

This high concentration is employed to induce aggregation during the MD simulation without requiring extremely long simulation times.[206-209] The input topology files for the simulations were built using Moltemplate.[205]

The standard 12-6 Lennard Jones potentials with a cutoff of 10 Å were used along with the standard geometric-mean combining rules and a 1.4 intra-nonbonded scaling of 0.5 was employed as recommended for the OPLS force field.[210] The electrostatic forces were modeled with a particle-particle particle-mesh solver (pppm),[211] providing ample accuracy while being much faster than the Ewald method.[212] The accuracy tolerance was set at 1.0×10^{-4} where accuracy is defined as the relative root mean square error in force per atom. The cutoff for Lennard Jones and short-range Coulombic interactions was 10 Å. The distance cutoff for the neighbors list was 13 Å. In all simulation preparation steps and production runs the Verlet integrator was used with a timestep of 1.0 fs.

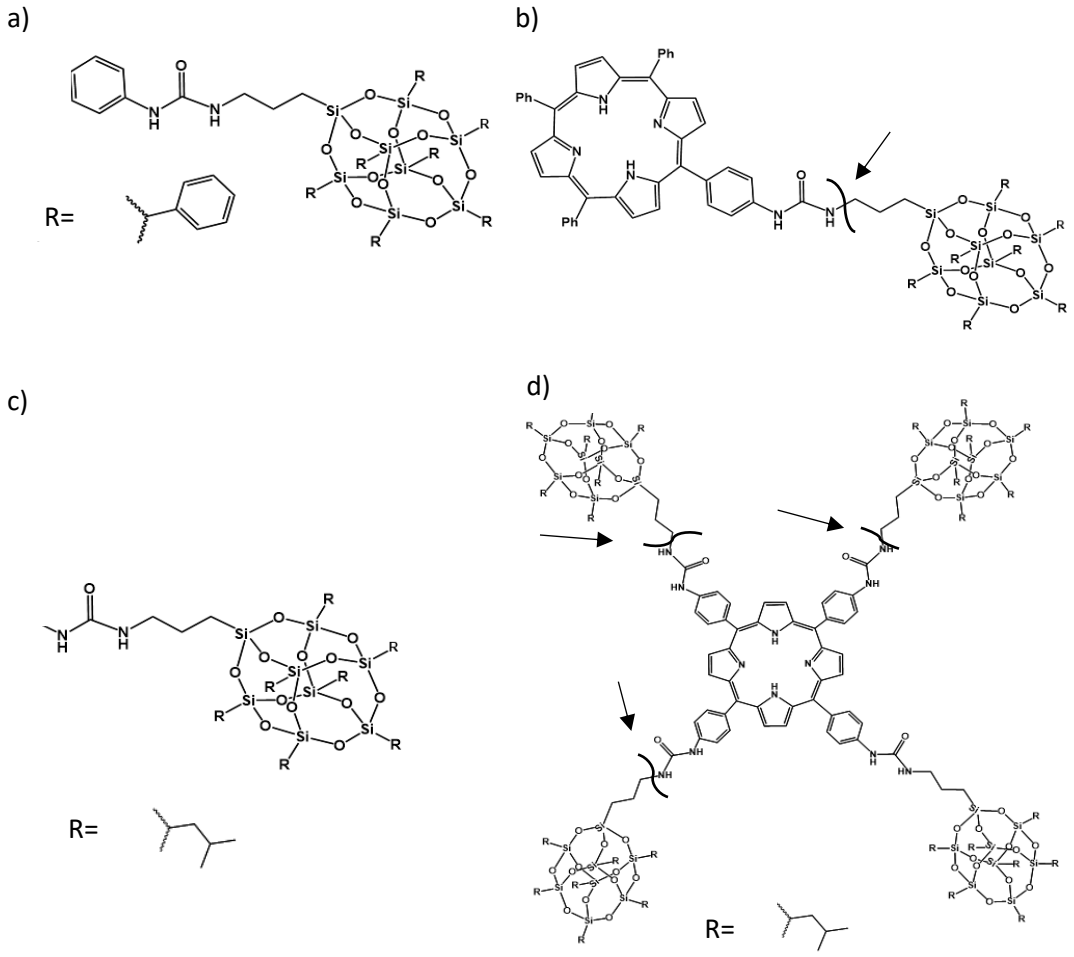

Figure 26. a) Fragment for POSSP-Ph parametrization. b) Point at which POSSP-Ph fragments were joined. c) IBPOSS fragment obtained from POSSP-IB. d) Points at which the POSSP-TIB fragments were joined.

The relaxation was performed by slowly heating the system from 1 K to 300 K while incrementally increasing the timestep from 0.1 to 1.0 fs. The water molecules were under NVT (constant particle number, volume and temperature), while the porphyrin or POSS-porphyrin molecules were under NVE (constant particle number, volume and energy). The temperature was rescaled and a limit of

0.1 Å on the movement of atoms was used. When the system reached 300 K at a timestep of 1.0 fs, different parts of the systems were run for 100 ps using NVT for water and NVE for the porphyrins, limiting the movement of atoms to 1.0 Å. Next, the entire system was run under NVT during 100 ps at 300 K. As the final relaxation step, the systems were run under NPT at 300 K and 1 bar for 100 ps, which always increased the volume of the boxes. Finally, water molecules were removed iteratively at a rate of 500 water molecules every 5 ps until the volume of the simulation box returned to $(10\ Å)^3$. Global linear and angular momentum of the system were removed every 1000 steps at the end of the relaxation stage using the fix momentum method from LAMMPS.

The production simulations were conducted under an NVT ensemble (Nose-Hoover) at 300 K with a temperature damping parameter of 100 fs. It is worth noting that when using the above protocol, no aggregates percolated across the simulation box except for an aggregate that formed in the POSSP-TIB system, which was found to percolate along one direction within the simulation box. Therefore, the simulation box was extended using two different ways to obtain an aggregate that did not percolate. In the first simulation of the POSSP-TIB system, the aggregate spanned the simulation box in one dimension (x-direction); therefore, interacted with itself along the periodic boundary. To correct this issue, we stopped the simulation at 80 ns to expand the box in the x dimension from 100 Å to 150 Å. All the molecules forming the aggregate were placed in a newly created space such that no molecules cross the periodic boundary. Then, 52,000 extra water molecules were added to fill the empty volume, and the same relaxation procedure was performed, followed by a second production run (POSSP-TIB (2)). To compare results, we also took the POSSP-TIB system as it was before starting the first simulation, increased the box size to 120 Å in every dimension. Then, we filled the volume with 60,000 extra water molecules, performed the

relaxation procedure described before and ran the simulation (POSSP-TIB (3)). Figure 27 shows that POSSP-TIB (2) and POSSP-TIB (3) simulations converge to the same solvation layer size, indicating that the final aggregation structure is similar. The properties of the molecular structures from both extended simulations were found to be consistent (Figure 27).

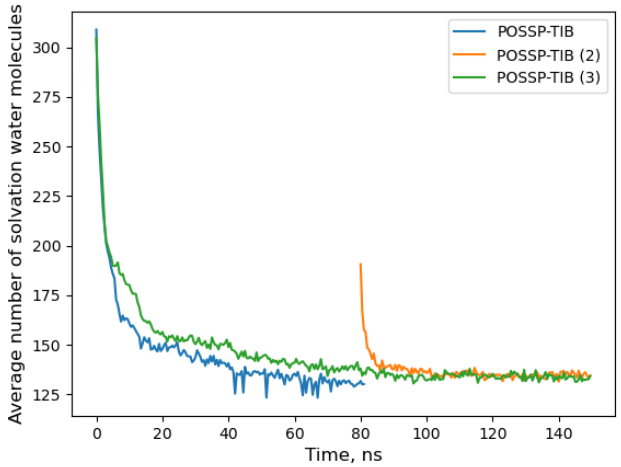

Figure 27. Average number of solvation waters per POSSP-TIB molecule for the three different set ups. The first simulation had a percolating aggregate. The second and third simulations have similar properties of the final aggregates, such has the average number of solvation waters.

3.2.2 Analysis of the morphology

We determined the aggregates of POSS-porphyrin molecules by following two criteria; first, we registered molecules that came closer than 6.0 Å from each other; and second, these molecules stayed within this separation distance for the rest of the simulation.

To characterize the relative orientation of a porphyrin molecule or porphyrin constituent, we defined a plane by employing a least-squares fitting procedure with respect to a planar surface to

the displacements of heavy atoms comprising the porphyrin core without including the phenyl groups. The plane orientation is determined by minimizing the normal displacements of the core heavy atoms to the plane. This plane is exemplified for TPP in Figure 28a. Furthermore, by checking which side of the plane the carbon atoms of the porphyrin core are found, specific conformation types as described in previous reports (e.g. saddle, wave, ruffled, dome or propeller) of each porphyrin molecule at each timestep along the trajectory was tracked.[213]

Two neighboring molecules are considered stacked when their defining planes are near parallel. The threshold is set so that the absolute value of the cosine of the angle between the two associated plane normal vectors are larger than 0.866 corresponding to less than +/- 30 degrees. The general trends of stacking angle and number of stacked pairs formed are insensitive to the threshold angle, they stay the same when a value of 0.95 is used.

a)

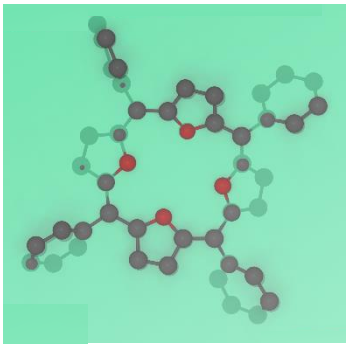

b)

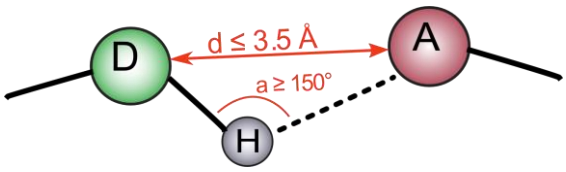

Figure 28. a) Molecular plane of TPP (in green). The atoms shown as shadows are below the plane. b) Definition for identifying H-bonds. D is the donor atom, A the acceptor atom.

3.2.3 Analysis of water solvation

Voronoi analysis was applied to characterize the solvation of water using the Voronoi-Delaunay method, implemented using the software Voro++.[214] This method avoids the need to establish a cutoff distance for the hydration layer, and is commonly used to determine the hydration shell volume in MD simulations.[215] A Radical Voronoi tessellation for each porphyrin or POSS-porphyrin molecule and for the water molecules that were at most 15 Å away were calculated. A Voronoi cell was assigned to every atom. The cell boundaries were weighted using the Van der Waals radii. From the tessellation, we were able to map contacts between water and porphyrin atoms by identifying atom pairs that had facets in common.[216] We recorded the area of these facets as an estimate to the atomic contact surface.[217] We consider the total molecular surface as the sum of all the areas of the atom cell facets minus the areas of the facets that are shared by bonded atoms. In addition, we used this information to monitor which porphyrin molecules were neighbors. The volumes of the Voronoi cells, often called Voronoi atoms, provide insight on the packing of the molecules and are equivalent to the specific volume (or reciprocal density).[215]

Among the water molecules contained the first solvation layer, all H-bonds between water and porphyrin molecules were identified. Moreover, any H-bonds that formed between neighboring porphyrins were identified. The definition used for determining H-bonds is described in Figure 28b following commonly used procedures employed in the literature.[218] The H-bonds are identified when the distance between Donor and Acceptor does not exceed 3.5 Å, and the angle between Donor – Hydrogen – Acceptor is not less than 150°.

The potential energy for every molecule at all timesteps was obtained using LAMMPS. The individual contributions to the potential energy that the software calculates includes the energy from bonding, dihedral angles, improper angles, van der Waals and electrostatics.[219]

3.3 Results and discussion

3.3.1 Aggregate morphology

The MD simulation of aqueous solutions involving the three POSS-porphyrin molecules with different substituents in the POSS was carried out at 300 K and 1 bar. The final structures are shown for the three cases in Figure 29 and Figure 30. After 120 ns the number of solvation water molecules per porphyrin molecule achieved steady values for all the systems (Figure 31). These two signatures were considered as an indication that equilibrium of the simulation has been reached. Subsequent analysis for all of the systems is performed over the range of 120-150 ns.

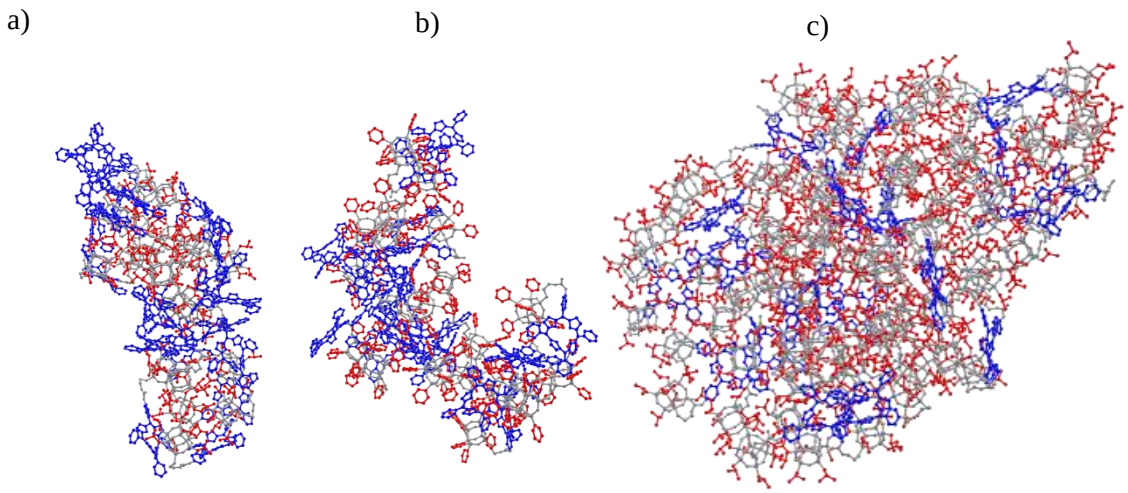

Figure 29. Morphology of aggregates at 150 ns simulation for a) POSSP-IB, b) POSSP-Ph, and c) POSSP-TIB. The color scheme shows the POSS cage in grey, POSS substituents in red and porphyrin in blue. Water molecules and H atoms omitted for clarity.

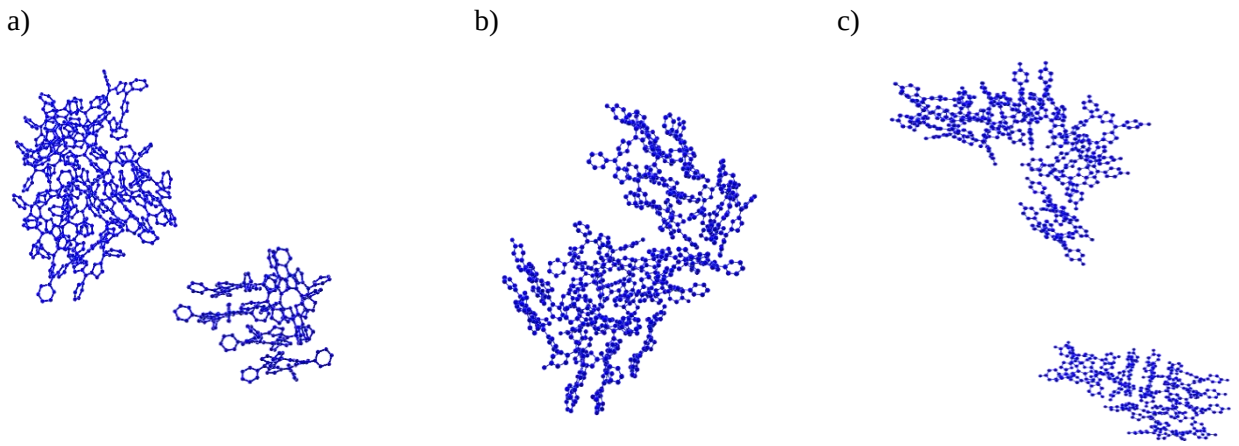

Figure 30. Morphology of aggregates at 150 ns simulation for a) TPP, b) ATPP, and c) TAPP. Water molecules and H atoms omitted for clarity.

In the case of the POSS-porphyrin systems, the MD simulations of the aggregation show the formation of larger aggregates as compared with the porphyrin controls as an indication of the influence of POSS in the self-assembly process of these molecules, Figure 30 shows the final aggregates of the control porphyrins. For POSSP-IB and POSSP-TIB, the hydrophobic effect between the POSS sections is dominating the self-assembly of the system. Therefore, the core of the aggregate is mainly formed by the POSS molecules, placing the porphyrin part of the molecule on the surface of the aggregate where it is exposed to water. Furthermore, the aminopropyl group of the POSS is flexible enough to allow the POSS to fold behind the porphyrin (Figure 32a and b) relative to the water interface. The consequence of the well-separated porphyrins in the final aggregate will decrease the self-quenching effect associated with porphyrins as shown recently by our group.[23] These characteristics are not seen in the morphology of the final self-assembly of POSSP-Ph (Figure 29).

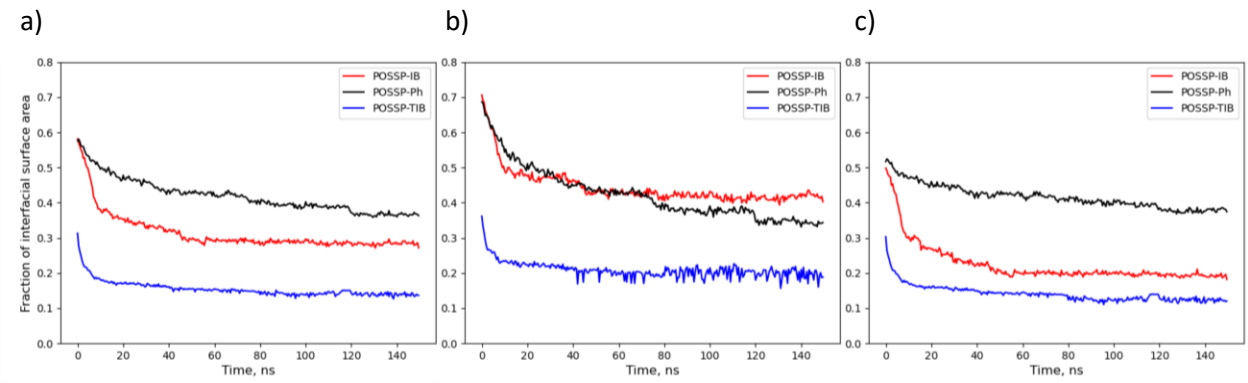

Figure 31. The fraction of molecular surface of a molecule that is in contact with water defines the fraction of interfacial surface area. a) Consideration of the whole molecule. b) Consideration of only the porphyrin. c) Consideration of only the POSS.

Previous MD simulation work has shown that the self-assembly of porphyrins is driven by the cooperative effect of hydrogen bonds (H-bonds), van der Waals forces and the hydrophobic effect.[220-221] In addition, it was found that there are generally more than one aggregation pathway.[220, 222] It was observed that unsubstituted porphyrins in water initially aggregated into a few small stacks, and by annealing the system, larger stacks would order.[223] Another study demonstrated that the aggregation of steroid-functionalized porphyrins is mainly driven by the hydrophobic effect, and underscored the importance of ring distortion, formation of intramolecular H-bonds related to OH-π interactions, and dispersion forces among the tetrapyrrolic platforms.[224]

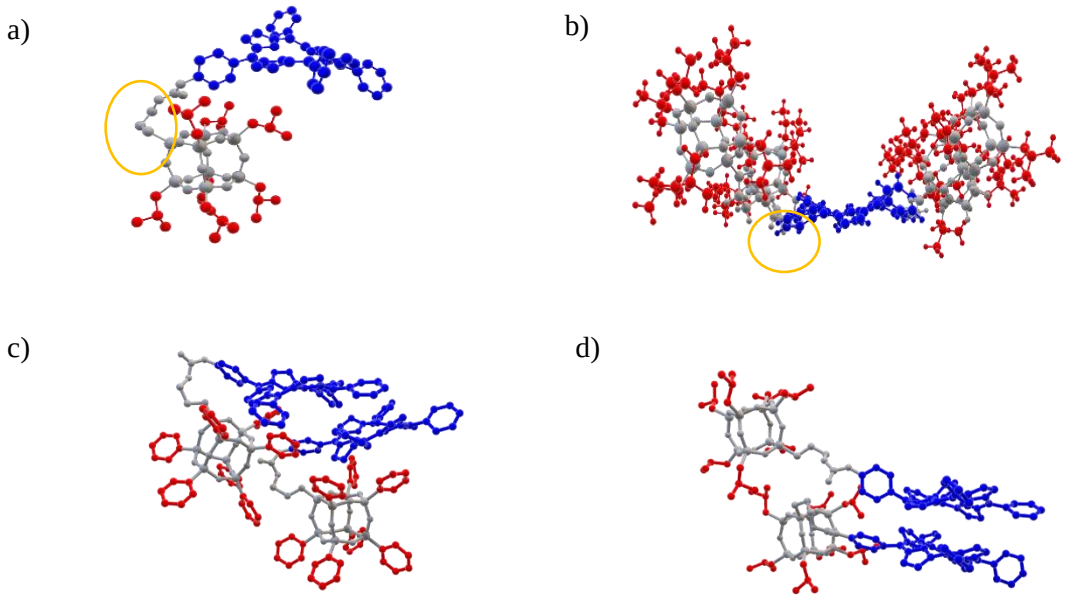

Figure 32. Representative POSS-porphyrin orientations. POSS cage in grey, POSS substituents in red and porphyrin in blue. Water and H atoms omitted for clarity. a) POSS-IB showing flexibility at the aminopropyl substituent. b) POSS-TIB showing flexibility at the aminopropyl substituent. c) POSSP-Ph J-aggregate. d) POSSP-IB H-aggregate.

The electronic coupling and energy transfer between porphyrins is strongly dependent on the distance that separates the porphyrins.[48, 53-54, 225] Therefore, adding a spacer between porphyrins has a direct impact in the optical properties and self-quenching. Different kinds of molecules have been used as spacers to avoid self-quenching, especially in their use as photosensitizers in photodynamic therapy.[23-24, 66-68] The arrangement of the molecules in the aggregates can give us insight into the driving forces of the self-assembly and elucidate macroscopic properties observed for the self-assembled systems.[226]

Here, we first used Voronoi analysis to determine the average number of neighboring molecules for each system. POSSP-IB and POSSP-TIB show an average of 7.9 and 9.3 neighboring molecules, respectively as an indication that the clusters are more tightly packed than found in POSSP-Ph, which has 6.2 neighboring molecules. In POSSP-IB and POSS-TIB, the number of porphyrin-porphyrin contacts is lower than in POSSP-Ph, but the number of POSS-POSS contacts is higher (Table 4[JV61]). This is a result of the higher hydrophobicity of the isobutyl POSS cage with respect to the phenyl POSS. In the case of the porphyrin controls, TPP and ATPP are also packed with 6.0 neighboring molecules each. TATPP has the lowest average number of neighboring molecules of 3.2, indicating a much looser packing. Table 4 and Figure 33 together elucidate how the POSS-porphyrins arrange with respect to each other in terms of the average number of POSS or porphyrin neighbors to POSS and porphyrin molecules. A neighbor can have more than one type of contact, so the total number of neighbors is not the sum of the first columns. As expected because of the higher hydrophobicity of isobutyl POSS, the majority of POSSP-IB and POSSP-TIB molecules have POSS-POSS contacts with their neighbors, contrary to POSSP-Ph where a smaller fraction of the molecules make contact through their POSS cages.

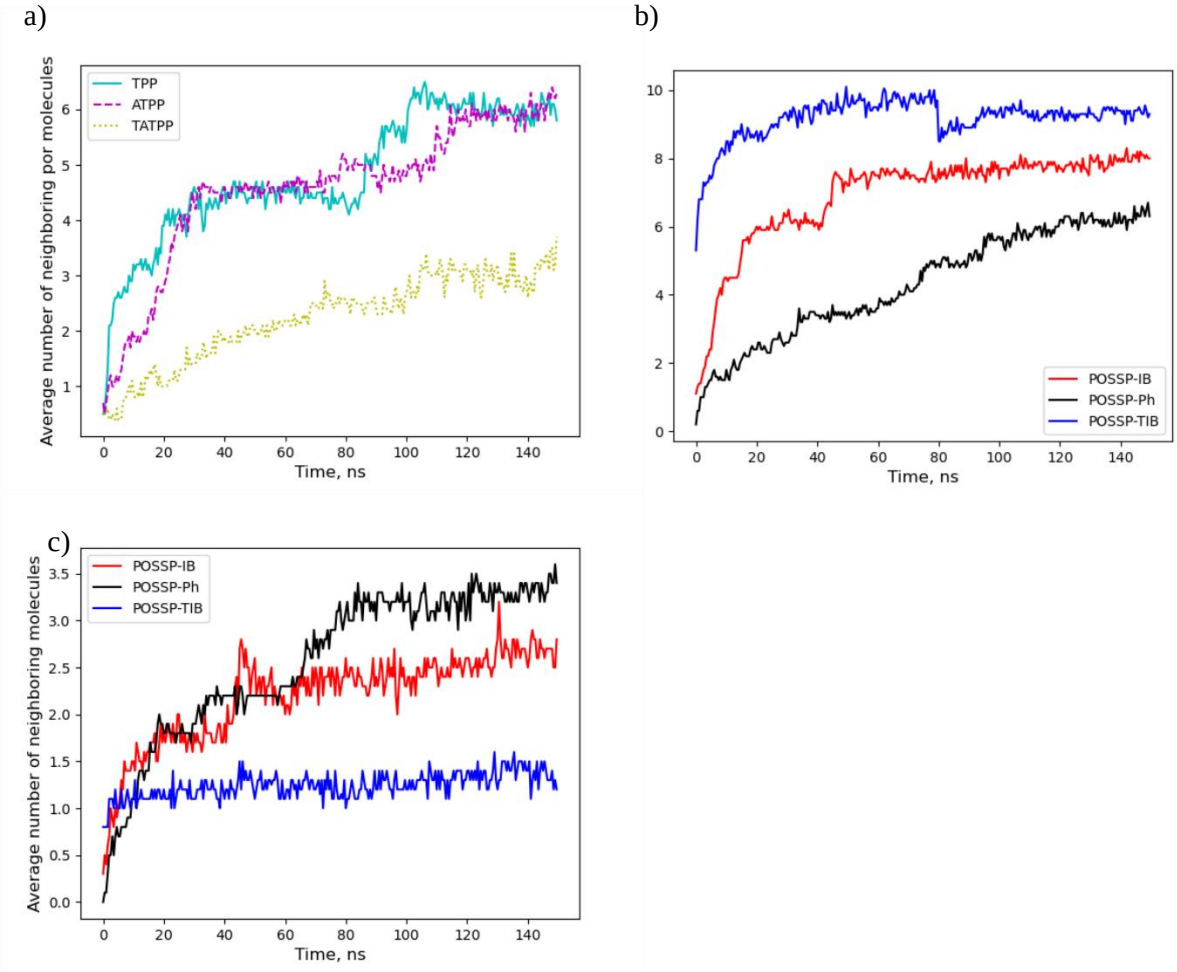

Figure 33. Average number of neighboring porphyrin or POSS-porphyrin molecules as determined from the Voronoi analysis. a) Porphyrin neighbors. b) POSS-porphyrin neighbors making contact anywhere. c) Any neighbors

The number of neighboring molecules is a consequence of the overall morphology of the system. The lower number of porphyrin-porphyrin contacts in POSSP-IB and POSSP-Ph results in a higher average distance between porphyrin moieties, also shown in Table 4. These data characterize the average distances between porphyrins after 120 ns, where it is seen that the porphyrin moieties are farther from each other in the POSSP-IB system compared to the POSSP-Ph system despite the

average distance between the center of mass of the whole POSS-porphyrin is smaller. This is due to the stronger tendency of the isobutyl groups to clump together in the center of the aggregate, which drives the porphyrins to separate. In the POSSP-Ph system, the molecules are oriented to have the porphyrins closer to each other, driven by the attractive forces between them.

Table 4. A[JV62]verage number of neighboring porphyrins by type of contact, 120-150 ns. Data obtained from the Voronoi analysis described in the methods section.

	Number of neighbors having porphyrin-porphyrin contacts	**Number of neighbors having POSS-POSS contacts**	**Number of neighbors having POSS-porphyrin contacts**	**Total number of neighbors**	**Average center of mass distance to closest neighbor, Å**	**Average porphyrin center of mass distance to closest neighbor, Å**
TPP	6.03 ± 0.04	NA	NA	6.03 ± 0.04	5.8 ± 1.3	
ATPP	6.00 ± 0.03	NA	NA	6.00 ± 0.03	7.3 ± 3.9	
TATPP	3.23 ± 0.02	NA	NA	3.23 ± 0.02	6.3 ± 4.4	
POSSP-IB	2.65 ± 0.02	5.33 ± 0.03	5.16 ± 0.02	7.88 ± 0.04	9.5 ± 1.6	10.0 ± 3.6
POSSP-Ph	3.33 ± 0.04	3.07 ± 0.02	5.05 ± 0.03	6.24 ± 0.04	11.8 ± 1.6	9.0 ± 1.8
POSSP-TIB	1.33 ± 0.01	9.31 ± 0.04	4.77 ± 0.03	9.31 ± 0.04	12.0 ± 2.8	13.2 ± 3.9

3.3.2 Analysis of solvation water molecules

To better understand the aggregation process, a detailed analysis of the molecular interactions of the POSS-porphyrin molecules and the solvent was carried out. Since it appears that hydrophobicity is playing a major role in the aggregation process of POSSP-IB and POSSP-TIB as compared with POSSP-Ph, we monitored the number of solvation water molecules during the self-assembly process. To deconvolute the effect of each part of the POSS-porphyrin molecule, a separate analysis of the POSS and porphyrin section was performed. We consider the number of water molecules in the first solvation layer to be proportional to the accessible surface area. Hence, the magnitude with which the solvation layer decreases during the simulation of the self-assembly process reflects the degree of hydrophobicity in the system.[227-228] Figure 31 shows the fraction of the POSS-porphyrin surface area that is in contact with water along the simulation. At the beginning, the number of water molecules in the hydration shell of each system is indicative of the maximum accessible surface area of each molecule. As expected, with the simulation time increasing, the POSS-porphyrin molecules self-assembled due to molecular interactions to minimize the number of water molecules in their solvation shell (Figure 31a). A constant value is reached after 120 ns, which is an indication that the equilibrium has been reached. A trend in the final number of water molecules in the solvation layer per POSS-porphyrin follows the hydrophobicity of the molecules with lower amount for POSSP-IB with around 28% of the POSSP-IB surface area covered by water while POSSP-Ph has around 37% of its surface covered by water. The same performance was observed for the control porphyrins with TPP 38% and ATPP 40% while TATPP has 50% of surface area coverage (Figure 34). For POSSP-TIB, only around 16% of its surface area is in contact with water, showing the greater degree of hydrophobicity given by the increased number of isobutyl POSS. The analysis of water molecules surrounding

only the porphyrin moiety for each POSS-porphyrin system is shown in Figure 31b. The porphyrin in the POSSP-IB system ended up with the largest fraction of area in contact with water (41%), confirming that in this system the porphyrins are more exposed to water in the surface of the aggregate. In the case of the porphyrin associated with POSSP-Ph, 35% of surface area was covered with water.

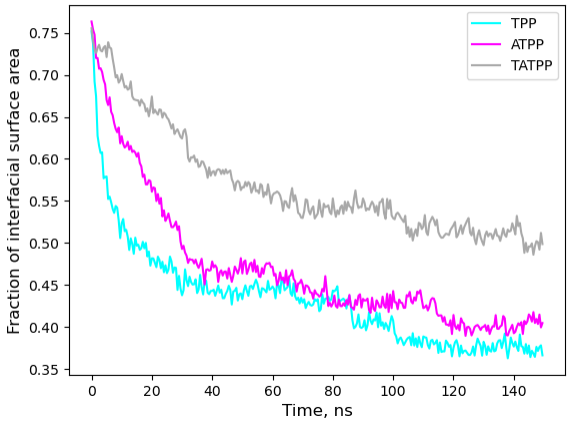

Figure 34. Contact area of the control porphyrins with water. Fraction of the surface of the whole molecule that is in contact with water.

Figure 31c depicts the analysis of water molecules around the POSS section. The relatively small percentage of POSS surface area in contact with water in both POSSP-IB and POSSP-TIB, 20% and 15%, respectively, demonstrates that for these molecules the self-assembly process is mainly driven by the hydrophobic effect. On the contrary, the amount of water molecules surrounding the phenyl POSS is 2-3 times higher than the isobutyl POSS (38% of surface area coverage) as a clear indication that phenyl is less hydrophobic. In addition, phenyl POSS cages are more stable in water because being more rigid, they do not cover the Si-O-Si cage as much, allowing more water to be

in contact with it. These geometrical and chemical properties provide a means for the phenyl POSS to form H-bonds with the O atoms. These considerations suggest that the self-assembly of this system is driven by π-π and H-bonding interactions. The analysis of water molecules surrounding the three control porphyrin systems is shown in Figure 34. The values of TPP and ATPP are similar to the porphyrin values of POSSP-IB and POSSP-Ph in Figure 31b, while TATPP has a higher contact area with water, showing higher hydrophilicity.

3.3.3 POSS and porphyrin molecular orientations

When the porphyrins aggregate, they tend to adopt certain positions relative to each other. In general, the porphyrin moieties interact with each other most likely due to π-π interactions to form stacks, T-shaped configurations or a combination of both. One feature in the self-assembly of porphyrins is the formation of stacks, which usually fall into two categories: H- or J-aggregates.[53] Figure 35 summarizes the criteria for this classification, it involves the stacking angle, θ.

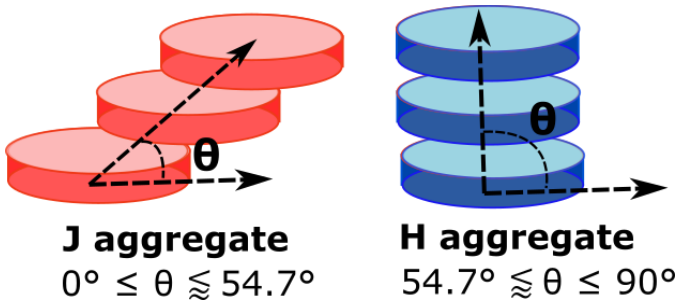

Figure 35. Kasha aggregates classification according to their stacking angle, θ.

Figure 36 shows the frequency of alignments between porphyrin pairs using scatter plots of angles between planes versus separation distances. Our MD simulations of control porphyrins show that the aggregated molecules form stacks and T-shapes as shown in Figure 37a. TPP and TATPP form

more stacks than ATPP. The amino groups in TATPP orient the molecules to stack in a parallel fashion, which allows H-bonds to form. In comparison, stacks are found to be more staggered in TPP and ATPP. The TPP molecules in water afford both H- and J-type aggregates, which were previously observed in other porphyrin systems.[223, 229] It is worth noting that stacks and T-shapes were seen on phenyl porphyrin dimers in liposome vesicles.[230]

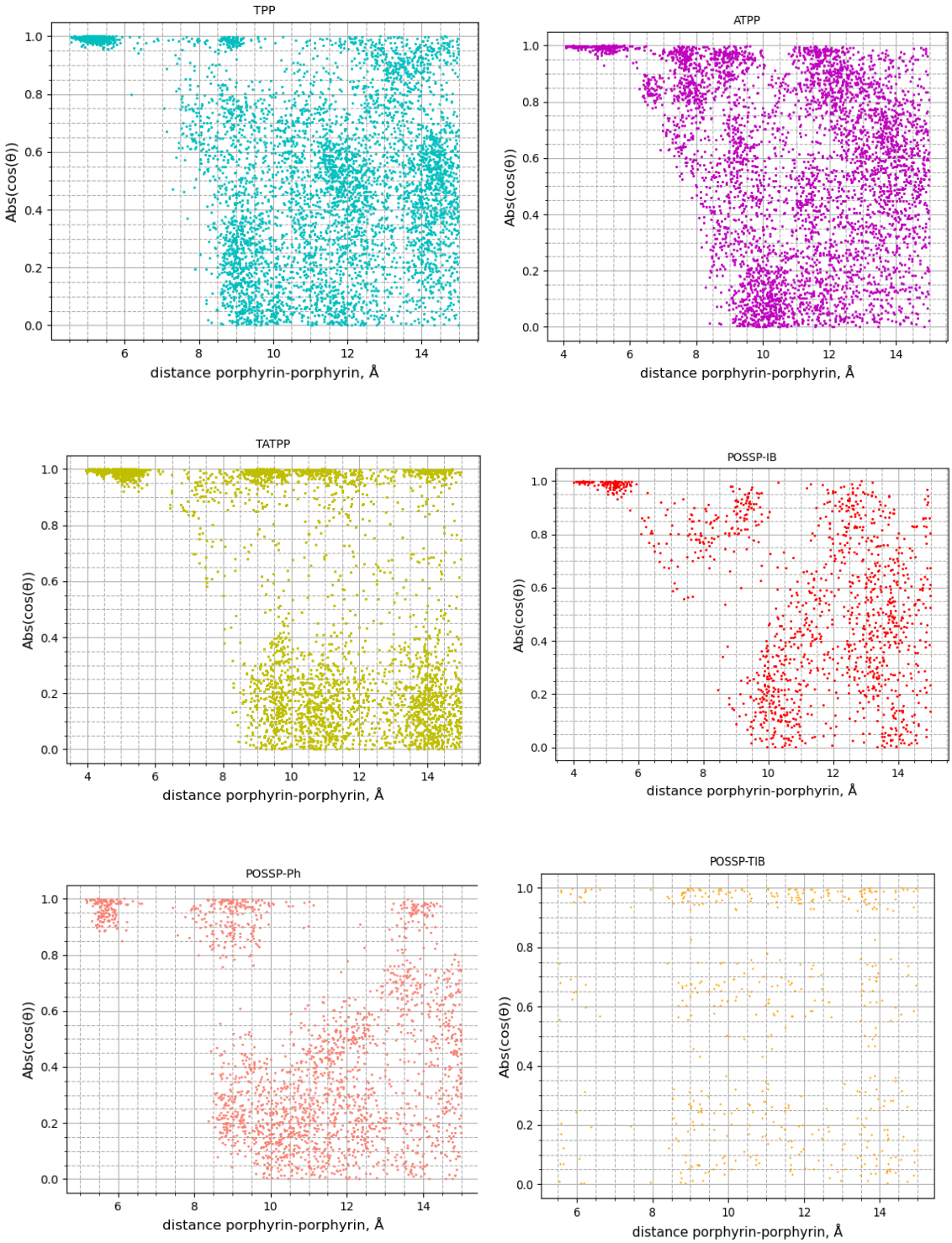

Figure 36. Angle between porphyrin planes vs distance between the porphyrin moieties of all pairs of molecules with a distance < 15 nm between porphyrin centroids from 120-150 ns.

Our MD simulation results show that most of the control porphyrin molecules form small stacks (2-3 molecules per stack) with variation in stacking angle distributions depending on the system (Figure 41). In TPP and ATPP, the coulombic repulsion between the porphyrin cores displaces the molecules, resulting in a stacking angle that spans the range between H- or J-aggregates. In contrast, the amino groups in TATPP form H-bonds with the other molecules in the stack, preventing the molecules from sliding with respect to each other, resulting mainly in H-aggregates. The porphyrin core only formed H-bonds to water from its inner nitrogen atoms. In all the control porphyrins, some stacks were found that trap a water molecule between two porphyrin cores (Figure 37c). It has been noted previously that bridging water between two layers of porphyrins can shape the final morphology.[70]

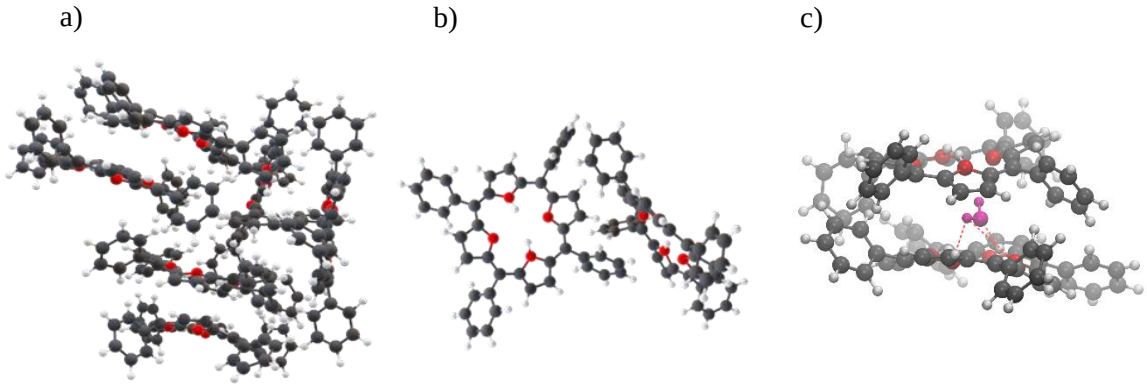

Figure 37. Representative porphyrin configurations. a) One of the TPP aggregates at 150 ns showing stacks and T-shaped configurations. b) Example of TPP T-shape. c) Water (in purple) in the middle of an H-stack of TPP forming H-bonds (red lines) with only one porphyrin. C atoms in grey, N atoms in red, H atoms in white.

It is also observed that the amino groups of ATPP and TATPP intermittently form H-bonds with the core of another porphyrin stabilizing T-shaped configurations, but not stacks. The porphyrins

that made contact in all POSS-porphyrins arranged into both stacks and T-shapes. Examples of molecular orientations are shown in Figure 37. Compared to the isobutyl substituted molecules, POSSP-Ph formed more stacks; and, on average, each porphyrin had contact with a larger number of other porphyrins (Table 4 and Table 7).

T-shapes, where the molecules are oblique to each other, have optical properties that are intermediate between H- or J-aggregates.[231-232] Depending on the angle between the molecules, the homo-FRET quenching could be reduced with respect to stacks.[48, 225] So, in general, T-shapes result in different optical properties where quenching would be less severe as in stacks. Visual inspection of the simulations reveals a common arrangement of the T-shaped pairs (Figure 37b). Figure 38a shows the trends of the different systems with respect to the formation of T-shapes. In particular, POSSP-TIB only formed one stack where each porphyrin was interacting with one neighbor porphyrin as a T-shape (Figure 38b). TATPP forms preferentially stacks than T-shapes due to the H-bonds between the amino groups that stabilize the stacks. The POSS-porphyrins form less T-shapes than TPP and ATPP because of the steric effect of the POSS cage, which is obvious in the case of POSSP-TIB. Most of the neighbors of the control porphyrins TPP and ATPP are forming a T-shape instead of a stack and this trend stays with the addition of any of the POSS cages.

In the same way that the POSS cage prevents the formation of porphyrin stacks, it also hinders the formation of T-shapes, and this effect is more accentuated in the isobutyl POSS molecules too.

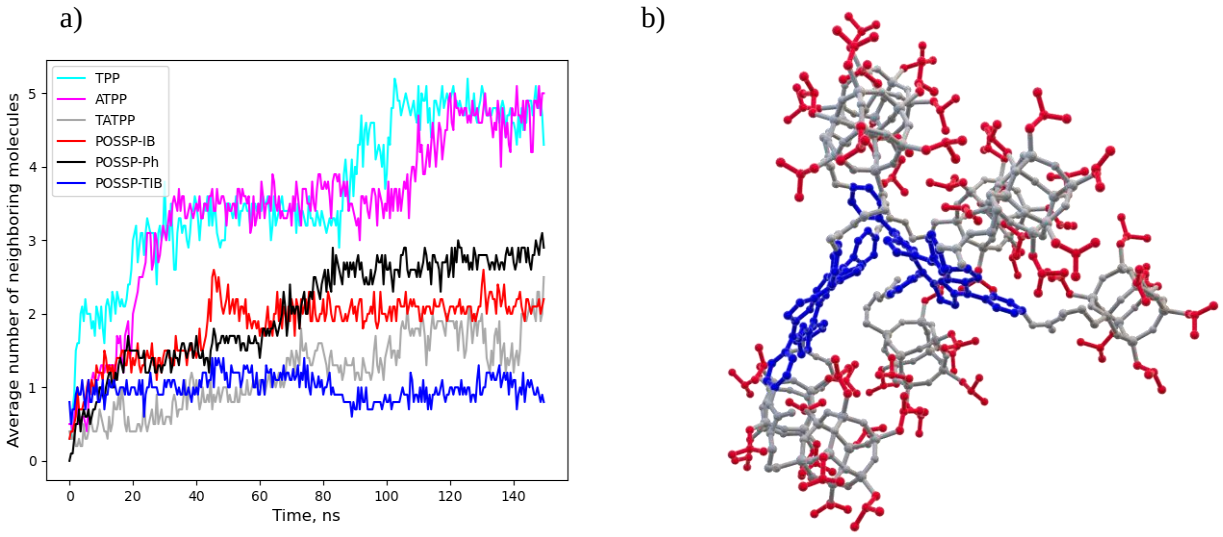

Figure 38. a) Average number of t-shaped pairs showing the reduction on number of T-shapes upon adding a POSS cage. b) Example of POSSP-TIB T-shape. POSS cage in grey, POSS substituents in red and porphyrin in blue. Water and H atoms omitted for clarity.

3.3.4 Molecular correlations

To study the intramolecular and intermolecular interaction between the porphyrin and POSS of the same POSSP, and between POSS of other POSSP molecules a radial distribution function (RDF) analysis was carried out. The analysis of RDFs in a MD simulation of peptide–perylenediimide dimers gleaned insight on the type of interactions that stabilized the preferred conformations of the dimer and predicted the overall balance between them.[233] Figure 39 depicts the RDFs between the POSS cage and porphyrins and POSS cage-cage. In Figure 39a, which shows the RDF between porphyrin and POSS belonging to the same molecule, the peak at 8.4 Å shows that the POSSP-Ph molecules have a propensity to have the porphyrins sitting on top of its own POSS cage as exemplified in Figure 32c, likely due to the coulombic interactions between the phenyl groups. From Figure 39a, the sharper peak for POSSP-Ph points to a more consistent, bent, molecular

conformation while POSSP-IB and POSSP-TIB with their broader peaks at 10-15 Å have the POSS cage and the porphyrin moiety moving more independently from each other. Figure 39b shows the POSS-POSS interaction distribution between different POSSP molecules. The isobutyl POSS in POSSP-IB and POSSP-TIB are able to get closer than the phenyl POSS in POSSP-Ph, probably because both the higher flexibility of the isobutyl groups compared to the phenyl substituents, and the strong hydrophobic interactions. This confirm that the aggregation of POSSP-IB and POSSP-TIB is driven mainly by the hydrophobic effect. Figure 40 includes other RDFs as a reference.

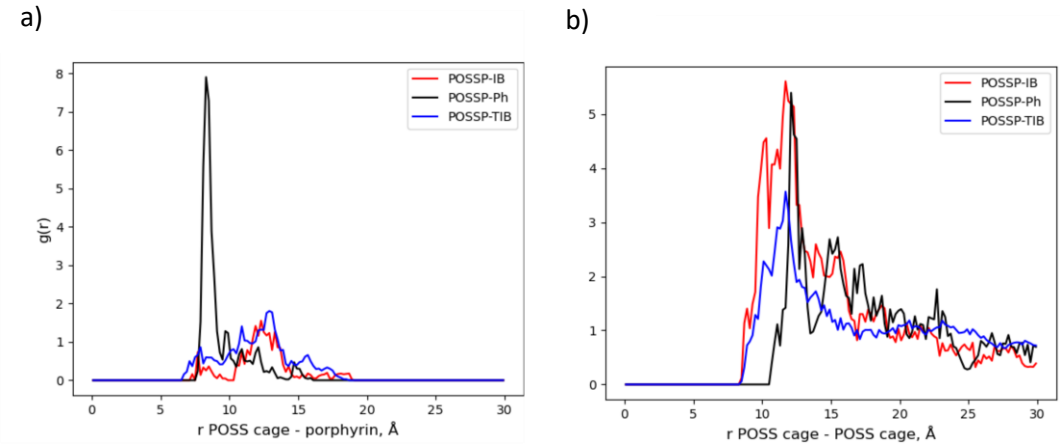

Figure 39. Radial distribution functions (averaged over 120-150 ns) of a) POSS cage to porphyrin in the same molecule, showing how in POSSP-Ph there is a larger number of porphyrins sitting on top of a POSS cage (first peak). b) POSS cage to POSS cage in different molecules, showing the isobutyl cages of POSSP-IB and POSSP-TIB tend to be closer together than phenyl POSS cages.

Table 5 summarizes the number of H-bonds associated with water or amino groups that are present in the self-assembled structure. The POSS cage in POSSP-Ph has a greater number of H-bonds to water per POSS because the phenyl groups, being more rigid, allowing more water to come closer

to the Si-O cage. The POSS cages also form H-bonds to the urea groups, but only in the same molecule.

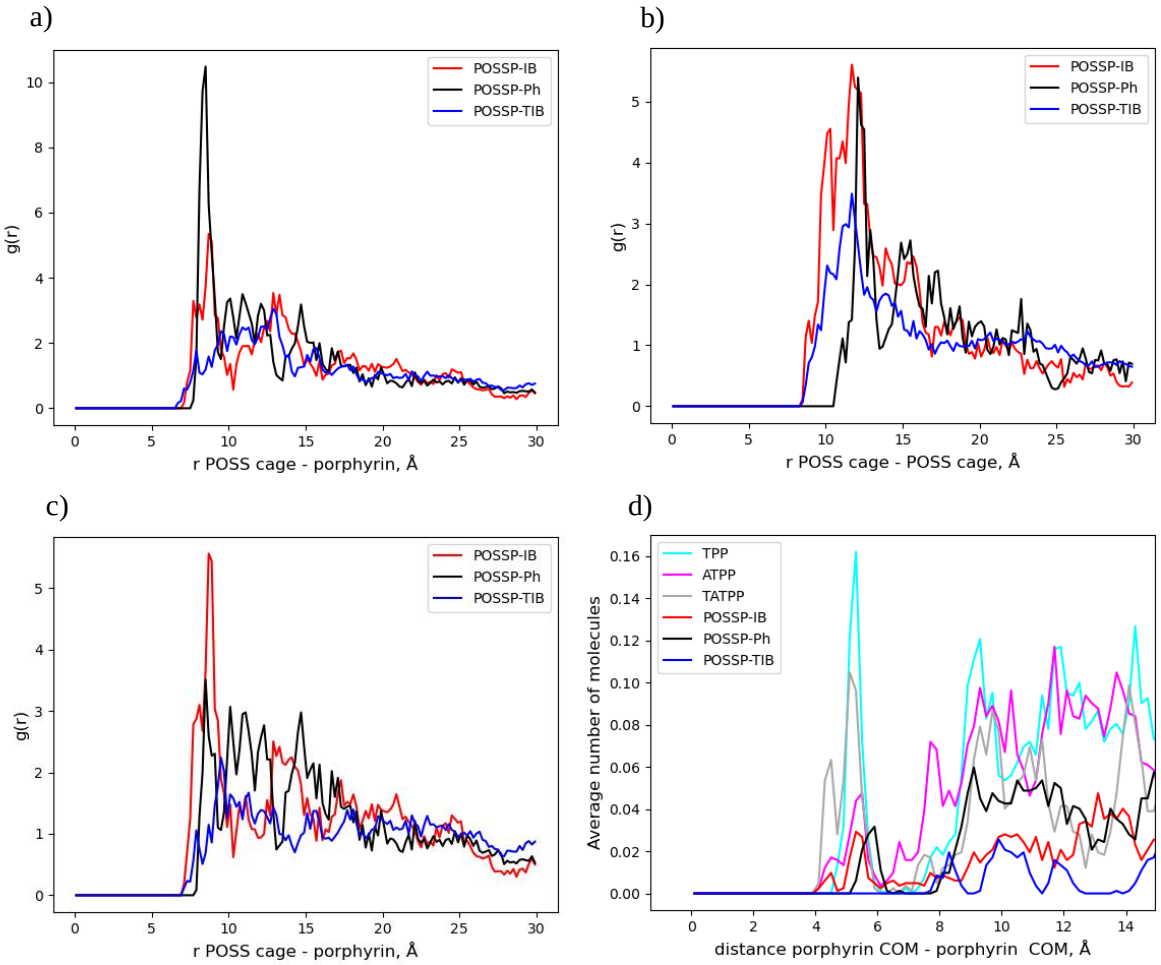

Figure 40. Radial distribution functions (averaged over 120-150 ns) of a) POSS cage to porphyrin in the same and different molecules. b) POSS cage to POSS cage in in the same and different molecules. c) POSS cage to porphyrin in different molecules. d) Frequency of distances between porphyrin moieties (averaged in the range 120-150 ns) including all molecules.

Table 5. Average [JV63]number of H bonds per molecule in the range of 120-150 ns.

	SiO to urea	**SiO to water**	**Amino or urea to amino or urea**	**Amino or urea to porphyrin**	**Amino or urea to water**	**Porphyrin core to water**	**SiO to urea same molecule**
TPP	NA	NA	NA	NA	NA	0.7 ± 0.04	NA
ATPP	NA	NA	0.0 ± 0.00	0.1 ± 0.02	2.1 ± 0.05	1.1 ± 0.05	NA
TATPP	NA	NA	0.7 ± 0.09	0.1 ± 0.02	9.0 ± 0.09	1.7 ± 0.05	NA
POSSP-IB	0.0 ± 0.00	0.7 ± 0.04	0.0 ± 0.00	0.0 ± 0.00	2.1 ± 0.05	1.3 ± 0.05	1.5 ± 0.02
POSSP-Ph	0.0 ± 0.00	2.3 ± 0.07	0.0 ± 0.00	0.0 ± 0.00	2.5 ± 0.06	1.4 ± 0.05	1.6 ± 0.02
POSSP-TIB	0.0 ± 0.00	4.8 ± 0.10	0.0 ± 0.00	0.0 ± 0.00	7.8 ± 0.15	0.9 ± 0.05	7.1 ± 0.07

Figure 41 shows the frequency of distance between the porphyrin moieties of the molecules when stacked. Because of geometry, the stacked molecules that are closer together are mainly H-aggregates while the more distant ones are J-aggregates. We identified three distance ranges, 4.0-4.7 Å (H-aggregates), 4.8-6.6 Å (mix) and 6.7-20.0 Å (J-aggregates) (Table 6). TATPP and POSSP-IB stacks that fall here are H-aggregates; but TPP, ATPP and POSPP-Ph are too close to the limit between H- and J-aggregates and cannot be classified. Stacks in the third range are always

J-aggregates. For the control porphyrins, TPP mainly formed stacks that are right at the limit between H- and J- aggregates, while almost all TATPP stacks were H-aggregates.

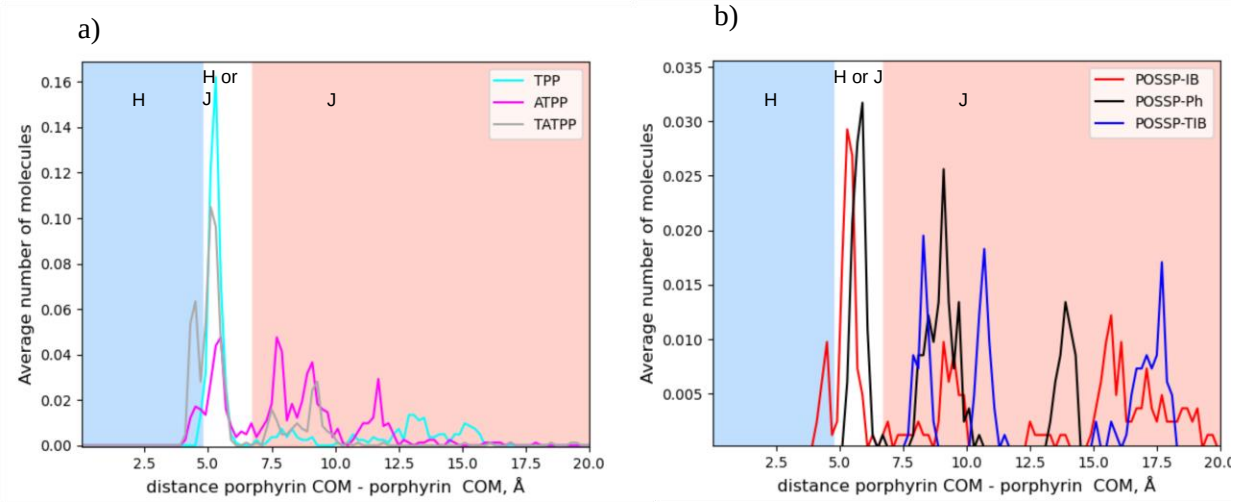

Figure 41. Frequency of distances between porphyrin moieties (averaged in the range 120-150 ns) of only stacked molecules, showing the distribution of H- and J-aggregates. a) control porphyrins b) POSS-porphyrins

POSS-porphyrins systems, as expected, resulted in much less stacks than the control porphyrins due to steric impediment. Table 7 indicates how many stacked molecules there are for each system. The arrangement of the stacks that emerge was influenced by the POSS moieties. POSSP-IB showed a tendency to form H-aggregates while POSPP-Ph and POSPP-TIB stacks were almost all J-aggregates (Figure 41b).

Table 6. Stacking angle by range of distance between porphyrins in stacked molecules. Averaged over the timesteps 120-150 ns.

Distance between porphyrin COMs	**4.0-4.7 Å**	**4.8-6.6 Å**	**6.7-20.0 Å**
TPP	73.9 ± 8.9°	48.9 ± 6.0°	24.1 ± 7.1°
ATPP	78.3 ± 3.5°	52.4 ± 6.5°	29.7 ± 10.3°
TATPP	78.1 ± 5.3°	66.2 ± 8.6°	34.9 ± 11.1°
POSSP-IB	78.7 ± 6.5°	64.8 ± 4.7°	17.6 ± 9.0°
POSSP-Ph	No stacks	56.7 ± 10.4°	25.6 ± 8.4°
POSSP-TIB	No stacks	No stacks	26.3 ± 6.5°

Table 7. Properties of the stacks formed averaged over the timesteps between 120-150 ns.

	TPP	**ATPP**	**TATPP**	**POSSP-IB**	**POSSP-Ph**	**POSSP-TIB**
Fraction of all the molecules that are forming part of a stack	91.8 ± 0.05%	83.5 ± 0.03%	95.6 ± 0.02%	45.6 ± 0.06%	51.3 ± 0.04%	33.3 ± 0.04%

Figure 32c and d provide examples of POSSP-IB and POSSP-Ph stacks. As described in Figure 40a, porphyrins in POSSP-Ph molecules are very attracted to the phenyl POSS of its own molecule and stick to it. This causes steric impediment at the porphyrin, hindering face to face stacking,

which explain why most of the POSSP-Ph form J-aggregates. POSSP-TIB, with its higher number of POSS cages per molecule, has also steric impediment at the porphyrin faces that staggers the stacks forming J-aggregates. As can be seen in Figure 42, the nitrogen atoms in the TPP porphyrin core are charged negatively while the acid protons have a positive charge. The molecules are not stacking exactly on top of each other but are slightly staggered to avoid having equal sign charges close to each other. With the staggering, the positively charged protons become closer to the negatively charged nitrogen atoms, favoring this arrangement and a stacking angle close to the limit between H- and J-aggregates (54.7º).

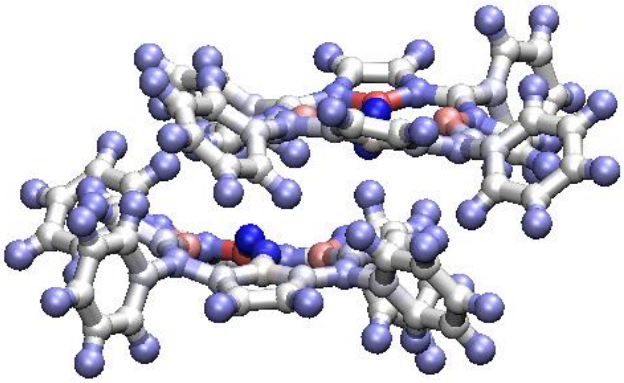

Figure 42. Stack of TPP showing partial charges of the atoms. Blue is positive, while red is negative. The more saturated the color, the higher the charge.

In all the molecules where the stacks were arranged face to face in an H-aggregate, we detected two main stabilizing factors. First, only in TATPP, H bonds between the amino groups keeping the molecules aligned face to face. Second, the presence of a water molecule in the middle of H-stacks, having an H bond with a nitrogen in at least one the porphyrin cores, sometimes with both, as shown in Figure 37d.

Table 8 quantifies the number of water molecules sandwiched inside porphyrin stacks, showing how most H-stacks include one. This water partly screens the coulombic interactions between porphyrin cores, allowing them to stack with less displacement.

Table 8. Percentage of stacked pairs that have a water sandwiched between the porphyrins and the water is forming a H bond with at least one porphyrin.

	H stacked pairs (stacking angle >60º)	**HJ stacked pairs (stacking angle between 50-60º)**	**J stacked pairs (stacking angle <50º)**
TPP	90.2% ± 0.4%	6.9% ± 0.4%	7.9% ± 0.1%
ATPP	98.9% ± 0.1%	22.1% ± 0.6%	48.9% ± 0.8%
TATPP	98.2% ± 0.1%	57.3% ± 0.7%	62.7% ± 1.0%
POSSP-IB	99.4% ± 0.1%	62.5% ± 0.8%	18.7% ± 0.3%
POSSP-Ph	100.0% ± 0.0%	0.0% ± 0.0%	50.8% ± 0.8%
POSSP-TIB	There are no H or HJ aggregates		34.6% ± 0.6%

3.4 Conclusions

The aggregation in water of three different POSSP molecules (POSSP-IB, POSSP-Ph and POSSP-TIB) was studied using MD. The POSSP molecules have different substituents in their POSS units including isobutyl and phenyl. MD simulations show that POSSP's aggregation is mainly driven by the hydrophobic effect related to the hydrophobicity of their substituents. However, in the case of POSSP-Ph, π-π and H-bonding interactions also play a role. The morphology analysis of the

final aggregates shows that isobutyl substituents, which are more hydrophobic than phenyl, produce tighter aggregates. In addition, in the case of POSSP-IB and POSSP-TIB, the isobutyl POSS cages cluster together in the middle of the aggregates leaving the porphyrins on the surface with a larger separation between them. This larger separation has a major impact on the photophysical properties of these molecules as was already shown experimentally by our group (Chapter 2).[23] The MD simulations also show that POSSP-Ph molecules are more stable in water. The phenyl substituents on the POSS cage are coulombically attracted to the porphyrins, resulting in a more homogeneous arrangement. These results demonstrate that the chemical nature of the substitutions on the POSS cages do impact the aggregation process and the morphology of the aggregates.

CHAPTER 4. FABRICATION AND CHARACTERIZATION OF POSS-PORPHYRIN PARTICLES USING THE REPRECIPITATION METHOD

4.1 Introduction

Self-assembled porphyrin particles have been studied for optical devices, theranostics, sensors, and catalysis. POSS-porphyrin molecules are hybrid building blocks that can be used in template-free processes leading to the formation of nano- and micro-objects via "bottom-up" strategies. Specific molecular packing and aggregation are efficient tools enabling the control of morphology, physicochemical characteristics and performance of POSS-porphyrin materials.[74-75] Formation of hierarchical superstructures by those unique self-assembling molecules can play an important role in fields such as energy, adsorption, separation, catalysis and biomedicine.[234] In this Chapter, we present our preliminary results on the fabrication of POSS-porphyrin particles using the reprecipitation method.

One common and simple method to prepare self-assembled particles is to add a non-solvent to a porphyrin solution while mixing vigorously, the so-called reprecipitation method,[99, 112-115] or in the presence of sonication.[116] Occasionally, the formed nanoparticles are stabilized with PEG or other surfactants. [115,112] Porphyrin nanoparticles have also been prepared by solubilizing a hydrophpbic porphyrin molecule in water by lowering the pH and then adding a basic surfactant such as CTAB, which has the double function of increasing the pH, turning the porphyrin insoluble, and stabilizing the produced colloid particles.[125] Herein, we used the reprecipitation method because it is a simple method that produces narrow size distributions and is reproducible.[112, 117-118] In the reprecipitation approach, also called mixed-solved precipitation method, the molecules are dispersed in a solvent with good solubility before combination with a solvent with poor solubility. The presence of the poor solvent decreases the thermal motion of the nanoparticles, which adjust their positions to

minimize the energy of the system until they reach an equilibrium and form a self-organized pattern with a minimum value of energy due to the increased organization.[235-236] This approach also has the advantage of being simple and reproducible.

By building POSS-porphyrin nanoparticles, a series of unique structural and optical features are expected for the final material compared to the parent porphyrin. Some of those changes are: the different stacking geometry and morphology, the impact on the fluorescence and singlet oxygen quantum yield, the band shifting on the UV-Vis absorption and fluorescence emission, and the effect on the fluorescence lifetime and self-quenching phenomena. Figure 43 shows the typical UV-vis spectrum of porphyrins. After self-assembly, changes in the absorption spectrum can yield information regarding the type of aggregation between the porphyrin molecules, whether it is J- or H-type.[113, 115-116] Although the self-assembly of the porphyrins could quench their fluorescence, it has been observed that in some cases that is not the case. In particular systems only a slight reduction in luminescence have been seen when comparing the colloid in water to the monomeric solution in an organic solvent.[112,237,99, 238]

In this chapter, we present our preliminary results on the synthesis of POSS-porphyrin materials using the reprecipitation method. Materials using TPP, ATPP and POSSP-IB were fabricated and characterized using SEM, UV-vis spectroscopy, steady state and time-resolved fluorescence spectroscopy, and dynamic and resonance light scattering.

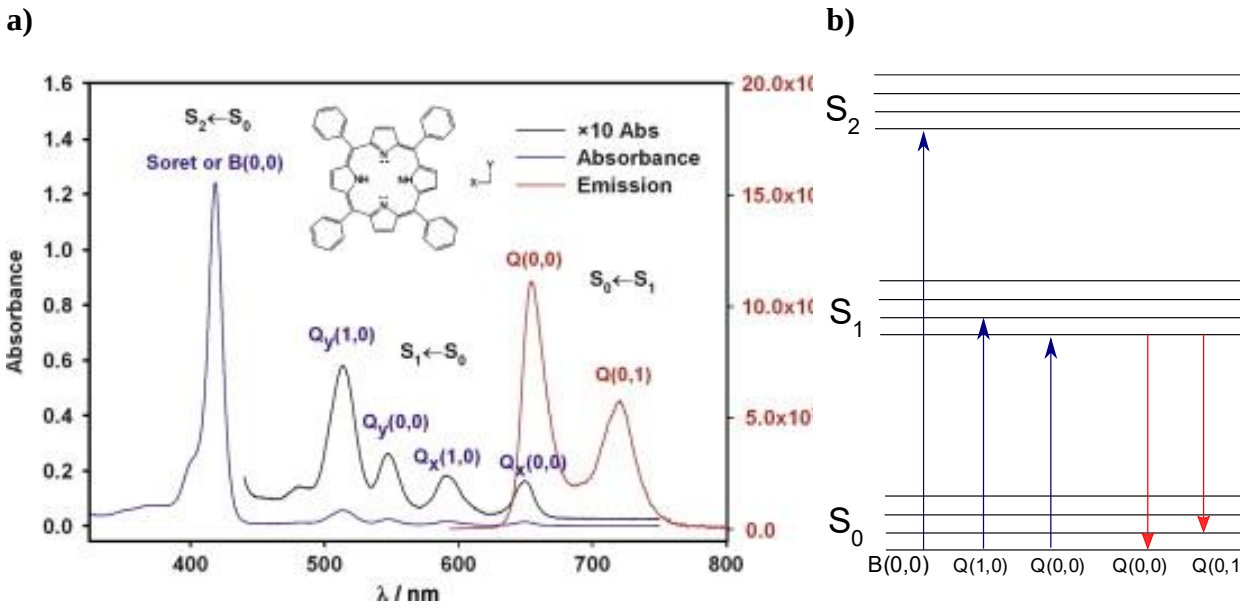

Figure 43. a) Typical porphyrin UV Vis transitions exemplified by TPP in toluene.[239] b) Jablonski diagram for the transitions

4.1.1 Resonance light scattering (RLS)

Besides absorbing light, aggregates also scatter it due to differences in polarizability with the solvent. This light scattering is enhanced at wavelengths were absorption takes place. This effect is called resonance light scattering (RLS). In monomeric solutions, RLS is weak compared to the absorption; however, as the volume of the aggregate increases, the absorption increases linearly. On the contrary, the light scattering depends on the square of the volume; so, it becomes more noticeable.[132] Therefore, RLS is observed as an elastic scattering signal at the wavelength of absorption related to the aggregate. This effect can also be enhanced when there is strong electronic coupling between the molecules in the aggregate, as happens frequently with chromophores.[132, 240] Figure 44 illustrates an example of the RLS technique for monitoring the aggregation of porphyrins with increasing ionic strength.

RLS spectra can be obtained using the synchronous scanning mode of a fluorimeter where emission and excitation are scanned in a given range and set to the same value throughout the scanning.[241]

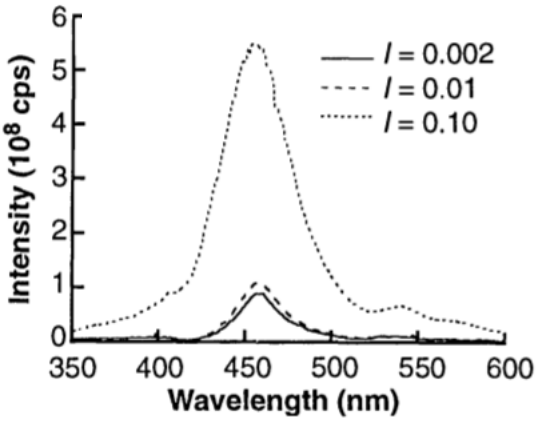

Figure 44. RLS profiles of an aggregating porphyrin as a function of ionic strength, I.[132]

Even though RLS is a technique that allows the "selective observation of aggregates"[52]; the interpretation needs to be carefully carried out since strongly absorbant samples can mask the scattering peaks.[132, 241]

4.2 Fabrication of porphyrin and POSS-porphyrin nanoparticles

4.2.1 Materials and methods

4.2.1.1 Materials

All commercial solvents were of reagent grade or higher and were used as received. 5-(4-aminophenyl)-10,15,20-(triphenyl)porphyrin (ATPP), 5,10,15,20-tetra(4-aminophenyl) porphyrin

(TAPP) and 5,10,15,20-(tetraphenyl)porphyrin (TPP) were purchased from Frontier Scientific (Logan, UT, USA). POSSP-IB was synthesized and characterized as described in Chapter 2.[23]

UV-vis spectra were recorded on a Cary 300 UV-visible spectrophotometer. Fluorescence and resonance light scattering (RLS) spectra were measured using a RF-5301 PC Shimadzu fluorimeter. Fluorescence time-resolved measurements were taken on a Jobin Yvon-Spex Fluorolog equipped with a 389 nm diode laser for time-resolved photoluminescence (PL) decay measurements. Dynamic light scattering (DLS) and ζ-potential measurements were carried out using a Malvern Instrument Zetasizer Nano (red laser 633 nm) (Malvern Instrument Ltd., Malvern, UK).

4.2.1.2 Methods

4.2.1.2.1 UV-Vis/Fluorescence spectroscopy

The UV–Vis spectra were recorded from 300 to 800 nm using the solutions in DI water of self-assembled ATPP, TPP, or POSSP-IB in quartz cuvettes (1 cm path length). The fluorescence spectra were obtained in the same solutions described above using an excitation wavelength of 420 nm. The fluorescence spectra were recorded from 600 to 800 nm.

4.2.1.2.2. Dynamic light scattering and ζ potential measurements.

The hydrodynamic diameter and ζ potential of the porphyrins or POSSP particles in DI water were assessed by DLS using Malvern Instrument Zetasizer Nano (red laser 633 nm). The equilibration time for the samples was set to 2 min, and three measurements taken on each sample. Measurements were performed in triplicates, and the data is reported as average ± SD.

4.2.1.2.3. Time-resolved fluorescence measurements.

The solutions of self-assembled porphyrins or POSSPs in DI water were measured along solutions of the same molecules in $CHCl_3$ (3.3 μM). Quartz cuvettes with 1 cm path length were used. The fluorescence was detected at 654 nm with a bandpass of 10 nm. The detector voltage was 950 V. Coaxial delay of 95 ns, measurement range was 100 ns and a peak preset of 10,000 counts. The excitation LED was set to a repetition rate of 1 MHz with a sync delay of 20 ns. The instrument response was measured using solvent blanks with the same instrument conditions.

4.2.2 Preparation method

The first generation of self-assembled particles was made using THF as a solvent and an aqueous sodium phosphate buffer (1 mM, pH = 7) as non-solvent (Figure 45). Variant I was made by adding 0.3 mL of a $1.0x10^{-4}$ M solution in THF of either a porphyrin or a POSSP molecule to 5 mL of phosphate buffer. The mixture was sonicated for 10 minutes. For Variant II, 0.3 mL of a $1.0x10^{-4}$ M solution in THF of either a porphyrin or a POSSP molecule to a mixture of 4 mL of phosphate buffer with 1 mL of THF. After sonication for 10 minutes, 1 mL of the phosphate buffer was added so the total volume of the aqueous solvent was 5 mL, same as in variant I. The difference between variants I and II was the initial amount of THF in the solution.

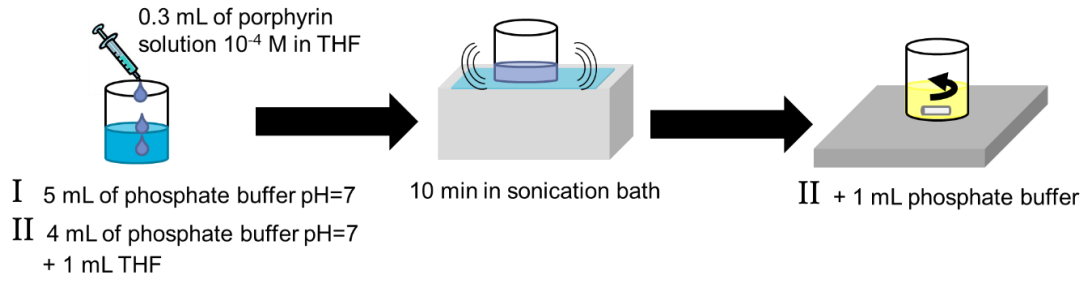

Figure 45. Preparation method for the first-generation particles.

To afford the second-generation of self-assembled particles $CHCl_3$ was used as a solvent, DI water was the non-solvent and methanol was used to create an initial homogeneous solvent mixture. According to its ternary phase diagram (Figure 46), the $CHCl_3$/methanol/water system is miscible at methanol concentrations above 40%. A volume of 0.1 mL of porphyrin or POSSP-IB [JV64]of a stock solution of $3.33x10^{-4}$ M in $CHCl_3$ is slowly added to a mixture of 10 mL of methanol and deionized water (50/50% vol.). The container is shaken until a single solvent phase is obtained. The solution is placed in a 25º C water bath for 24 h; in this way, $CHCl_3$ and methanol solvents evaporate. At the end, a yellow aqueous solution is formed as an indication that nanoparticles have been formed. The material is stored in water.

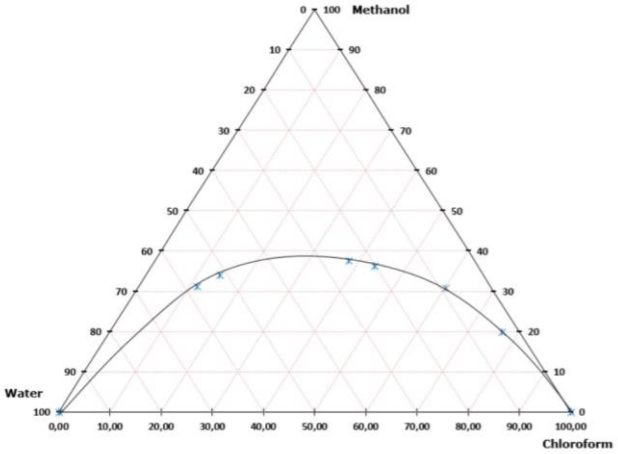

Figure 46. Ternary phase diagram of the miscibility of the water/methanol/$CHCl_3$ system. The black curve separates the monophasic system (above) from the biphasic (below).[242]

The rest of the control porphyrin and POSSP molecules was not prepared using this second-generation method due to issues unrelated to the laboratory, but this is proposed as future work.

4.2.3 Results

4.2.3.1 First-generation particles

The size of the self-assembled [JV65]particles was analyzed out using DLS (Table 9).

Table 9. Dynamic light scattering and ζ-potential data. First-generation particles

First-generation self-assembled particles	**Variant**	**Z-average (d/nm)**	**PDI**	**Z-potential (mV)**
TPP	I	96 ± 1	0.17 ± 0.02	-15 ± 1
ATPP	I	169 ± 2	0.20 ± 0.03	-59 ± 1
ATPP	II	207 ± 3	0.08 ± 0.01	-60 ± 5
TAPP	I	186 ± 7	0.24 ± 0.01	-38 ± 1
POSSP-IB	I	243 ± 24	0.4 ± 0.05	-84 ± 6
POSSP-Ph	I	116 ± 2	0.14 ± 0.01	-42 ± 3
POSSP-Ph	II	146 ± 3	0.16 ± 0.02	-51 ± 1
POSSP-TIB[JV66]	I	970 ± 30	0.38 ± 0.13	-12 ± 1

DLS data (Table 9) show that POSSP-TIB and POSSP-IB tend to have a hydrodynamic diameter larger than the control porphyrins, but POSSP-Ph hydrodynamic diameter is within the control

porphyrins range. Comparing variants I and II for ATPP and POSSP-Ph, variant II samples tend to have larger hydrodynamic diameters. This could be an effect of the LaMer mechanism of particle growth.[243] Variant II, having a larger initial volume of solvent (THF), would increase the critical monomer concentration at which the "burst -nucleation" is triggered, resulting in fewer nuclei formed at this step. Having fewer nuclei would result in an increased final particle size.

Commercial THF includes butylated hydroxytoluene (BHT) as a peroxide inhibitor. While testing the first-generation self-assembled particles, we realized that BHT has been found to quench singlet oxygen,[244-245] and has also been found to quench fluorescent molecules.[246] We carefully removed BHT from a small volume of THF by filtering through activated carbon and Celite. This BHT-free THF was used to make a sample of self-assembled TPP I. At the same time, we prepared another TPP I sample, but using normal THF containing BHT. The difference in fluorescence intensity was appreciable visually using an UV lamp, the sample where BHT-free THF was used had a much higher emission intensity. We hypothesize that BHT can be incorporated into the porphyrin self-assembly, which results in quenching the fluorescence.

Given the disadvantages found for the use of THF and the possible formation of phosphate nanoparticles that could also be interfering with the self-assembly process, we decided to develop a second procedure using a different organic solvent and only DI water as a non-solvent. Another modification was made to refine the second protocol; sonication was removed since it involved a significant increase of the samples temperature. The procedure for the second-generation particles is described above and it involves $CHCl_3$ as the solvent, DI water as the non-solvent and methanol to homogenize the initial mixture.

For the second-generation self-assembly procedure, the structural characterization of TPP, ATPP and POSSP-IB particles was carried out using DLS. DLS data revealed a higher hydrodynamic

diameter for the particles obtained with the control porphyrins TPP and ATPP (327 ± 24 and 334 ± 4 nm) compared with POSSP-IB (286 nm) (Table 10).[JV67][PL68] The surface charge for the three particles is negative as indicated by the ζ-potential values with the ones fabricated using ATPP having the lowest value (-54 ± 14 mV).

Table 10. Dynamic light scattering and ζ-potential data of the second-generation particles.

Second generation particles	**Z-average (d/nm)**	**PDI**	**Z-potential (mV)**
POSSP-IB	286	0.2	-21
ATPP	334 ± 4	0.08 ± 0	-54 ± 14
TPP	327 ± 24	0.16 ± 0.03	-29 ± 2

The photophysical properties of the nanoparticles were investigated using UV-vis spectroscopy, steady state and time-resolved fluorescence spectroscopy, and resonance light scattering. Figure 47a shows the UV-Vis spectra of the nanoparticles. For both materials fabricated with the control porphyrins, TPP and ATPP, the Soret band becomes split; while the Soret band of the POSSP-IB particles does not.[JV69] It is difficult to compare the bands of the self-assemblies to the monomers because of the difference in solvents. The lambda maxima (λ_{max}) for the Soret bands of TPP, ATPP, and POSSP-IB in THF (monomers) are at 416, 419, and 416 nm, respectively (Table 1, Chapter 2).

From Figure 47 we can notice that the Soret band of the POSSP-IB particle is slightly different from the monomer in THF (λ_{max} = 421 vs λ_{max} = 416 nm), but for the control porphyrins this

difference is quite remarkable; λ_{max} = 435-446 vs λ_{max} = 416 nm for TPP, and λ_{max} = 425-462 vs λ_{max} = 419 nm for ATPP. Since we do not know the position of the λ_{max} for the Soret band associated to the monomers in water, we cannot tell if the self-assemblies bands are red or blue shifted with respect to the monomers bands. Interestingly, comparing the Q bands of the self-assemblies in Figure 47 to the Q bands of the monomers in THF in Figure 12, we noticed that the positions are very similar, having differences of maximum 3 nm between the particles and the monomers.

a) b)

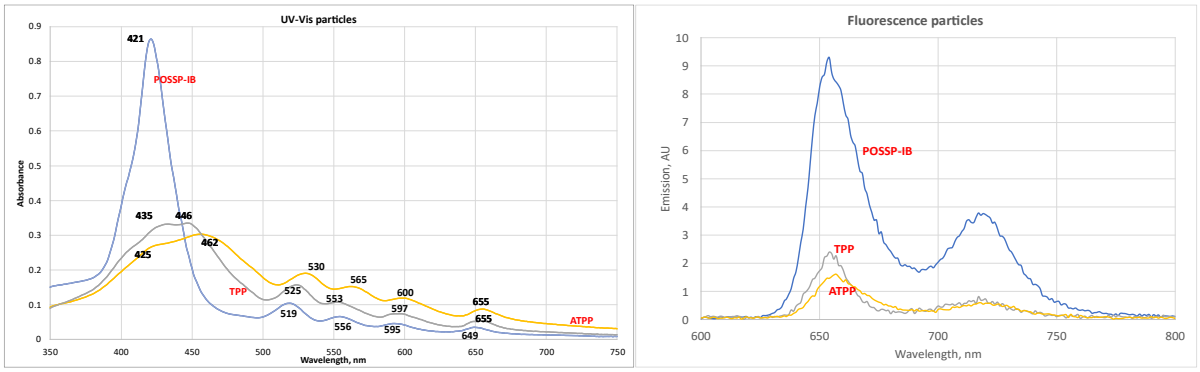

[JV70]

Figure 3. a) UV-Vis of the self-assembled particles and b) Fluorescence spectra of the self-assembled particles

The fluorescence spectra of the nanoparticles show that all of them emit at the same wavelength, 656 and 719 nm, which are typical wavelengths for the emission of porphyrins[JV71]. The steady state fluorescence of the POSSP-IB particles at the same concentration is around four [JV72]times higher than the nanoparticles obtained with the control porphyrins, TPP and ATPP. Time-resolved fluorescence spectroscopy was carried out for the individual molecules (TPP, ATPP and POSSP-IB) in $CHCl_3$[JV73][PL74][PL75] (Figure 48a)[JV76]. In a similar way, the nanoparticles were

characterized using time-resolved fluorescence spectroscopy in water (Figure 48b)[JV77]. The fluorescence lifetime values were fitted from the instrument response and samples curves of the individual molecules and nanoparticles using the software DecayFit (http://www.fluortools.com) (Table 11). ATPP and TPP particles were better modeled by a two-term polynomial, describing two fluorescence lifetimes components. Fluorescence lifetime values have a complex relation to the solvent used since they depend on the solvent refractive index,[247-248] oxygen concentration, pH,[249] and H-bond donating capacity.[250] Therefore, comparison between fluorescence lifetime values obtained in different solvents is complicated. However, we can compare the values of the molecules/particles that were obtained using the same solvent.

a) b)

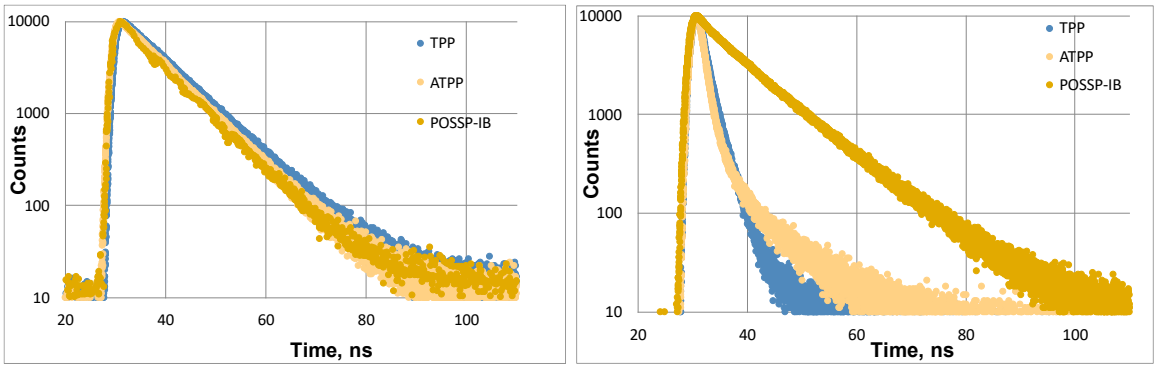

Figure 48. Fluorescence lifetime of a) monomers in $CHCl_3$ and b) self-assembled particles in DI water.

Table 11. Fluorescence lifetime in nanoseconds.

	Monomers	**Particles (in H_2O) (n = 2)**

	(in $CHCl_3$)	First term, weighting factor	Second term, weighting factor
ATPP	8.4	3.5 ± 0.3, 0.90	8.2 ± 0.3, 0.10
TPP	8.8	2.3 ± 0.1, 0.96	5.0 ± 0.3, 0.04
POSSP-IB	8.6	9.0 ± 0.1	NA

To analyze the aggregation of the molecules in the nanoparticles, resonance light scattering (RLS) was used (Figure 49). At the Soret band region (approx. 410 - 450 nm), the RLS signal is considerably stronger for TPP and ATPP than for POSSP-IB. This can be an evidencing that TPP and ATPP has either larger volumes or higher concentration of particles where strong electronic coupling is happening (H- or J-aggregates).

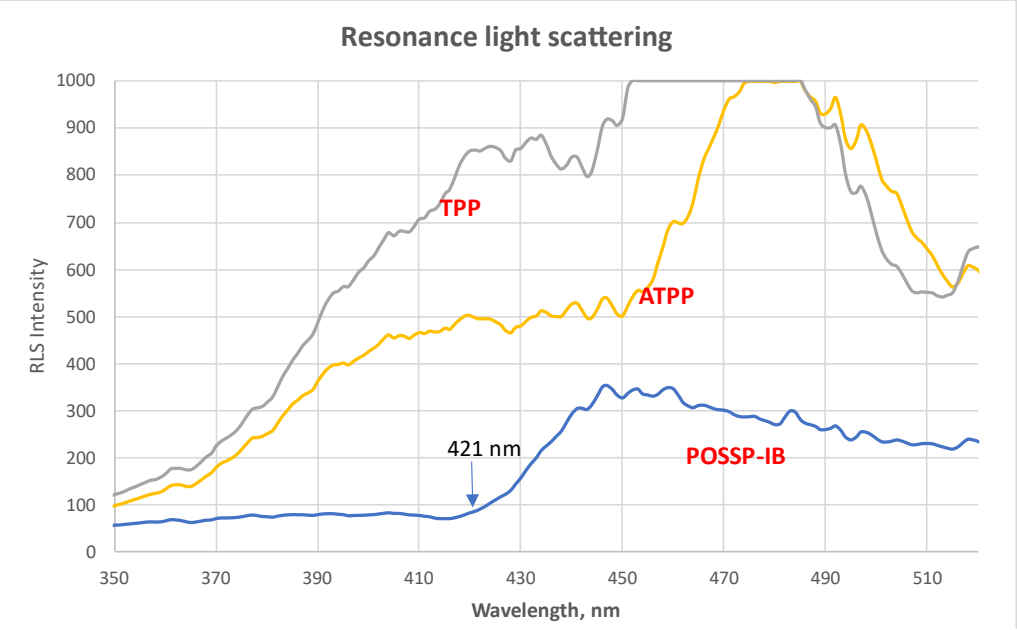

Figure 49. RLS of self-assembled TPP, ATPP and POSSP-IB

4.2.4 Discussion

POSSP nanoparticles fabricated using the first synthetic approach showed a dependence on the molecule identity and on the initial ratio of solvent/non-solvent to afford nanomaterials with different sizes. Unfortunately, the use of a phosphate buffer and THF as a solvent was not the best choice because they were interfering with the morphology and fluorescence emission of the fabricated nanoparticles.

POSS-porphyrin self-assemblies in water have been reported as quasi-spherical.[64-65] Also, an isobutyl POSS porphyrin was reported to self-assemble in organic solvents as vesicles or rods of different sizes depending on the solvent mixture and the initial concentration of the POSS-porphyrin.[74, 251] Sheet-like, spheres, nanorods and nanothorns[JV78] were formed with TATPP in organic solvents depending on the solvent mixture and the porphyrin concentration. Spheres are formed at low concentrations; however, as the concentration increases, the growth rate of the nanoparticles is higher, increasing the anisotropy and creating other shapes.[252][JV79] In all these examples, the shape of the resulting particles is determined by the balance of forces between the molecules and the solvent, and by the interaction of the molecules themselves. For the self-assembled particles of this project, we could not determine their shape because, although we analyzed the samples using TEM and SEM microscopies, we did not confirm the identity of the particles analyzed with a secondary analysis.

The split in the Soret bands of the particles synthesized with TPP and ATPP can be explained by an excitonic splitting related to the electronic coupling of molecules in close proximity like H- or J-aggregates.[55, 253] In POSSP-IB there is no evident splitting or evidence of electronic coupling, pointing to the role of POSS cage as a spacer to provide enough distance between porphyrin moieties. Furthermore, the higher fluorescence intensity obtained for the POSSP-IB particles is also another evidence confirming the POSS effect. Several reports in the literature, our own

experiments and MD simulations support the role of POSS cages as a spacer to prevent the quenching of fluorescence and of singlet oxygen geration.[23-24, 66-68]

The fluorescence lifetime values for the parent porphyrin molecules in $CHCl_3$ are similar to those of POSSP-IB, which is consistent with the rest of the photophysical properties measured for the monomers in Chapter 2. On the contrary, the fluorescence lifetime performance in water is quite different between the particles fabricated with TPP, ATPP or POSSP-IB. We notice that the life time plots for control porphyrins are made of two fluorescence decay components, pointing to the presence of two different arrangements in the material, most likely different aggregates and/or monomers. In the literature, the longer lifetime component has been associated to monomers or H-aggregates, while the shorter lifetime component is related to J-aggregates,[254] or unspecific aggregates.[255] In addition, a shorter fluorescence lifetime component can be a sign of self-quenching.[56] [JV80] The nanoparticles synthesized with POSSP-IB only showed the long fluorescence decay term, as an indication of the absence of self-quenching aggregates. This is another experimental evidence that supports the role of POSS cage in separating porphyrin molecules inside the framework.

RLS is a technique that detects scattering coming from electronically coupled chromophores at the coupling wavelengths.[132] The signals of the materials made of POSSP-IB and control porphyrins show that the scattering coming from POSSP-IB particles at the Soret wavelength is much weaker than the one related to the control porphyrins. Since scattering increases with the volume and concentration of the electronic coherent aggregates, where porphyrins are close enough to have electronic coupling, it is assumed that the lower scattering from POSSP-IB nanoparticles correlates with fewer aggregates, which is also supported by our MD simulations described in Chapter 3.

4.3 Conclusions

Our preliminary data demonstrate that by tuning the conditions in the reprecipitation method, we can fabricate nanoparticles using TPP, ATPP and POSSP-IB as precursors. The morphology of the particles synthesized with TPP or ATPP have rod- and disk-like shapes as have been previously reported in the literature.[74, 251-252] The POSSP-IB precursor forms mainly spherical nanoparticles, most likely due to the hydrophobic aggregation driven by the POSS-IB unit as we found in Chapter 3. The photophysical properties of the nanoparticles synthesized with TPP or ATPP show that there is a strong aggregation between porphyrins as indicated by the split S-band, reduction in the fluorescence intensity, lifetime values and RLS data. These data point out toward a strong aggregation self-quenching effect. On the contrary, the photophysical properties of nanoparticles fabricated using the POSSP-IB molecule as precursor show reduced aggregation self-quenching effect, most likely due to the presence of the POSS cage unit. Overall, the use of POSS-IB units has a positive impact on the photophysical properties of the nanoparticles, allowing the porphyrin molecules to preserve their fluorescence and most likely also their singlet oxygen quantum yield.[JV81]

CHAPTER 5. CONCLUSIONS AND FUTURE WORK

5.1 Conclusions

POSS and porphyrin molecules present remarkable features to develop novel building units for the fabrication of nanoscale size materials with controlled morphology, size, and chemical properties.[64-65, 74, 251] The self-assembly of POSS-porphyrin molecules has a great impact on the optical and electronic properties of the porphyrin, especially on the aggregation induced quenching phenomenon.[74, 251] In this work, we synthesized and characterized three POSS-porphyrin molecules with different functional groups in the POSS cage unit, isobutyl or phenyl (POSSP-IB or POSSP-Ph); and number of substitutions on the core porphyrin, mono or tetra (POSSP-IB or POSSP-TIB). By taking advantage of the well-known silane chemistry for the functionalization of POSS, we obtained POSS-porphyrins in relatively high yield and easy separation. This can be a promising alternative to avoid the direct functionalization of porphyrin molecules, which is usually tedious, with multiple synthetic steps, long separation protocols, and results in very low yields. Considering the broad scope of POSS chemistry,[10, 32, 256] this approach can be expanded to other functional groups. In fact, our research lab has already reported on the incorporation of hydrophilic groups to POSS-porphyrin derivatives.[23]

The POSS-porphyrin derivatives were used in photodynamic therapy and the fabrication of nanoparticles. In both scenarios, the POSS-porphyrin were exposed to aqueous environment where the self-assembly of these molecules is expected. The rational design of the POSS-porphyrin molecules pursued to evaluate the impact of the hydrophobic, aromatic and steric effect on the self-assembly of these molecules. Our experimental results for the photochemical properties of these molecules in PDT, and preliminary data of photophysical features of the nanoparticles fabricated with POSSP-IB, clearly demonstrated that there is a major impact of the POSS cage

unit on the performance of these POSSP derivatives. The POSSP molecules with hydrophobic substituents afforded aggregates/nanoparticles in aqueous environment with the highest singlet oxygen quantum yield, strongest PDT effect on cancer cells, and reduced aggregation self-quenching effect. Similar outcomes have been reported for other systems containing POSS cages, which have been explained by considering the role of POSS as molecular spacers to increase the separation between the photosensitizer molecules. [23-24, 66-68] It is important to mention that the substituents on the POSS cages may also have an impact on the morphology of the nanoparticles obtained by the reprecipitation approach based on the preliminary results with the POSSP-IB, but this hypothesis still need to be further studied by evaluating other POSSP derivatives.

Molecular dynamic simulations can be a useful tool to have a better understanding in some of the processes and outcomes that happen in the self-assembly of molecules.[79, 135-138, 196] In this project, MD simulations were critical to come out with a rational explanation for the PDT results and the photophysical performance of nanoparticles. The simulation data show that the combination of the hydrophobic POSS cage and coulombic interactions between porphyrins drives the formation of aggregates where the POSS cages form the core and the porphyrins the shell of the aggregate for both POSSP-IB and POSSP-TIB. Interestingly, as shown in our measurement/calculations, this arrangement pushes the porphyrin farther apart from each other avoiding the aggregation self-quenching effect, which is in correlation with our experimental results. MD simulations also show that in the case of POSSP-Ph, other molecular forces are playing a role in the formation of the aggregate. As a result, a different arrangement of the POSSP-Ph molecules is found where there is more interaction between porphyrins with the ultimate outcome of having a more effective aggregation self-quenching effect. The use of MD simulations to understand the interactions of POSSP-IB and POSSP-Ph with the lipid bilayer was also relevant to explain the PDT results. The

morphology of the aggregate obtained with the POSSP-IB allows a higher penetration in the lipid bilayer. As shown in previous reports the penetration of porphyrin molecules in the cell membrane is critical for the PDT outcome.[57, 144]

5.2 Future work

Several experiments are still needed to complete the project in Chapter 4 of this Thesis to fabricate and characterize the self-assembled particles using POSSP-Ph and POSSP-TIB.

Despite the outstanding outcome for PDT obtained with the POSSP-IB and POSSP-TIB molecules, the poor solubility of these molecules in water is still a major challenge for biomedical applications. In Chapter 4, we already showed that these POSS-porphyrins can be assembled in particles that can be suspended in water, we propose test these particles for PDT. The water stability of the POSSP self-assembled particles would allow testing higher concentrations of the photosensitizer in the PDT experiments without the use of cosolvents (like DMSO).

Another approach to overcome the solubility issues would be to take advantage of the fact that POSS chemistry allows a wide range of modifications for these molecules. In fact, our group has already synthesized POSSP derivatives with hydrophilic groups like amine and ammonium. But, the photochemical and PDT properties of those molecules were not as impressive as the ones for the three POSSP derivatives reported in this Thesis.[23] As future work, it is proposed to synthesize and evaluate POSSP derivatives with other type of hydrophilic substituents; in particular, groups containing glycol monomers or zwitterions that are well-known to enhance the solubility in water.[257-258]

The MD simulations depicted in this Thesis show that when molecular forces other than hydrophobic start to play a major role in the self-assembly of the molecules, like in the case of POSSP-Ph, the arrangement of the final aggregate tends to afford higher number of stacks. This outcome has a direct impact on the aggregation self-quenching effect and was corroborated by our experimental data. Hence, it is of particular interest to carry out the MD simulations of POSSP derivatives with hydrophilic groups. We envision that the MD results will help to explain the experimental results that we have for the POSSP derivatives with amine and ammonium groups. It will also be of interest to simulate the other proposed POSSP compounds with glycol chains and zwitterions to use MD simulation as a predictive tool to determine whether those modifications may bring other molecular forces as part of the self-assembly process.

The simulations also showed how the different substituents of POSS influence the stacking angle of the few stacks formed, POSSP-Ph and POSSP-TIB forming J-aggregates and POSSP-IB forming H-aggregates. Controlling the way in which the porphyrin stacks are arranged would be useful for optical and electronic applications. However, the simulations of POSSPs showed the formation of different configurations along with the stacks (T-shapes and solitary porphyrins not in contact with other porphyrins). In the simulations, it could be noted that the linker between the POSS and the porphyrins, a propyl urea group, was fairy flexible and allowed a wide range of orientations of the porphyrin relative to the POSS. Controlling the degrees of freedom (rigidity) of a molecule can guide its self-assembly to favor one outcome over the many possible.[259-260] Therefore, we hypothesize that having a more rigid linker would produce a more uniform arrangement of the self-assemblies. So, we propose as future work to run a series of simulations using rigid linkers to test this hypothesis.

An interesting POSS cage derivative that can be investigated in the future is a Janus POSS cage with one side made of hydrophobic substituents and the other one of hydrophilic groups. Janus POSS cage molecules are not new,[261] and we can further explore both experimentally and through MD simulations the use of these molecules for PDT and self-assembly.

REFERENCES

1. Ben, H.-J.; Ren, X.-K.; Song, B.; Li, X.; Feng, Y.; Jiang, W.; Chen, E.-Q.; Wang, Z.; Jiang, S., Synthesis, crystal structure, enhanced photoluminescence properties and fluoride detection ability of S-heterocyclic annulated perylene diimide-polyhedral oligosilsesquioxane dye. *Journal of Materials Chemistry C* **2017,** *5* (10), 2566-2576.
2. Long, K.; Liu, Y.; Li, Y.; Wang, W., Self-assembly of trigonal building blocks into nanostructures: molecular design and biomedical applications. *Journal of Materials Chemistry B* **2020,** *8* (31), 6739-6752.
3. Lehn, J.-M., Toward self-organization and complex matter. *Science* **2002,** *295* (5564), 2400-2403.
4. Ozin, G. A.; Hou, K.; Lotsch, B. V.; Cademartiri, L.; Puzzo, D. P.; Scotognella, F.; Ghadimi, A.; Thomson, J., Nanofabrication by self-assembly. *Materials Today* **2009,** *12* (5), 12-23.
5. Su, Z.; Zhang, R.; Yan, X.; Guo, Q.; Huang, J.; Shan, W.; Liu, Y.; Liu, T.; Huang, M.; Cheng, S. Z., The role of architectural engineering in macromolecular self-assemblies via non-covalent interactions: A molecular LEGO approach. *Progress in Polymer Science* **2020**, 101230.
6. Whitesides, G. M.; Boncheva, M., Beyond molecules: Self-assembly of mesoscopic and macroscopic components. *Proceedings of the National Academy of Sciences* **2002,** *99* (8), 4769-4774.
7. Zhang, W.-B.; Yu, X.; Wang, C.-L.; Sun, H.-J.; Hsieh, I.-F.; Li, Y.; Dong, X.-H.; Yue, K.; Van Horn, R.; Cheng, S. Z., Molecular nanoparticles are unique elements for macromolecular science: From "nanoatoms" to giant molecules. *Macromolecules* **2014,** *47* (4), 1221-1239.
8. Kuo, S.-W.; Chang, F.-C., POSS related polymer nanocomposites. *Progress in Polymer Science* **2011,** *36* (12), 1649-1696.
9. Li, Z.; Kong, J.; Wang, F.; He, C., Polyhedral oligomeric silsesquioxanes (POSSs): An important building block for organic optoelectronic materials. *Journal of Materials Chemistry C* **2017,** *5* (22), 5283-5298.
10. Li, G.; Wang, L.; Ni, H.; Pittman, C. U., Polyhedral oligomeric silsesquioxane (POSS) polymers and copolymers: a review. *Journal of Inorganic and Organometallic Polymers* **2001,** *11* (3), 123-154.
11. Cordes, D. B.; Lickiss, P. D.; Rataboul, F., Recent developments in the chemistry of cubic polyhedral oligosilsesquioxanes. *Chemical reviews* **2010,** *110* (4), 2081-2173.
12. Carniato, F.; Boccaleri, E.; Marchese, L.; Fina, A.; Tabuani, D.; Camino, G., Synthesis and characterisation of metal isobutylsilsesquioxanes and their role as inorganic–organic nanoadditives for enhancing polymer thermal stability. *European journal of inorganic chemistry* **2007,** *2007* (4), 585-591.
13. Feher, F. J.; Newman, D. A.; Walzer, J. F., Silsesquioxanes as models for silica surfaces. *Journal of the American Chemical Society* **1989,** *111* (5), 1741-1748.
14. Fabritz, S.; Hörner, S.; Avrutina, O.; Kolmar, H., Bioconjugation on cube-octameric silsesquioxanes. *Organic & biomolecular chemistry* **2013,** *11* (14), 2224-2236.
15. Dong, F.; Lu, L.; Ha, C.-S., Silsesquioxane-Containing Hybrid Nanomaterials: Fascinating Platforms for Advanced Applications. *Macromolecular Chemistry and Physics* **2019,** *220* (3), 1800324.

16. Du, Y.; Liu, H., Cage-like silsesquioxanes-based hybrid materials. *Dalton Transactions* **2020,** *49* (17), 5396-5405.
17. Hartmann-Thompson, C., *Applications of Polyhedral Oligomeric Silsesquioxanes*. Springer: 2011; Vol. 03.
18. Liu, S.; Guo, R.; Li, C.; Lu, C.; Yang, G.; Wang, F.; Nie, J.; Ma, C.; Gao, M., POSS hybrid hydrogels: A brief review of synthesis, properties and applications. *European Polymer Journal* **2021,** *143*, 110180.
19. Susheel Kalia, K. P., *Polymer/POSS Nanocomposites and Hybrid Materials*. Springer: 2018.
20. Janeta, M.; John, Ł.; Ejfler, J.; Szafert, S., High-Yield Synthesis of Amido-Functionalized Polyoctahedral Oligomeric Silsesquioxanes by Using Acyl Chlorides. *Chemistry–A European Journal* **2014,** *20* (48), 15966-15974.
21. Zhao, X.; Zhang, W.; Wu, Y.; Liu, H.; Hao, X., Facile fabrication of OA-POSS modified near-infrared-emitting CdSeTe alloyed quantum dots and their bioapplications. *New J Chem* **2014,** *38* (7), 3242-3249.
22. Tanaka, K.; Inafuku, K.; Naka, K.; Chujo, Y., Enhancement of entrapping ability of dendrimers by a cubic silsesquioxane core. *Organic & biomolecular chemistry* **2008,** *6* (21), 3899-3901.
23. Siano, P.; Johnston, A.; Loman-Cortes, P.; Zhin, Z.; Vivero-Escoto, J. L., Evaluation of Polyhedral Oligomeric Silsesquioxane Porphyrin Derivatives on Photodynamic Therapy. *Molecules* **2020,** *25* (21), 4965.
24. Chen, J.; Xu, Y.; Gao, Y.; Yang, D.; Wang, F.; Zhang, L.; Bao, B.; Wang, L., Nanoscale Organic–Inorganic Hybrid Photosensitizers for Highly Effective Photodynamic Cancer Therapy. *ACS applied materials & interfaces* **2018,** *10* (1), 248-255.
25. Fabritz, S.; Heyl, D.; Bagutski, V.; Empting, M.; Rikowski, E.; Frauendorf, H.; Balog, I.; Fessner, W.-D.; Schneider, J. J.; Avrutina, O., Towards click bioconjugations on cube-octameric silsesquioxane scaffolds. *Organic & biomolecular chemistry* **2010,** *8* (9), 2212-2218.
26. Trastoy, B.; Pérez-Ojeda, M. E.; Sastre, R.; Chiara, J. L., Octakis (3-azidopropyl) octasilsesquioxane: A Versatile Nanobuilding Block for the Efficient Preparation of Highly Functionalized Cube-Octameric Polyhedral Oligosilsesquioxane Frameworks Through Click Assembly. *Chemistry–A European Journal* **2010,** *16* (12), 3833-3841.
27. Ray, J. G.; Ly, J. T.; Savin, D. A., Peptide-based lipid mimetics with tunable core properties via thiol–alkyne chemistry. *Polymer Chemistry* **2011,** *2* (7), 1536-1541.
28. Fan, L.; Wang, X.; Cao, Q.; Yang, Y.; Wu, D., POSS-based supramolecular amphiphilic zwitterionic complexes for drug delivery. *Biomaterials science* **2019,** *7* (5), 1984-1994.
29. Ervithayasuporn, V.; Wang, X.; Kawakami, Y., Synthesis and characterization of highly pure azido-functionalized polyhedral oligomeric silsesquioxanes (POSS). *Chemical communications* **2009,** (34), 5130-5132.
30. Heyl, D.; Rikowski, E.; Hoffmann, R. C.; Schneider, J. J.; Fessner, W. D., A "clickable" hybrid nanocluster of cubic symmetry. *Chemistry–A European Journal* **2010,** *16* (19), 5544-5548.
31. Suarez, J. R.; Trastoy, B.; Perez-Ojeda, M. E.; Marin-Barrios, R.; Chiara, J. L., Nonafluorobutanesulfonyl Azide: A Shelf-Stable Diazo Transfer Reagent for the Synthesis of Azides from Primary Amines. *Advanced Synthesis & Catalysis* **2010,** *352* (14-15), 2515-2520.

32. Fan, L.; Wang, X.; Wu, D., Polyhedral Oligomeric Silsesquioxanes (POSS)-based Hybrid Materials: Molecular Design, Solution Self-Assembly and Biomedical Applications. *Chinese Journal of Chemistry* **2021,** *39* (3), 757-774.
33. Olivero, F.; Renò, F.; Carniato, F.; Rizzi, M.; Cannas, M.; Marchese, L., A novel luminescent bifunctional POSS as a molecular platform for biomedical applications. *Dalton Transactions* **2012,** *41* (25), 7467-7473.
34. Janaszewska, A.; Gradzinska, K.; Marcinkowska, M.; Klajnert-Maculewicz, B.; Stanczyk, W. A., In vitro studies of polyhedral oligo silsesquioxanes: evidence for their low cytotoxicity. *Materials* **2015,** *8* (9), 6062-6070.
35. Almutary, A.; Sanderson, B., Toxicity of four novel Polyhedral Oligomeric Silsesquioxane (POSS) particles used in anti-cancer drug delivery. *J. Appl. Pharm. Sci* **2017,** *7*, 101-105.
36. Ni, C.; Wu, G.; Zhu, C.; Yao, B., The preparation and characterization of amphiphilic star block copolymer nano micelles using silsesquioxane as the core. *The Journal of Physical Chemistry C* **2010,** *114* (32), 13471-13476.
37. Shakiba, M.; Chen, J.; Zheng, G., Porphyrin nanoparticles in photomedicine. In *Applications of Nanoscience in Photomedicine*, Elsevier: 2015; pp 511-526.
38. Tian, J.; Huang, B.; Nawaz, M. H.; Zhang, W., Recent advances of multi-dimensional porphyrin-based functional materials in photodynamic therapy. *Coordination Chemistry Reviews* **2020,** *420*, 213410.
39. Plaetzer, K.; Krammer, B.; Berlanda, J.; Berr, F.; Kiesslich, T., Photophysics and photochemistry of photodynamic therapy: fundamental aspects. *Lasers in medical science* **2009,** *24* (2), 259-268.
40. Ormond, A.; Freeman, H., Dye sensitizers for photodynamic therapy. *Materials* **2013,** *6* (3), 817-840.
41. Swavey, S.; Tran, M., Porphyrin and Phthalocyanine Photosensitizers as PDT Agents: ANewModalityfortheTreatmentofMelanoma. *Recent Advances in the biology, therapy and management of melanoma* **2013**, 253.
42. Ormond, A. B.; Freeman, H. S., Dye sensitizers for photodynamic therapy. *Materials* **2013,** *6* (3), 817-840.
43. Kessel, D., *Photodynamic therapy of neoplastic disease*. CRC Press: 1990; Vol. 1.
44. Josefsen, L. B.; Boyle, R. W., Unique diagnostic and therapeutic roles of porphyrins and phthalocyanines in photodynamic therapy, imaging and theranostics. *Theranostics* **2012,** *2* (9), 916.
45. Sève, A.; Couleaud, P.; Lux, F.; Tillement, O.; Arnoux, P.; André, J.-C.; Frochot, C., Long-distance energy transfer photosensitizers arising in hybrid nanoparticles leading to fluorescence emission and singlet oxygen luminescence quenching. *Photochemical & Photobiological Sciences* **2012,** *11* (5), 803-811.
46. Wu, W.; Shao, X.; Zhao, J.; Wu, M., Controllable photodynamic therapy implemented by regulating singlet oxygen efficiency. *Advanced Science* **2017,** *4* (7), 1700113.
47. Ghosh, M.; Nath, S.; Hajra, A.; Sinha, S., Fluorescence self-quenching of tetraphenylporphyrin in liquid medium. *Journal of luminescence* **2013,** *141*, 87-92.
48. Zhegalova, N. G.; He, S.; Zhou, H.; Kim, D. M.; Berezin, M. Y., Minimization of self-quenching fluorescence on dyes conjugated to biomolecules with multiple labeling sites via asymmetrically charged NIR fluorophores. *Contrast media & molecular imaging* **2014,** *9* (5), 355-362.

49. Bader, A. N.; Hofman, E. G.; Voortman, J.; en Henegouwen, P. M. v. B.; Gerritsen, H. C., Homo-FRET imaging enables quantification of protein cluster sizes with subcellular resolution. *Biophysical journal* **2009,** *97* (9), 2613-2622.
50. Nicoli, F.; Barth, A.; Bae, W.; Neukirchinger, F.; Crevenna, A. H.; Lamb, D. C.; Liedl, T., Directional photonic wire mediated by homo-Förster resonance energy transfer on a DNA origami platform. *ACS nano* **2017,** *11* (11), 11264-11272.
51. Sahoo, H., Förster resonance energy transfer–A spectroscopic nanoruler: Principle and applications. *Journal of Photochemistry and Photobiology C: Photochemistry Reviews* **2011,** *12* (1), 20-30.
52. Conroy, E. M.; Li, J. J.; Kim, H.; Algar, W. R., Self-quenching, dimerization, and homo-FRET in hetero-FRET assemblies with quantum dot donors and multiple dye acceptors. *The Journal of Physical Chemistry C* **2016,** *120* (31), 17817-17828.
53. Zhou, J.-D.; Zhang, W.-Q.; Liu, L.-L.; Xie, Z.-Q.; Ma, Y.-G., Aggregation structures of organic conjugated molecules on their optoelectronic properties. *Chinese Chemical Letters* **2016,** *27* (8), 1350-1356.
54. Burin, A. L.; Armbruster, M. E.; Hariharan, M.; Lewis, F. D., Sum rules and determination of exciton coupling using absorption and circular dichroism spectra of biological polymers. *Proceedings of the National Academy of Sciences* **2009,** *106* (4), 989-994.
55. Kasha, M.; Rawls, H.; El-Bayoumi, M. A., The exciton model in molecular spectroscopy. *Pure and applied Chemistry* **1965,** *11* (3-4), 371-392.
56. Hestand, N. J.; Spano, F. C., Expanded theory of H-and J-molecular aggregates: the effects of vibronic coupling and intermolecular charge transfer. *Chemical reviews* **2018,** *118* (15), 7069-7163.
57. Hurst, A. N.; Scarbrough, B.; Saleh, R.; Hovey, J.; Ari, F.; Goyal, S.; Chi, R. J.; Troutman, J. M.; Vivero-Escoto, J. L., Influence of cationic meso-substituted porphyrins on the antimicrobial photodynamic efficacy and cell membrane interaction in Escherichia coli. *International journal of molecular sciences* **2019,** *20* (1), 134.
58. Vega, D.; Lodge, P.; Vivero-Escoto, J., Redox-responsive porphyrin-based polysilsesquioxane nanoparticles for photodynamic therapy of cancer cells. *International journal of molecular sciences* **2016,** *17* (1), 56.
59. Vivero-Escoto, J. L.; Vega, D. L., Stimuli-responsive protoporphyrin IX silica-based nanoparticles for photodynamic therapy in vitro. *RSC Advances* **2014,** *4* (28), 14400-14407.
60. Vivero-Escoto, J.; Elnagheeb, M., Mesoporous silica nanoparticles loaded with cisplatin and phthalocyanine for combination chemotherapy and photodynamic therapy in vitro. *Nanomaterials* **2015,** *5* (4), 2302-2316.
61. Juneja, R.; Lyles, Z.; Vadarevu, H.; Afonin, K. A.; Vivero-Escoto, J. L., Multimodal Polysilsesquioxane Nanoparticles for Combinatorial Therapy and Gene Delivery in Triple-Negative Breast Cancer. *ACS applied materials & interfaces* **2019,** *11* (13), 12308-12320.
62. Vega, D. L.; Lodge, P.; Vivero-Escoto, J. L., Redox-Responsive Porphyrin-Based Polysilsesquioxane Nanoparticles for Photodynamic Therapy of Cancer Cells. *International journal of molecular sciences* **2016,** *17* (1), 16.
63. Vivero-Escoto, J. L.; Vega, D. L., Stimuli-responsive protoporphyrin IX silica-based nanoparticles for photodynamic therapy in vitro. *RSC Adv.* **2014,** *4* (28), 14400-14407.
64. Kim, Y.-J.; Lee, H.-I.; Kim, J.-K.; Kim, C.-H.; Kim, Y.-J., Peptide 18-4/chlorin e6-conjugated polyhedral oligomeric silsesquioxane nanoparticles for targeted photodynamic therapy of breast cancer. *Colloids and Surfaces B: Biointerfaces* **2020,** *189*, 110829.

65. Lee, H.-I.; Kim, Y.-J., Enhanced cellular uptake of protoporphyrine IX/linolenic acid-conjugated spherical nanohybrids for photodynamic therapy. *Colloids and Surfaces B: Biointerfaces* **2016,** *142*, 182-191.
66. Jin, J.; Zhu, Y.; Zhang, Z.; Zhang, W., Enhancing the efficacy of photodynamic therapy through a porphyrin/POSS alternating copolymer. *Angewandte Chemie International Edition* **2018,** *57* (50), 16354-16358.
67. Chen, J.; Shan, J.; Xu, Y.; Su, P.; Tong, L.; Yuwen, L.; Weng, L.; Bao, B.; Wang, L., Polyhedral oligomeric silsesquioxane (POSS)-based cationic conjugated oligoelectrolyte/porphyrin for efficient energy transfer and multiamplified antimicrobial activity. *ACS applied materials & interfaces* **2018,** *10* (40), 34455-34463.
68. Bao, B.; Zhai, X.; Liu, T.; Su, P.; Zhou, L.; Xu, Y.; Gu, B.; Wang, L., Cubic POSS engineering of photosensitizer-doped semiconducting polymer nanoparticles for enhanced fluorescence imaging and amplified photodynamic therapy. *Polymer Chemistry* **2020,** *11* (44), 7035-7041.
69. Zhu, Y.-X.; Jia, H.-R.; Chen, Z.; Wu, F.-G., Photosensitizer (PS)/polyhedral oligomeric silsesquioxane (POSS)-crosslinked nanohybrids for enhanced imaging-guided photodynamic cancer therapy. *Nanoscale* **2017,** *9* (35), 12874-12884.
70. Zhang, P.; Zhang, Z.; Jiang, X.; Rui, L.; Gao, Y.; Zhang, W., Unimolecular micelles from POSS-based star-shaped block copolymers for photodynamic therapy. *Polymer* **2017,** *118*, 268-279.
71. Li, S.; Chang, K.; Sun, K.; Tang, Y.; Cui, N.; Wang, Y.; Qin, W.; Xu, H.; Wu, C., Amplified singlet oxygen generation in semiconductor polymer dots for photodynamic cancer therapy. *ACS applied materials & interfaces* **2016,** *8* (6), 3624-3634.
72. Shen, X.; Li, L.; Wu, H.; Yao, S. Q.; Xu, Q.-H., Photosensitizer-doped conjugated polymer nanoparticles for simultaneous two-photon imaging and two-photon photodynamic therapy in living cells. *Nanoscale* **2011,** *3* (12), 5140-5146.
73. Bhattacharyya, S.; Barman, M. K.; Baidya, A.; Patra, A., Singlet oxygen generation from polymer nanoparticles–photosensitizer conjugates using fret cascade. *The Journal of Physical Chemistry C* **2014,** *118* (18), 9733-9740.
74. Zhang, Y.; Yue, T.; Cao, H.; Gao, Y.; Zhang, W., Photocontrollable Supramolecular Self-Assembly of a Porphyrin Derivative that Contains a Polyhedral Oligomeric Silsesquioxane (POSS). *Asian Journal of Organic Chemistry* **2017,** *6* (8), 1034-1042.
75. Ma, L.; Geng, H.; Song, J.; Li, J.; Chen, G.; Li, Q., Hierarchical self-assembly of polyhedral oligomeric silsesquioxane end-capped stimuli-responsive polymer: from single micelle to complex micelle. *The Journal of Physical Chemistry B* **2011,** *115* (36), 10586-10591.
76. Mann, S., Self-assembly and transformation of hybrid nano-objects and nanostructures under equilibrium and non-equilibrium conditions. *Nature materials* **2009,** *8* (10), 781.
77. Grzybowski, B. A.; Wilmer, C. E.; Kim, J.; Browne, K. P.; Bishop, K. J., Self-assembly: from crystals to cells. *Soft Matter* **2009,** *5* (6), 1110-1128.
78. Chi, H.; Wang, M.; Xiao, Y.; Wang, F.; KS, J., Self-assembly and applications of amphiphilic hybrid poss copolymers. *Molecules* **2018,** *23* (10), 2481.
79. Wang, X.; Gao, P.; Yang, Y.; Guo, H.; Wu, D., Dynamic and programmable morphology and size evolution via a living hierarchical self-assembly strategy. *Nature communications* **2018,** *9* (1), 1-15.

80. Li, J.; Zhou, Z.; Ma, L.; Chen, G.; Li, Q., Hierarchical assembly of amphiphilic POSS-cyclodextrin molecules and azobenzene end-capped polymers. *Macromolecules* **2014,** *47* (16), 5739-5748.
81. Huang, M.; Yue, K.; Huang, J.; Liu, C.; Zhou, Z.; Wang, J.; Wu, K.; Shan, W.; Shi, A.-C.; Cheng, S. Z., Highly asymmetric phase behaviors of polyhedral oligomeric silsesquioxane-based multiheaded giant surfactants. *ACS nano* **2018,** *12* (2), 1868-1877.
82. Zhang, W.; Chu, Y.; Mu, G.; Eghtesadi, S. A.; Liu, Y.; Zhou, Z.; Lu, X.; Kashfipour, M. A.; Lillard, R. S.; Yue, K., Rationally controlling the self-assembly behavior of triarmed POSS–organic hybrid macromolecules: from giant surfactants to macroions. *Macromolecules* **2017,** *50* (13), 5042-5050.
83. Hirai, T.; Leolukman, M.; Hayakawa, T.; Kakimoto, M.-a.; Gopalan, P., Hierarchical nanostructures of organosilicate nanosheets within self-organized block copolymer films. *Macromolecules* **2008,** *41* (13), 4558-4560.
84. Tada, Y.; Yoshida, H.; Ishida, Y.; Hirai, T.; Bosworth, J. K.; Dobisz, E.; Ruiz, R.; Takenaka, M.; Hayakawa, T.; Hasegawa, H., Directed self-assembly of POSS containing block copolymer on lithographically defined chemical template with morphology control by solvent vapor. *Macromolecules* **2012,** *45* (1), 292-304.
85. Zhang, W.; Yuan, J.; Weiss, S.; Ye, X.; Li, C.; Müller, A. H., Telechelic hybrid poly (acrylic acid) s containing polyhedral oligomeric silsesquioxane (POSS) and their self-assembly in water. *Macromolecules* **2011,** *44* (17), 6891-6898.
86. Ni, Y.; Zheng, S., Nanostructured thermosets from epoxy resin and an Organic− Inorganic amphiphile. *Macromolecules* **2007,** *40* (19), 7009-7018.
87. Kim, B.-S.; Mather, P. T., Morphology, microstructure, and rheology of amphiphilic telechelics incorporating polyhedral oligosilsesquioxane. *Macromolecules* **2006,** *39* (26), 9253-9260.
88. Zheng, L.; Hong, S.; Cardoen, G.; Burgaz, E.; Gido, S. P.; Coughlin, E. B., Polymer nanocomposites through controlled self-assembly of cubic silsesquioxane scaffolds. *Macromolecules* **2004,** *37* (23), 8606-8611.
89. Miao, J.; Cui, L.; Lau, H. P.; Mather, P. T.; Zhu, L., Self-assembly and chain-folding in hybrid coil− coil− cube triblock oligomers of polyethylene-b-poly (ethylene oxide)-b-polyhedral oligomeric silsesquioxane. *Macromolecules* **2007,** *40* (15), 5460-5470.
90. Handke, B.; Klita, Ł.; Niemiec, W., Self-assembly of dodecaphenyl POSS thin films. *Surface Science* **2017,** *666*, 70-75.
91. Li, Y.; Zhang, W.-B.; Hsieh, I.-F.; Zhang, G.; Cao, Y.; Li, X.; Wesdemiotis, C.; Lotz, B.; Xiong, H.; Cheng, S. Z., Breaking symmetry toward nonspherical Janus particles based on polyhedral oligomeric silsesquioxanes: Molecular design,“click” synthesis, and hierarchical structure. *Journal of the American Chemical Society* **2011,** *133* (28), 10712-10715.
92. Du, F.; Tian, J.; Wang, H.; Liu, B.; Jin, B.; Bai, R., Synthesis and luminescence of POSS-containing perylene bisimide-bridged amphiphilic polymers. *Macromolecules* **2012,** *45* (7), 3086-3093.
93. Du, F.; Wang, H.; Bao, Y.; Liu, B.; Zheng, H.; Bai, R., Conjugated coordination polymers based on 8-hydroxyquinoline ligands: impact of polyhedral oligomeric silsesquioxanes on solubility and luminescence. *Journal of Materials Chemistry* **2011,** *21* (29), 10859-10864.
94. Lucenti, E.; Botta, C.; Cariati, E.; Righetto, S.; Scarpellini, M.; Tordin, E.; Ugo, R., New organic–inorganic hybrid materials based on perylene diimide–polyhedral oligomeric

silsesquioxane dyes with reduced quenching of the emission in the solid state. *Dyes Pigments* **2013,** *96* (3), 748-755.
95. Li, Q.; Dong, L.; Wang, X.; Huang, J.; Xie, H.; Xiong, C., Self-assembled quantum dots–polyhedral oligomeric silsesquioxane nanohybrids with enhanced photoluminescence. *Scripta Materialia* **2012,** *66* (9), 646-649.
96. Mao, Y.; Zhao, Q.; Wu, J.; Pan, T.; Zhou, B.; Tian, Y., A highly sensitive and fast-responding oxygen sensor based on POSS-containing hybrid copolymer films. *Journal of Materials Chemistry C* **2017,** *5* (44), 11395-11402.
97. Chen, J.; Jia, S.; Ji, X.; Nourrein, M.; Xiang, H.; Zhou, Z.; Wang, C.-L.; Sun, B.; Zhu, M., The morphologies and fluorescence quantum yields of perylene diimide dye-doped PS and PHVB microspheres. *RSC Advances* **2018,** *8* (62), 35534-35538.
98. Zhang, Y.; Zhang, L.; Liu, H.; Sun, D.; Li, X., Synthesis and aggregation properties of a series of dumbbell polyhedral oligosilsesquioxane-perylene diimide triads. *CrystEngComm* **2015,** *17* (6), 1453-1463.
99. Medforth, C. J.; Wang, Z.; Martin, K. E.; Song, Y.; Jacobsen, J. L.; Shelnutt, J. A., Self-assembled porphyrin nanostructures. *Chemical Communications* **2009,** (47), 7261-7277.
100. Wang, Y.; Vaneski, A.; Yang, H.; Gupta, S.; Hetsch, F.; Kershaw, S. V.; Teoh, W. Y.; Li, H.; Rogach, A. L., Polyhedral oligomeric silsesquioxane as a ligand for CdSe quantum dots. *The Journal of Physical Chemistry C* **2013,** *117* (4), 1857-1862.
101. Sun, J.; Chen, Y.; Zhao, L.; Chen, Y.; Qi, D.; Choi, K. M.; Shin, D. S.; Jiang, J., Porphyrin-POSS Molecular Hybrids. *Chemistry–A European Journal* **2013,** *19* (38), 12613-12618.
102. Sun, H.-J.; Tu, Y.; Wang, C.-L.; Van Horn, R. M.; Tsai, C.-C.; Graham, M. J.; Sun, B.; Lotz, B.; Zhang, W.-B.; Cheng, S. Z., Hierarchical structure and polymorphism of a sphere-cubic shape amphiphile based on a polyhedral oligomeric silsesquioxane–[60] fullerene conjugate. *Journal of Materials Chemistry* **2011,** *21* (37), 14240-14247.
103. Dolphin, D., *The Porphyrins V5: Physical Chemistry*. Elsevier Science: 2012.
104. Scholes, G. D.; Rumbles, G., Excitons in nanoscale systems. In *Materials For Sustainable Energy: A Collection of Peer-Reviewed Research and Review Articles from Nature Publishing Group*, World Scientific: 2011; pp 12-25.
105. Verma, S.; Ghosh, A.; Das, A.; Ghosh, H. N., Exciton-Coupled Charge-Transfer Dynamics in a Porphyrin J-Aggregate/TiO2 Complex. *Chemistry–A European Journal* **2011,** *17* (12), 3458-3464.
106. Balaban, T. S., Tailoring porphyrins and chlorins for self-assembly in biomimetic artificial antenna systems. *Accounts of chemical research* **2005,** *38* (8), 612-623.
107. Sengupta, S.; Würthner, F., Chlorophyll J-aggregates: From bioinspired dye stacks to nanotubes, liquid crystals, and biosupramolecular electronics. *Accounts of chemical research* **2013,** *46* (11), 2498-2512.
108. Pšenčík, J.; Butcher, S. J.; Tuma, R., Chlorosomes: structure, function and assembly. In *The Structural Basis of Biological Energy Generation*, Springer: 2014; pp 77-109.
109. Bricks, J. L.; Slominskii, Y. L.; Panas, I. D.; Demchenko, A. P., Fluorescent J-aggregates of cyanine dyes: basic research and applications review. *Methods and applications in fluorescence* **2017,** *6* (1), 012001.
110. Chang, Y.-C.; Wang, C.-L.; Pan, T.-Y.; Hong, S.-H.; Lan, C.-M.; Kuo, H.-H.; Lo, C.-F.; Hsu, H.-Y.; Lin, C.-Y.; Diau, E. W.-G., A strategy to design highly efficient porphyrin sensitizers for dye-sensitized solar cells. *Chemical Communications* **2011,** *47* (31), 8910-8912.

111. Splan, K. E.; Hupp, J. T., Permeable nonaggregating porphyrin thin films that display enhanced photophysical properties. *Langmuir* **2004,** *20* (24), 10560-10566.
112. Drain, C. M.; Smeureanu, G.; Patel, S.; Gong, X.; Garno, J.; Arijeloye, J., Porphyrin nanoparticles as supramolecular systems. *New Journal of Chemistry* **2006,** *30* (12), 1834-1843.
113. Perepogu, A. K.; Bangal, P. R., Preparation and characterization of free-standing pure porphyrin nanoparticles. *Journal of chemical sciences* **2008,** *120* (5), 485-491.
114. Zhai, J.; Li, H.; Sun, X., A novel application of porphyrin nanoparticles as an effective fluorescent assay platform for nucleic acid detection. *RSC Advances* **2011,** *1* (1), 36-39.
115. Gong, X.; Milic, T.; Xu, C.; Batteas, J. D.; Drain, C. M., Preparation and characterization of porphyrin nanoparticles. *Journal of the American Chemical Society* **2002,** *124* (48), 14290-14291.
116. Kashani-Motlagh, M. M.; Rahimi, R.; Kachousangi, M. J., Ultrasonic method for the preparation of organic porphyrin nanoparticles. *Molecules* **2009,** *15* (1), 280-287.
117. Motlagh, M. M. K.; Rahimi, R.; Kachousangi, M. J. In *Ultrasonic method for the preparation of organic nanoparticles of porphyrin*, International Electronic Conference on Synthetic Organic Chemistry, 12th, 2008.
118. Kashani-Motlagh, M. M.; Rahimi, R.; Kachousangi, M. J., Ultrasonic method for the preparation of organic porphyrin nanoparticles. *Molecules* **2010,** *15* (1), 280-287.
119. Wang, S.-P.; Lin, W.; Wang, X.; Cen, T.-Y.; Xie, H.; Huang, J.; Zhu, B.-Y.; Zhang, Z.; Song, A.; Hao, J., Controllable hierarchical self-assembly of porphyrin-derived supra-amphiphiles. *Nature communications* **2019,** *10* (1), 1399.
120. Fan, J.; Whiteford, J. A.; Olenyuk, B.; Levin, M. D.; Stang, P. J.; Fleischer, E. B., Self-Assembly of porphyrin arrays via coordination to transition metal bisphosphine complexes and the unique spectral properties of the product metallacyclic ensembles. *Journal of the American Chemical Society* **1999,** *121* (12), 2741-2752.
121. Zhang, N.; Wang, L.; Wang, H.; Cao, R.; Wang, J.; Bai, F.; Fan, H., Self-assembled one-dimensional porphyrin nanostructures with enhanced photocatalytic hydrogen generation. *Nano letters* **2017,** *18* (1), 560-566.
122. van der Weegen, R.; Teunissen, A. J.; Meijer, E., Directing the Self-Assembly Behaviour of Porphyrin-Based Supramolecular Systems. *Chemistry–A European Journal* **2017,** *23* (15), 3773-3783.
123. Wang, D.; Niu, L.; Qiao, Z.-Y.; Cheng, D.-B.; Wang, J.; Zhong, Y.; Bai, F.; Wang, H.; Fan, H., Synthesis of self-assembled porphyrin nanoparticle photosensitizers. *ACS nano* **2018,** *12* (4), 3796-3803.
124. Chen, Y.; Li, A.; Huang, Z.-H.; Wang, L.-N.; Kang, F., Porphyrin-based nanostructures for photocatalytic applications. *Nanomaterials* **2016,** *6* (3), 51.
125. Wang, J.; Zhong, Y.; Wang, L.; Zhang, N.; Cao, R.; Bian, K.; Alarid, L.; Haddad, R. E.; Bai, F.; Fan, H., Morphology-controlled synthesis and metalation of porphyrin nanoparticles with enhanced photocatalytic performance. *Nano letters* **2016,** *16* (10), 6523-6528.
126. Castriciano, M. A.; Leone, N.; Cardiano, P.; Manickam, S.; Scolaro, L. M.; Schiavo, S. L., A new supramolecular polyhedral oligomeric silsesquioxanes (POSS)–porphyrin nanohybrid: synthesis and spectroscopic characterization. *Journal of Materials Chemistry C* **2013,** *1* (31), 4746-4753.
127. Würthner, F.; Kaiser, T. E.; Saha-Möller, C. R., J-aggregates: from serendipitous discovery to supramolecular engineering of functional dye materials. *Angewandte Chemie International Edition* **2011,** *50* (15), 3376-3410.

128. Araya-Hermosilla, R.; Araya-Hermosilla, E.; Torres-Gallegos, C.; Alarcón-Alarcón, C.; Moreno-Villoslada, I., Sensing Cu2+ by controlling the aggregation properties of the fluorescent dye rhodamine 6G with the aid of polyelectrolytes bearing different linear aromatic density. *Reactive and Functional Polymers* **2013,** *73* (11), 1455-1463.
129. Kasha, M.; Rawls, H. R.; El-Bayoumi, M. A., The exciton model in molecular spectroscopy. *Pure and applied Chemistry* **1965,** *11* (3-4), 371-392.
130. Nagamura, T.; Kamata, S., A three-dimensional extended dipole model for interaction and alignment of chromophores in monolayer assemblies. *Journal of Photochemistry and Photobiology A: Chemistry* **1990,** *55* (2), 187-196.
131. Van der Auweraer, M.; Scheblykin, I., One-dimensional J-aggregates: Dependence of the properties of the exciton band on the model of the intermolecular coupling. *Chemical physics* **2002,** *275* (1-3), 285-306.
132. Pasternack, R. F.; Collings, P. J., Resonance light scattering: a new technique for studying chromophore aggregation. *Science* **1995,** *269* (5226), 935-939.
133. Hospital, A.; Goñi, J. R.; Orozco, M.; Gelpí, J. L., Molecular dynamics simulations: advances and applications. *Advances and applications in bioinformatics and chemistry: AABC* **2015,** *8*, 37.
134. Hollingsworth, S. A.; Dror, R. O., Molecular dynamics simulation for all. *Neuron* **2018,** *99* (6), 1129-1143.
135. Zhang, X.; Chan, E. R.; Glotzer, S. C., Self-assembled morphologies of monotethered polyhedral oligomeric silsesquioxane nanocubes from computer simulation. *The Journal of chemical physics* **2005,** *123* (18), 184718.
136. Roy, S.; Feng, J.; Scionti, V.; Jana, S. C.; Wesdemiotis, C., Self-assembled structure formation from interactions between polyhedral oligomeric silsesquioxane and sorbitol in preparation of polymer compounds. *Polymer* **2012,** *53* (8), 1711-1724.
137. Chan, E. R.; Striolo, A.; McCabe, C.; Cummings, P. T.; Glotzer, S. C., Coarse-grained force field for simulating polymer-tethered silsesquioxane self-assembly in solution. *The Journal of chemical physics* **2007,** *127* (11), 114102.
138. Wang, X.; Gao, P.; Wang, J.; Yang, Y.; You, Y.; Wu, D., A Robust Strategy for Precise Fabrication of Rigid–Flexible Coupling Dendrimers toward Self-Coordinated Hierarchical Assembly. *CCS Chemistry* **2020**, 1093-1104.
139. Wadhwa, R.; Yadav, N. S.; Katiyar, S. P.; Yaguchi, T.; Lee, C.; Ahn, H.; Yun, C.-O.; Kaul, S. C.; Sundar, D., Molecular dynamics simulations and experimental studies reveal differential permeability of withaferin-A and withanone across the model cell membrane. *Scientific reports* **2021,** *11* (1), 1-15.
140. Zhang, S.; Mu, Y.; Zhang, J. Z.; Xu, W., Effect of self-assembly of fullerene nano-particles on lipid membrane. *Plos One* **2013,** *8* (10), e77436.
141. Nademi, Y.; Iranagh, S. A.; Yousefpour, A.; Mousavi, S. Z.; Modarress, H., Molecular dynamics simulations and free energy profile of Paracetamol in DPPC and DMPC lipid bilayers. *Journal of Chemical Sciences* **2014,** *126* (3), 637-647.
142. Marrink, S. J.; De Vries, A. H.; Tieleman, D. P., Lipids on the move: simulations of membrane pores, domains, stalks and curves. *Biochimica et Biophysica Acta (BBA)-Biomembranes* **2009,** *1788* (1), 149-168.
143. Tieleman, P.; Vattulainen, I.; Tajkhorshid, E.; Essex, J. W.; Ulmschneider, M. B.; Schulten, K.; Robertson, J. L.; Roux, B.; Khalid, S., *Molecular Simulations and Biomembranes: From Biophysics to Function*. Royal Society of Chemistry: 2010.

144. Cordeiro, R. M.; Miotto, R.; Baptista, M. S., Photodynamic efficiency of cationic meso-porphyrins at lipid bilayers: insights from molecular dynamics simulations. *The Journal of Physical Chemistry B* **2012,** *116* (50), 14618-14627.
145. Zhou, J.; Zhao, Y.; Yu, K.; Zhou, X.; Xie, X., Synthesis, thermal stability and photoresponsive behaviors of azobenzene-tethered polyhedral oligomeric silsesquioxanes. *New Journal of Chemistry* **2011,** *35* (12), 2781-2792.
146. Wheeler, P. A.; Fu, B. X.; Lichtenhan, J. D.; Weitao, J.; Mathias, L. J., Incorporation of metallic POSS, POSS copolymers, and new functionalized POSS compounds into commercial dental resins. *Journal of Applied Polymer Science* **2006,** *102* (3), 2856-2862.
147. York, M.; Evans, R. A., The use of polyhedral oligomeric silsesquioxane (POSS) as a soluble support for organic synthesis: A case study with a POSS-bound isocyanate scavenger reagent. *Tetrahedron Letters* **2010,** *51* (35), 4677-4680.
148. Angeli, N. G.; Lagorio, M. G.; Román, E. A. S.; Dicelio, L. E., Meso-Substituted Cationic Porphyrins of Biological Interest. Photophysical and Physicochemical Properties in Solution and Bound to Liposomes¶. *Photochemistry and photobiology* **2000,** *72* (1), 49-56.
149. Marin, D. M.; Payerpaj, S.; Collier, G. S.; Ortiz, A. L.; Singh, G.; Jones, M.; Walter, M. G., Efficient intersystem crossing using singly halogenated carbomethoxyphenyl porphyrins measured using delayed fluorescence, chemical quenching, and singlet oxygen emission. *Physical Chemistry Chemical Physics* **2015,** *17* (43), 29090-29096.
150. Chen, L.; Chen, J.; Zhou, G.; Wang, Y.; Xu, C.; Wang, X., Molecular dynamics simulations of the permeation of bisphenol A and pore formation in a lipid membrane. *Scientific reports* **2016,** *6* (1), 1-7.
151. Tieleman, D. P.; Berendsen, H., Molecular dynamics simulations of a fully hydrated dipalmitoylphosphatidylcholine bilayer with different macroscopic boundary conditions and parameters. *The Journal of chemical physics* **1996,** *105* (11), 4871-4880.
152. Berendsen, H. J.; van der Spoel, D.; van Drunen, R., GROMACS: a message-passing parallel molecular dynamics implementation. *Computer physics communications* **1995,** *91* (1-3), 43-56.
153. Hess, B.; Kutzner, C.; Van Der Spoel, D.; Lindahl, E., GROMACS 4: algorithms for highly efficient, load-balanced, and scalable molecular simulation. *Journal of chemical theory and computation* **2008,** *4* (3), 435-447.
154. Dodda, L. S.; Cabeza de Vaca, I.; Tirado-Rives, J.; Jorgensen, W. L., LigParGen web server: an automatic OPLS-AA parameter generator for organic ligands. *Nucleic acids research* **2017,** *45* (W1), W331-W336.
155. Dodda, L. S.; Vilseck, J. Z.; Tirado-Rives, J.; Jorgensen, W. L., 1.14* CM1A-LBCC: localized bond-charge corrected CM1A charges for condensed-phase simulations. *The Journal of Physical Chemistry B* **2017,** *121* (15), 3864-3870.
156. Udier–Blagović, M.; Morales De Tirado, P.; Pearlman, S. A.; Jorgensen, W. L., Accuracy of free energies of hydration using CM1 and CM3 atomic charges. *Journal of computational chemistry* **2004,** *25* (11), 1322-1332.
157. Dodda, L. Command files needed to install LigParGen locally. https://github.com/leelasd/LigParGen-CommandFiles (accessed 05/20/2020).
158. Berger, O.; Edholm, O.; Jähnig, F., Molecular dynamics simulations of a fluid bilayer of dipalmitoylphosphatidylcholine at full hydration, constant pressure, and constant temperature. *Biophysical journal* **1997,** *72* (5), 2002-2013.

159. Monticelli, L.; Simões, C.; Belvisi, L.; Colombo, G., Assessing the influence of electrostatic schemes on molecular dynamics simulations of secondary structure forming peptides. *Journal of Physics: Condensed Matter* **2006,** *18* (14), S329.
160. Cordomí, A.; Caltabiano, G.; Pardo, L., Membrane protein simulations using AMBER force field and Berger lipid parameters. *Journal of chemical theory and computation* **2012,** *8* (3), 948-958.
161. Tieleman, D. P.; MacCallum, J. L.; Ash, W. L.; Kandt, C.; Xu, Z.; Monticelli, L., Membrane protein simulations with a united-atom lipid and all-atom protein model: lipid–protein interactions, side chain transfer free energies and model proteins. *Journal of Physics: Condensed Matter* **2006,** *18* (28), S1221.
162. Neale, C.; Pomès, R., Combination rules for united-atom lipids and OPLSAA proteins. *Unpublished document. http://www. pomeslab. com/files/lipidCombinationRules. pdf. Accessed* **2011,** *2*.
163. Chakrabarti, N.; Neale, C.; Payandeh, J.; Pai, E. F.; Pomès, R., An iris-like mechanism of pore dilation in the CorA magnesium transport system. *Biophysical journal* **2010,** *98* (5), 784-792.
164. Berendsen, H.; Grigera, J.; Straatsma, T., The missing term in effective pair potentials. *Journal of Physical Chemistry* **1987,** *91* (24), 6269-6271.
165. Martínez, L.; Andrade, R.; Birgin, E. G.; Martínez, J. M., PACKMOL: a package for building initial configurations for molecular dynamics simulations. *Journal of computational chemistry* **2009,** *30* (13), 2157-2164.
166. Hess, B.; Bekker, H.; Berendsen, H. J.; Fraaije, J. G., LINCS: a linear constraint solver for molecular simulations. *Journal of computational chemistry* **1997,** *18* (12), 1463-1472.
167. Darden, T.; York, D.; Pedersen, L., Particle mesh Ewald: An N· log (N) method for Ewald sums in large systems. *The Journal of chemical physics* **1993,** *98* (12), 10089-10092.
168. Essmann, U.; Perera, L.; Berkowitz, M. L.; Darden, T.; Lee, H.; Pedersen, L. G., A smooth particle mesh Ewald method. *The Journal of chemical physics* **1995,** *103* (19), 8577-8593.
169. Nagle, J., Area/lipid of bilayers from NMR. *Biophysical journal* **1993,** *64* (5), 1476-1481.
170. Evans, D. J.; Holian, B. L., The nose–hoover thermostat. *The Journal of chemical physics* **1985,** *83* (8), 4069-4074.
171. Parrinello, M.; Rahman, A., Polymorphic transitions in single crystals: A new molecular dynamics method. *Journal of Applied physics* **1981,** *52* (12), 7182-7190.
172. Lemkul, J. A.; Bevan, D. R., Assessing the stability of Alzheimer's amyloid protofibrils using molecular dynamics. *The Journal of Physical Chemistry B* **2010,** *114* (4), 1652-1660.
173. Kumar, S.; Rosenberg, J. M.; Bouzida, D.; Swendsen, R. H.; Kollman, P. A., The weighted histogram analysis method for free-energy calculations on biomolecules. I. The method. *Journal of computational chemistry* **1992,** *13* (8), 1011-1021.
174. Hub, J. S.; De Groot, B. L.; Van Der Spoel, D., g_wham□ A Free Weighted Histogram Analysis Implementation Including Robust Error and Autocorrelation Estimates. *Journal of chemical theory and computation* **2010,** *6* (12), 3713-3720.
175. Humphrey, W.; Dalke, A.; Schulten, K., VMD: visual molecular dynamics. *Journal of molecular graphics* **1996,** *14* (1), 33-38.
176. Dewprashad, B.; Eisenbraun, E., Fundamentals of epoxy formulation. *Journal of chemical education* **1994,** *71* (4), 290.

177. Giovanelli, L.; Lee, H.-L.; Lacaze-Dufaure, C.; Koudia, M.; Clair, S.; Lin, Y.-P.; Ksari, Y.; Themlin, J.-M.; Abel, M.; Cafolla, A. A., Electronic structure of tetra (4-aminophenyl) porphyrin studied by photoemission, UV–Vis spectroscopy and density functional theory. *Journal of Electron Spectroscopy and Related Phenomena* **2017,** *218*, 40-45.
178. Caminos, D. A.; Spesia, M. B.; Durantini, E. N., Photodynamic inactivation of Escherichia coli by novel meso-substituted porphyrins by 4-(3-N, N, N-trimethylammoniumpropoxy) phenyl and 4-(trifluoromethyl) phenyl groups. *Photochemical & Photobiological Sciences* **2006,** *5* (1), 56-65.
179. Van Leeuwen, M.; Beeby, A.; Fernandes, I.; Ashworth, S. H., The photochemistry and photophysics of a series of alpha octa (alkyl-substituted) silicon, zinc and palladium phthalocyanines. *Photochemical & Photobiological Sciences* **2013,** *13* (1), 62-69.
180. Engelmann, F. M.; Mayer, I.; Gabrielli, D. S.; Toma, H. E.; Kowaltowski, A. J.; Araki, K.; Baptista, M. S., Interaction of cationic meso-porphyrins with liposomes, mitochondria and erythrocytes. *Journal of bioenergetics and biomembranes* **2007,** *39* (2), 175-185.
181. Hudis, C. A.; Gianni, L., Triple-negative breast cancer: an unmet medical need. *The oncologist* **2011,** *16*, 1-11.
182. Foulkes, W. D.; Smith, I. E.; Reis-Filho, J. S., Triple-negative breast cancer. *New England journal of medicine* **2010,** *363* (20), 1938-1948.
183. Sambi, M.; Haq, S.; Samuel, V.; Qorri, B.; Haxho, F.; Hill, K.; Harless, W.; Szewczuk, M. R., Alternative therapies for metastatic breast cancer: multimodal approach targeting tumor cell heterogeneity. *Breast Cancer: Targets and Therapy* **2017,** *9*, 85.
184. Yanovsky, R. L.; Bartenstein, D. W.; Rogers, G. S.; Isakoff, S. J.; Chen, S. T., Photodynamic therapy for solid tumors: A review of the literature. *Photodermatology, photoimmunology & photomedicine* **2019,** *35* (5), 295-303.
185. Shi, X.; Zhang, C. Y.; Gao, J.; Wang, Z., Recent advances in photodynamic therapy for cancer and infectious diseases. *Wiley Interdisciplinary Reviews: Nanomedicine and Nanobiotechnology* **2019,** *11* (5), e1560.
186. Lyles, Z. K.; Tarannum, M.; Mena, C.; Inada, N. M.; Bagnato, V. S.; Vivero-Escoto, J. L., Biodegradable Silica-Based Nanoparticles with Improved and Safe Delivery of Protoporphyrin IX for the In Vivo Photodynamic Therapy of Breast Cancer. *Advanced Therapeutics* **2020,** *3* (7), 2000022.
187. Kadri, N. B.; Gdovin, M.; Alyassin, N.; Avila, J.; Cruz, A.; Cruz, L.; Holliday, S.; Jordan, Z.; Ruiz, C.; Watts, J., Photodynamic acidification therapy to reduce triple negative breast cancer growth in vivo. American Society of Clinical Oncology: 2016.
188. Medina, M. A.; Oza, G.; Sharma, A.; Arriaga, L.; Hernández Hernández, J. M.; Rotello, V. M.; Ramirez, J. T., Triple-negative breast cancer: a review of conventional and advanced therapeutic strategies. *International journal of environmental research and public health* **2020,** *17* (6), 2078.
189. O'Connor, A. E.; Gallagher, W. M.; Byrne, A. T., Porphyrin and nonporphyrin photosensitizers in oncology: preclinical and clinical advances in photodynamic therapy. *Photochemistry and photobiology* **2009,** *85* (5), 1053-1074.
190. Shinoda, W., Permeability across lipid membranes. *Biochimica et Biophysica Acta (BBA)-Biomembranes* **2016,** *1858* (10), 2254-2265.
191. Cohen, B. E., Membrane thickness as a key factor contributing to the activation of osmosensors and essential Ras signaling pathways. *Frontiers in cell and developmental biology* **2018,** *6*, 76.

192. Boucher, P.-A.; Joós, B.; Zuckermann, M. J.; Fournier, L., Pore formation in a lipid bilayer under a tension ramp: modeling the distribution of rupture tensions. *Biophysical journal* **2007,** *92* (12), 4344-4355.
193. Reddy, A. S.; Warshaviak, D. T.; Chachisvilis, M., Effect of membrane tension on the physical properties of DOPC lipid bilayer membrane. *Biochimica et Biophysica Acta (BBA)-Biomembranes* **2012,** *1818* (9), 2271-2281.
194. Kučerka, N.; Nagle, J. F.; Sachs, J. N.; Feller, S. E.; Pencer, J.; Jackson, A.; Katsaras, J., Lipid bilayer structure determined by the simultaneous analysis of neutron and X-ray scattering data. *Biophysical journal* **2008,** *95* (5), 2356-2367.
195. Heller, H.; Schaefer, M.; Schulten, K., Molecular dynamics simulation of a bilayer of 200 lipids in the gel and in the liquid crystal phase. *The Journal of Physical Chemistry* **1993,** *97* (31), 8343-8360.
196. Yue, K.; Huang, M.; Marson, R. L.; He, J.; Huang, J.; Zhou, Z.; Wang, J.; Liu, C.; Yan, X.; Wu, K., Geometry induced sequence of nanoscale Frank–Kasper and quasicrystal mesophases in giant surfactants. *Proceedings of the National Academy of Sciences* **2016,** *113* (50), 14195-14200.
197. Plimpton, S. *Fast parallel algorithms for short-range molecular dynamics*; Sandia National Labs., Albuquerque, NM (United States): 1993.
198. Laboratories, S. N. LAMMPS. http://lammps.sandia.gov.
199. Ryckaert, J.-P.; Ciccotti, G.; Berendsen, H. J., Numerical integration of the cartesian equations of motion of a system with constraints: molecular dynamics of n-alkanes. *Journal of computational physics* **1977,** *23* (3), 327-341.
200. Elber, R.; Ruymgaart, A. P.; Hess, B., SHAKE parallelization. *The European Physical Journal Special Topics* **2011,** *200* (1), 211-223.
201. Jorgensen, W. L.; Tirado–Rives, J., Molecular modeling of organic and biomolecular systems using BOSS and MCPRO. *Journal of computational chemistry* **2005,** *26* (16), 1689-1700.
202. Jorgensen, W., BOSS-Biochemical and organic simulation system. *The encyclopedia of computational Chemistry* **1998,** *5*, 3281-3285.
203. YABE, M.; MORI, K.; UEDA, K.; TAKEDA, M., Development of PolyParGen software to facilitate the determination of molecular dynamics simulation parameters for polymers. *Journal of Computer Chemistry, Japan-International Edition* **2019,** *5*, 2018-0034.
204. Allison, J. R.; Welsh, I. D., CherryPicker: An Algorithm for the Automated Parameterisation of Large Biomolecules for Molecular Simulation. *Frontiers in chemistry* **2019,** *7*, 400.
205. Jewett, A. I.; Zhuang, Z.; Shea, J.-E., Moltemplate a coarse-grained model assembly tool. *Biophysical Journal* **2013,** *104* (2), 169a.
206. Fogolari, F.; Corazza, A.; Viglino, P.; Zuccato, P.; Pieri, L.; Faccioli, P.; Bellotti, V.; Esposito, G., Molecular dynamics simulation suggests possible interaction patterns at early steps of β2-microglobulin aggregation. *Biophysical journal* **2007,** *92* (5), 1673-1681.
207. Pagano, K.; Bemporad, F.; Fogolari, F.; Esposito, G.; Viglino, P.; Chiti, F.; Corazza, A., Structural and dynamics characteristics of acylphosphatase from Sulfolobus solfataricus in the monomeric state and in the initial native-like aggregates. *Journal of Biological Chemistry* **2010,** *285* (19), 14689-14700.
208. Fogolari, F.; Corazza, A.; Varini, N.; Rotter, M.; Gumral, D.; Codutti, L.; Rennella, E.; Viglino, P.; Bellotti, V.; Esposito, G., Molecular dynamics simulation of β2-microglobulin in

denaturing and stabilizing conditions. *Proteins: Structure, Function, and Bioinformatics* **2011,** *79* (3), 986-1001.
209. Zajac, G.; Machalska, E.; Kaczor, A.; Kessler, J.; Bouř, P.; Baranska, M., Structure of supramolecular astaxanthin aggregates revealed by molecular dynamics and electronic circular dichroism spectroscopy. *Physical Chemistry Chemical Physics* **2018,** *20* (26), 18038-18046.
210. Jorgensen, W. L.; Maxwell, D. S.; Tirado-Rives, J., Development and testing of the OPLS all-atom force field on conformational energetics and properties of organic liquids. *Journal of the American Chemical Society* **1996,** *118* (45), 11225-11236.
211. Hockney, R. W.; Eastwood, J. W., *Computer simulation using particles*. crc Press: 1988.
212. Pollock, E.; Glosli, J., Comments on P3M, FMM, and the Ewald method for large periodic Coulombic systems. *Computer Physics Communications* **1996,** *95* (2-3), 93-110.
213. Marques, H. M.; Brown, K. L., Molecular mechanics and molecular dynamics simulations of porphyrins, metalloporphyrins, heme proteins and cobalt corrinoids. *Coordination chemistry reviews* **2002,** *225* (1-2), 123-158.
214. Rycroft, C. *Voro++: A three-dimensional Voronoi cell library in C++*; Lawrence Berkeley National Lab.(LBNL), Berkeley, CA (United States): 2009.
215. Voloshin, V. P.; Medvedev, N. N.; Andrews, M. N.; Burri, R. R.; Winter, R.; Geiger, A., Volumetric properties of hydrated peptides: Voronoi–Delaunay analysis of molecular simulation runs. *The Journal of Physical Chemistry B* **2011,** *115* (48), 14217-14228.
216. Cazals, F.; Proust, F.; Bahadur, R. P.; Janin, J., Revisiting the Voronoi description of protein–protein interfaces. *Protein Science* **2006,** *15* (9), 2082-2092.
217. McConkey, B. J.; Sobolev, V.; Edelman, M., Quantification of protein surfaces, volumes and atom–atom contacts using a constrained Voronoi procedure. *Bioinformatics* **2002,** *18* (10), 1365-1373.
218. Liu, Z.; Zou, Y.; Zhang, Q.; Chen, P.; Liu, Y.; Qian, Z., Distinct Binding Dynamics, Sites and Interactions of Fullerene and Fullerenols with Amyloid-β Peptides Revealed by Molecular Dynamics Simulations. *International Journal of Molecular Sciences* **2019,** *20* (8), 2048.
219. Corporation, S. LAMMPS Documentation. https://lammps.sandia.gov/doc/Manual.html.
220. Siggel, U.; Bindig, U.; Endisch, C.; Komatsu, T.; Tsuchida, E.; Voigt, J.; Fuhrhop, J. H., Photophysical and photochemical properties of porphyrin aggregates. *Berichte der Bunsengesellschaft für physikalische Chemie* **1996,** *100* (12), 2070-2075.
221. Keller, N.; Calik, M.; Sharapa, D.; Soni, H. R.; Zehetmaier, P. M.; Rager, S.; Auras, F.; Jakowetz, A. C.; Görling, A.; Clark, T., Enforcing extended porphyrin J-aggregate stacking in covalent organic frameworks. *Journal of the American Chemical Society* **2018,** *140* (48), 16544-16552.
222. Mabesoone, M. F.; Markvoort, A. J.; Banno, M.; Yamaguchi, T.; Helmich, F.; Naito, Y.; Yashima, E.; Palmans, A. R.; Meijer, E., Competing interactions in hierarchical porphyrin self-assembly introduce robustness in pathway complexity. *Journal of the American Chemical Society* **2018,** *140* (25), 7810-7819.
223. Ghadamgahi, M.; Ajloo, D., The effects of urea, guanidinium chloride and sorbitol on porphyrin aggregation: Molecular dynamics simulation. *Journal of Chemical Sciences* **2013,** *125* (3), 627-641.
224. Lorecchio, C.; Venanzi, M.; Mazzuca, C.; Lettieri, R.; Palleschi, A.; Thi, T. H. N.; Cardová, L.; Drasar, P.; Monti, D., Tuning the chiroptical and morphological properties of steroidal-porphyrin aggregates: a mechanistic, structural, and MM investigation. *Organic & biomolecular chemistry* **2014,** *12* (23), 3956-3963.

225. Wang, H.; Yue, B.; Xie, Z.; Gao, B.; Xu, Y.; Liu, L.; Sun, H.; Ma, Y., Controlled transition dipole alignment of energy donor and energy acceptor molecules in doped organic crystals, and the effect on intermolecular Förster energy transfer. *Physical Chemistry Chemical Physics* **2013,** *15* (10), 3527-3534.
226. Frederix, P. W.; Patmanidis, I.; Marrink, S. J., Molecular simulations of self-assembling bio-inspired supramolecular systems and their connection to experiments. *Chemical Society Reviews* **2018,** *47* (10), 3470-3489.
227. Samanta, U.; Bahadur, R. P.; Chakrabarti, P., Quantifying the accessible surface area of protein residues in their local environment. *Protein engineering* **2002,** *15* (8), 659-667.
228. Moret, M.; Zebende, G., Amino acid hydrophobicity and accessible surface area. *Physical Review E* **2007,** *75* (1), 011920.
229. Arba, M.; Ihsan, S.; Tjahjono, D. H., Computational approach toward targeting the interaction of porphyrin derivatives with Bcl-2. *Journal of Applied Pharmaceutical Science* **2018,** *8* (12), 060-066.
230. Lott, G. A.; Perdomo-Ortiz, A.; Utterback, J. K.; Widom, J. R.; Aspuru-Guzik, A.; Marcus, A. H., Conformation of self-assembled porphyrin dimers in liposome vesicles by phase-modulation 2D fluorescence spectroscopy. *Proceedings of the National Academy of Sciences* **2011,** *108* (40), 16521-16526.
231. Bujdák, J., The effects of layered nanoparticles and their properties on the molecular aggregation of organic dyes. *Journal of Photochemistry and Photobiology C: Photochemistry Reviews* **2018,** *35*, 108-133.
232. Cannon, B. L.; Patten, L. K.; Kellis, D. L.; Davis, P. H.; Lee, J.; Graugnard, E.; Yurke, B.; Knowlton, W. B., Large Davydov splitting and strong fluorescence suppression: an investigation of exciton delocalization in DNA-templated Holliday junction dye aggregates. *The Journal of Physical Chemistry A* **2018,** *122* (8), 2086-2095.
233. Srivastava, A.; Garg, A.; Das, D.; Debnath, A., Molecular dynamics simulations of a stacked $$\uppi $$ π-conjugated soft material: binding energy and preferential geometry for self-assembly. *Bulletin of Materials Science* **2020,** *43* (1), 1-8.
234. **!!! INVALID CITATION !!! 41-45**.
235. Wu, S.; Gao, G.; Zhang, S.; Zhu, W.; Wang, L.; Chen, R.; Zhang, W.; Wang, J.; Yang, F.; Li, J., Mixed-solvent precipitation: A facile approach for nanoparticle self-assembled monolayers. *Applied Surface Science* **2019,** *465*, 526-531.
236. Zhu, G.; Huang, Z.; Xu, Z.; Yan, L.-T., Tailoring interfacial nanoparticle organization through entropy. *Accounts of chemical research* **2018,** *51* (4), 900-909.
237. Guo, B.; Cai, X.; Xu, S.; Fateminia, S. M. A.; Liu, J.; Liang, J.; Feng, G.; Wu, W.; Liu, B., Decoration of porphyrin with tetraphenylethene: converting a fluorophore with aggregation-caused quenching to aggregation-induced emission enhancement. *Journal of Materials Chemistry B* **2016,** *4* (27), 4690-4695.
238. Zhang, G.; Chen, Q.; Zhang, Y.; Kong, L.; Tao, X.; Lu, H.; Tian, Y.; Yang, J., Bulky group functionalized porphyrin and its Zn (II) complex with high emission in aggregation. *Inorganic Chemistry Communications* **2014,** *46*, 85-88.
239. Uttamlal, M.; Holmes-Smith, A. S., The excitation wavelength dependent fluorescence of porphyrins. *Chemical Physics Letters* **2008,** *454* (4-6), 223-228.
240. Parkash, J.; Robblee, J. H.; Agnew, J.; Gibbs, E.; Collings, P.; Pasternack, R. F.; De Paula, J. C., Depolarized resonance light scattering by porphyrin and chlorophyll a aggregates. *Biophysical journal* **1998,** *74* (4), 2089-2099.

241. Collings, P. J.; Gibbs, E. J.; Starr, T. E.; Vafek, O.; Yee, C.; Pomerance, L. A.; Pasternack, R. F., Resonance light scattering and its application in determining the size, shape, and aggregation number for supramolecular assemblies of chromophores. *The Journal of Physical Chemistry B* **1999,** *103* (40), 8474-8481.
242. Breil, C.; Abert Vian, M.; Zemb, T.; Kunz, W.; Chemat, F., "Bligh and Dyer" and Folch methods for solid–liquid–liquid extraction of lipids from microorganisms. Comprehension of solvatation mechanisms and towards substitution with alternative solvents. *International journal of molecular sciences* **2017,** *18* (4), 708.
243. Vreeland, E. C.; Watt, J.; Schober, G. B.; Hance, B. G.; Austin, M. J.; Price, A. D.; Fellows, B. D.; Monson, T. C.; Hudak, N. S.; Maldonado-Camargo, L., Enhanced nanoparticle size control by extending LaMer's mechanism. *Chemistry of Materials* **2015,** *27* (17), 6059-6066.
244. Hajimohammadi, M.; Vaziri Sereshk, A.; Schwarzinger, C.; Knör, G., Suppressing Effect of 2-Nitrobenzaldehyde on Singlet Oxygen Generation, Fatty Acid Photooxidation, and Dye-Sensitizer Degradation. *Antioxidants* **2018,** *7* (12), 194.
245. Lee, J. H.; Jung, M. Y., Direct spectroscopic observation of singlet oxygen quenching and kinetic studies of physical and chemical singlet oxygen quenching rate constants of synthetic antioxidants (BHA, BHT, and TBHQ) in methanol. *Journal of food science* **2010,** *75* (6), C506-C513.
246. Wu, D.; Yan, J.; Tang, P.; Li, S.; Xu, K.; Li, H., Binding properties and structure–affinity relationships of food antioxidant butylated hydroxyanisole and its metabolites with lysozyme. *Food chemistry* **2015,** *188*, 370-376.
247. Sun, Y. P.; Fox, M. A., Fluorescence of 9-cyanoanthracene in supercritical ethane: a very unusual dependence of fluorescence lifetime on solvent refractive index. *The Journal of Physical Chemistry* **1993,** *97* (2), 282-283.
248. Chung, P.-H.; Tregidgo, C.; Suhling, K., Determining a fluorophore's transition dipole moment from fluorescence lifetime measurements in solvents of varying refractive index. *Methods and applications in fluorescence* **2016,** *4* (4), 045001.
249. Kano, K.; Nakajima, T.; Takei, M.; Hashimoto, S., Self aggregation of cationic porphyrin in water. *Bulletin of the Chemical Society of Japan* **1987,** *60* (4), 1281-1287.
250. Hilaire, M. R.; Mukherjee, D.; Troxler, T.; Gai, F., Solvent dependence of cyanoindole fluorescence lifetime. *Chemical physics letters* **2017,** *685*, 133-138.
251. Liu, F.; Zhang, Y.; Xu, L.; Zhang, W., Morphology-Controlled Self-Assembly of an Organic/Inorganic Hybrid Porphyrin Derivative Containing Polyhedral Oligomeric Silsesquioxane (POSS). *Chemistry–A European Journal* **2015,** *21* (14), 5540-5547.
252. Liu, Q.-Y.; Jia, Q.-Y.; Zhu, J.-Q.; Shao, Q.; Fan, J.-F.; Wang, D.-M.; Yin, Y.-S., Highly ordered arrangement of meso-tetrakis (4-aminophenyl) porphyrin in self-assembled nanoaggregates via hydrogen bonding. *Chinese Chemical Letters* **2014,** *25* (5), 752-756.
253. Koch, F.; Kullmann, M.; Selig, U.; Nuernberger, P.; Götz, D. C.; Bringmann, G.; Brixner, T., Coherent two-dimensional electronic spectroscopy in the Soret band of a chiral porphyrin dimer. *New Journal of Physics* **2013,** *15* (2), 025006.
254. Maiti, N. C.; Ravikanth, M.; Mazumdar, S.; Periasamy, N., Fluorescence dynamics of noncovalently linked porphyrin dimers, and aggregates. *The Journal of Physical Chemistry* **1995,** *99* (47), 17192-17197.

255. Andrade, S. M.; Teixeira, R.; Costa, S. M.; Sobral, A. J., Self-aggregation of free base porphyrins in aqueous solution and in DMPC vesicles. *Biophysical chemistry* **2008,** *133* (1-3), 1-10.
256. Ghanbari, H.; Cousins, B. G.; Seifalian, A. M., A nanocage for nanomedicine: polyhedral oligomeric silsesquioxane (POSS). *Macromolecular rapid communications* **2011,** *32* (14), 1032-1046.
257. Paczesny, J.; Binkiewicz, I.; Janczuk, M.; Wybrańska, K.; Richter, Ł.; Hołyst, R., Langmuir and Langmuir–Blodgett films of unsymmetrical and fully condensed polyhedral oligomeric silsesquioxanes (POSS). *The Journal of Physical Chemistry C* **2015,** *119* (48), 27007-27017.
258. Xu, Y.; Huang, J.; Li, Y.; Wang, M.; Cao, Y.; Yuan, C.; Zeng, B.; Dai, L., A novel hybrid polyhedral oligomeric silsesquioxane-based copolymer with zwitterion: Synthesis, characterization, self-assembly behavior and pH responsive property. *Macromolecular Research* **2017,** *25* (8), 817-825.
259. Pandey, S.; Johnson, D.; Kaplan, R.; Klobusicky, J.; Menon, G.; Gracias, D. H., Self-assembly of mesoscale isomers: the role of pathways and degrees of freedom. *Plos One* **2014,** *9* (10), e108960.
260. King, E. M.; Gebbie, M. A.; Melosh, N. A., Impact of Rigidity on Molecular Self-Assembly. *Langmuir* **2019,** *35* (48), 16062-16069.
261. Han, D.; Wen, T.-j.; Han, G.; Deng, Y.-y.; Deng, Y.; Zhang, Q.; Fu, Q., Synthesis of Janus POSS star polymer and exploring its compatibilization behavior for PLLA/PCL polymer blends. *Polymer* **2018,** *136,* 84-91.

APPENDIX: POSS PORPHYRINS STRUCTURAL CHARACTERIZATION

Aminopropyl hepta(isobutyl) POSS

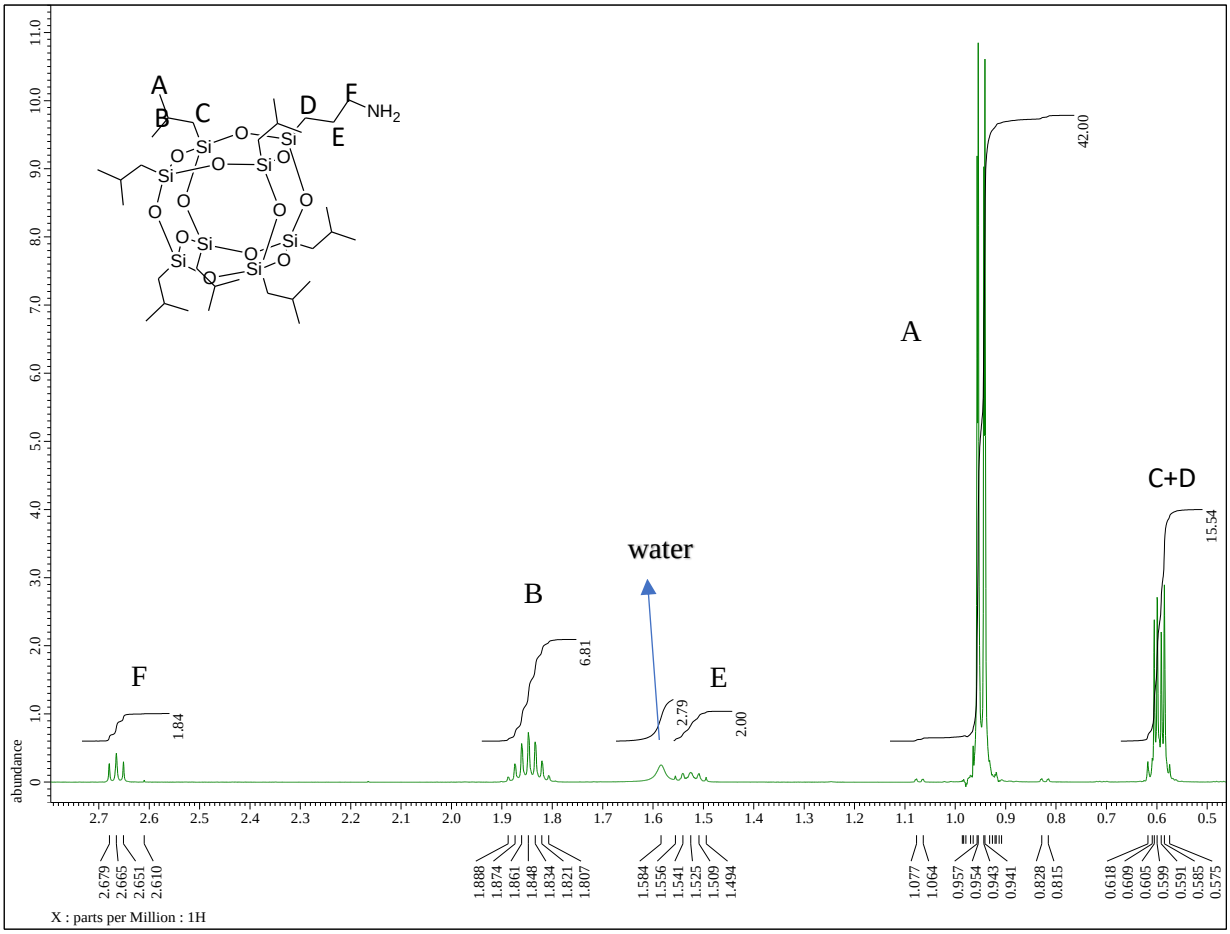

Figure A1. ^{1}H NMR Aminopropyl hepta(isobutyl) POSS

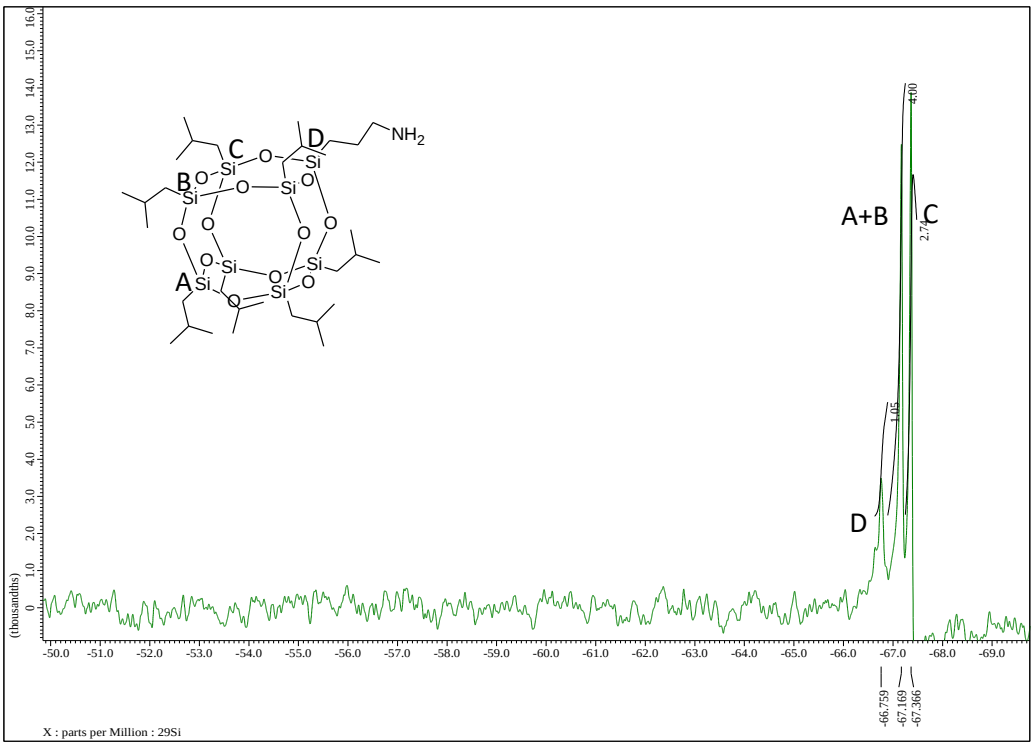

Figure A2. ^{29}Si NMR Aminopropyl hepta(isobutyl) POSS

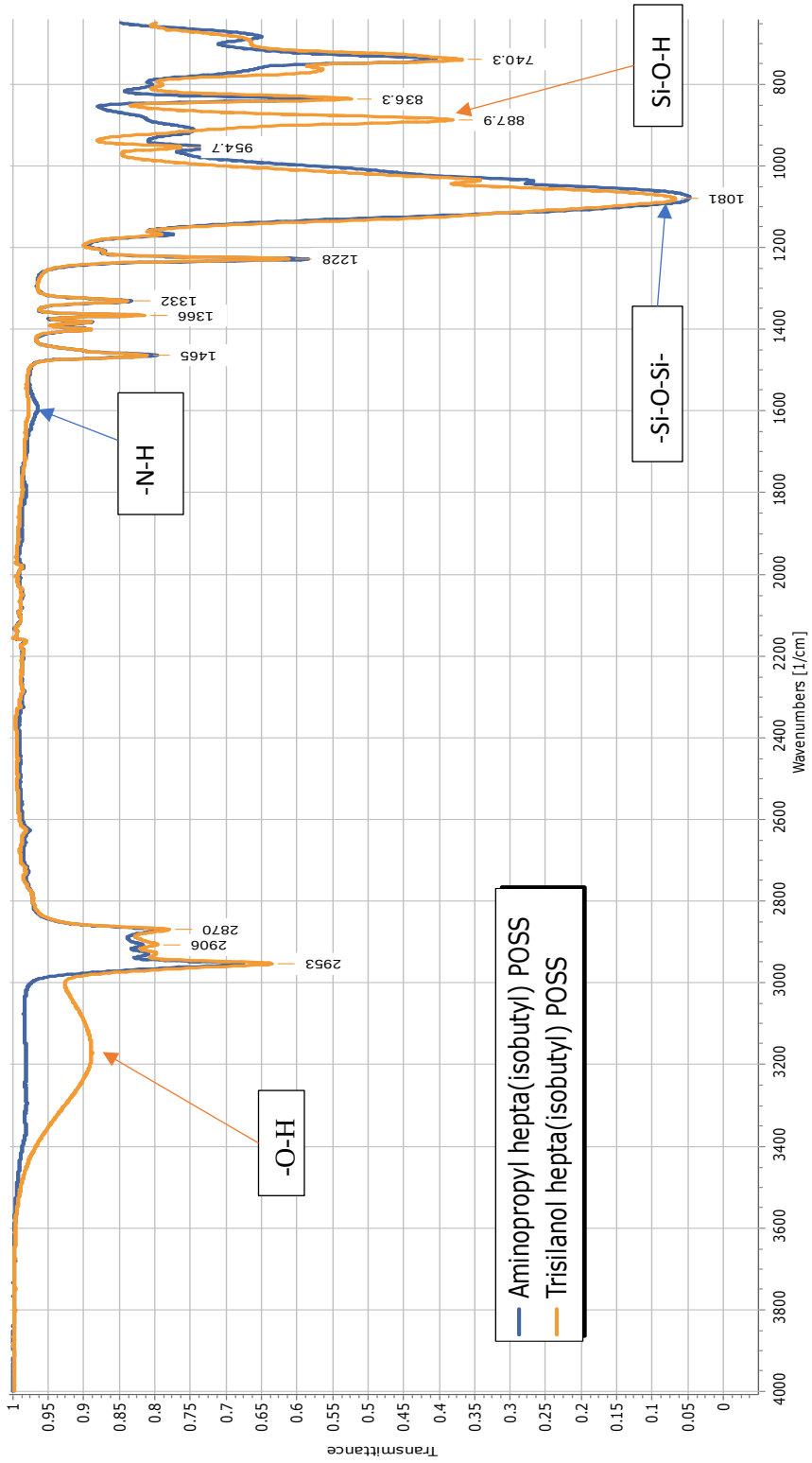

Figure A3. FT-IR Aminopropyl hepta(isobutyl) POSS

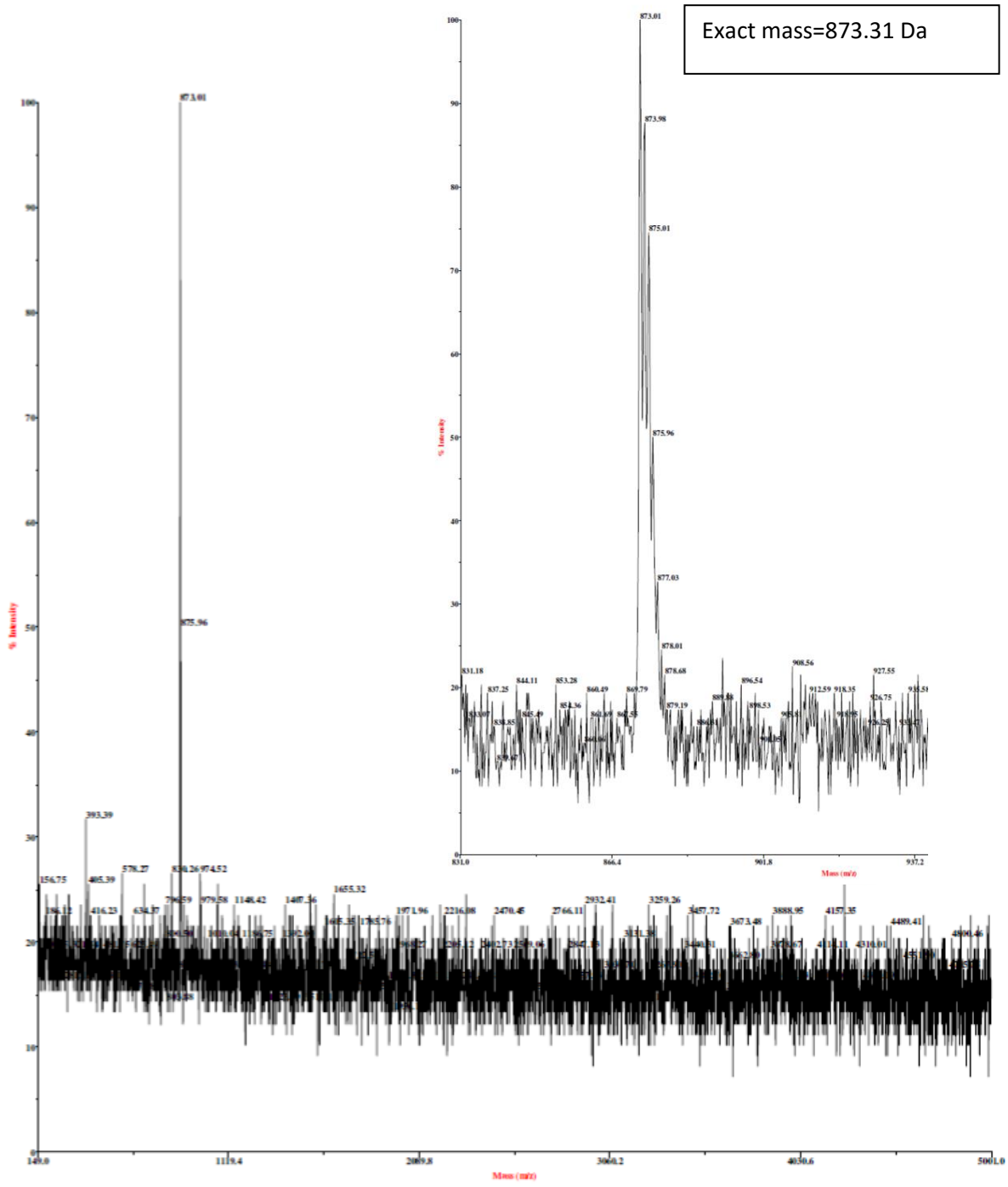

Figure A4. MALDI-TOF MS for [JV82]Aminopropyl hepta(isobutyl)

POSS

Propyl isocyanate hepta(isobutyl) POSS

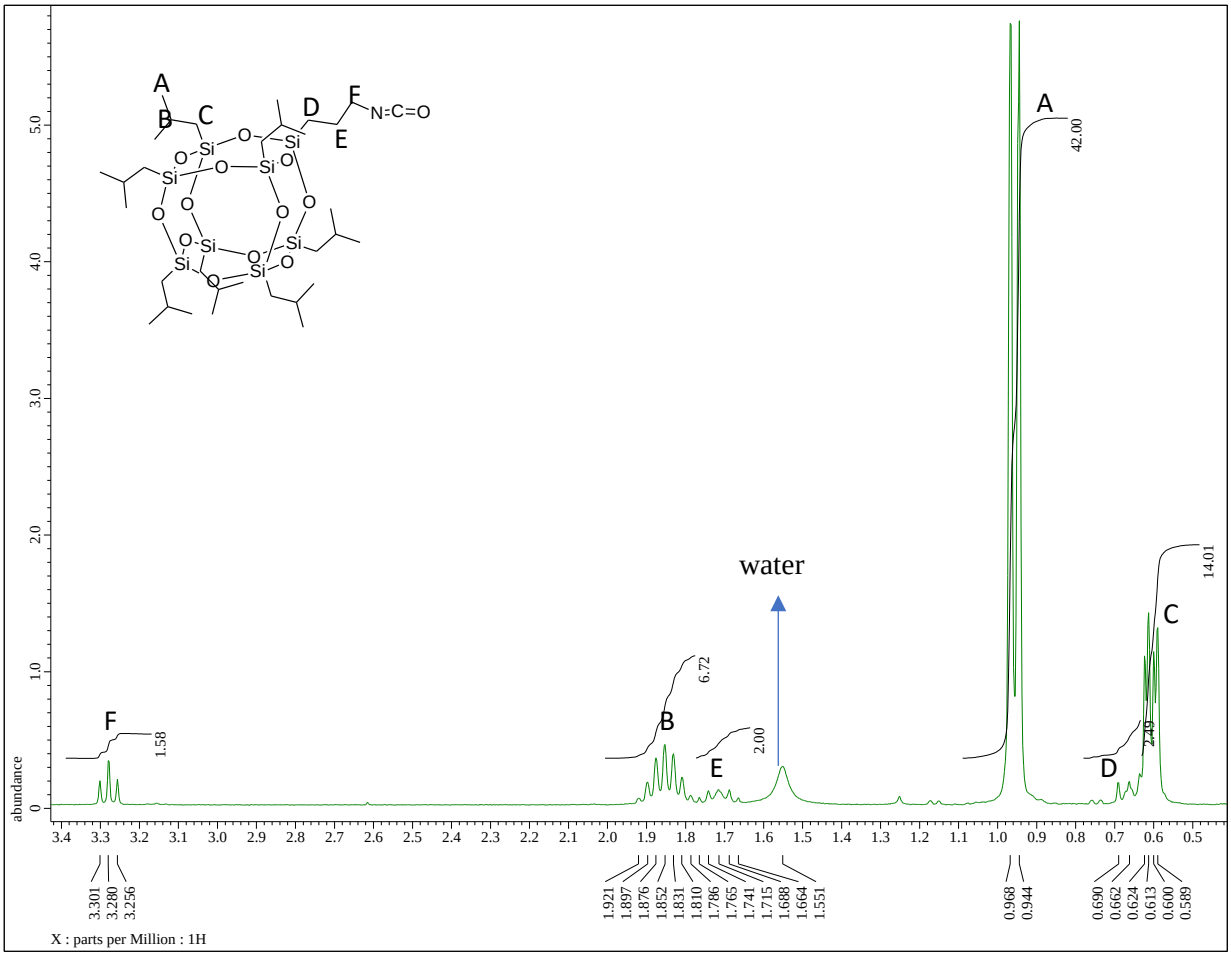

Figure A5. ^{1}H NMR Propyl-isocyanate hepta(isobutyl) POSS[JV83]

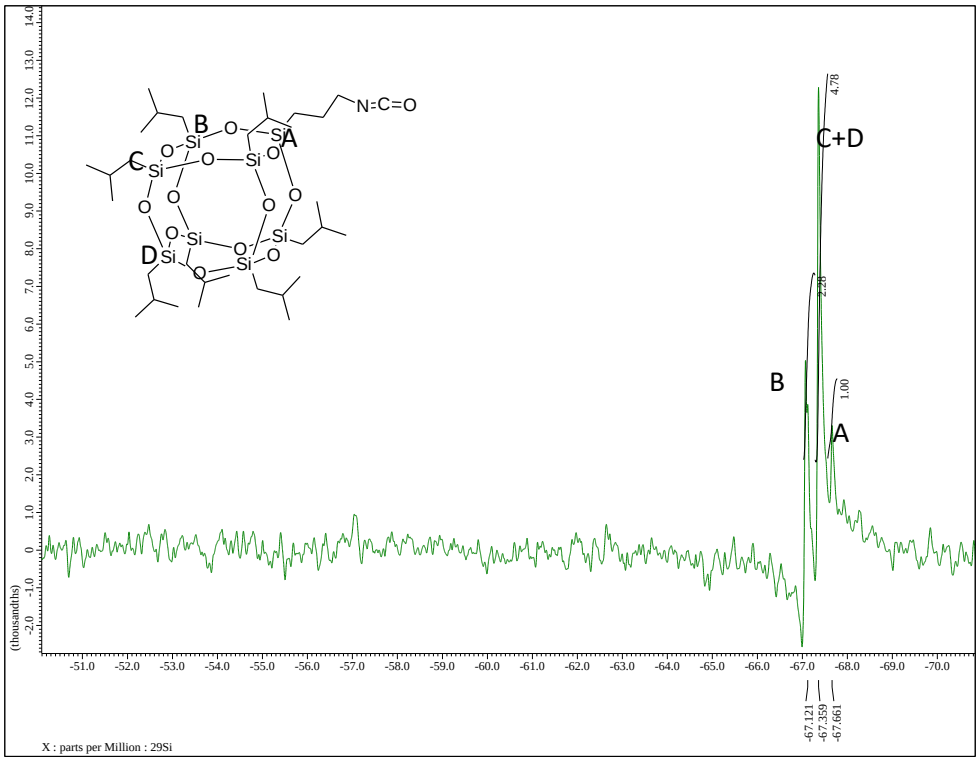

Figure A6. ^{29}Si NMR Propyl-isocyanate hepta(isobutyl) POSS

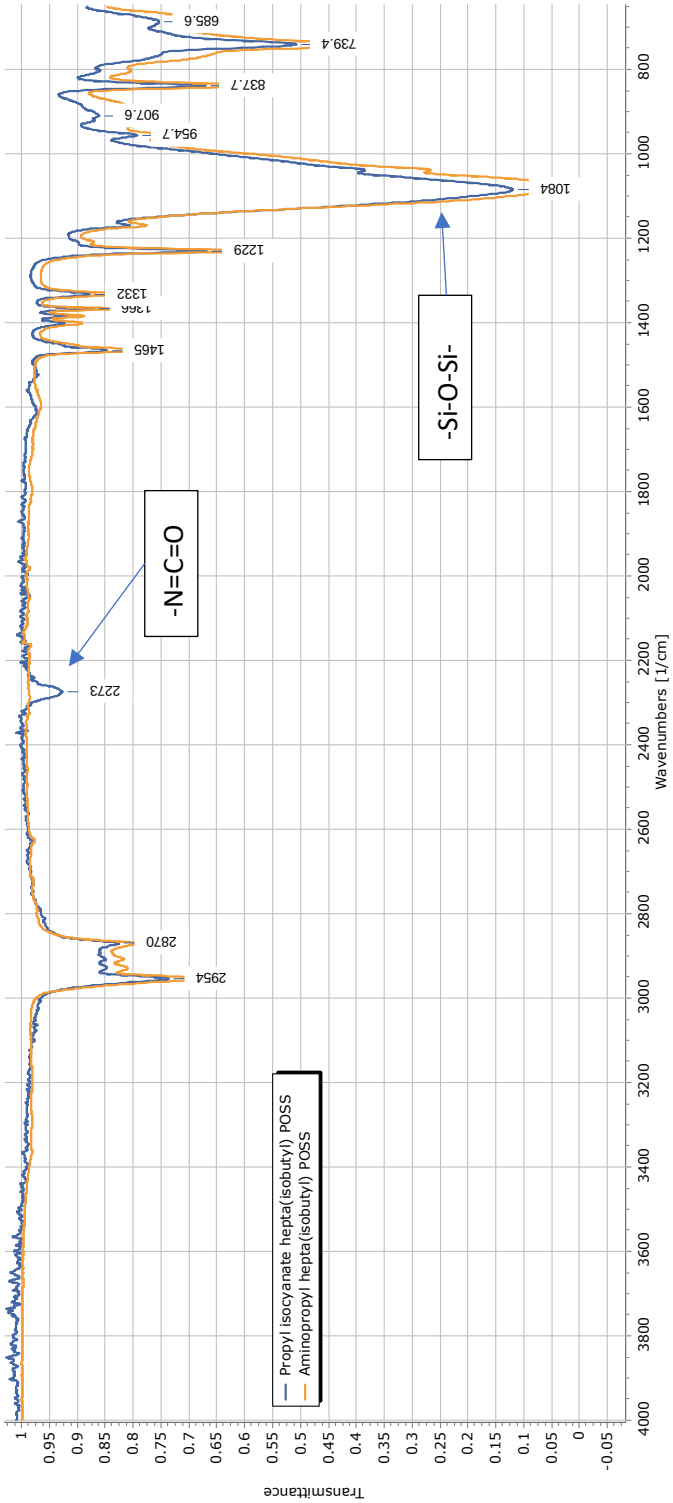

Figure A7. FT-IR Propyl-isocyanate hepta(isobutyl) POSS

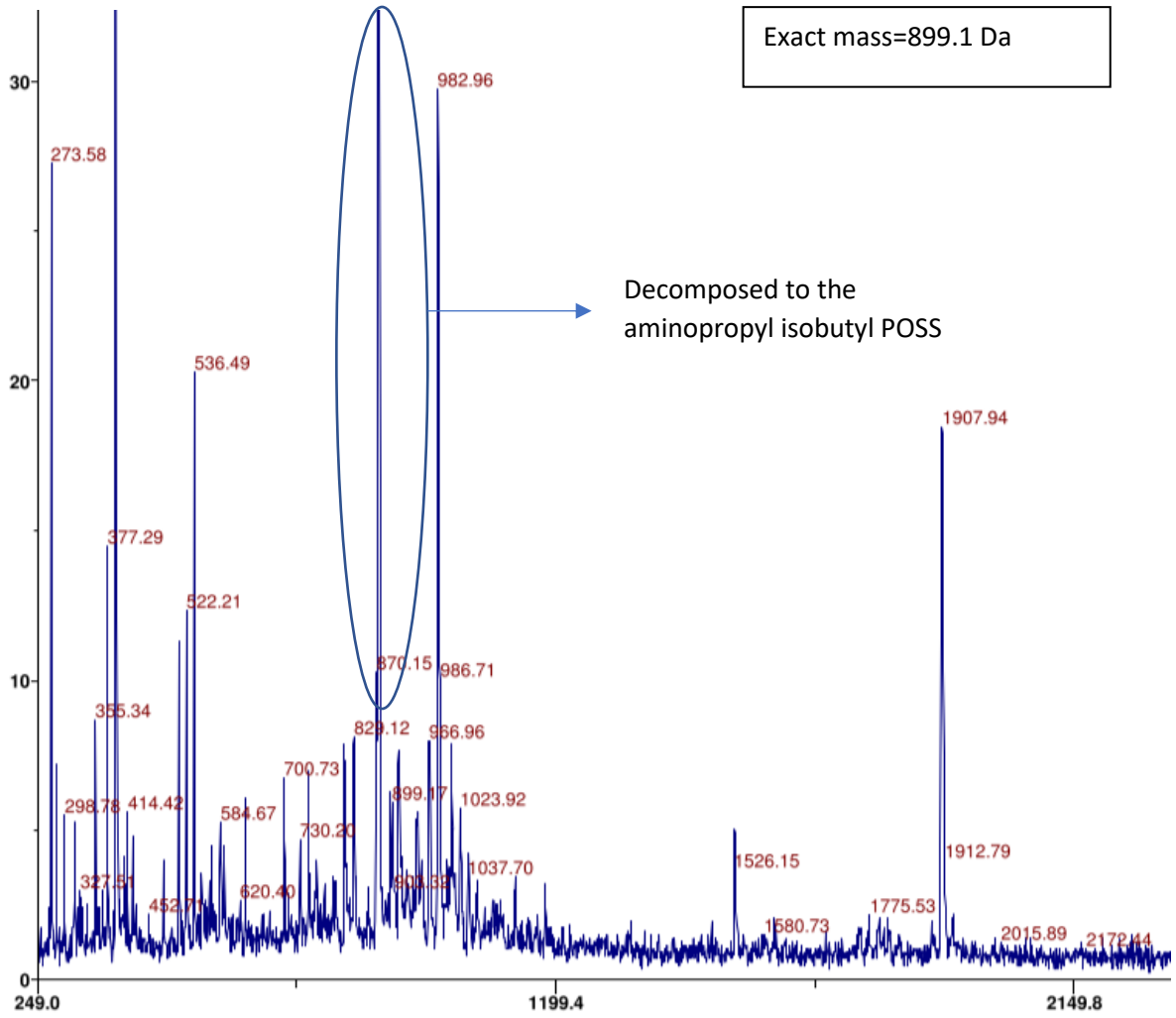

Figure A8. MALDI-TOF MS Propyl-isocyanate hepta(isobutyl) POSS[JV84]

POSSP-IB

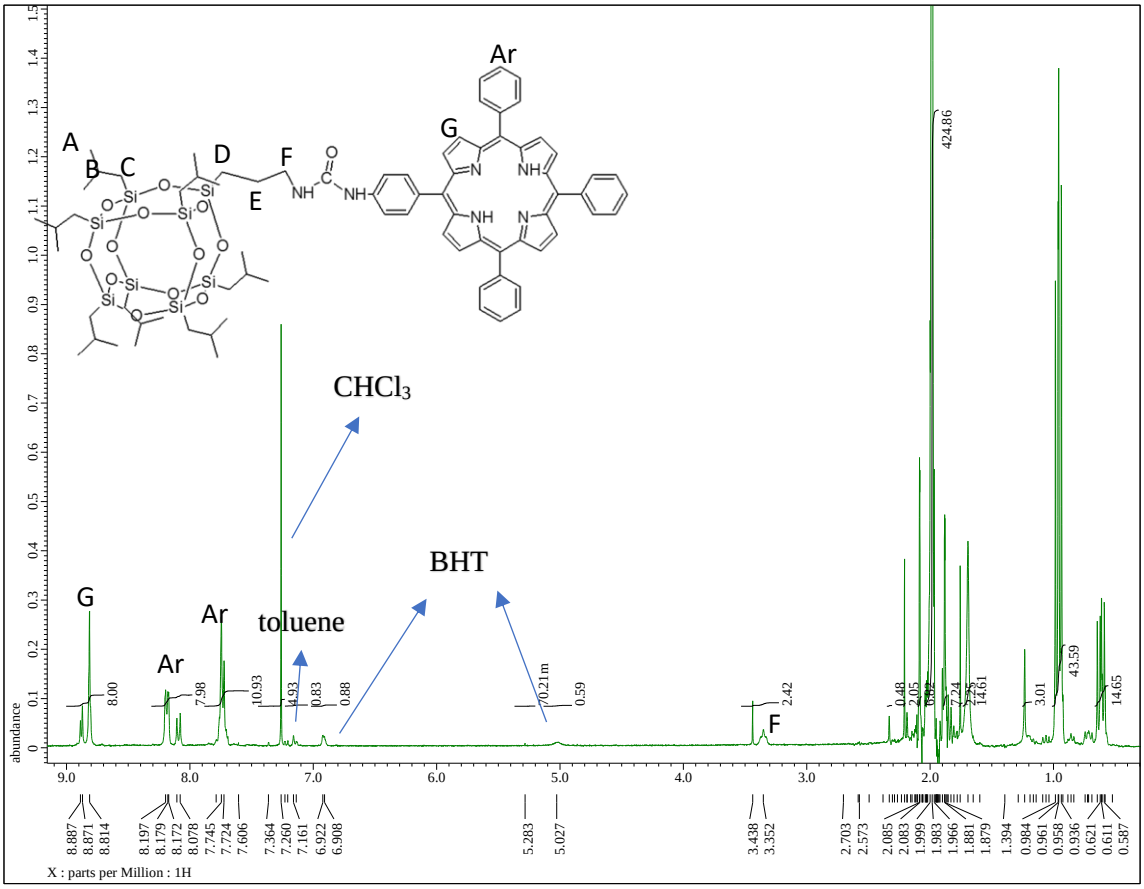

Figure A9. ^{1}H NMR POSSP-IB[JV85]

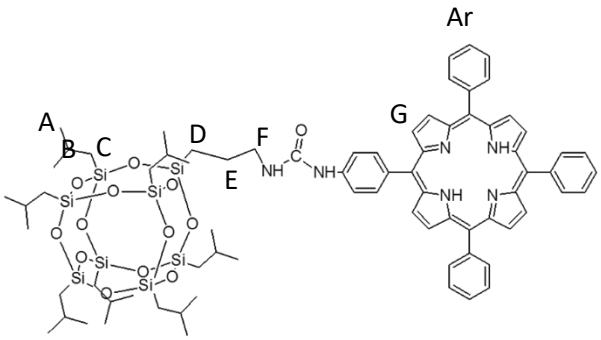

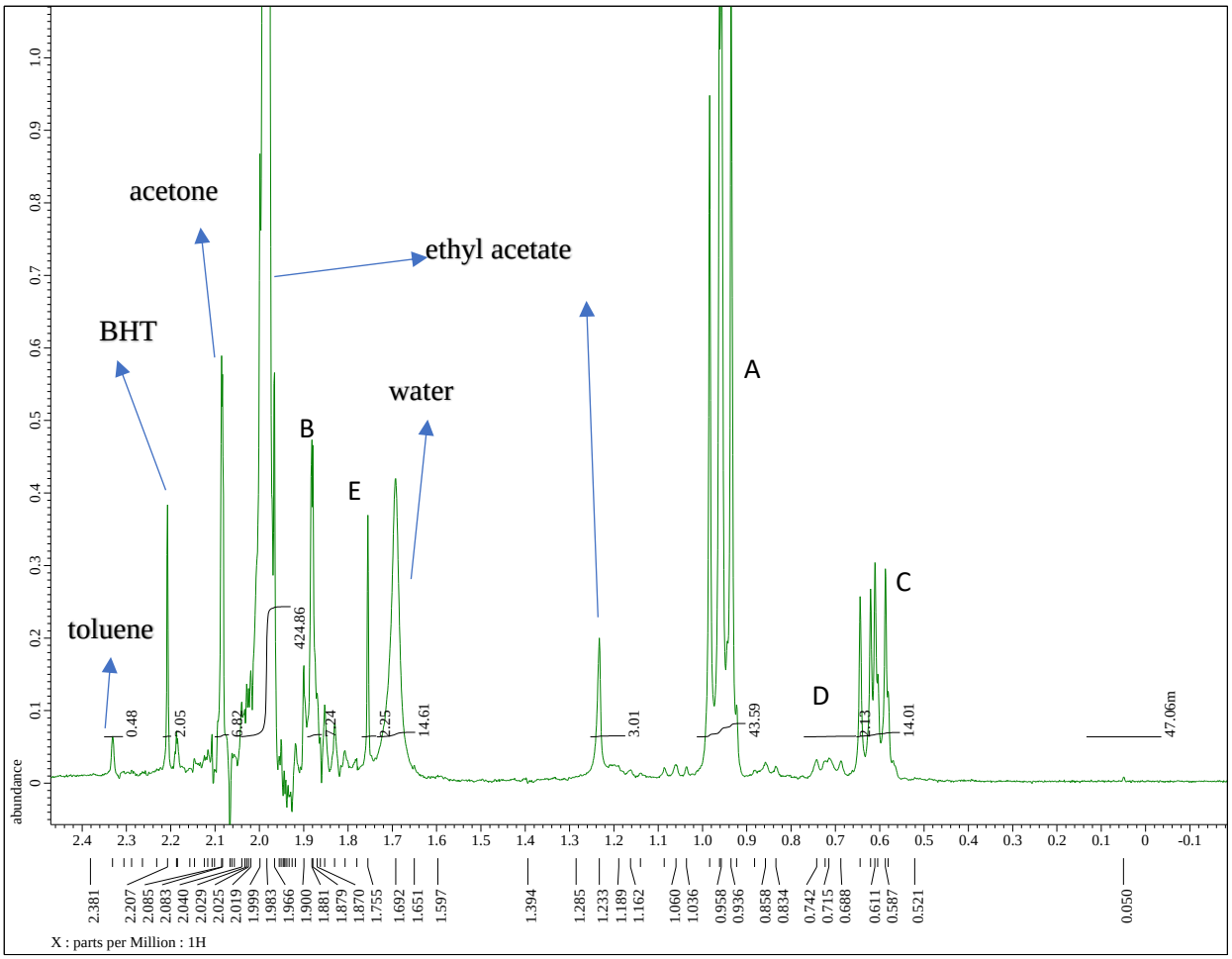

Figure A10. ^{1}H NMR POSSP-IB (aliphatic region)

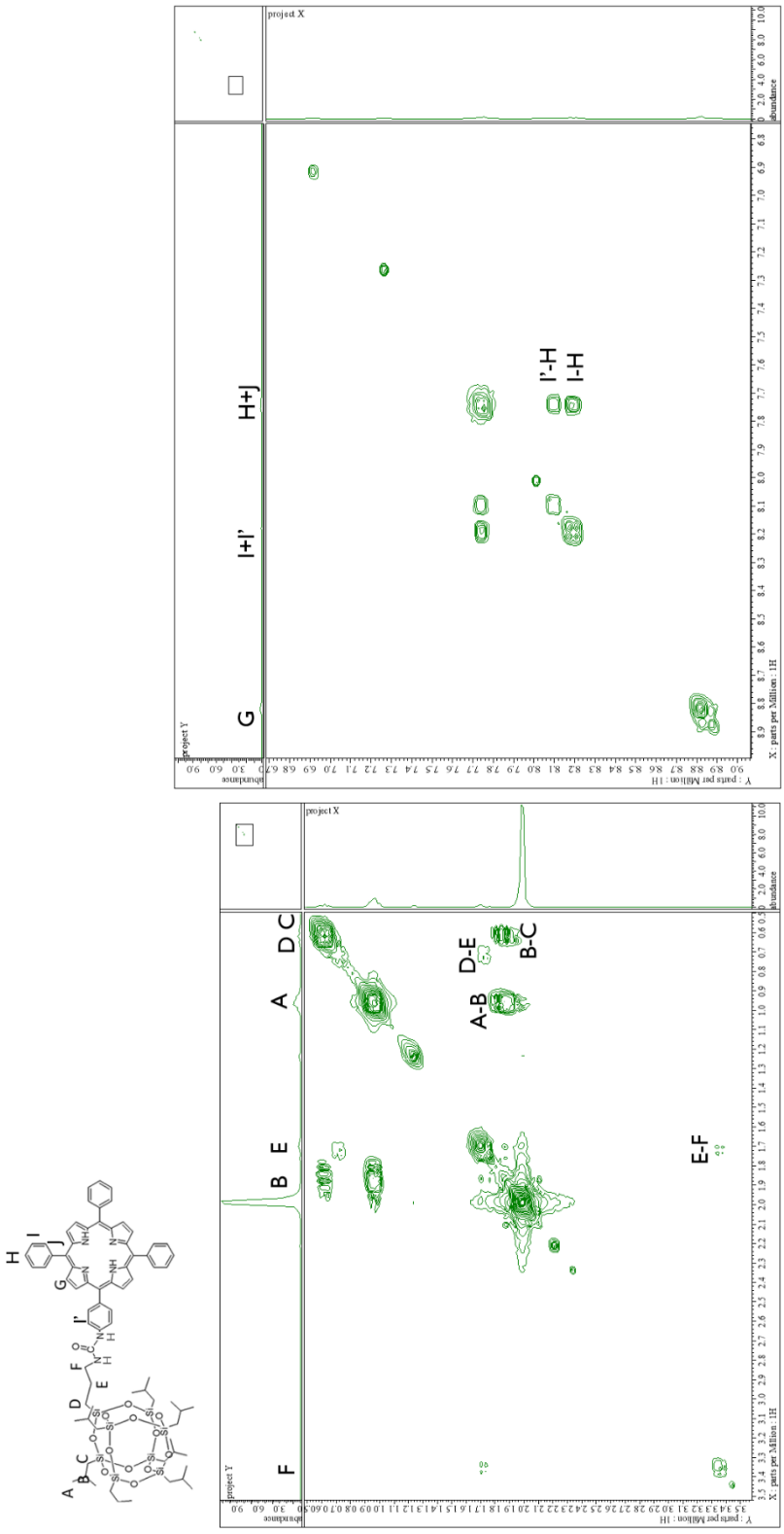

Figure A11. COSY NMR POSSP-IB

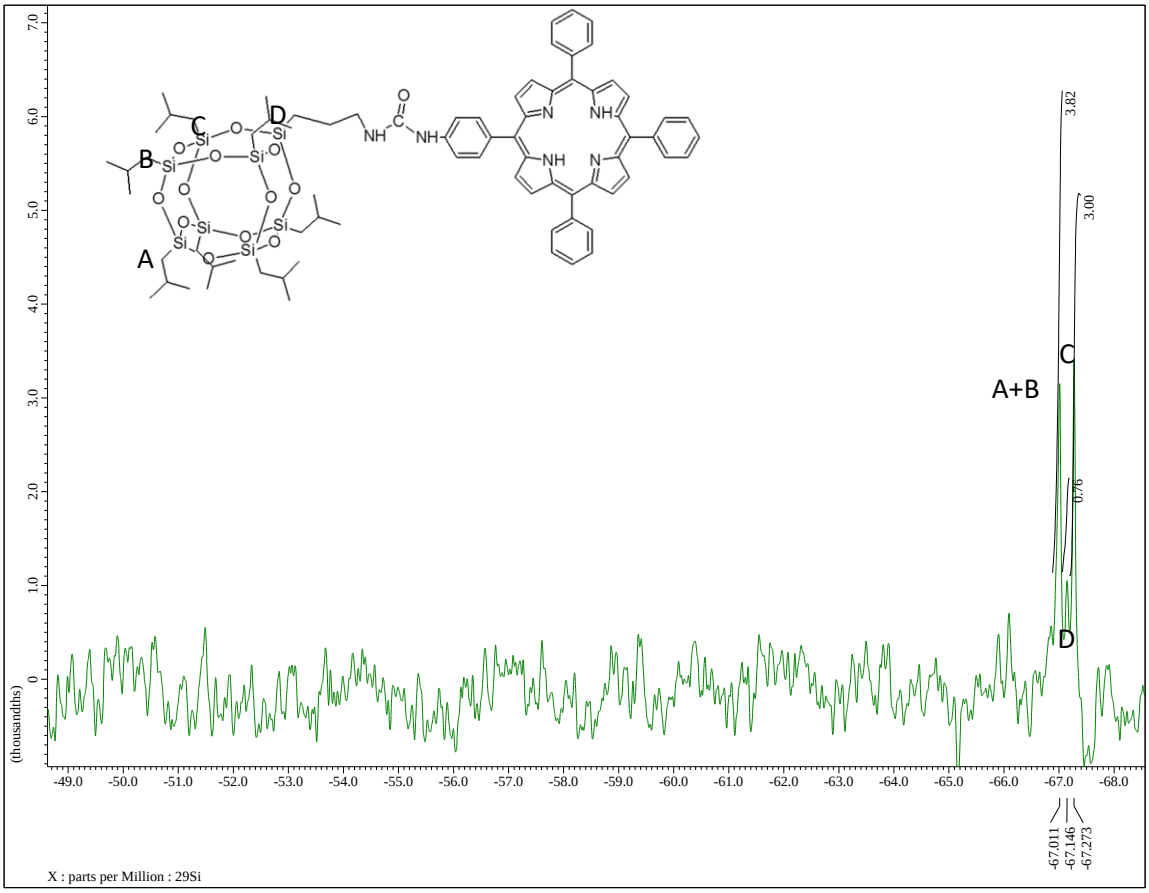

Figure A12. ^{29}Si NMR POSSP-IB

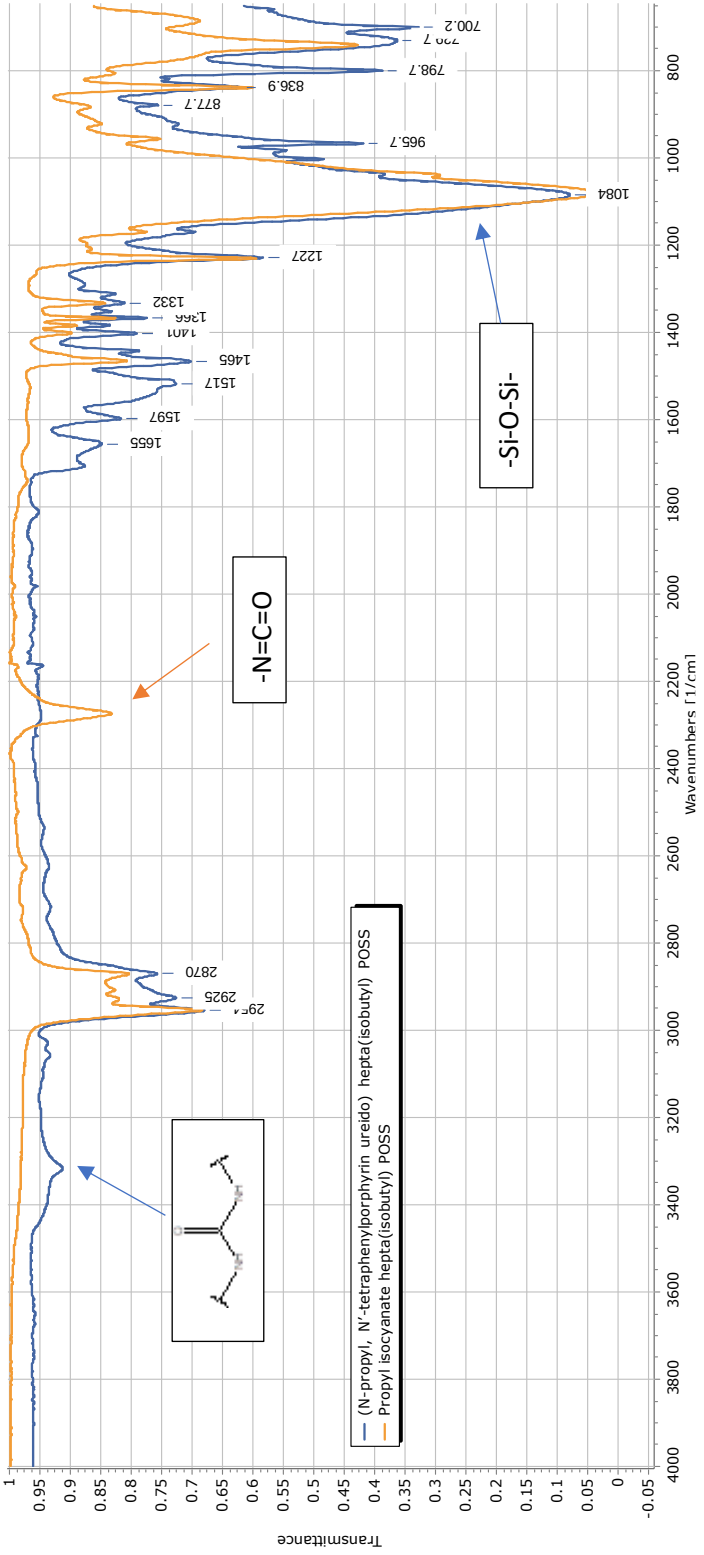

Figure A13. FT-IR POSSP-IB

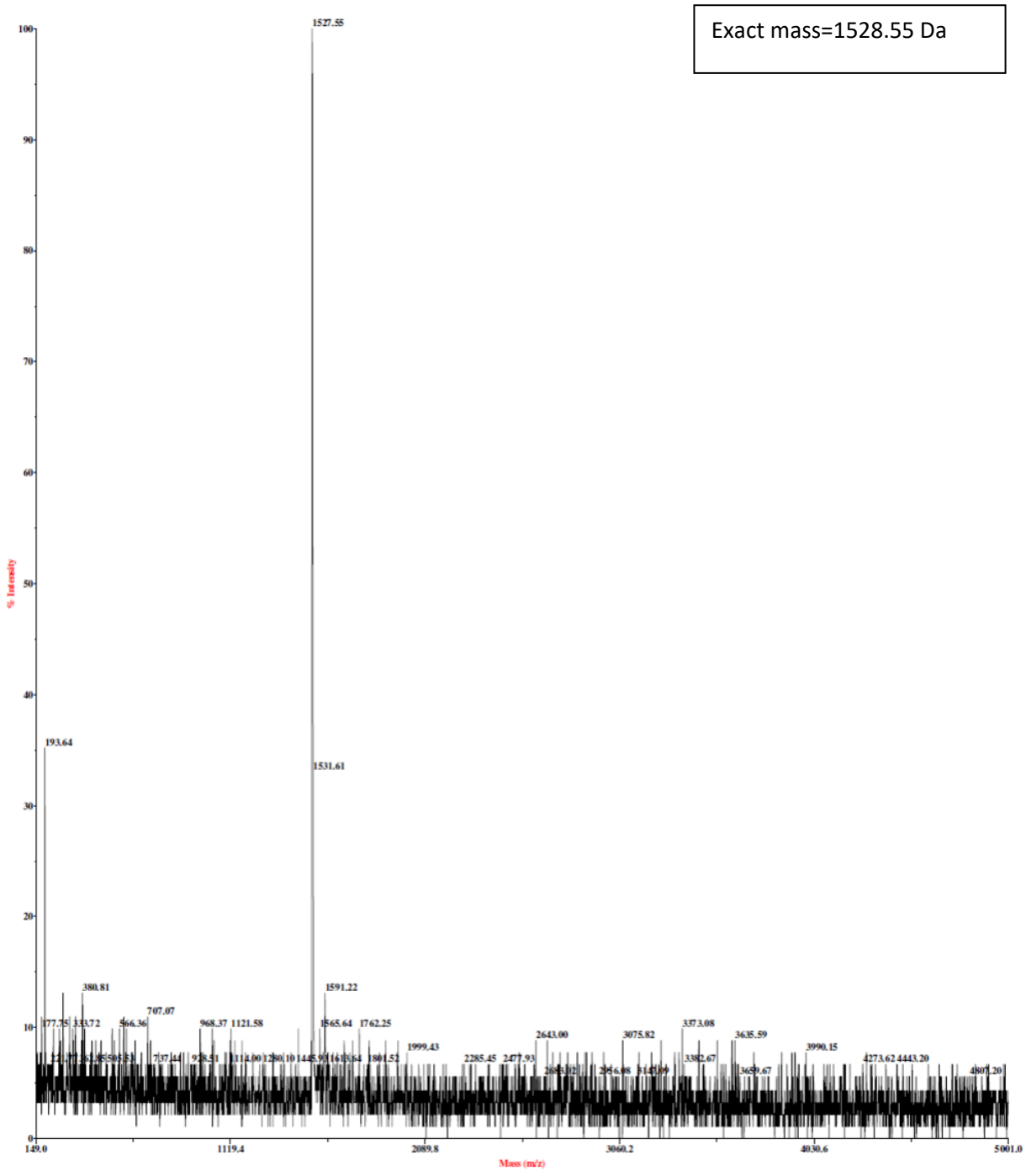

Figure A14. MALDI-TOF MS [JV86]for POSSP-IB

Aminopropyl hepta(phenyl) POSS

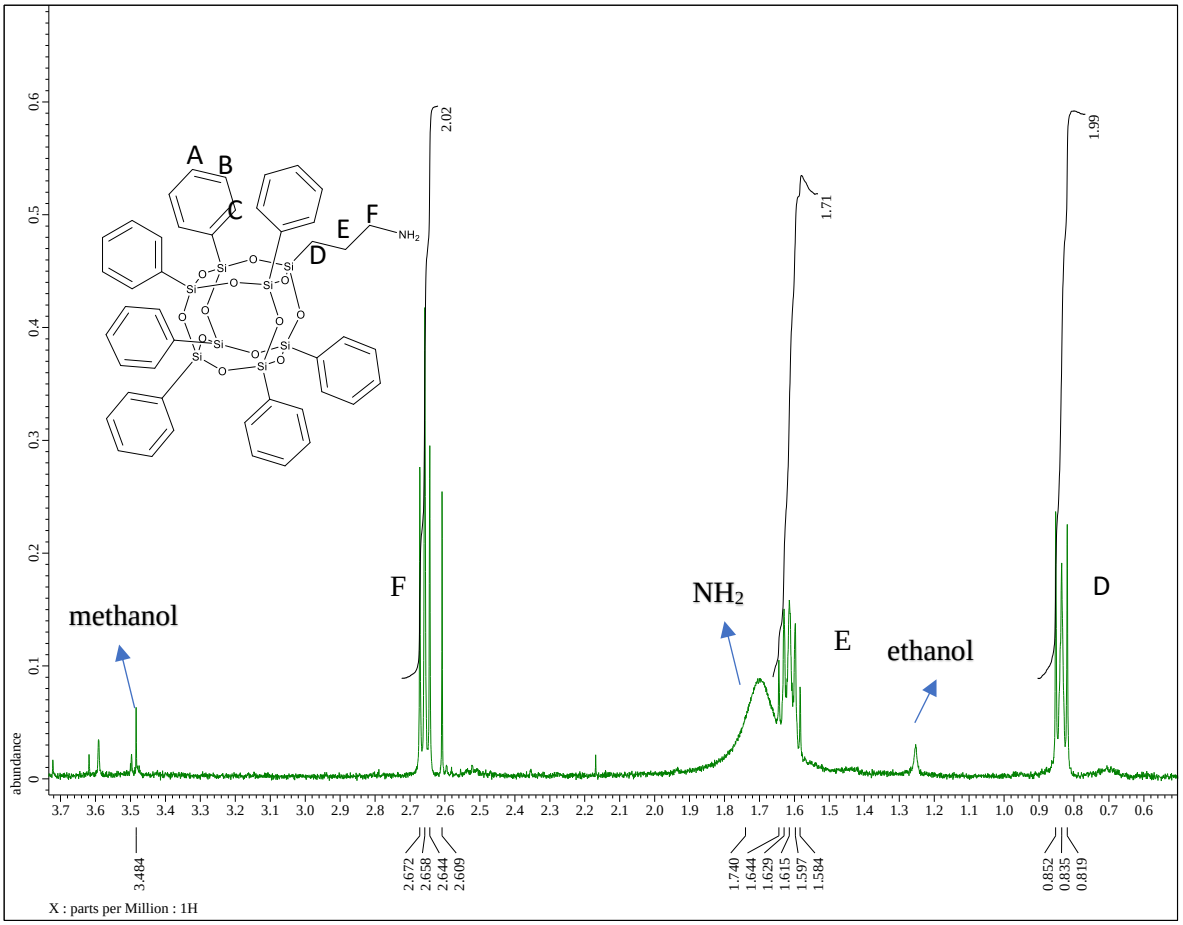

Figure A15. ^{1}H NMR Aminopropyl hepta(phenyl) POSS

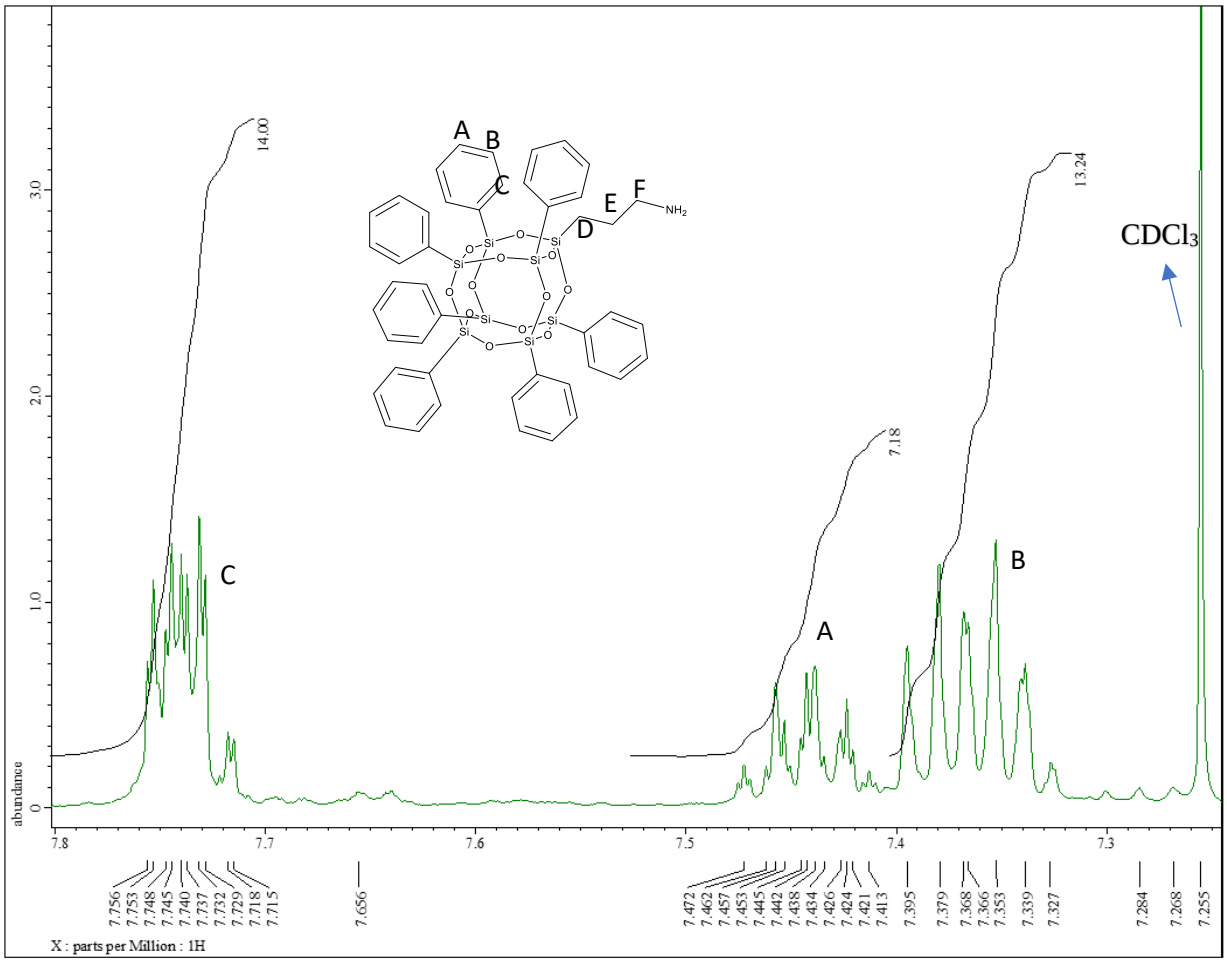

Figure A16. ^{1}H NMR Aminopropyl hepta(phenyl) POSS.

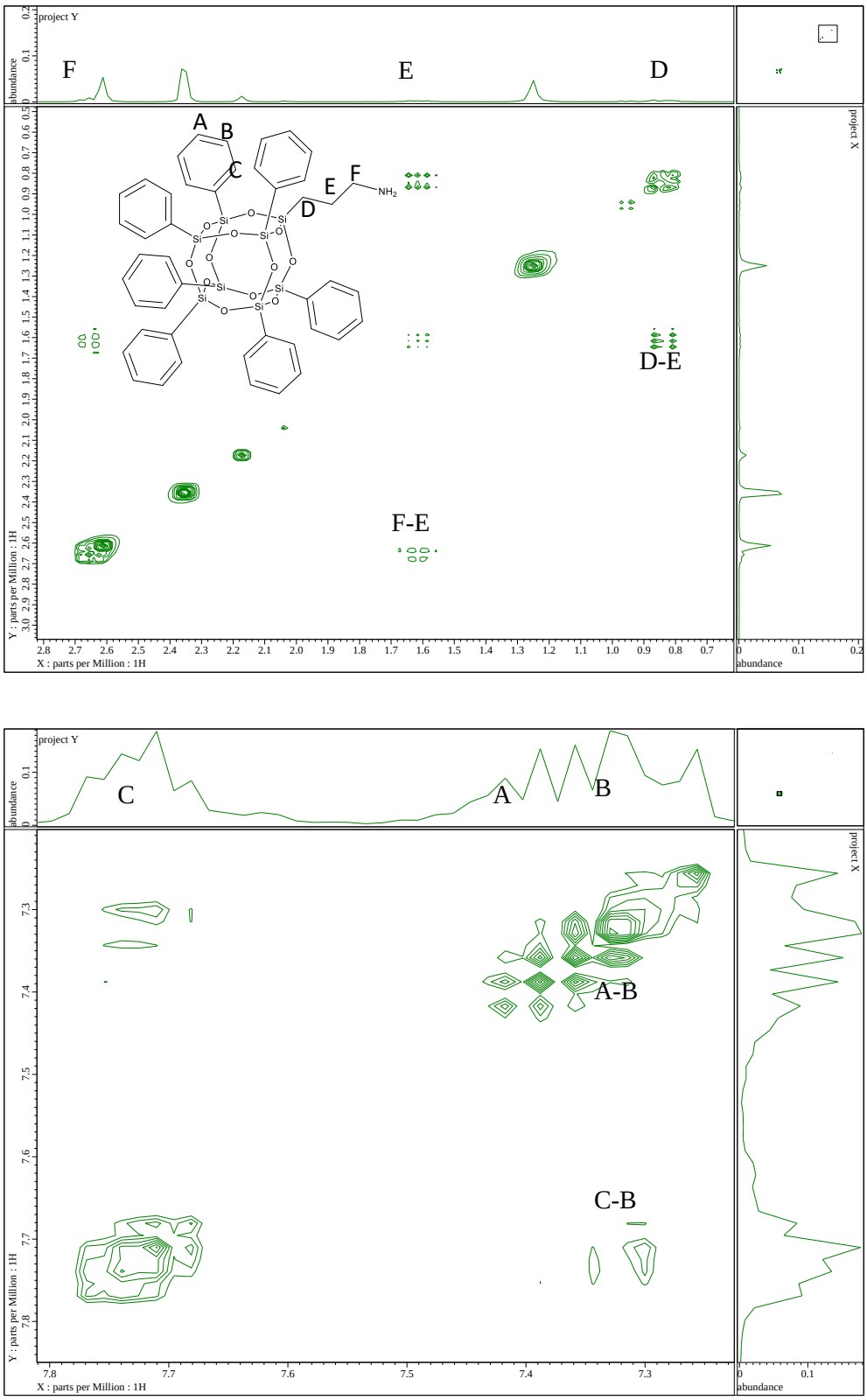

Figure A17. COSY NMR Aminopropyl hepta(phenyl) POSS

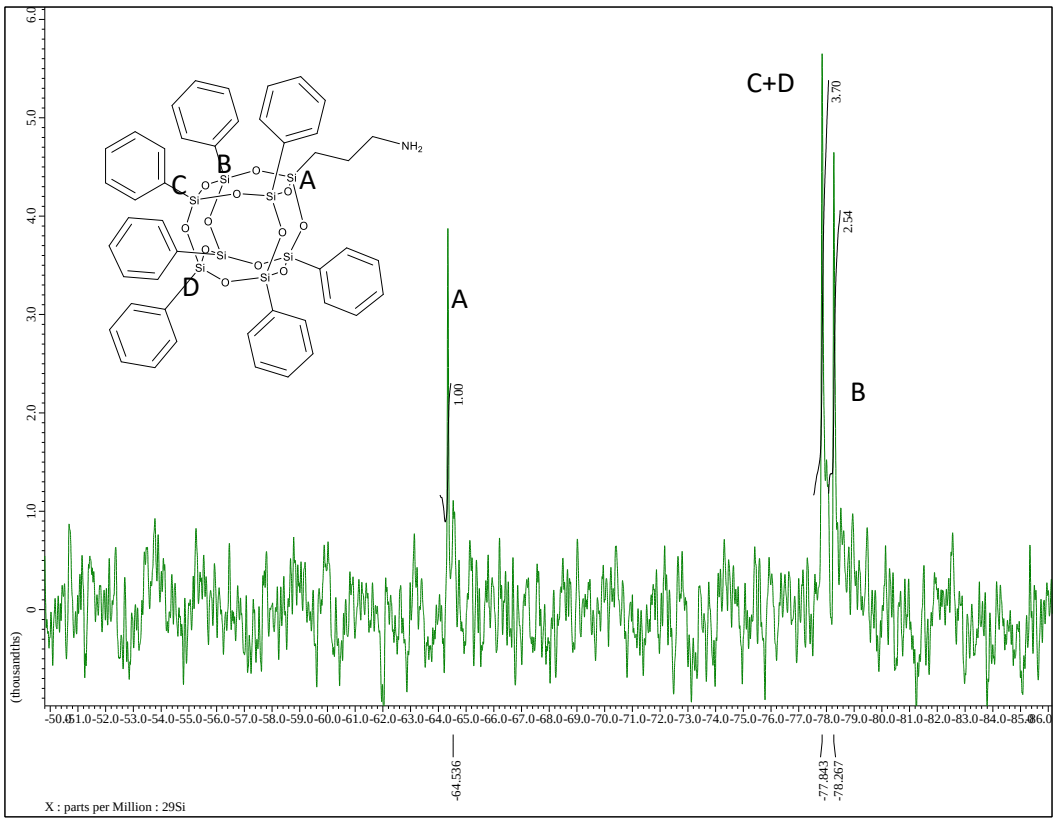

Figure A18. ^{29}Si NMR Aminopropyl hepta(phenyl) POSS

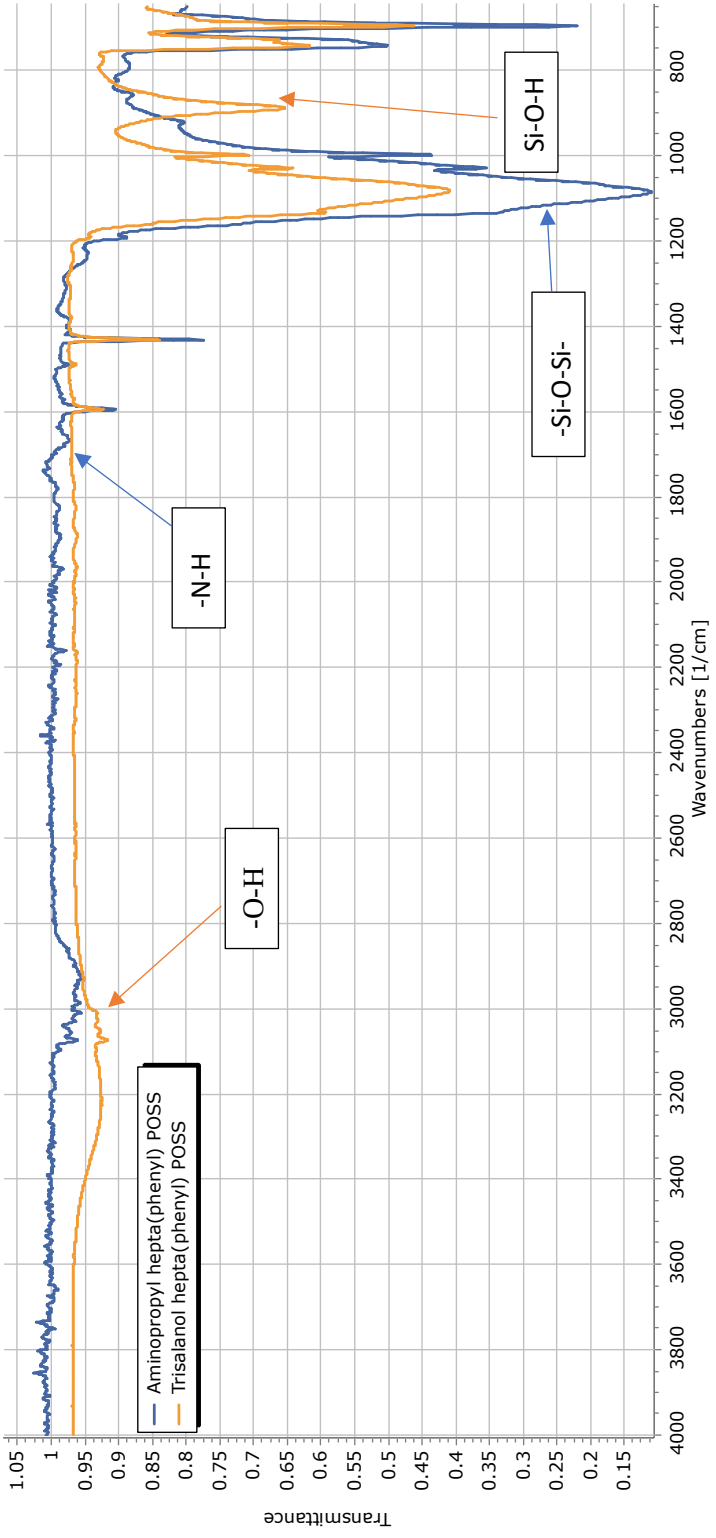

Figure A19. FT-IR Aminopropyl hepta(phenyl) POSS

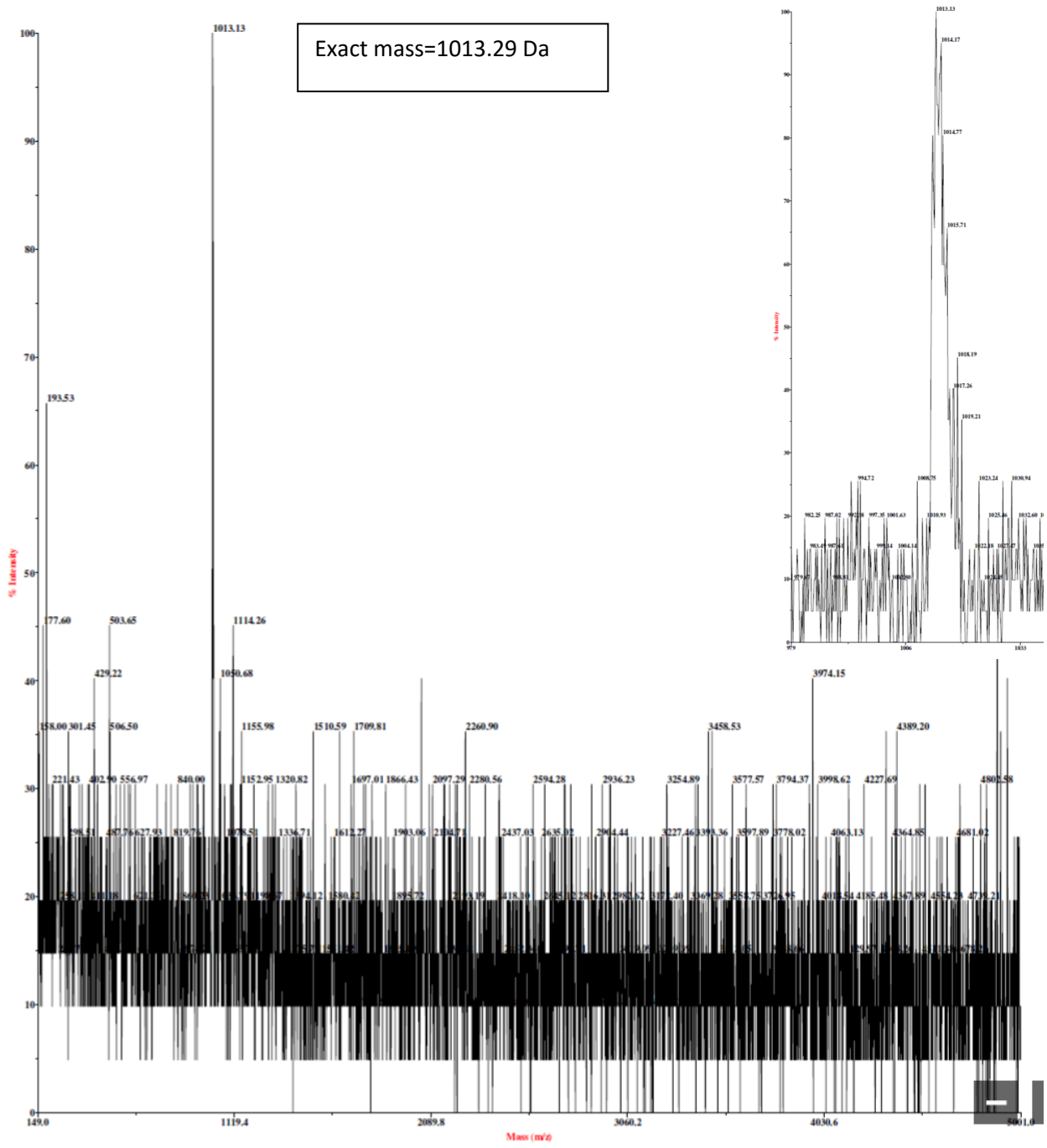

Figure A20. MALDI-TOF MS Aminopropyl hepta(phenyl) POSS

Propyl isocyanate hepta(phenyl) POSS

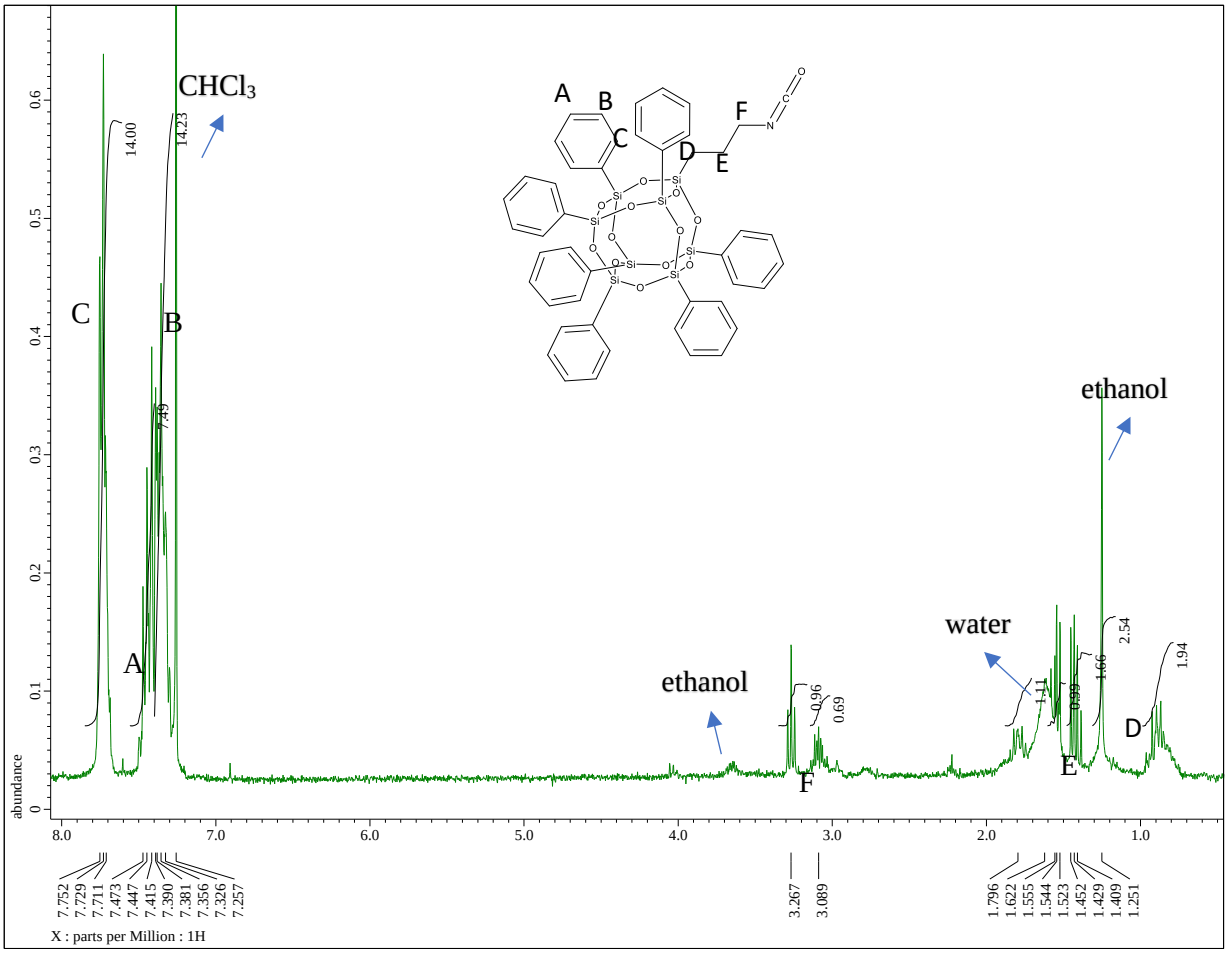

Figure A21. ^{1}H NMR propyl isocyanate hepta(phenyl) POSS.

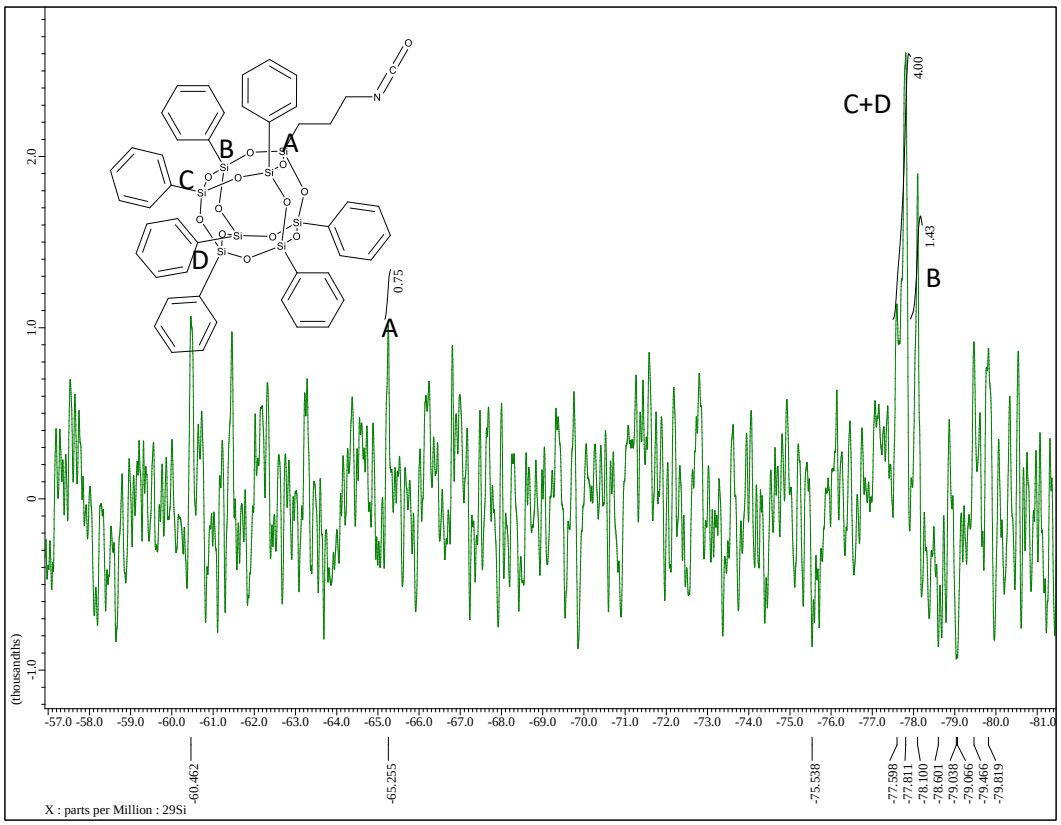

Figure A22. ^{29}Si NMR propyl isocyanate hepta(phenyl) POSS[JV87]

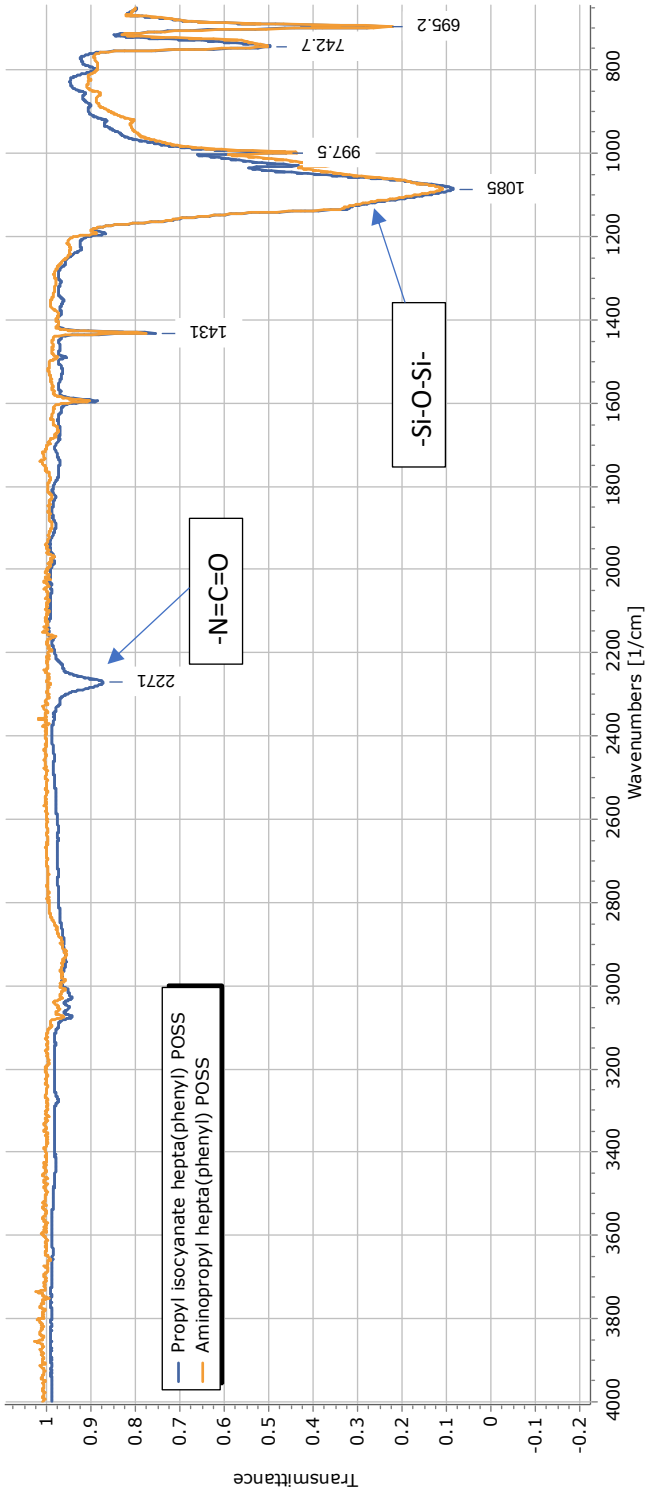

Figure A23. FT-IR propyl isocyanate hepta(phenyl) POSS

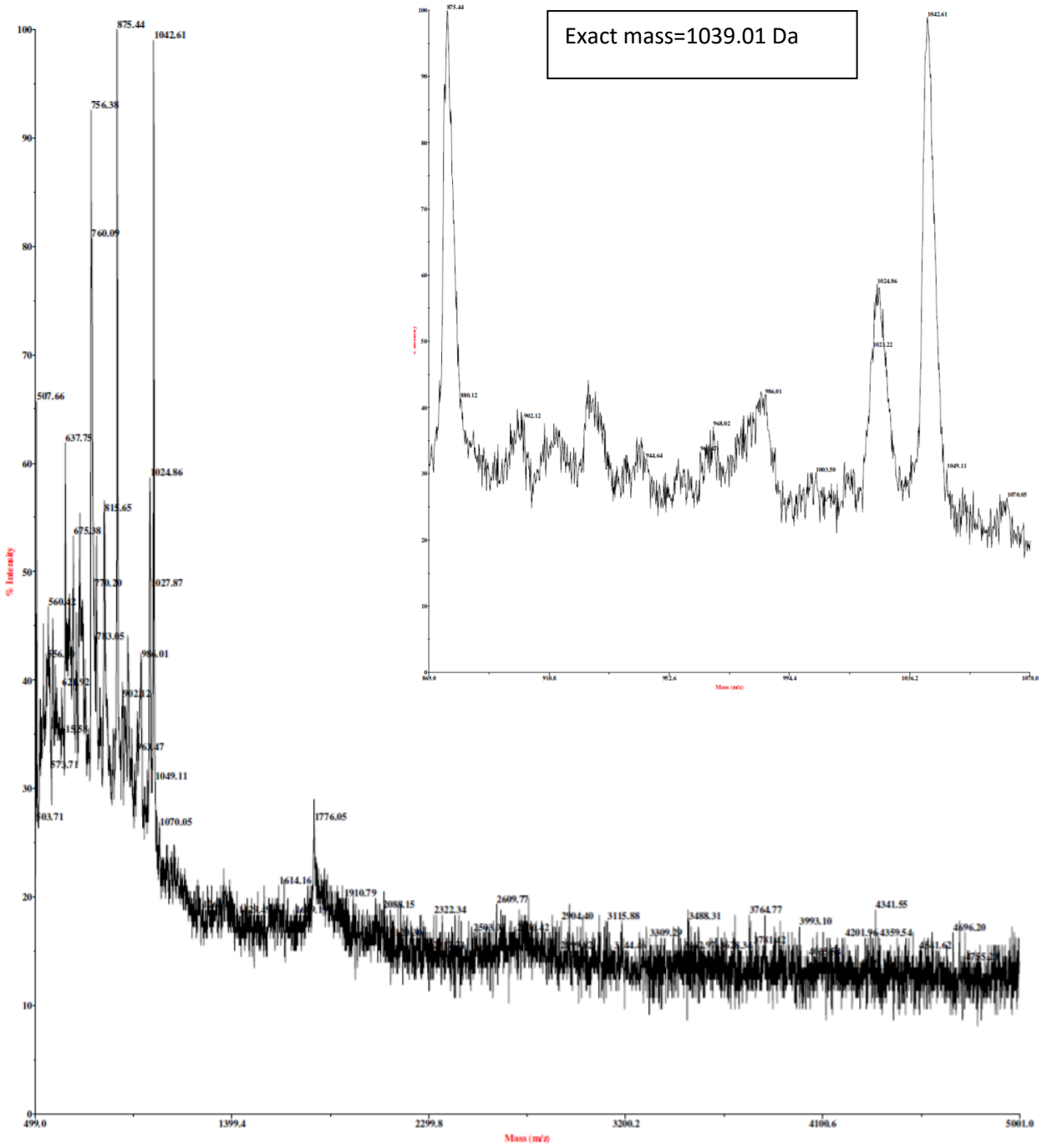

Figure A24. MALDI-TOF MS propyl isocyanate hepta(phenyl) POSS

POSSP-Ph

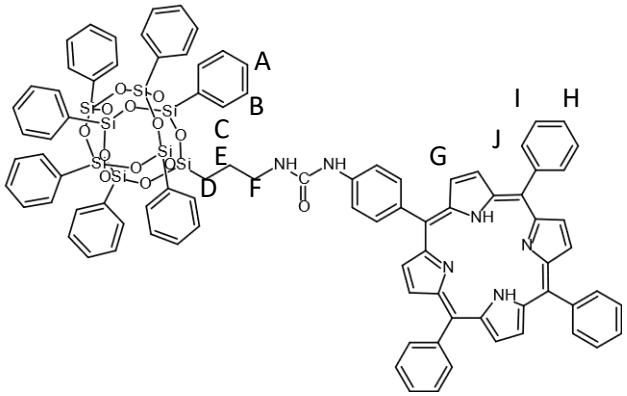

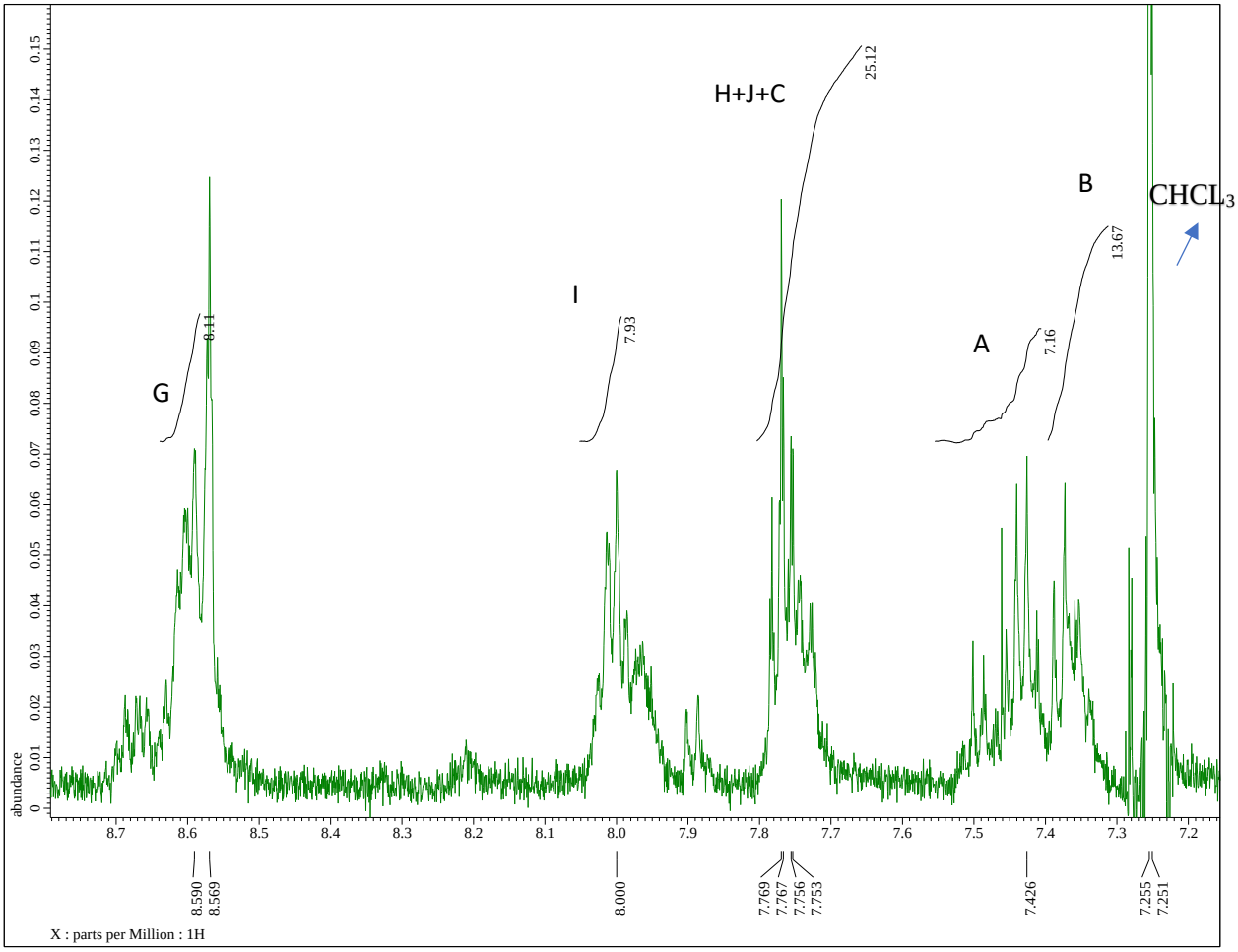

Figure A25. ^{1}H NMR POSSP-Ph

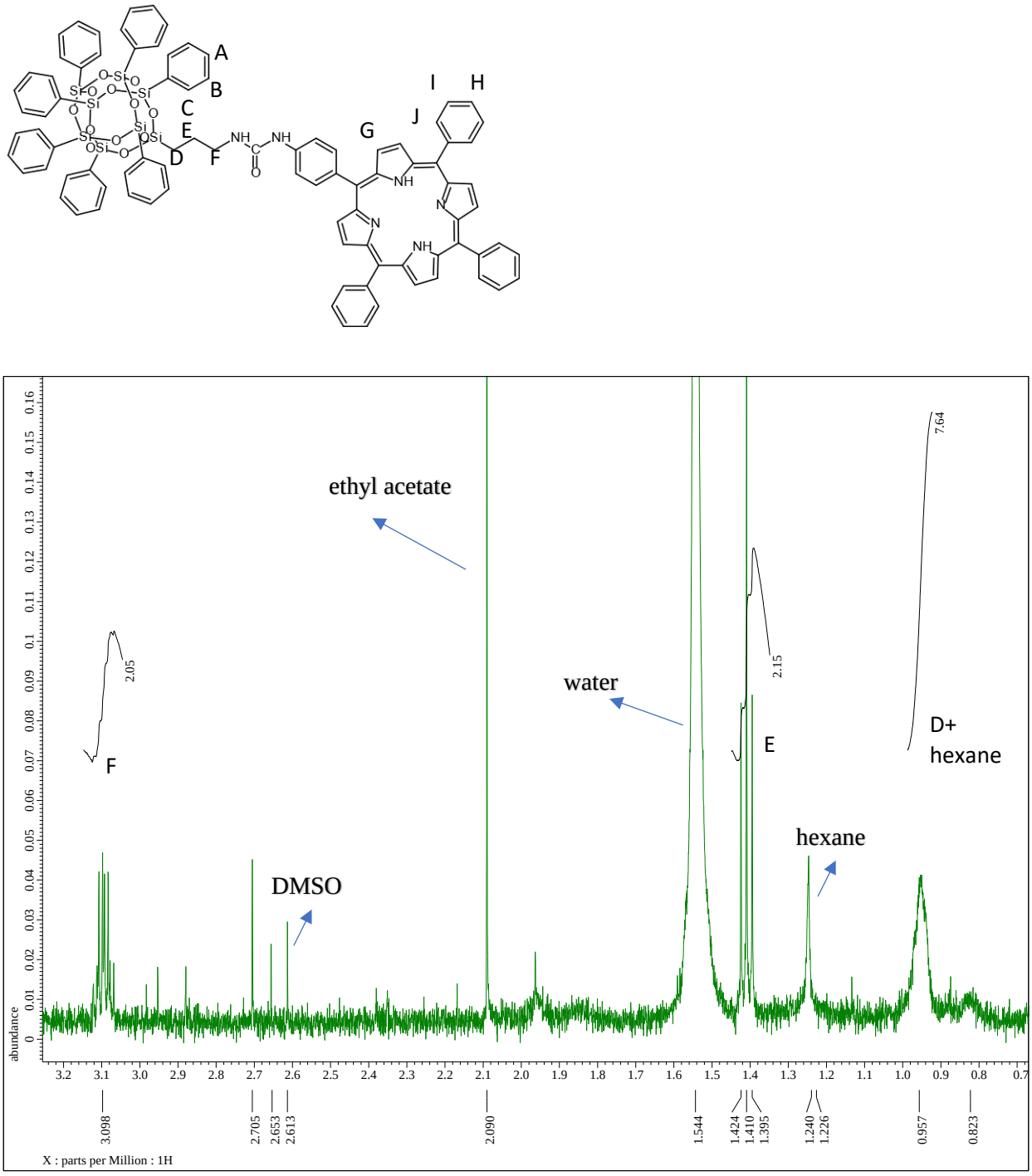

Figure A26. ^{1}H NMR POSSP-Ph

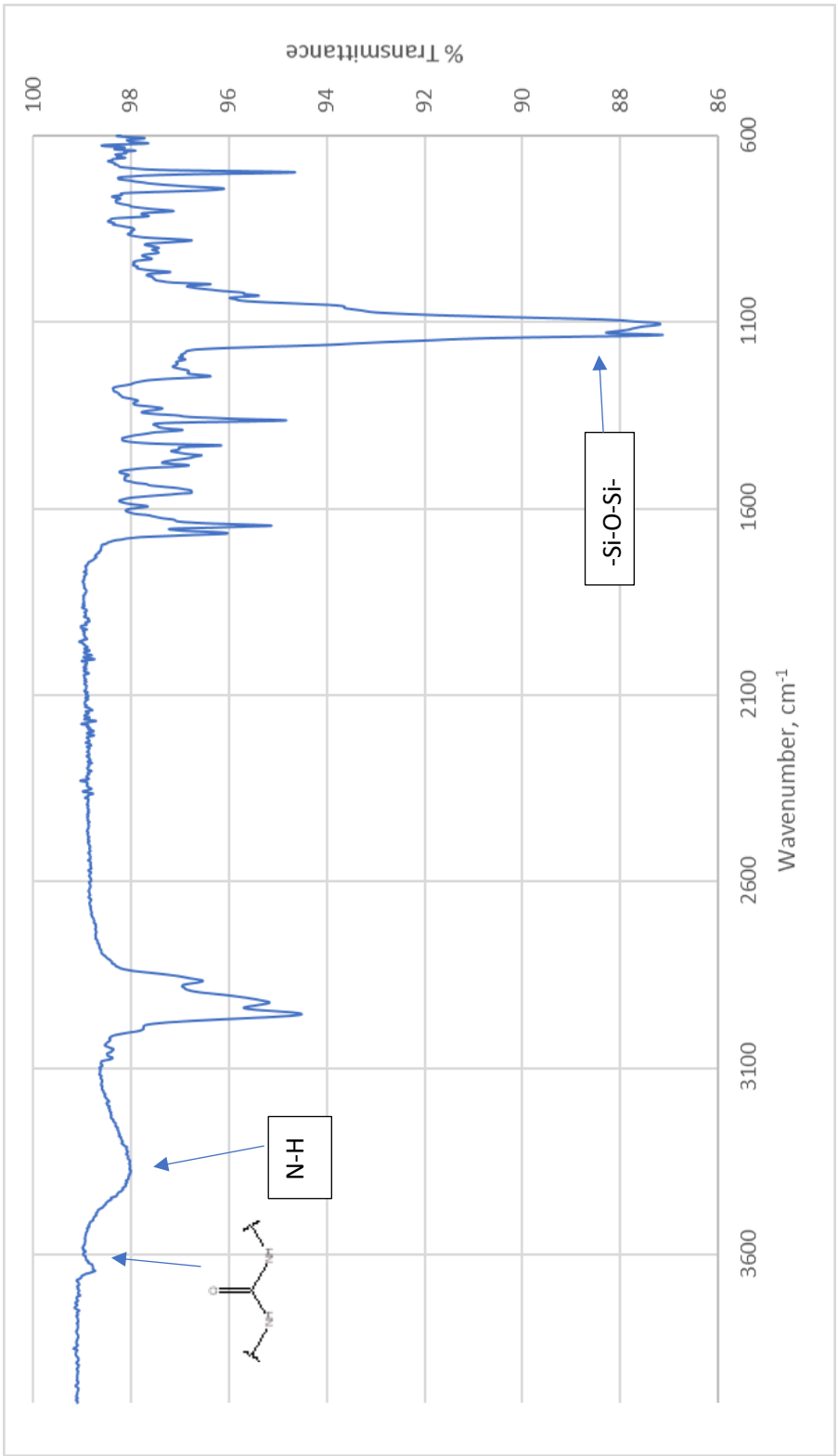

Figure A27. FT-IR POSSP-Ph

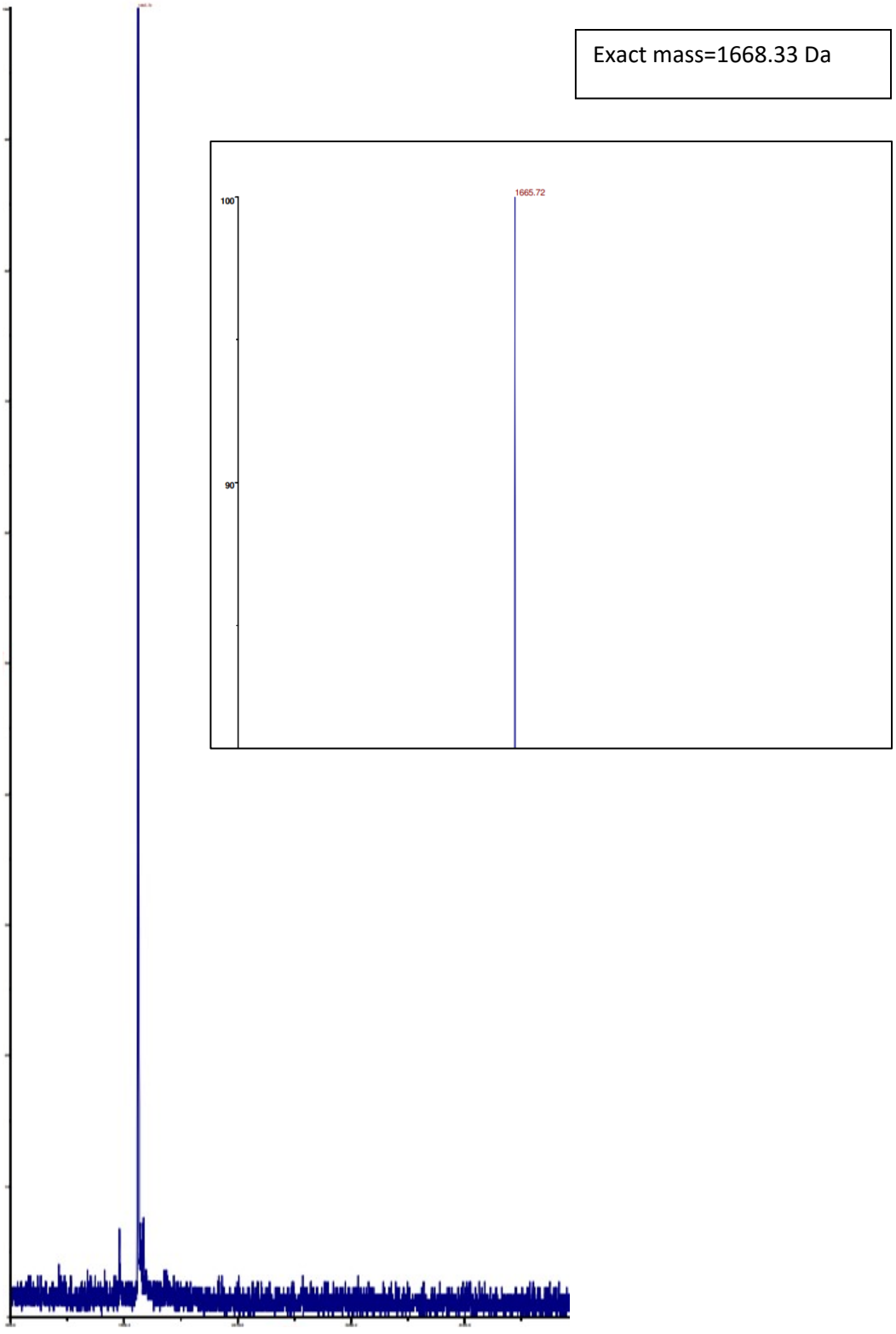

Figure A28. MALDI-TOF MS [JV88]for POSSP-Ph

POSSP-TIB

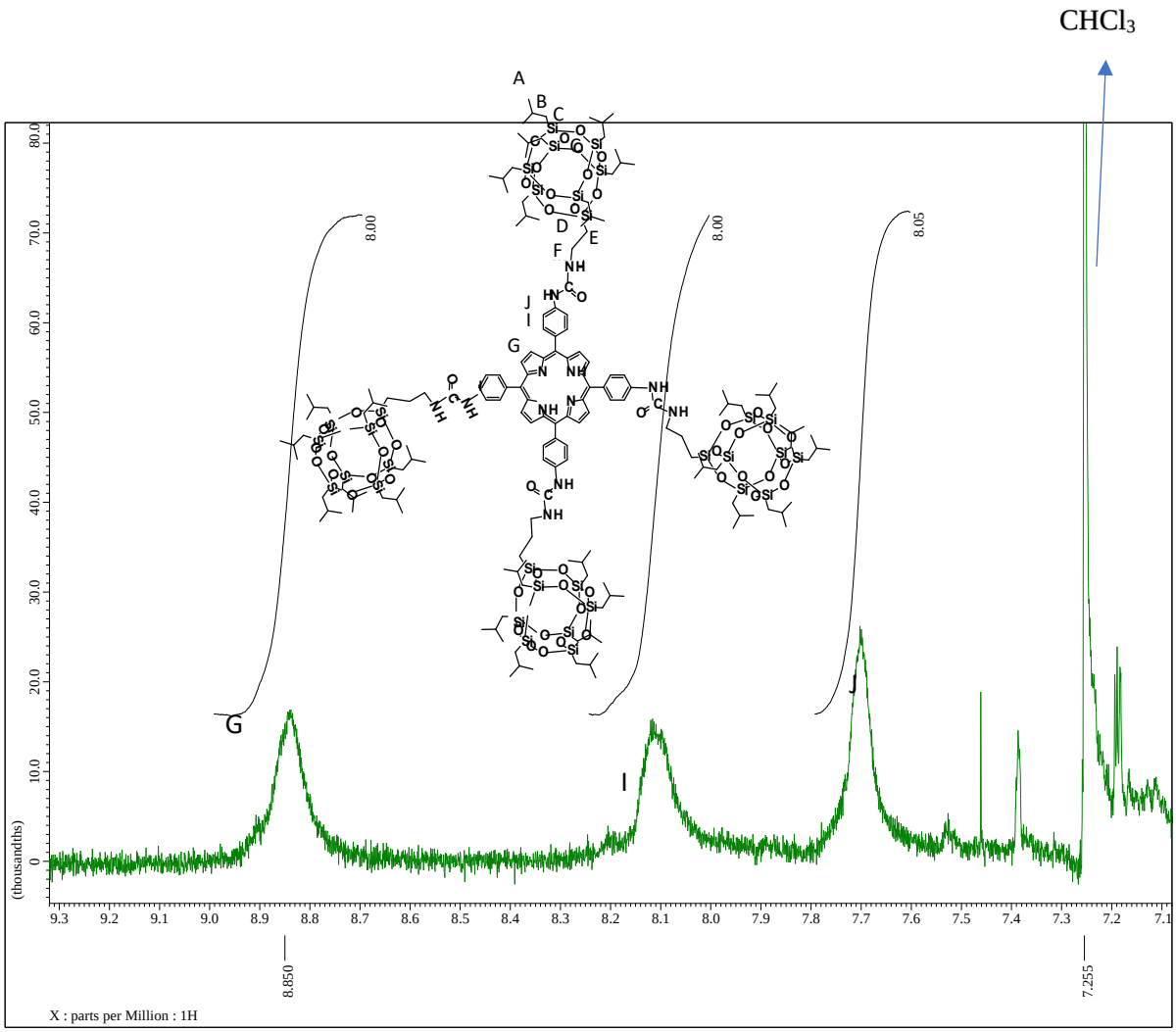

Figure A29. ^{1}H NMR POSSP-TIB

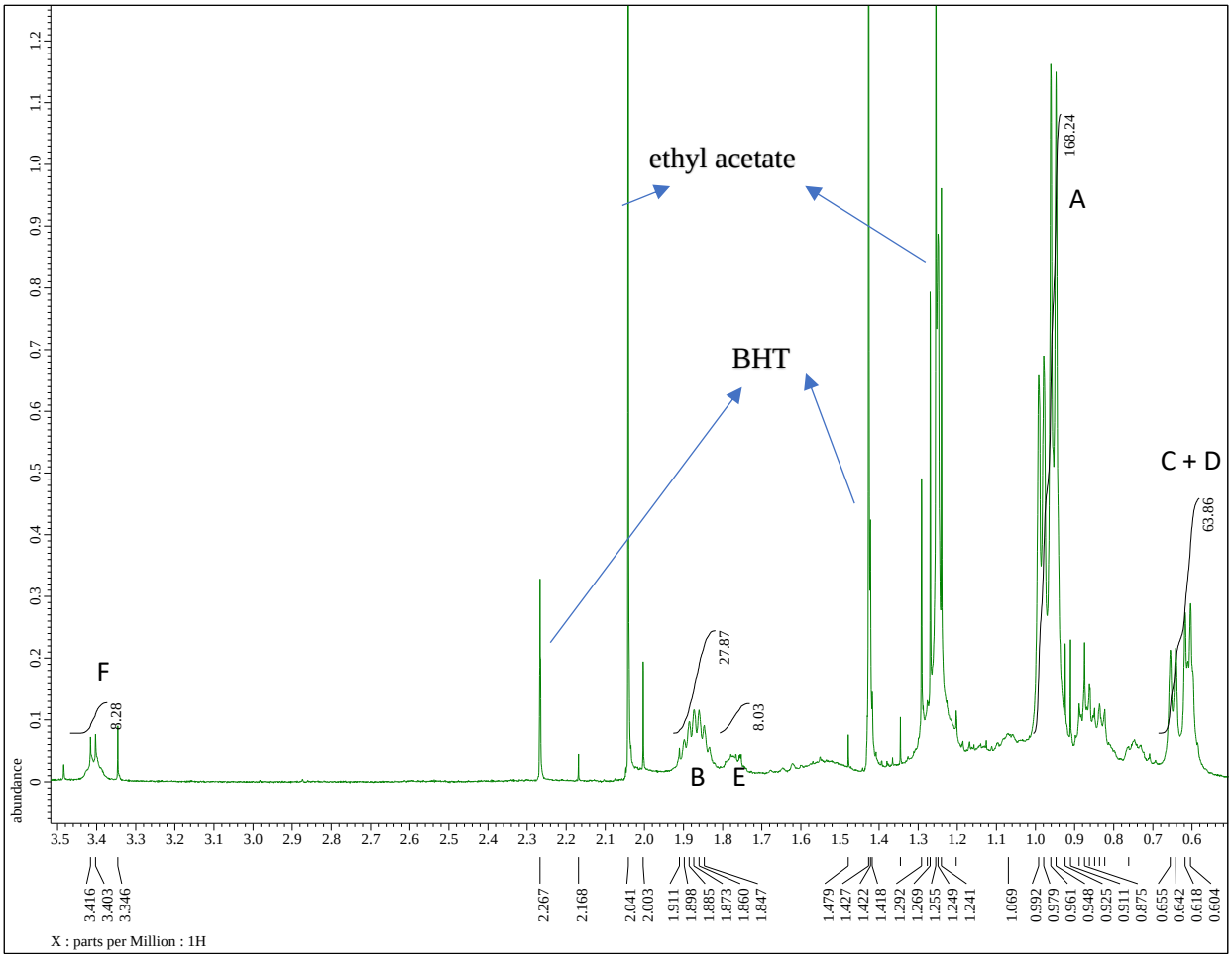

Figure A30. ^{1}H NMR POSSP-TIB[JV89]

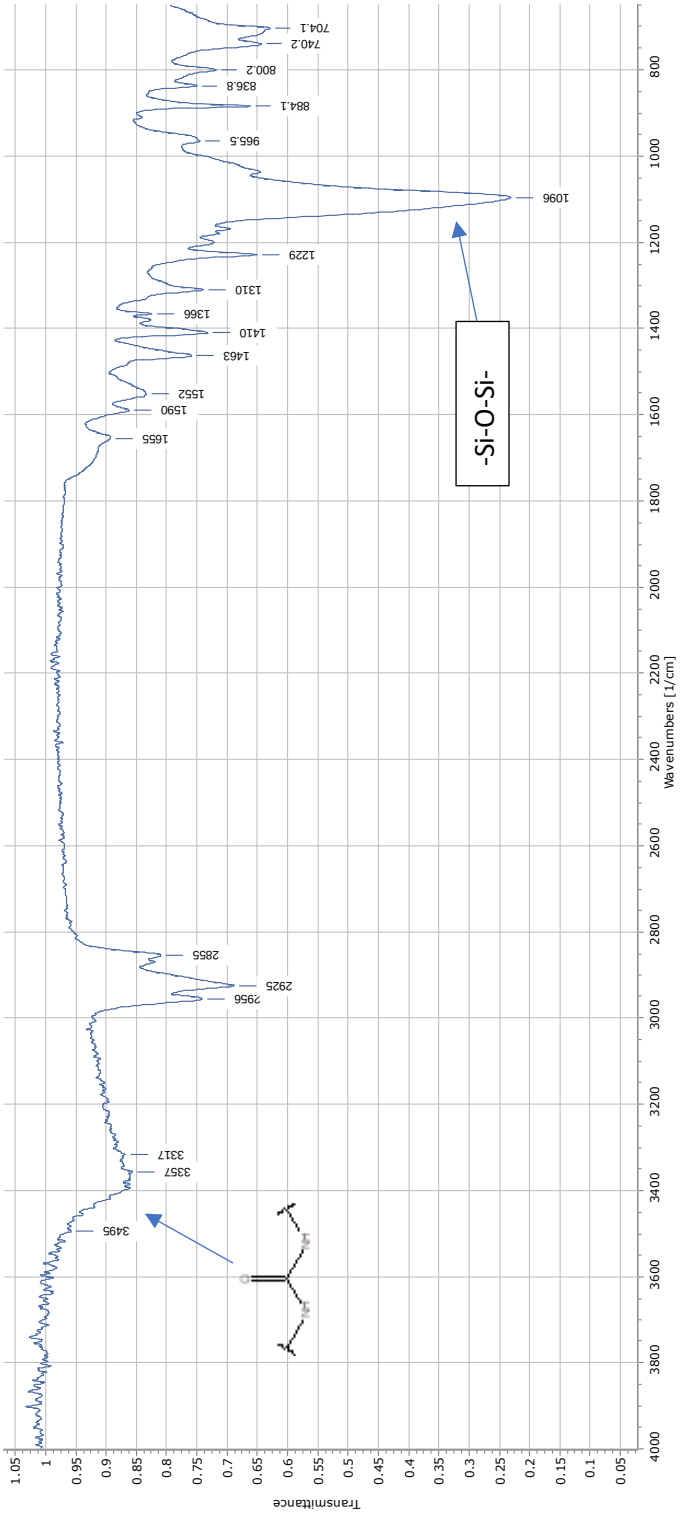

Figure A31. FT-IR POSSP-TIB

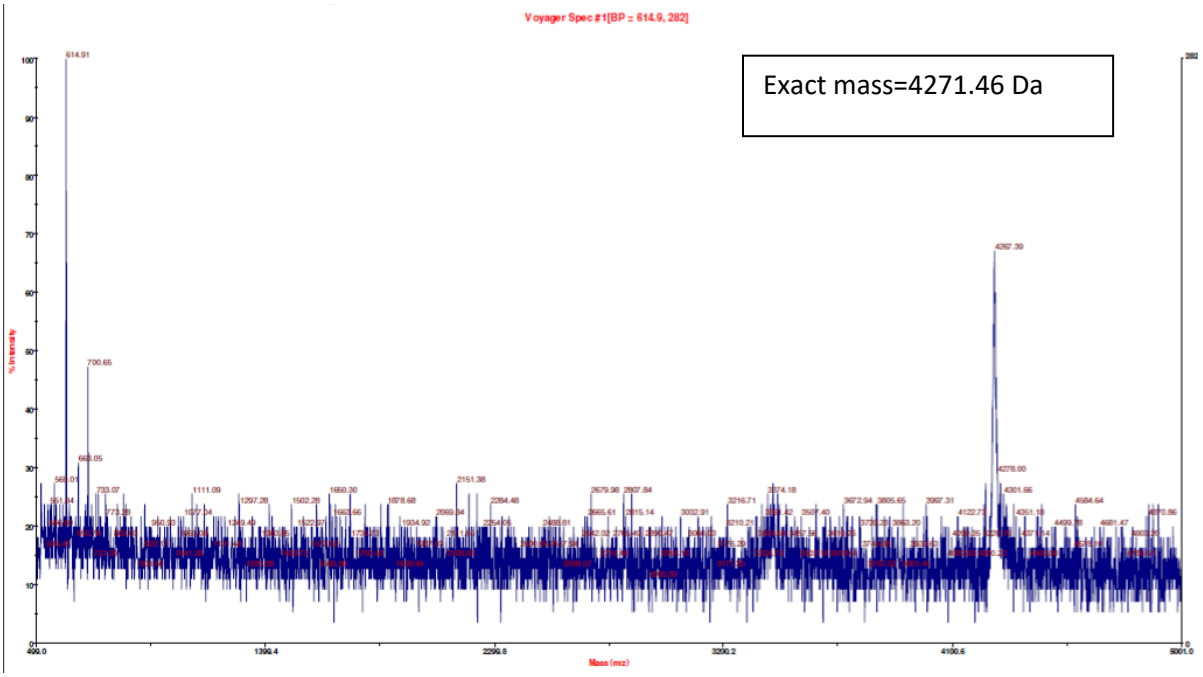

Figure A32. MALDI-TOF MS POSSP-TIB